La dispersión de los homínidos fuera de África ha sido desde el inicio del estudio de la paleontología humana un tema recurrente. Conocer cuándo comenzó la migración fuera del continente africano es algo que sigue siendo objeto de estudio de manera intensa actualmente. Por estos motivos, obtener una cronología clara de aquellos yacimientos en los que hay presencia humana es importante, ya que aportaría más información para establecer un mejor contexto cronológico de esa migración fuera de África. El paleomagnetismo puede ser una herramienta útil y fácilmente aplicable, pues tiene un registro temporal muy amplio y no es destructiva para los restos al aplicarse sobre el sedimento. Con esta idea en mente, en este trabajo se ha procedido a realizar análisis paleomagnéticos, concretamente la obtención de magnetoestratigrafías, en una serie de yacimientos localizados en el Sur de España y Norte de África con presencia humana durante el Paleolítico inferior (Pleistoceno inferior y medio), con la intención de ampliar la información cronológica existente para intentar determinar con un marco temporal más exacto cuándo se produjo la presencia humana en esas localidades.

Claudia Álvarez Posada Contexto Cronológico de las primeras expansiones humanas en la Cuenca Circummediterránea mediante la aplicación del paleomagnetismo

Contexto cronológico de las primeras expansiones humanas en la cuenca circummediterránea mediante la aplicación del paleomagnetismo

TESIS DOCTORAL

Claudia Álvarez Posada

2018

DIRIGIDA POR Dr. Josep M. Parés

UNIVERSIDAD DE BURGOS

CENIEH
Centro Nacional de Investigación sobre la Evolución Humana

UNIVERSIDAD DE BURGOS

Contexto cronológico de las primeras expansiones humanas en la cuenca circummediterránea mediante la aplicación del paleomagnetismo

Tesis Doctoral

Claudia Álvarez Posada

2018

Programa de Doctorado

Evolución humana, paleoecología del cuaternario y técnicas aplicadas en la investigación

D. Josep M. Parés casanova, coordinador del Programa de investigación de Geocronología del Centro Nacional de Investigación sobre Evolución Humana (CENIEH),

Certifica que la Tesis Doctoral

"Contexto cronológico de las primeras expansiones humanas en la cuenca circummediterránea mediante la aplicación del paleomagnetismo"

ha sido realizada bajo su dirección en el CENIEH por la licenciada Dña. Claudia Álvarez Posada, dentro del Programa de Doctorado de Evolución Humana, Paleoecologia del Cuaternario y Técnicas de estudio aplicadas a la investigación de la universidad de Burgos, y mediante la presente

Informa Favorablemente de su presentación.

Para que conste a los efectos necesarios, firmado en Burgos, a 30 de Julio de 2018.

Fdo. Josep M. Parés

La Presente Tesis Doctoral ha sido financiada por el Ministerio de Ciencia e Innovación (MICINN) del Gobierno de España con la ayuda BES-2011-048877 del Subprograma de Formación de Personal Investigador (FPI) correspondiente al proyecto CGL2010-16821 (Primeras expansiones Humanas en la Región Circummediterránea: Contexto Geocronológico). Así mismo durante el desarrollo de la presente tesis se ha disfrutado de ayudas para la realización de estancias en el *Paleomagnetic Laboratory, Fort Hoofddijk, Faculty of Geosciences,* Universidad de Utrecht, Holanda (EEBB-I-13-06414) , y en el *Palaeomagnetism and Rock Magnetism Research Group, Departament of Earth Sciences*, en la Universidad de Oxford, Reino Unido (EEBB-I-14-09041).

El proceso de desarrollo de esta Tesis se ha llevado a cabo en el Centro Nacional de investigación sobre la Evolución Humana (CENIEH), en Burgos.

Durante el desarrollo de esta Tesis Doctoral, a parte de los artículos que conforman la misma, la doctoranda ha participado en diferentes congresos y ha colaborado en distintos estudios publicados en revistas de ámbito nacional e internacional:

- **Claudia Álvarez Posada** , 2014. *Magnetismo, campo magnético terrestre y su aplicación cronológica: Paleomagnetismo.* Revista de divulgación Científica Pangea.

- **Claudia Álvarez Posada**, Josep M. Parés. *Paleomagnetic analysis of river terraces of the Arlanza, Arlanzón and Duero Rivers (N Spain) and chronological context,* 14th Castle Meeting. New Trends on Paleo, Rock and Environmental Magnetism. Evora, Portugal 31 August - 6 September 2014. Póster.

-**Claudia Álvarez Posada**, Josep María Parés, Ángel Carrancho Alonso, Juan José Villalaín, Aouraghe Hassan, Haddoumi Hamid, El Hammouti Kamal, El Harradji Abderrahman, Robert Sala, María Gema Chacón. *Paleomagnetic Analysis of the Northern Margin of the Basin of Aïn Beni Mathar-Guefait (Eastern Morocco).* XVII World UISPP Congress. Burgos, España. Del 1 al 7 de septiembre de 2014. Póster.

- **Claudia Álvarez Posada**, *Paleomagnetic Studies in The Northern Margin of Aïn Bni Mathar - Guefait basin (High Plateau, Morocco).* II Jornadas de Prehistoria Africana realizadas en el Centro de Investigación sobre la Evolución Humana en Burgos, Del 15 al 16 de abril de 2015. Comunicación Oral.

- Melanie Bartz, Gilles Rixhon, Mathieu Duval, Georgina E. King, **Claudia Álvarez Posada**, Josep M. Parés, Helmut Brückner, 2018. *Successful combination of electron spin resonance, luminiscence and palaeomagnetic dating*

methods allows reconstruction of the Pleistocene evolution of the lower Molouya river (NE Morocco). Quaternary Science Reviews 185, 153-171

- Melanie Bartz, Lee J. Arnold, Martina Demuro, Mathieu Duval, Georgina E. King, Gilles Rixhon, **Claudia Álvarez Posada**, Josep M. Parés, Helmut Brückner, 2018. *Single-grain TT-OSL dating results confirm an Early Pleistocene age for the lower Moulouya River deposits (NE Morocco).* Quaternary Geochronology, doi.org/10.1016/j.quageo.2018.04.007

Agradecimientos

Agradecimientos

La realización de la presente tesis ha supuesto para mí una fase muy importante en mi vida, tanto en lo académico como en lo personal, en la que he recorrido nuevos caminos y hecho frente a nuevos retos. Me ha dado la oportunidad de conocer a personas estupendas y de retomar el contacto con antiguos compañeros. Este agradecimiento es para todas aquellas personas que han contribuido a hacer de esta experiencia un viaje memorable.

En primer lugar, quiero dar las gracias a mi director de tesis, Josep M. Parés, por la confianza depositada en mí para la realización de esta tesis doctoral, cuando lo más que sabía de magnetismo era que quedaba registrado en las dorsales oceánicas. Gracias por haberme guiado en este camino, por lo mucho que he aprendido y sobre todo por haber hecho que disfrute del proceso de investigación. Muchísimas gracias por esta oportunidad increíble y por la paciencia que has demostrado conmigo.

Quiero agradecer también enormemente el apoyo total que me han brindado desde todo el equipo de Paleomagnetismo de la Universidad de Burgos. Juan José Villalaín y Ángel Carrancho Alonso, gracias por vuestros sabios consejos y ayuda siempre que los he necesitado.

Gracias a Cor Langereis y al grupo de Paleomagnetismo de la Universidad de Utrecht por esos dos meses aprendiendo tanto en Holanda. Mención especial para Daniel Pastor Galán e Inés Iglesias Hernández por acogerme esos meses y hacerme sentir como en casa.

A Conall MacNiocaill del grupo de Paleomagnetismo y Magnetismo de Rocas de la Universidad de Oxford (Inglaterra) por la estancia de dos meses aprendiendo sobre el manejo y mantenimiento de magnetómetros.

A los compañeros del CENIEH, los que ya no están en el centro y los que siguen, que me han ofrecido su soporte y ayuda: Mark Sier, Carlos Saíz, Javier Iglesias, Mathieu Duval, Ana Isabel Ortega, Isabel Sarro Moreno. Y gracias también al resto del personal y trabajadores del CENIEH.

Gracias al Equipo de Investigación de Atapuerca y sus directores, José María Bermúdez de Castro, Eudald Carbonell y Juan Luis Arsuaga por facilitarme el acceso y muestreo en los yacimientos.

Gracias también a las personas que he conocido por el camino, quienes me han aportado y enriquecido esta experiencia de varias y muy diversas formas. Gema Chachón Navarro y Robert Sala Ramos: os quiero dar las gracias por permitirme colaborar con vosotros y por ello enseñarme un lugar tan fascinante como es Marruecos. Jordi Rosell, gracias por dejarme incordiaros en el yacimiento con el muestreo y por esos momentos de excavación en TD4. Cesar Viseras y Sila Pla-Pueyo, gracias a ambos por vuestro tiempo y esfuerzo para acompañarme en el muestreo en la Cuenca de Guadix - Baza.

Mención especial merece la familia que elegimos a lo largo de nuestra vida, aquellos con los que compartimos las frustraciones de los artículos, los resul-

tados negativos pero también los éxitos cuando los ha habido y con quienes me he desahogado o celebrado con unas cañas mediante. Verónica Mardones, gracias por esos momentos de locura transitoria necesaria y por dejarme estar en Haru cuando ya no aguantaba más en la biblioteca. Carmen Herrera, gracias precisamente por acogerme en la biblioteca y ayudarme con todo lo referente a registros e información. Esta experiencia no habría sido lo mismo sin ese grupo del SESHI, peliculeros de serie B, tanto los que acudíais como los que no: Carlos Pérez Garrido, Cecilia García Campos, Davinia Moreno García, Guillermo Rodríguez-Gómez, Isidoro Campaña Lozano, Laura Sánchez Romero, Lucía Bermejo Albarrán, Marina Martínez de Pinillos, Mario Modesto Mata, Nuria Basdediós Prieto, Theodoro Karampaglidis, Virginia Martínez Pillado. Gracias.

Y luego está la familia en la que nacemos, la que está ahí pase lo que pase y la que siempre te apoya. Gracias a mis padres, por su paciencia, su comprensión y su cariño. Por enseñarme que el esfuerzo y el trabajo duro tienen su recompensa, por dejarme ser quien soy y fomentar mi curiosidad y ganas de saber. Cruz Posada García, mamá, simplemente gracias por estar siempre ahí. Y Rodrigo Álvarez González, papá, estés donde estés, gracias. Gracias a mis hermanas, Julieta, Laura, Paula y Susana, y a mi tía Elvira y mi prima Eva, por interesarse siempre por lo que hago e incluso tratar de entender lo que estudio, escuchándome aunque les suene a chino.

A todos. Muchas gracias.

ÍNDICE

Índice

Abstract / Resumen

Abstract

The dispersion of the hominins outside Africa has been a recurrent topic since the beginning of the study of human paleontology. Knowing when *Homo* migration began outside the african continent is something that is still being intensively studied. Theories have been changing over time, from the idea of a "short" dispersion, no more than half a million years ago, to the most accepted idea today, claiming it happened more than a million years ago. The new discoveries in the Middle East (Ubeidiya, Gesher Benot Ya'aqov), Eurasia (Dmanisi) and Europe (Le Vallonet, Ca'Belverede, Ceprano, Atapuerca and others), reinforce this hypothesis, and also that this colonization is the result of intermittent and sucesive waves. However, a controversial and intense subject remains.

That is why obtaining clear chronology of those sites where there is a human presence is an important key, as it would provide more information to establish a better chronological context of that migration outside of Africa. There are numerous dating methods that have been developed and improved over time, such as electron spin resonance, biostratigraphy, luminescence, etc., but sometimes it is difficult to establish a correct correlation between all of them, which it can even lead to inconsistent results. Therefore, paleomagnetism can be a useful and easily applicable tool, since it has a very broad temporal

record (> 180 million years, up to the present) and is not destructive for the remains because it is applied in sediments.

With this idea in mind, in this thesis we have carried out paleomagnetic analyses in order to obtain magnetostratigraphies in various localities in Spain and Northern Africa that have human evidence during the Lower Paleolithic (Lower and Middle Pleistocene), such as Fuente - 3 and Solana del Zamborino paleontological sites, both located in the Guadix-Baza Basin, in Orce (Granada, Spain); the paleontological site of Gran Dolina, in Atapuerca (Burgos, Spain); as well as in the Duero Basin itself, and in the Aïn Bni Mathar Basin (Aïn Bni Mathar, Morocco). The main objective has been to expand the existing chronological information to provide a better time framework of the deposits and to establish when the human presence occurred in those sites.

To this end, an exhaustive fieldwork has been carried out, obtaining several stratigraphic logs, either in exposed localities or based on bore holes, and thus collecting more than 1200 individual samples which have been analyzed in the National Research Center for Human Evolution, as well as in the Paleomagnetic Laboratory, Fort Hoofddijk, Faculty of Geosciences, University of Utrecht, The Netherlands; and in the Palaeo-Magnetism and Rock Magnetism Research Group, Department of Earth Sciences, at the University of Oxford, United Kingdom. The results of the paleomagnetic analyses, in combination with other chronology techniques (biostratigraphy, cosmogenic nuclidess, electron spin resonance, luminiscence), allow testing the presence or absence of the Jaramillo Subcron, (0.99 - 1.07 Ma) and to determine if the human presence in the deposits in question occurred before or after to one million years.

Consequently, in view of the results presented in this thesis, paleomagnetism, in combination with other chronological methods provides further evi-

dence for human presence close to a million years ago in TD4 level from Gran Dolina (Atapuerca) and ever older in Fuente Nueva 3 (Baza Basin) Using a similar approach, we also reevaluate the age of the lithic industry in the Solana del Zamborino site (Guadix Basin).

Resumen

La dispersión de los homínidos fuera de África ha sido desde el inicio del estudio de la paleontología humana, un tema recurrente. Conocer cuándo comenzó la migración fuera del continente africano es algo que sigue siendo objeto de estudio de manera intensa actualmente. Las teorías han ido cambiando a lo largo del tiempo, desde la idea de una dispersión "corta", hace no más de medio millón de años, hasta la más aceptada hoy día, de que ocurrió hace algo más de un millón de años. Los nuevos descubrimientos, tanto en Oriente Medio (Ubeidiya, Gesher Benot Ya'aqov), como en Eurasia (Dmanisi) y Europa (Le Vallonet, Ca'Belverede, Ceprano, Atapuerca entre otros), refuerzan esta hipótesis, y también que haya sido una colonización efectuada de manera intermitente y en oleadas sucesivas. Sin embargo, sigue siendo un tema controvertido sujeto a intensos debates.

Por estos motivos, obtener una cronología clara de aquellos yacimientos en los que hay presencia humana es un punto importante, pues aportaría más información para establecer un mejor contexto cronológico de esa migración fuera de África. Son numerosos los métodos de datación que se han desarrollado y mejorado con el tiempo como, por ejemplo, la resonancia del espín electrónico, la bioestratigrafía, la luminiscencia, etc. Pero a veces es complicado establecer una correlación acertada entre todos ellos, lo que puede dar lugar incluso a resultados incoherentes. Ante todo esto, el paleomagnetismo puede

ser una herramienta útil y fácilmente aplicable, pues tiene un registro temporal muy amplio (> 180 millones de años, hasta la actualidad) y además no es destructivo para los restos, pues se aplica en los sedimentos.

Con esta idea en mente, en esta tesis hemos procedido a realizar análisis paleomagnéticos, específicamente la obtención de magnetostratigrafías, en varias localidades del Sur de España y Norte de África con evidencia humana durante el Paleolítico Inferior (Pleistoceno Inferior y Medio), como son los yacimientos de Fuente - 3 y Solana del Zamborino, ambos ubicados en la cuenca de Guadix-Baza, en Orce (Granada, España); el yacimiento de Gran Dolina, en Atapuerca (Burgos, España); así como en la propia Cuenca del Duero, y en la Cuenca Aïn Bni Mathar (Aïn Bni Mathar, Marruecos). El objetivo principal ha sido ampliar la información cronológica existente para proporcionar una mejor cronología de los depósitos y tratar de establecer, con un marco temporal más preciso, cuándo ocurrió la presencia humana en esos sitios.

Para ello, se ha llevado a cabo un exhaustivo trabajo de campo, obteniendo varios registros estratigráficos, en las localidades *in situ* o aprovechando sondeos anteriores, recogiendo en el proceso más de 1200 muestras individuales que se han analizado en el Centro Nacional de Investigación sobre Evolución Humana (CENIEH), así como en el Laboratorio Paleomagnético, Fort Hoofddijk, Facultad de Geociencias, Universidad de Utrecht, Países Bajos; y en el Grupo de Investigación de Paleomagnetismo y Magnetismo de Rocas, Departamento de Ciencias de la Tierra, en la Universidad de Oxford, Reino Unido. Los resultados de los análisis paleomagnéticos realizados, en colaboración con otras técnicas de cronología (bioestratigrafía, nucleidos cosmogénicos, resonancia del espín electrónico, luminiscencia), establecen la presencia o ausencia del Subcronde Jaramillo (0.99 - 1.07 Ma) para determinar si la presencia humana en los depósitos en cuestión se produjo antes o cerca de un millón de años.

En consecuencia, a la vista de los resultados presentados en esta tesis, el paleomagnetismo, en combinación con otros métodos cronológicos proporciona evidencia adicional de la presencia humana cercana al millón de años en el nivel TD4 de Gran Dolina (Atapuerca) e incluso más antigua en el yacimiento de Fuente Nueva 3 (Cuenca de Baza). Usando un enfoque similar, se ha re evaluado la edad de la industria lítica hallada en el yacimiento de Solana del Zamborino (Cuenca de Guadix).

Capítulo 1. Introducción

Capítulo 1. Introducción

Entender el origen de la especie humana es el eje principal de la Paleoantropología desde el comienzo de la misma como ciencia. Actualmente está aceptado que nuestra especie se originó en África, siendo *Homo habilis* (2,5 Ma) el primer integrante del género *Homo* (Leaky et al., 1964; Leakey et al., 1971; Boaz y Clark Howell, 1977) en las regiones de Kenia y Tanzania. Sin embargo, una vez consensuado el dónde, lo que ya no está tan claro es el cómo, el por qué y sobre todo el cuándo ha ocurrido la dispersión del género *Homo;* en qué momento dejó de ser una población localizada en el continente africano y se lanzó a la colonización de otros territorios. Surgen numerosos interrogantes, tales como si fue una sola migración o hubo varias oleadas, qué rutas de salida siguieron esos primeros exploradores y, sobre todo, cuándo ocurrió esa migración. Durante las últimas décadas del siglo XX y principios del XXI han sido numerosas las publicaciones científicas que, a tenor de los descubrimientos que se han ido sucediendo, han tratado de dar respuestas a esas cuestiones.

1.1 ¿Cuándo se migró hacia Europa?

En la década de los 90 del siglo pasado, algunos autores abogaban por la teoría de una cronología "corta" para la salida hacia el continente europeo, con una primera presencia del género *Homo* no más allá del medio millón de años, a raíz de la falta de registros seguros del Pleistoceno inferior y medio (Roebroeks, 1994; Roebroeks y Kolfschoten, 1994; Dennell y Roebroeks, 1996). Sin embargo, yacimientos como el de Le Vallonet en Francia (Lumley et al., 1989), Ca'Belverede di Monte Poggiolo (Antoniazzi et al., 1993; Peretto et al., 1998) y Ceprano (Ascenzi et al., 1996) en Italia; Fuente Nueva 3 (Duval et al., 2012b; Oms et al., 2000, 1996; Turq et al., 1996) y Gran Dolina (Carbonell et al., 1996, 1995) en España, presentaban industria lítica del Modo 1 e indicaban una colonización anterior de Europa, más próxima al millón de años. Esa posibilidad de un poblamiento más antiguo se reforzó posteriormente con el descubrimiento y datación de Dmanisi en Georgia (Gabounia y Vekua, 1995; Gabounia et al., 2002; Lordkipanidze et al., 2005) que junto con los recientes hallazgos de Sima del Elefante en Atapuerca (Carbonell et al., 2008), indican una cronología algo más antigua, alrededor de 1,2 millones de años para esa primera colonización de Europa. En conjunto, la evidencia fósil obtenida y analizada en los últimos años, parece indicar que los primeros humanos que migraron y colonizaron Europa lo hicieron durante el Pleistoceno inferior (Carbonell et al., 1995, 2008; Dean y Delson, 1995; Arzarello et al., 2007; García et al., 2010; Beyin, 2011; Duval et al., 2012a; Parés et al., 2013a, 2013b).

Sin embargo, dada la discontinuidad de la evidencia fósil, en los últimos años se ha teorizado sobre la posibilidad de que esta dispersión se produjera de manera intermitente y en diferentes oleadas (Muttoni et al., 2011; Bermúdez de Castro y Martinón-Torres, 2013; Mosquera et al., 2013; Palombo, 2013).

1.2 ¿Cómo se llegó a Europa?

El cómo, o más bien por dónde llegaron los primeros homínidos a Europa, es también otra pieza clave del estudio de la dispersión humana desde el continente africano.

Tradicionalmente se han barajado tres posibilidades: desplazamiento a través de lo que se conoce como el Corredor del Levante; paso por el Canal de Sicilia; y el paso por el Estrecho de Gibraltar (Figura 1.1). En las dos últimas, aunque implican el cruzar grandes masas de agua, hay que tener en consideración las variaciones en el nivel del mar que permitirían el paso por esas regiones, como bien recogen Abbate y Sagri (2012).

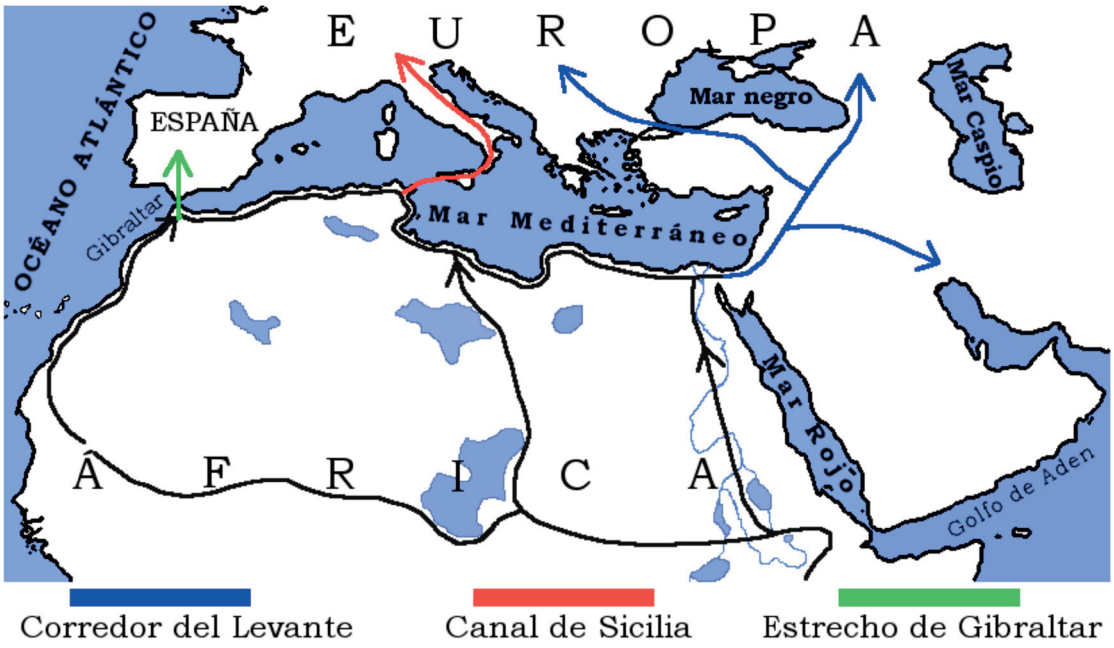

Figura 1.1 Potenciales rutas para la dispersión humana durante el Pleistoceno Medio fuera de África. Modificada de Abbate y Sagri (2012). Se incluyen en el mapa las tres rutas potenciales (Corredor del Levante, Canal de Sicilia y Estrecho de Gibraltar), así como los corredores internos de desplazamiento por el continente africano.

Aunque algunos autores plantean la posibilidad de que se produjera una colonización por las tres vías (Arribas y Palmqvist, 1999), hoy en día, la teoría de colonización más aceptada es la que implica el paso por el Corredor del

Levante, ayudando a consolidar esta posibilidad yacimientos como el de Ubeidiya (Belmaker et al., 2002) y Gesher Benot Ya'aqov (Goren-Inbar et al., 2000).

1.3 ¿Por qué?

Dentro del debate de la migración, otro de los puntos que sigue en continua revisión es el porqué de la salida de los homínidos del continente africano y su dispersión por Europa y el resto de continentes. Actualmente se plantean dos alternativas, la primera es la relación de los homínidos con el medio que les rodea y la posibilidad de obtener alimento aprovechando lo dejado por los grandes cazadores (es decir siendo carroñeros) e incorporando de esta manera el consumo de carne de manera progresiva a su dieta (Turner, 1992; Arribas y Palmqvist, 1999; Rodríguez et al., 2012, 2013; Espigares et al., 2013). Así como también por el consumo de animales más pequeños (Blasco et al., 2013), para, posteriormente, competir directamente con los grandes depredadores.

En este contexto habría que tener en cuenta también los cambios climáticos que condicionarían las migraciones de los grandes mamíferos, afectando la presencia y disponibilidad de los recursos, obligando a esos primeros humanos a desplazarse (Van der Made y Mateos, 2010; Jiménez-Arenas et al., 2011; Blain et al., 2013; Van der Made, 2013).

La segunda teoría, sin embargo, aborda una posibilidad condicionada por el desarrollo técnico de la industria lítica, en la que la aparición del Modo 2 en África, más efectivo que el Modo 1, acabaría en un primer momento empujando a las poblaciones usuarias del Modo 1 a buscar nuevas regiones para, posteriormente, acabar reemplazándolo (Carbonell et al., 1999, 2010).

1.4 ¿Entonces?

Está claro que actualmente no hay una respuesta clara para las cuestiones antes mencionadas de cuándo, cómo y porqué se produjo el poblamiento de Europa. Pero sí podemos decir que algunas teorías están más afianzadas que otras, al menos en cuanto a la ruta de salida fuera de África, ya no sólo para los primeros homínidos, sino también para los humanos modernos, y que lleva al Corredor del Levante como ruta migratoria de preferencia. Recientes publicaciones de yacimientos como el de Ksâr `Akil en el Líbano (Bosch et al., 2015) refuerzan esa posibilidad. Cabe añadir que el estudio de otras fuentes de información, por ejemplo, el ADN, aplicadas a la evolución humana, como la llevada a cabo en 2007 por Rowold et al., ya indicaban el Corredor del Levante como ruta prominente para las migraciones fuera del continente africano.

Se hace evidente que, a día de hoy, el cómo, el cuándo y porqué el género *Homo* colonizó Europa (y el resto de continentes) sigue siendo un debate intenso y vigente, sin una respuesta clara.

1.4 Referencias

Abbate, E., Sagri, M., 2012. Early to Middle Pleistocene Homo dispersals from Africa to Eurasia: Geological, climatic and environmental constraints. Quaternary International 267, 3–19.

Antoniazzi, A., Ferrari, M., Peretto, C., 1993. Il giacimento di Ca'Belvedere di Monte Poggiolo del Pleistocene inferiore con industria litica (Forlì). Bolletino de Paleontologia italiana 84, 1–56.

Arribas, A., Palmqvist, P., 1999. On the ecological connection between sabre-tooths and hominids: Faunal dispersal events in the Lower Pleistocene

and a review of the evidence for the first human arrival in Europe. Journal of Archaeological Science 26, 571–585.

Arzarello, M., Marcolini, F., Pavia, G., Pavia, M., Petronio, C., Petrucci, M., Rook, L., Sardella, R., 2007. Evidence of earliest human occurrence in Europe: The site of Pirro Nord (Southern Italy). Naturwissenschaften 94, 107–112.

Ascenzi, A., Biddittu, I., Cassoli, P.F., Segre, A.G., Segre-Naldini, E., 1996. A calvarium of late Homo erectus from Ceprano, Italy. Journal of Human Evolution 31, 409–423.

Belmaker, M., Tchernov, E., Condemi, S., Bar-Yosef, O., 2002. New evidence for hominid presence in the Lower Pleistocene of the Southern Levant. Journal of Human Evolution 43, 43–56.

Bermúdez de Castro, J.M., Martinón-Torres, M., 2013. A new model for the evolution of the human Pleistocene populations of Europe. Quaternary International 295, 102–112.

Beyin, A., 2011. Upper Pleistocene Human Dispersals out of Africa: A Review of the Current State of the Debate. International Journal of Evolutionary Biology 2011, 1–17.

Blain, H.-A.A., Cuenca-Bescós, G., Burjachs, F., López-García, J.M., Lozano-Fernández, I., Rosell, J., 2013. Early Pleistocene palaeoenvironments at the time of the Homo antecessor settlement in the Gran Dolina cave (Atapuerca, Spain). Journal of Quaternary Science 28, 311–319.

Blasco, R., Rosell, J., Fernández Peris, J., Arsuaga, J.L., Bermúdez de Castro, J.M., Carbonell, E., 2013. Environmental availability, behavioural diversity and diet: A zooarchaeological approach from the TD10-1 sublevel of

Gran Dolina (Sierra de Atapuerca, Burgos, Spain) and Bolomor Cave (Valencia, Spain). Quaternary Science Reviews 70, 124–144.

Boaz, N.T., Clark Howell, F., 1977. A gracile hominid cranium from upper member G of the Shungura Formation, Ethiopia. American Journal of Physical Anthropology 46, 93–108.

Bosch, M.D., Mannino, M.A., Prendergast, A.L., O'Connell, T.C., Demarchi, B., Taylor, S.M., Niven, L., van der Plicht, J., Hublin, J.-J., 2015. New chronology for Ksâr 'Akil (Lebanon) supports Levantine route of modern human dispersal into Europe. Proceedings of the National Academy of Sciences 112, 7683–7688.

Carbonell, E., Bermudez de Castro, J., Arsuaga, J., Diez, J., Rosas, A., Cuenca-Bescos, G., Sala, R., Mosquera, M., Rodriguez, X., 1995. Lower Pleistocene hominids and artifacts from Atapuerca-TD6 (Spain). Science 269, 826–830.

Carbonell, E., Bermúdez De Castro, J.M., Parés, J.M., Pérez-González, A., Cuenca-Bescós, G., Ollé, A., Mosquera, M., Huguet, R., Van Der Made, J., Rosas, A., Sala, R., Vallverdú, J., García, N., Granger, D.E., Martinón-Torres, M., Rodríguez, X.P., Stock, G.M., Vergès, J.M., Allué, E., Burjachs, F., Cáceres, I., Canals, A., Benito, A., Díez, C., Lozano, M., Mateos, A., Navazo, M., Rodríguez, J., Rosell, J., Arsuaga, J.L., 2008. The first hominin of Europe. Nature 452, 465–469.

Carbonell, E., Mosquera, M., Rodríguez, X.P., Sala, R., 1996. The first human settlement of Europe. Journal of Anthropological Research 52, 107–114.

Carbonell, E., Mosquera, M., Rodríguez, X.P., Sala, R., Van Der Made, J., 1999. Out of Africa: The Dispersal of the Earliest Technical Systems Reconsidered. Journal of Anthropological Archaeology 18, 119–136.

Carbonell, E., Sala Ramos, R., Rodríguez, X.P., Mosquera, M., Ollé, A., Vergès, J.M., Martínez-Navarro, B., Bermúdez de Castro, J.M., 2010. Early hominid dispersals: A technological hypothesis for " out of Africa." Quaternary International 223–224, 36–44.

Dean, D., Delson, E., 1995. Homo at the gates of Europe. Nature 373, 472-473.

Dennell, R., Roebroeks, W., 1996. The earliest colonization of Europe: The short chronology revisited. Antiquity 70, 535–542.

Duval, M., Falguères, C., Bahain, J.J., 2012a. Age of the oldest hominin settlements in Spain: Contribution of the combined U-series/ESR dating method applied to fossil teeth. Quaternary Geochronology 10, 412–417.

Duval, M., Falguères, C., Bahain, J.-J.J., Grün, R., Shao, Q., Aubert, M., Dolo, J.-M.M., Agustí, J., Martínez-Navarro, B., Palmqvist, P., Toro-Moyano, I., 2012b. On the limits of using combined U-series/ESR method to date fossil teeth from two Early Pleistocene archaeological sites of the Orce area (Guadix-Baza basin, Spain). Quaternary Research 77, 482–491.

Espigares, M.P., Martínez-Navarro, B., Palmqvist, P., Ros-Montoya, S., Toro, I., Agustí, J., Sala, R., 2013. Homo vs. Pachycrocuta: Earliest evidence of competition for an elephant carcass between scavengers at Fuente Nueva-3 (Orce, Spain). Quaternary International 295, 113–125.

Gabounia, L., de Lumley, M.A., Vekua, A., Lordkipanidze, D., de Lumley, H., 2002. Découverte d'un nouvel hominidé à Dmanissi (Transcaucasie, Géorgie). Comptes Rendus - Palevol 1, 243–253.

Gabounia, L., Vekua, A., 1995. A Plio-Pleistocene hominid from Dmanisi, East Georgia, Caucasus. Nature 373, 509–512.

Garcia, T., Féraud, G., Falguères, C., de Lumley, H., Perrenoud, C., Lordkipanidze, D., 2010. Earliest human remains in Eurasia: New $^{40}Ar/^{39}Ar$ dating of the Dmanisi hominid-bearing levels, Georgia. Quaternary Geochronology 5, 443–451.

Goren-Inbar, N., Feibel, C.S., Verosub, K.L., Melamed, Y., Kislev, M.E., Tchernov, E., Saragusti, I., 2000. Pleistocene milestones on the out-of-Africa corridor at Gesher Benot Ya'aqov, Israel. Science 289, 944–947.

Jiménez-Arenas, J.M., Santonja, M., Botella, M., Palmqvist, P., 2011. The oldest handaxes in Europe: Fact or artefact? Journal of Archaeological Science 38, 3340–3349.

Leakey, M.D., Clarke, R.J., Leakey, L.S.B., 1971. New hominid skull from Bed I, Olduvai Gorge, Tanzania. Nature 232, 308–312.

Leaky, L.S.B., Tobias, P. V., Napier, J.R., 1964. A NEW SPECIES OF THE GENUS HOMO FROM OLDUVAI GORGE. Nature 202, 464–466.

Lordkipanidze, D., Vekua, A., Ferring, R., Rightmire, G.P., Agusti, J., Kiladze, G., Mouskhelishvili, A., Nioradze, M., Ponce de León, M.S., Tappen, M., Zollikofer, C.P.E., 2005. Anthropology: the earliest toothless hominin skull. Nature 434, 717–718.

Lumley, H. de, Kahlke, H.D., Moigne, A.M., Moulle, P.E., 1989. Les faunes de grands mammifères de la grotte du Vallonet, Roquebrune-Cap Martin, Alpes-Maritimes. L'anthropologie 92, 501–613.

Mosquera, M., Ollé, A., Rodríguez, X.P., 2013. From Atapuerca to Europe: Tracing the earliest peopling of Europe. Quaternary International 295, 130–137.

Muttoni, G., Scardia, G., Kent, D. V., Morsiani, E., Tremolada, F., Cremaschi, M., Peretto, C., 2011. First dated human occupation of Italy at ~0.85Ma during the late Early Pleistocene climate transition. Earth and Planetary Science Letters 307, 241–252.

Oms, O., Agustí, J., Gabàs, M., Anadón, P., 2000. Lithostratigraphical correlation of micromammal sites and biostratigraphy of the Upper Pliocene to Lower Pleistocene in the Northeast Guadix-Baza Basin (southern Spain). Journal of Quaternary Science 15, 43–50.

Oms, O., Dinarés Turell, J., Parés, J.M., 1996. Resultados paleomagnéticos iniciales de la sección Plio-Pleistocena de Fuente Nueva. Revista de la Sociedad Geológica de España 9, 89–95.

Palombo, M.R., 2013. What about causal mechanisms promoting early hominin dispersal in Eurasia? A research agenda for answering a hotly debated question. Quaternary International 295, 13–27.

Parés, J.M., Arnold, L., Duval, M., Demuro, M., Pérez-González, A., Bermúdez de Castro, J.M., Carbonell, E., Arsuaga, J.L., 2013a. Reassessing the age of Atapuerca-TD6 (Spain): New paleomagnetic results. Journal of Archaeological Science 40, 4586–4595.

Parés, J.M., Duval, M., Arnold, L.J., 2013b. New views on an old move: Hominin migration into Eurasia. Quaternary International 295, 5–12.

Peretto, C., Amore, F.O., Antoniazzi, A., Bahain, J.J., Cattani, L., Cavallini, E., Esposito, P., Falguères, C., Gagnepain, J., Hedley, I., Laurent, M., Lebreton, V., Longo, L., Milliken, S., Monegatti, P., Ollé, A., Pugliese, A., Renault-Miskovsky, J., Sozzi, M., Ungaro, S., Vannuci, S., Vergès, J.M., Wagner, J.J., Yokoyama, Y., 1998. Industrie lithique de Ca'Belvedere di Monte Poggio-

lo: Stratigraphie, matière première, typologie, remontages et traces d'utilisation. Paleoanthropologie, paleontologie 102, 343–465.

Rodríguez, J., Martín-González, J.A., Goikoetxea, I., Rodríguez-Gómez, G., Mateos, A., 2013. Mammalian paleobiogeography and the distribution of Homo in early Pleistocene Europe. Quaternary International 295, 48–58.

Rodríguez, J., Rodríguez-Gómez, G., Martín-González, J.A., Goikoetxea, I., Mateos, A., 2012. Predator-prey relationships and the role of Homo in Early Pleistocene food webs in Southern Europe. Palaeogeography, Palaeoclimatology, Palaeoecology 365–366, 99–114.

Roebroeks, W., 1994. Updating the earliest occupation of Europe. Current Anthropology 35, 301–305.

Roebroeks, W., Kolfschoten, T. van, 1994. The earliest occupation of Europe: A short chronology. Antiquity 68, 489–503.

Rowold, D.J., Luis, J.R., Terreros, M.C., Herrera, R.J., 2007. Mitochondrial DNA geneflow indicates preferred usage of the Levant Corridor over the Horn of Africa passageway. Journal of Human Genetics 52, 436–447.

Turner, A., 1992. Large carnivores and earliest European hominids: changing determinants of resource availability during the Lower and Middle Pleistocene. Journal of Human Evolution 22, 109–126.

Turq, A., Martinez-Navarro, B., Palmquist, P., Arribas, A., Agusti, J., Rodriguez-Vidal, J., 1996. Le Plio-Pléistocène de la région d'Orce, province de Grenade, Espagne : bilan et perspectives de recherche. Paléo 8, 161–204.

Van der Made, J., 2013. First description of the large mammals from the locality of Penal, and updated faunal lists for the Atapuerca ungulates - Equus

altidens, Bison and human dispersal into Western Europe. Quaternary International 295, 36–47.

Van der Made, J., Mateos, A., 2010. Longstanding biogeographic patterns and the dispersal of early Homo out of Africa and into Europe. Quaternary International 223–224, 195–200.

Capítulo 2. Objetivos

Capitulo 2. Objetivos

Tal como se ha mencionado en la introducción, cuándo se produjo la ocupación del continente europeo no está ni mucho menos solucionado, por tanto, en aquellos lugares en los que hay evidencia humana es importante establecer un marco cronológico lo más concreto posible, para así tratar de entender mejor en qué momento ocurrió esa dispersión humana en el Paleolítico.

En lo que se refiere a las dataciones cronológicas de esas primeras poblaciones humanas, son numerosas las metodologías aplicadas hoy en día, tales como la resonancia del espín electrónico (ESR en sus siglas en inglés), la bioestratigrafía, la luminiscencia, los nucleidos cosmogénicos, el análisis de la industria lítica asociada a los yacimientos, entre otros.

Sin embargo, pese a la gran cantidad de información que aporta el uso de tanta variedad de métodos, o quizás debido a ello, es a veces complicado establecer una correcta correlación entre todos los datos aportados como, por ejemplo, desde la asociación de la industria lítica con la información aportada por la bioestratigrafía, pasando por la dificultad de obtener dataciones absolutas consistentes dado el margen de error presente en esas metodologías y los resultados, a veces incongruentes entre métodos. En este sentido, el paleomagnetismo se perfila como una herramienta útil y versátil para establecer dataciones que aporten más información y un mejor contexto

cronológico a los yacimientos, ya que es un método que ofrece un registro muy amplio, con un marco temporal que abarca desde hace 180 millones de años hasta la actualidad.

Con esta idea en mente, el objetivo general de la presente tesis, es la aplicación de esta metodología en una serie de yacimientos, y al entorno en el que se encuentran, en lo que se conoce como la Cuenca Circummediterránea, correspondientes tanto a la Península Ibérica como localizaciones en el Norte de África, y que presentan evidencia de presencia humana durante el Paleolítico inferior (Pleistoceno inferior y medio). Se pretende asi proporcionar un mejor marco cronológico, incrementando la información existente, ya sea porque se aplica por vez primera esta metodología o porque puede haber conflicto o incongruencias con las dataciones realizadas previamente o porque se pueden ampliar análisis paleomagnéticos previos.

Así mismo se quiere demostrar la versatilidad y utilidad del paleomagnetismo como metodología cronológica, aportando un mejor contexto temporal a esas primeras dispersiones humanas.

A continuación se explican brevemente los objetivos desarrollados a lo largo del curso de esta tesis, tanto los que han dado lugar a resultados publicados en revistas de impacto, como aquellos que están todavía en proceso.

2.1 Análisis paleomagnético en distintos yacimientos del Pleistoceno inferior y medio de la Península Ibérica

Como se ha indicado, el área de estudio se ha localizado en la Cuenca Circummediterránea, focalizándose en el sur y centro de la Peninsula Ibérica, en concreto en los yacimientos de Fuente Nueva y Solana del Zamborino (ambos en la zona correspondiente a la Cuenca de Guadix-Baza, Granada), y

en el yacimiento de Atapuerca (Burgos, Castilla y León). Estos trabajos han dado lugar a artículos publicados que forman parte de la presente tesis.

2.1.1 Aplicación del paleomagnetismo en el yacimiento de Fuente Nueva 3 (Cuenca de Guadix-Baza, Granada)

El yacimiento de Fuente Nueva 3 (FN-3), en la Cuenca de Guadix – Baza (Granada, España) es considerado uno de los yacimientos más antiguos con evidencia de ocupación humana en el oeste de Europa. Por tanto, establecer un buen marco temporal es sumamente importante.

En concreto, en este yacimiento se han realizado análisis paleomagnéticos previos (Oms et al., 2000, 2011) que indicaban una polaridad predominantemente inversa, coincidente con el cron Matuyama (0,78 – 2,59 Ma), en un marco temporal basado en la evidencia bioestratigráfica comprendido entre los subcrones Jaramillo y Olduvai (0,99 – 1,07 y 1,7 – 1,9 Ma respectivamente).

Dada la irregularidad del terreno y los pocos afloramientos presentes en la zona, es complicado el obtener un muestreo continuado, por lo que en 2011 se llevaron a cabo dos sondeos cercanos al yacimiento de FN-3 sobre los que se realizó un nuevo análisis magnetoestratigráfico con la idea de establecer la presencia, o no, del subcron Jaramillo, y aportar así un mejor contexto geocronológico del yacimiento.

Este estudio fue publicado en la revista Quaternary International, volumen 389, de la página 224 a la 234 bajo el titulo “New Magnetostratigraphic and numerical age of Fuente Nueva - 3 site (Guadix – Baza basin, Spain)”, y conforma el cuarto capitulo de la presente tesis doctoral.

2.1.2 Nuevos análisis magnetoestratigráficos en el yacimiento de Solana del Zamborino (Cuenca Guadix – Baza, Granada)

La Cuenca de Guadix – Baza es una zona que ha aportado una gran información con respecto a los periodos Mioceno y Pleistoceno dada la gran cantidad de restos faunísticos que se han preservado en el entorno (Rook y Martínez-Navarro, 2010; Turq et al., 1996; Viseras et al., 2005).

En algunos casos, dicha fauna se ha encontrado asociada a industria lítica, como es el caso del yacimiento conocido como Solana del Zamborino, situado en el sector oeste de la Cuenca Guadix – Baza. Dicho yacimiento ha sido objeto de bastante controversia con respecto a los análisis magnéticos llevados a cabo por Scott y Gibert (2009) y los resultados obtenidos, los cuales afectaban notablemente a la cronología considerada para la industria lítica encontrada.

Dada la dificultad del yacimiento en lo que se refiere a la obtención de las muestras, pues se encuentra situado en una zona de dificil acceso, además de la complejidad en cuanto al proceso del relleno sedimentario de la sección de la cuenca donde se encuentra situado, que se ha producido con aportes de distintos origenes (Pla-Pueyo, 2009), se hacía necesario un nuevo análisis magnetoestratigráfico para establecer un mejor contexto temporal de dichas herramientas y, por tanto, acotar mejor la presencia humana en la zona.

En este sentido, se ha realizado un estudio que no sólo comprende el yacimiento en sí, si no también hasta unos 60 metros por debajo. Este trabajo se publicó con el titulo *"New magnetostratigraphic evidence for the Acheulean tools at the archaeo – palaeontological site "Solana del Zamborino"(Guadix – Baza Basin, S Spain)"* en la revista Scientific Reports, volumen 7, issue 1, y constituye el quinto capitulo de la presente tesis.

2.1.3 Nuevo análisis paleomagnético del yacimiento de Gran Dolina en Atapuerca (Burgos, España)

Los yacimientos de la Sierra de Atapuerca, en Burgos, son unos de los yacimientos paleontólogicos de Europa que aportan una mayor cantidad de información en lo que a evolución humana se refiere, pues preservan una gran cantidad de sedimentos y fósiles correspondientes al Pleistoceno inferior y medio (Aguirre et al., 1990; Carbonell et al., 1999; Bermúdez de Castro et al., 2013).

Uno de estos yacimientos es el de Gran Dolina (TD), donde los niveles inferiores de TD4 y TD6 han aportado evidencia de la presencia humana en Europa antes de los 800.000 años, con el descubrimiento de *Homo antecessor* en el nivel estratigráfico TD6, y la presencia de industria lítica en TD4. Gracias al desarrollo de las sucesivas campañas de excavación en los yacimientos, se ha ido facilitando cada vez más el acceso a los mismos y se han podido ampliar las dataciones realizadas. Una de las más recientes es la llevada a cabo por Moreno et al. (2015) aplicando la resonancia del espín electrónico y que ha dado una edad de 0,91 ± 0,25 Ma para el límite inferior de TD4, una fecha claramente post Jaramillo. Con la intención de aportar más información cronológica a las dataciones ESR y por tanto establecer un mejor contexto temporal a la industria lítica de TD4, se llevó a cabo un análisis paleomagnético de los niveles TD4 a TD6 para determinar la presencia o no en dichos niveles del subcron Jaramillo.

Este análisis se ha publicado en la revista Quaternary Geochronology, volúmen 45, páginas 1 a 8, con el titulo *"A post Jaramillo age for the artefact-bearing layer TD4 (Gran Dolina, Atapuerca): New paleomagnetic evidence"*, y forma parte de un estudio conjunto de los sedimentos que componen el relleno que conforman los distintos niveles estratigráficos de Gran Dolina,

pues se han tomado muestras de la secuencia desde TD1 a TD6 aprovechando ese mejor acceso a esos niveles, proporcionado por las sucesivas campañas de excavación. Este segundo trabajo se ha publicado con el titulo "Chronology of the cave interior sediments at Gran Dolina archaeological site, Atapuerca (Spain)" en la revista Quaternary Science Reviews, volumne 186, paginas 1 a 16.

Ambos artículos constituyen el sexto y séptimo capítulo respectivamente de la presente tesis doctoral.

2.2 Aplicación del paleomagnetismo en la Cuenca de Aïn Bni Mathar (Marruecos)

Para entender las primeras migraciones humanas es imprescindible estudiar y aportar una cronología a los yacimientos del Paleolítico inferior presentes en el norte de África, como los situados en la cuenca de Aïn Bni Mathar, en cuyas terrazas se han encontrado numerosas evidencias de industria lítica que llevan estudiandose desde el 2006 de manera conjunta por el Instituto de Paleoecología Humana i Evolució Social (IPHES) y la Université Mohamed I. Establecer una cronología adecuada es crítico para contextualizar las migraciones humanas en el interior del continente africano y su salida del mismo hacia nuevos territorios, y determinar si ésta quizás ocurrió desde comienzos del Pleistoceno inferior (Parés et al., 2013; Sahnouni et al., 2010).

Como consecuencia, durante el desarrollo de esta tesis, se llevó a cabo una colaboración con estas instituciones para aportar un contexto cronológico a dicha industria, lo que dió lugar a la realización de una serie de muestreos en la localidad de Guefait (dentro de la propia cuenca de Aïn Bni Mathar) de los que se han procesado y analizado más de 300 muestras, que actualmente forman parte de un trabajo multidisciplinar cuyos resultados estan en proceso

de publicación. La información paleomagnetica preliminar consituye parte del octavo capítulo de la presente tesis.

2.3 Análisis paleomagnéticos en el estudio de la evolución de la Cuenca del Duero

La cuenca del Duero, al igual que la mayoría de las cuencas cenozoicas de la Península Ibérica, se encuentra rellena de sedimentos continentales, que, en el caso del Duero, es una alternancia sedimentaria de origen detrítico fluvial, y carbonatada lacustre. Su evolución ha sido altamente compleja, ya que los sectores o subcuencas que la conforman presentan comportamientos propios que han condicionado su relleno deposicional de tal manera que no ha sido uniforme en el tiempo ni en el espacio, y el cuál queda reflejado en los numerosos niveles de terrazas presentes. Por lo tanto, entender cómo ha evolucionado la cuenca desde un contexto cronológico permitiría una mejor comprensión de los yacimientos presentes, como es el caso de la importante relación que guardan las terrazas de la cuenca en la región noreste de la misma con el complejo kárstico en el que se encuentran los yacimientos de Atapuerca.

Por lo tanto, y dado que los estudios paleomagnéticos llevados a cabo en la cuenca del Duero son escasos (Montes et al., 2006; Ruiz et al., 1996), se ha realizado el muestreo y análisis paleomagnético de una serie de terrazas de la cuenca, así como la realización de magnetoestratigrafías en tres secuencias estratigráficas de la misma tomando como referencia el nivel superior de calizas del páramo.

Los resultados preliminares obtenidos constituyen parte del octavo capítulo de la presente tesis.

2.4 Referencias

Aguirre, E., Arsuaga, J.L., Bermúdez de Castro, J.M., Carbonell, E., Ceballos, M., Díez, C., Enamorado, J., Fernández-Jalvo, Y., Gil, E., Gracia, A., Martín-Nájera, A., Martínez, I., Morales, J., Ortega, A.I., Rosas, A., Sánchez, A., Sánchez, B., Sesé, C., Soto, E., Torres, T.J., 1990. The Atapuerca sites and the ibeas hominids. Human Evolution 5, 55–73.

Bermúdez de Castro, J.M., Martinón-Torres, M., 2013. A new model for the evolution of the human Pleistocene populations of Europe. Quaternary International 295, 102–112.

Carbonell, E., Mosquera, M., Rodríguez, X.P., Sala, R., Van Der Made, J., 1999. Out of Africa: The Dispersal of the Earliest Technical Systems Reconsidered. Journal of Anthropological Archaeology 18, 119–136.

Montes, M., Beamud, B., Garcés, M., Nozal Martín, F., López Olmedo, F., 2006. Magnetoestratigrafía del sureste de la Cuenca del Duero (Aragonienense-Vallesiense): datos preliminares. Geotemas 9, 171–175.

Moreno, D., Falguères, C., Pérez-González, A., Voinchet, P., Ghaleb, B., Despriée, J., Bahain, J.J., Sala, R., Carbonell, E., Bermúdez de Castro, J.M., Arsuaga, J.L., 2015. New radiometric dates on the lowest stratigraphical section (TD1 to TD6) of Gran Dolina site (Atapuerca, Spain). Quaternary International 30, 535–540.

Oms, O., Agustí, J., Gabàs, M., Anadón, P., 2000. Lithostratigraphical correlation of micromammal sites and biostratigraphy of the Upper Pliocene to Lower Pleistocene in the Northeast Guadix-Baza Basin (southern Spain). Journal of Quaternary Science 15, 43–50.

Oms, O., Anadón, P., Agustí, J., Julià, R., 2011. Geology and chronology of the continental Pleistocene archeological and paleontological sites of the Orce area (Baza basin, Spain). Quaternary International 243, 33–43.

Parés, J.M., Duval, M., Arnold, L.J., 2013. New views on an old move: Hominin migration into Eurasia. Quaternary International 295, 5–12.

Pla-Pueyo, S., 2009. Contexto estratigráfico y sedimentario de los yacimientos de grandes mamíferos del sector centralal de la Cuenca de Guadix (Cordillera Bética). Tesis Doctoral. Universidad de Granada.

Rook, L., Martínez-Navarro, B., 2010. Villafranchian: The long story of a Plio-Pleistocene European large mammal biochronologic unit. Quaternary International 219, 134–144.

Ruiz, V.C., Mediavilla López, R., Osete, M.L., Villalaín, J.J., 1996. Magnetostratigraphy of Neogene in Duero Basin Central Area. Geogaceta 20, 1017–1020.

Sahnouni, M., van der Made, J., Everett, M., 2010. Early North Africa: Chronology, ecology, and hominin behavior: Insights from Ain Hanech and El-Kherba, northeastern Algeria. Quaternary International 223-224, 436-438.

Scott, G.R., Gibert, L., 2009. The oldest hand-axes in Europe. Nature 461, 82–85.

Turq, A., Martinez-Navarro, B., Palmquist, P., Arribas, A., Agusti, J., Rodriguez-Vidal, J., 1996. Le Plio-Pléistocène de la région d'Orce, province de Grenade, Espagne : bilan et perspectives de recherche. Paléo 8, 161–204.

Viseras, C., Soria, J.M., Fernández, J., García, F., 2005. The neogene-quaternary basins of the betic cordillera : an overview. Geophysical Research Abstracts 7, 11123–11128.

Capítulo 3 . METODOLOGÍA

Capítulo 3. Metodología

El método utilizado, e hilo conductor de esta tesis, en los yacimientos anteriormente mencionados es el paleomagnetismo, disciplina que se fundamenta en el estudio del campo magnético del pasado de nuestro planeta y más concretamente en la aplicación del mismo para obtener lo que se conoce como magnetoestratigrafías de las secuencias analizadas. Para su correcta comprensión, se va a exponer un pequeño resumen de lo que es el paleomagnetismo, sus características, funcionalidad y aplicación.

3.1 Magnetismo y el campo magnético terrestre

El magnetismo es el fenómeno físico por el cual los objetos ejercen fuerzas de atracción y repulsión sobre otros materiales. Este fenómeno ha sido comprobado desde antiguo, siendo el filósofo griego Tales de Mileto el primero en estudiar las propiedades magnéticas de la magnetita; y desde que en China se inventara la brújula en el sigo II a.C., ha sido ampliamente utilizado como herramienta para navegantes y exploradores.

Pese a ello, no es hasta el siglo XVII cuando el médico alemán William Gilbert publica su obra *Die Magnete, magneticisque corporibus, et de magno magnete tellure (Sobre los imanes, los cuerpos mágneticos y el gran imán terrestre)* que se sientan las bases del estudio profundo del magnetismo. Gilbert, en su obra, clasificó los materiales en conductores y aislantes, descubrió la

imantación por influencia y fue el primero en percatarse de que la imantación del hierro se pierde al calentarlo al rojo. Sin embargo, no es hasta 1830 que Oersted descubrió que un hilo conductor al se que se le aplica una corriente eléctrica generaba a su vez un campo magnético a su alrededor. Es a partir de ese momento cuando se suceden numerosos experimentos relacionados con el magnetismo en la electricidad (Ámpere, Faraday, etc.) hasta que en 1873, James Maxwell agrupó todas esas observaciones, lo que dio lugar a un nuevo campo de estudio: el electromagnetismo, el cual ha permitido determinar que nuestro planeta genera a su vez su propio campo magnético, lo que se conoce como campo magnético terrestre o CMT.

Pero, ¿qué es realmente el CMT? Hoy en día sabemos que la Tierra se organiza en capas, conocidas como corteza, manto y núcleo, éste último se divide a su vez en núcleo interno sólido, compuesto en su mayor parte de hierro; y un núcleo externo líquido, formado por hierro y níquel, en continuo movimiento. Esto da lugar a que se produzcan corrientes de convección en el interior del planeta. Podría decirse que es similar a una dinamo autoinducida: el movimiento de los materiales del núcleo líquido genera corrientes eléctricas que a su vez generan corrientes magnéticas que generan de nuevo corrientes eléctricas y así sucesivamente, retroalimentándose constantemente.

Por tanto, la forma más sencilla para explicar el CMT sería asumir que en el interior de nuestro planeta el núcleo interno genera un campo magnético esencialmente dipolar, alineado con el eje de rotación del mismo; lo que se conoce como teoría del dipolo axial geocéntrico. Sin embargo, esto no es del todo cierto. Registros actuales del CMT demuestran que los polos magnéticos no coinciden exactamente con los geográficos. Actualmente existe una variación de 11,5º, así que es más correcto decir que el CMT es un dipolo geocéntrico inclinado con respecto al eje de la Tierra, lo que se ha denominado como modelo

dipolar y que explica aproximadamente el 90% de campo magnético terrestre (figura 3.1).

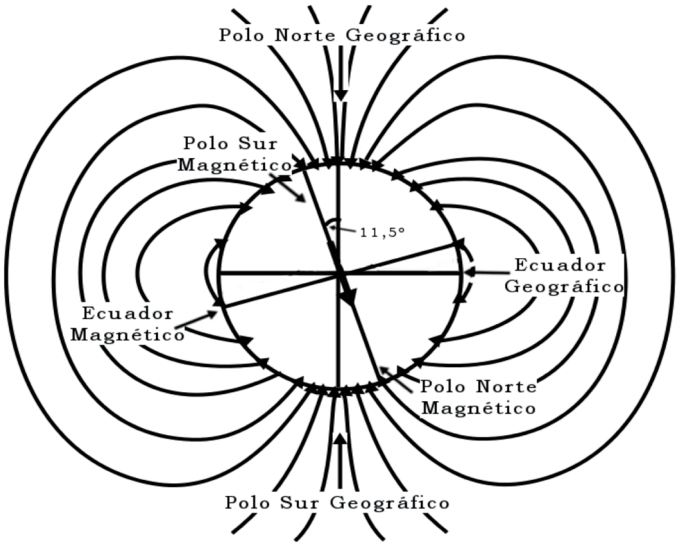

Figura 3.1. Esquema del dipolo geocéntrico inclinado. Las líneas que van del Polo Sur geográfico al Polo Norte geográfico son lo que se conocen como las líneas de fuerza del campo magnético, y representan la estructura del mismo en tres dimensiones. Modificado de Butler 1998

El 10% restante es lo que se conoce como componente no dipolar del campo, el hecho de que los polos magnéticos y geográficos no coincidan indican que el modelo dipolar no es del todo exacto (Butler, 1998; Tauxe, 2010). Esto puede explicarse si en vez de considerar el CMT como un dipolo completamente geocéntrico, se considera como un dipolo excéntrico, como si hubiera múltiples dipolos que, a medida que nos alejamos del núcleo, van perdiendo intensidad.

Además, ese campo magnético que posee nuestro planeta queda impreso en la corteza terrestre, en función de las propiedades magnéticas de los sedimentos, las cuales pueden agruparse en tres categorías diferentes: diamagnéticos, paramagnéticos y ferromagnéticos. Todas ellas dependen de lo que se denomina como momento magnético total, el cual es la suma de los momentos magnéticos orbitales y el momento magnético intrínseco de las partículas que componen los átomos de la materia. Por tanto, a nivel macroscópico, esa suma total puede calificarse como imanación o magnetización específica (M) la cual, junto con la presencia de un campo magnético externo, condicionará las propiedades magnéticas de los materiales.

La más relevante para el paleomagnetismo es la ferromagnética, pues al aplicar un campo magnético sobre un material ferromagnético, la imantación aumenta al aumentar el campo hasta alcanzar un valor máximo que se conoce como magnetización de saturación, parte de la cual queda retenida cuando se retira el campo magnético externo. Cosa que no ocurre en materiales diamagnéticos o paramagnéticos. Esa magnetización que queda, puede decirse, grabada, en los materiales ferromagnéticos es lo que se conoce como magnetismo remanente, o magnetización remanente natural (NRM en sus siglas en inglés) y los mecanismos por los que los minerales ferromagnéticos adquieren esta NRM son los siguientes:

- Magnetización termorremanente o Termorremanencia (TRM en sus siglas en inglés): es la que adquieren los materiales que se enfrían de manera gradual desde una temperatura superior a la que se conoce como Temperatura de Curie (T_C), la cual es aquella temperatura en la que un mineral ferromagnético pierde sus características y se vuelve paramagnético.

- Magnetización remanente deposicional (DRM en sus siglas en inglés): es la que adquieren los granos ferromagnéticos en presencia de un campo magnético ambiental; al depositarse se alinean estadísticamente en función de la orientación del mismo. También está la que se denomina post-deposicional (p-DRM) y es la que adquieren los granos reorientados tras la deposición y antes de la consolidación del sedimento.

- Magnetización remanente química (CRM en sus siglas en inglés): es la que se produce cuando se forma un nuevo mineral magnético en presencia de un campo magnético, ya sea por alteración química y/o cristalográfica de un mineral preexistente o por nucleación y crecimiento del grano a través de un volumen crítico.

Por tanto, la NRM es uno de los fundamentos básicos del paleomagnetismo, ya que una correcta interpretación de esta propiedad puede aportar información sobre la orientación del campo magnético de la Tierra a lo largo del tiempo, convirtiéndose en un registro temporal muy valioso, y el Paleomagnetismo en una herramienta de datación muy relevante.

3.2 Paleomagnetismo y su aplicación cronológica: escala temporal de polaridad geomagnética

Sin embargo, el estudio del CMT es algo más complejo, ya que no basta con saber cómo ha quedado registrado en los sedimentos, sino que hay que interpretarlo, y para ello hay que entender el campo magnético de manera matemática, como una magnitud vectorial. Esto permite descomponerlo tridimensionalmente en una serie de vectores que presentan una dirección y módulo específico, F o Intensidad, cuyos parámetros pueden observarse en la figura 3.2:

- Declinación (D): la componente horizontal del campo (H) señala al norte magnético y tiene una desviación con respecto al norte geográfico. Ese ángulo que se mide en el sentido de las agujas del reloj (valores positivos), por lo que va de 0º a 360º, es lo que se conoce como declinación magnética.

- Inclinación (I): es la desviación del vector H con respecto a la horizontal; es decir, si por ejemplo pudiésemos observar una aguja magnética de una

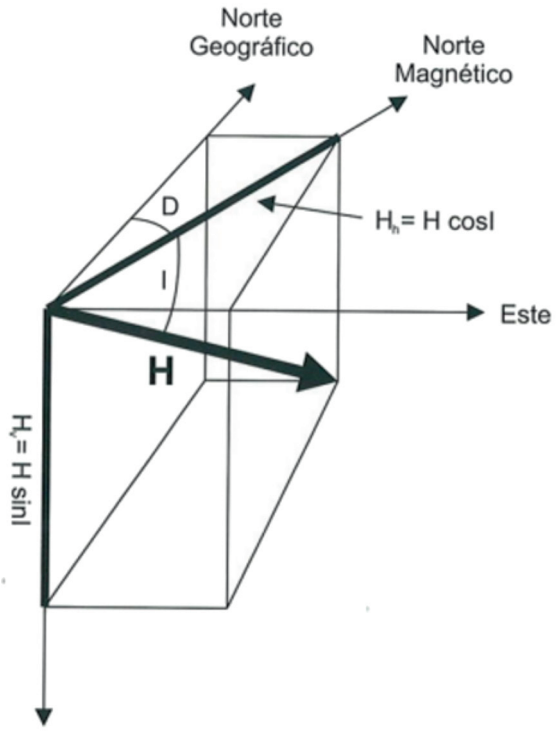

Figura 3.2. Descomposición vectorial del CMT, definido por la declinación (D) y la inclinación (I). Modificado de Butler 1998

brújula suspendida en el aire, veríamos que no queda completamente horizontal; la zona imantada que señala el norte, se inclinaría hacia abajo en el hemisferio norte y hacia arriba en el hemisferio sur. Ese ángulo con respecto a la horizontal es lo que se denomina inclinación magnética. Por convenio es positiva si apunta hacia el interior de la Tierra, es decir, de 0° a 90° desde el polo norte magnético hasta el Ecuador, y negativa, de 0° a -90° entre el Ecuador hasta el Polo sur magnético.

Por tanto, el CMT puede definirse en cualquier punto de nuestro planeta mediante esos tres parámetros: declinación, inclinación e intensidad, los cuales varían con el paso del tiempo. Dicha variación ha permitido caracterizar tres fenómenos en lo que se refiere a los cambios del CMT, es decir, variaciones en la dirección (declinación e inclinación) e intensidad (magnitud) del campo, que han permitido establecer un control cronológico del mismo: las inversiones geomagnéticas o inversiones de polaridad, las excursiones geomagnéticas y la variación secular.

- Inversiones geomagnéticas: el dipolo magnético cambia su polaridad, los polos magnéticos N y S intercambian su posición. Porqué ocurre no se sabe con exactitud, aunque está relacionado con la disminución de la intensidad (Tauxe, 2010). Se produce a escala global y la duración de cada inversión se estima en unos 5000 años (Coe et al., 2000; Cox, 1969; Opdyke and Channell, 1996) aunque no hay un consenso establecido.

- Variación secular: son también cambios en la dirección y magnitud del campo con el tiempo, pero en este caso son periodos comprendidos de decenas a centenares de años.

- Excursiones geomagnéticas: de nuevo, son desviaciones en la dirección del campo, pero en este caso no son necesariamente de carácter global y a menudo están asociadas a transiciones de polaridad (Laj and Channell, 2007). Son

bastante controvertidas, ya que no está claro sí se pueden considerar como una variación secular muy moderada o inversiones de polaridad que no llegaron a realizarse.

Son estos cambios, sobre todo las inversiones geomagnéticas, las que presentan el mayor interés en geocronología, siendo el campo más estudiado del paleomagnetismo. Junto con otras técnicas cronológicas (p.ej. datación radiométrica, serie de Ar^{40}/Ar^{39}, etc.) han permitido construir lo que se conoce como Escala Temporal de Polaridad Geomagnética (o GPTS en sus siglas en inglés) la cuál es un registro de inversiones de polaridad a escala global. Las primeras realizaciones de esta escala fueron llevadas a cabo por Cox et al., (1964, 1963) en donde se definió la secuencia en dos tipos de polaridades dominantes, polaridad normal (campo similar al actual) y polaridad inversa (campo contrario al actual). Se estableció por convenio un color negro para la primera, y blanco para la segunda, y definiendo los periodos de tiempo amplios en los que predominaba una u otra polaridad como épocas y los intervalos más cortos como eventos, aunque esta terminología se cambió en 1979 por las definiciones cron y subcron respectivamente.

Sobre esta base, y a lo largo del tiempo se ha ido desarrollando la GPTS (Figura 3.3), la cual ha ido ajustándose y adaptándose en función de la mejora y desarrollo de los métodos radiométricos, variaciones orbitales de la Tierra, cambios climáticos registrados en el sedimento, etc., que han ido aportando más información y datos (Cande and Kent, 1995; Gee and Kent, 2007; Gradstein et al., 2004; Kent and Gradstein, 1985; Lowrie and Kent, 2004).

El principal objetivo de la GPTS es servir como herramienta de datación de secuencias estratigráficas mediante lo que se conoce como magnetoestratigrafías: básicamente consiste en obtener muestras en campo a lo largo de secuencias estratigráficas, de las cuales se mide la NRM para determinar su

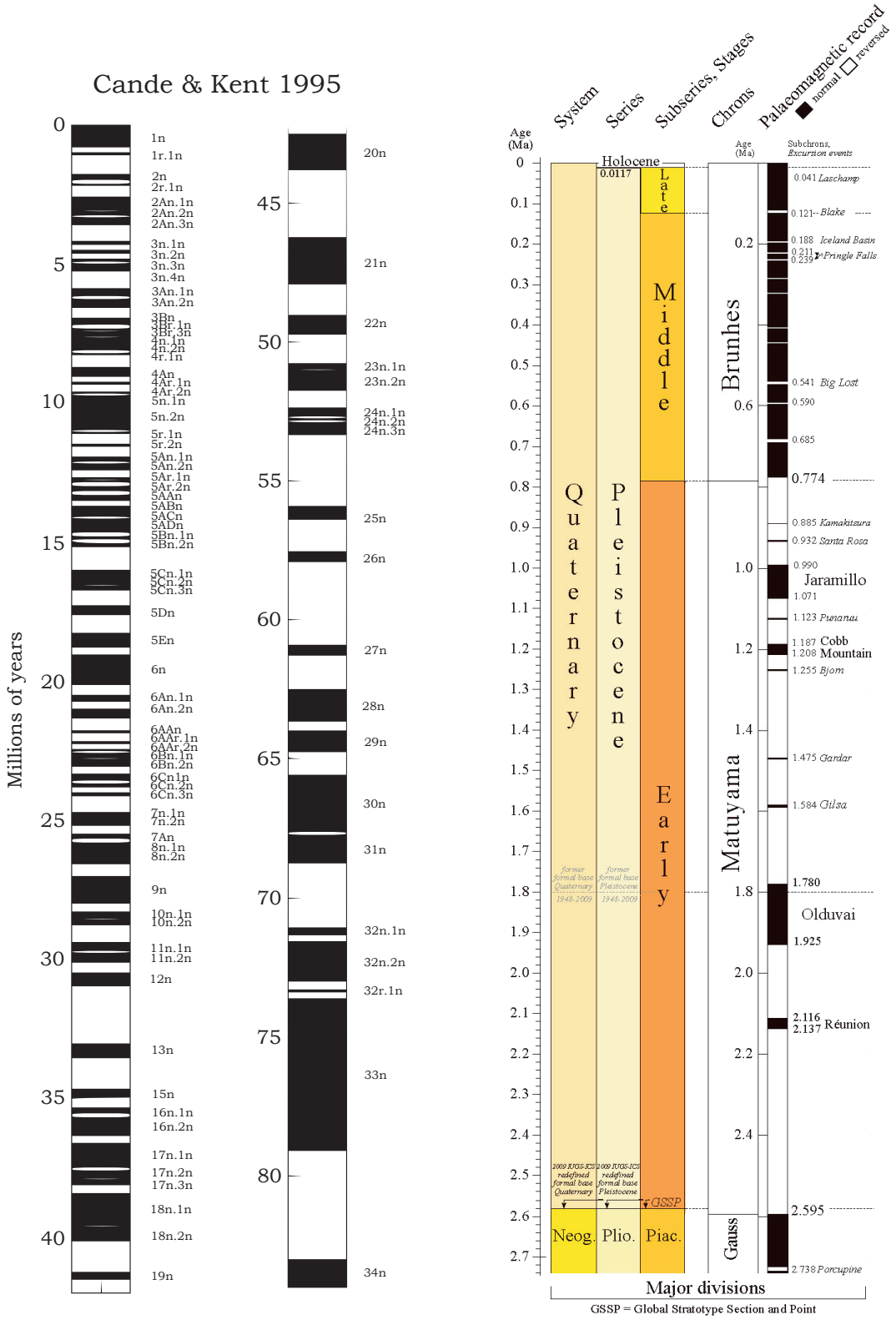

Figura 3.3. A la izquierda la GPTS realizada por Cande y Kent en 1995, correspondiente al periodo comprendido para el Cenozoico y finales del Cretácico superior (0 a 85 millones de años), y a la derecha, la tabla correspondiente a los últimos 2.7 millones de años, el Cuaternario, sólo las inversiones magnéticas, obtenida de la tabla de correlación cronoestratigráfica llevada a cabo por la Comisión Internacional de Estratigrafía (ICS, http://www.stratigraphy.org/index.php/ics-chart-timescale) versión 2016.

polaridad, lográndose así una secuencia de cambios de polaridad para una sección estratigráfica concreta. Las distintas polaridades conseguidas se correlacionan con la GPTS obteniéndose así un marco temporal para esa secuencia estratigráfica específica. Al ser un método de datación relativa, se hace imprescindible que vaya acompañada de otros métodos de datación, tales como resonancia del espín electrónico, luminiscencia, bioestratigrafía, entre otros.

3.3 Obtención del material para su análisis: muestreo

La premisa fundamental de la toma de muestras para magnetoestratigrafía, y para paleomagnetismo en general, es que dichas muestras han de estar orientadas en campo de la manera más precisa posible. Generalmente dicha orientación se establece referenciada a un sistema de coordenadas (eje cartesiano) en el que el eje Z define el sentido del muestreo como se representa en la figura 3.4 (Butler 1998): el eje Z es el eje central (Z positivo en el afloramiento); el eje X está en el plano vertical (ortogonal a Z); y el eje Y es horizontal.

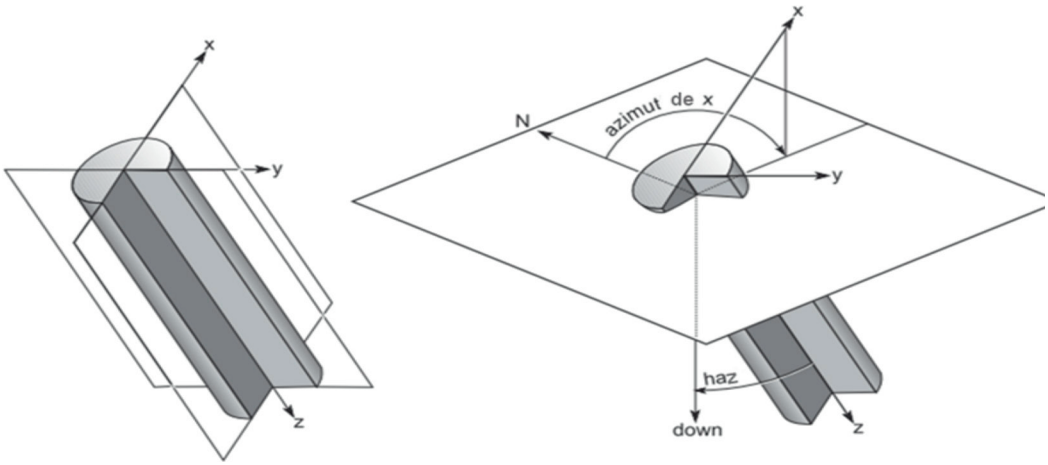

Figura 3.4. El diagrama de la izquierda es una representación esquemática de una muestra cilíndrica (o testigo) obtenida *in situ*. El eje Z apunta al afloramiento; el eje X está en el plano vertical; el eje Y es horizontal. El diagrama de la derecha muestra los ángulos de orientación para las muestras individuales. Los ángulos medidos son el diámetro del eje Z (ángulo de Z desde la vertical) y el acimut geográfico de la proyección horizontal del eje + X medido en el sentido de las agujas del reloj desde el norte geográfico. Tomado de Butler 1998.

En el campo, la orientación de la muestra se determina midiendo (1) el acimut de la proyección horizontal del eje + X (acimut del plano X-Z) y (2) el haz (ángulo desde la vertical = [90° - inmersión]) del + eje Z.

No existe en realidad un procedimiento estándar para el muestreo, la orientación *in situ* es una premisa fundamental, pero tampoco tiene un protocolo normalizado. La toma de muestras viene casi siempre condicionada por el tipo de material del que se obtienen las mismas, dependiendo de si son materiales duros (rocas calizas, carbonatos, etc.) o blandos (arcillas compactadas, arenas, etc.).

En la presente tesis, en el caso de los materiales duros, el muestreo se ha realizado mediante una perforadora eléctrica o a gasolina (Foto 3.5a) para obtener ejemplares cilíndricos que se orientan *in situ* con la ayuda de un clinómetro (Foto 3.5b) tomando así la inclinación y la declinación de la muestra en el campo.

Para los materiales blandos se ha utilizado normalmente un cuchillo de cerámica, para no contaminar el material, con el que se talla una muestra de mano, la cual se suele consolidar con silicato de sodio, elemento no magnético que ayuda a mantener la integridad de la muestra, y se suele orientar marcando el norte magnético sobre la superficie horizontal obtenida (Foto 3.6).

El siguiente paso es cortar los ejemplares obtenidos, a unas dimensiones específicas para obtener así ejemplares o muestras individuales que serán posteriormente analizadas. En el caso de los cilindros se ha procurado obtener unas dimensiones de aproximadamente 11cm^3 y las muestras individuales de los bloques de mano se han cortado en cubos de aproximadamente 8cm^3 (figura 3.7).

Figura 3.5. Ejemplo de toma de muestras llevada a cabo en Aín Bni Mathar, (Marruecos) realizada en muestras duras, mediante una perforadora a gasolina, a), y la posterior orientación de los ejemplares cilíndricos obtenidos, mediante el clinómetro, b). Fotos ©Claudia Álvarez Posada.

Figura 3.6. Toma de muestra de materiales blandos, obteniendo un bloque de mano, en el yacimiento de Solana del Zamborino. Las flechas indican el Norte magnético actual. Foto ©Claudia Álvarez Posada.

Figura 3.7. ejemplo de muestras individuales que van a ser medidas en laboratorio. La flecha roja es el sentido del muestreo tomado en campo. Suele indicar la dirección de las muestras con respecto al norte en el momento de su obtención

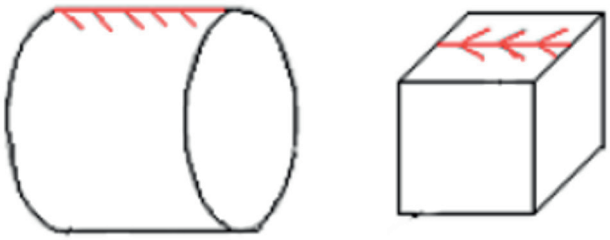

En los yacimientos analizados en esta tesis, la línea de trabajo ha consistido en general, en realizar primero una columna estratigráfica de la sección a muestrear y posteriormente obtener las muestras distanciándolas entre 1m, 1,5m aproximadamente siempre que fuera posible, y en caso de acceso complicado o dificultad del terreno, muestrear donde se pudiera acceder. Sin embargo, la excepción ha sido el yacimiento de FN-3, ya que en este caso se han

obtenido los ejemplares directamente de dos sondeos verticales realizados en el yacimiento, la columna estratigráfica correspondiente se ha realizado en función de dichos sondeos, y la obtención de las muestras se ha llevado a cabo cortando longitudinalmente las secciones de los sondeos en donde había material muestreable y mediante el uso de un cuchillo de cerámica.

3.4 Análisis en laboratorio de las muestras individuales y representación gráfica de los datos obtenidos

La magnetización remanente natural, NRM, es la suma vectorial de todos los componentes de la magnetización que queda registrada en la formación de los sedimentos, tanto de la adquirida en el momento de formación del material (magnetización primaria) como de la adquirida posteriormente (magnetización secundaria) El análisis básico para la obtención de magnetoestratigrafías es aislar lo que se conoce como la componente de magnetización remanente característica o primaria, conocida como *Characteristic Remanent Magnetization*, o ChRM en sus siglas en inglés.

Para poder aislar la ChRM hay dos tipos de técnicas de lavado o desmagnetización, que permiten descartar las magnetizaciones secundarias: aplicación de incrementos de temperatura (*Thermal demagnetization* o TH en inglés) o el uso de campos alternos (*Alternating fields* o AF en inglés). Ambas técnicas se basan en los siguientes parámetros:

- Temperatura: se centra sobre todo en la temperatura de Curie (T_C), que como se explicó anteriormente en la temperatura por encima de la cual los componentes ferromagnéticos pierden sus propiedades magnéticas y es característica de cada mineral. Influye también la temperatura de desbloqueo (T_{UB}), que es aquella por debajo de la T_C en la que el tiempo de relajación de los granos que conforman el mineral es muy corto.

- Tiempo de relajación: magnitud que puede definirse como el tiempo necesario para que la magnetización inicial (M_o) decaiga $^1/e$ (parecido a una vida media de la remanencia inicial) y el cual varía desde cientos de años hasta segundos (*e*: es el número de Euler).

- Coercitividad: se puede definir como el campo requerido para reorientar la magnetización de las partículas de una dirección en otra opuesta. Su valor es el del campo magnético necesario para hacer cero la magnetización o provocar la desmagnetización.

La desmagnetización térmica aprovecha la relación entre la temperatura y el tiempo de relajación de las partículas ferromagnéticas. En laboratorio se puede determinar una temperatura (T) inferior a la de Curie (T_C) con un tiempo de relajación muy corto, es decir una T_{UB} del orden de segundos. Al calentar las muestras por encima de esa temperatura de desbloqueo, aquellas partículas que tengan una $T_{UB} < T$ estarán en equilibrio con el campo magnético ambiental, magnetizándose en la misma dirección que este. Si esto ocurre en un entorno donde el campo magnético es cero, no habrá magnetización sobre esas partículas, y si se va enfriando progresivamente la muestra, esas partículas se reorientan de manera aleatoria, perdiendo su magnetización neta, mientras aquellas partículas con unta $T_{UB} > T$ no se habrán desbloqueado, y seguirán aportando magnetización a la NRM resultante, que se mide tras cada aplicación de T, la cual se va incrementando en cada paso, hasta que se alcanza la T_C, momento en el que el material pierde sus características magnéticas y se convierte en diamagnético. La TH se hace de manera progresiva, aplicando cada vez temperaturas más elevadas.

En el uso de campos alternos, se aplica un campo magnético alterno que disminuye gradualmente, en un entorno neutro, magnéticamente hablando. Aquellas partículas cuya coercitividad sea menor o igual que el campo apli-

cado se magnetizarán en el mismo sentido que éste. Asumiendo que hay un rango de coercitividades diferentes en las muestras, las partículas de baja estabilidad se distribuirán al 50%, unas orientadas en la misma dirección del campo aplicado, y la otra en dirección contraria, anulándose entre ellas, y por tanto dejando de contribuir a la magnetización NRM resultante. El proceso se repite hasta que el campo alterno se haya anulado, obteniéndose así la desmagnetización de todas las partículas de la muestra.

Una vez lavadas y procesadas las muestras individuales, se proyectan los datos de inclinación y declinación obtenidos, correspondientes a la NRM, en lo que se conoce como diagramas ortogonales o diagramas de Zijderveld (Zijderveld, 1967) y que son diagramas que aunque proyectados en dos dimensiones, representan vectores en 3D, por lo que normalmente se correlacionan los ejes X, Y, Z con la dirección Norte (N), Este (E) y Down (vertical hacia abajo) (Figura 3.8a).

Lo que se representa en estos diagramas son los cambios de intensidad y dirección de la magnetización a lo largo de las diferentes etapas de desmagnetización de las muestras. Cada punto indica un valor de declinación e inclinación. La primera se proyecta en el plano horizontal y por convención con puntos sólidos (figura 3.8b), y la segunda en el plano vertical y con puntos huecos (figura 3.8c).

Sin embargo, los diagramas de Zijderveld no son los únicos sistemas para representar los datos paleomagnéticos obtenidos. Otro sistema muy extendido es el uso de las proyecciones de igual área, que consiste en proyectar una esfera en un plano horizontal en una representación polar. Es decir, en estas proyecciones el eje vertical corresponde al eje N-S, mientras que el horizontal representa el eje E-W (figura 3.9). Este tipo de representaciones permite

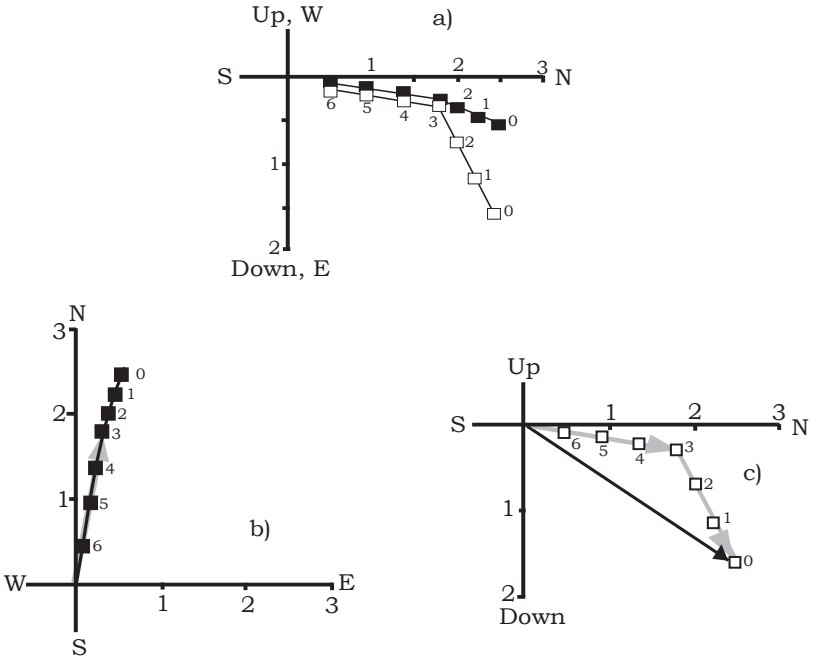

Figura 3.8. a) Las proyecciones vertical y horizontal se combinan en un único diagrama vectorial b) La proyección del vector NRM se muestra en el plano horizontal (N frente a E). c) Se representa la proyección del vector NRM en el plano vertical orientado N-S según el eje de abscisas. La flecha negra es la proyección vertical del vector NRM antes de la desimanación mientras que las flechas grises indican las componentes magnéticas eliminadas en esos pasos. Modificado de Carrancho Alonso (2010)

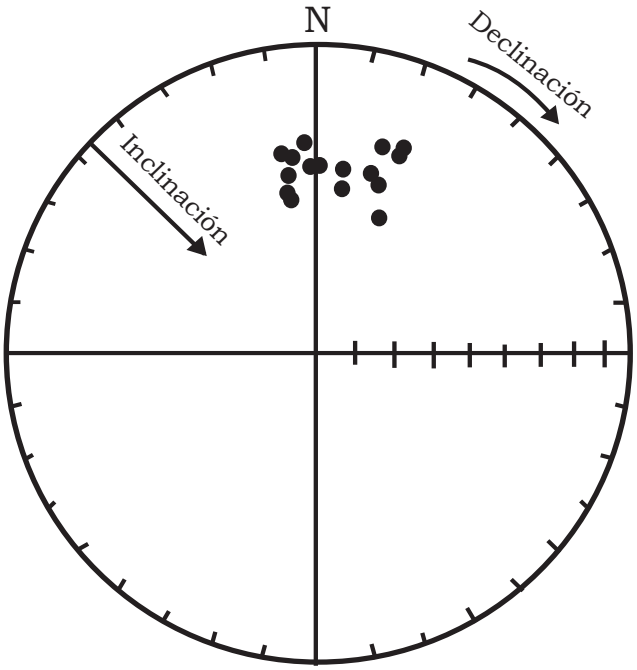

Figura 3.9 Representación gráfica de una proyección de igual área correspondiente a un proceso de desimanación de muestras del yacimiento de Solana del Zamborino (Cuenca Guadix – Baza). La declinación se mide a lo largo del margen externo del círculo, por tanto, va de 0º a 360º, mientras que la inclinación aumenta de 0º a 90º desde el margen del círculo hacia el interior del mismo

estudiar la distribución de un conjunto de muestras al proyectar sobre la esfera la componente característica (ChRM) de cada una de ellas.

Obviamente, todos estos datos se tratan estadísticamente para reducir los posibles errores presentes en las direcciones paleomagnéticas obtenidas, las cuales pueden deberse a errores implícitos al orientar la muestra en campo, lavado incompleto de las muestras, remagnetización en el campo magnético actual, etc.

El método estadístico seguido más a menudo en paleomagnetismo es el desarrollado por Fisher (1953). Para una mejor comprensión de la estadística fisheriana y del paleomagnetismo en general, recomendamos la lectura de los libros de Butler (1998) y Tauxe (2010).

3.5 Referencias

Butler, R., 1998. Paleomagnetism: Magnetic domains to geologic terranes, Electronic edition.

Carrancho Alonso, Á., 2010. Arqueomagnetismo y magnetismo de las rocas en registros arqueológicos holocenos. Aplicación a sedimentos kársticos (yacimientos de la Sierra de Atapuerca y Cueva de El Mirón) y recreaciones experimentales. Tesis Doctoral.Universidad de Burgos.

Cande, S.C., Kent, D. V., 1995. Revised calibration of the geomagnetic polarity timescale for the late Cretaceous and Cenozoic. Journal of Geophysical Research 100, 6093–6095.

Coe, R.S., Hongre, L., Glatzmaier, G.A., 2000. An examination of simulated geomagnetic reversals from a palaeomagnetic perspective. Physical and Engineering Sciences.

Cox, A., 1969. Geomagnetic Reversals. Science 163, 237–245.

Cox, A., Doell, R., Dalrymple, G., 1964. Reversals of the earth's magnetic field. Science 144, 1537–1543.

Cox, A., Doell, R.R., Dalrymple, G.B., 1963. Geomagnetic polarity epochs and pleistocene geochronometry. Nature 198, 1049–1051.

Fisher, R., 1953. Dispersion on a Sphere. Proceedings of the Royal Society A: Mathematical, Physical and Engineering Sciences 217, 295–305.

Gee, J.S., Kent, D.V., 2007. Source of Oceanic Magnetic Anomalies and the Geomagnetic Polarity Timescale, in: Treatise on Geophysics. Elsevier, pp. 455–507.

Gradstein, F.M., Ogg, J.G., Smith, A.G., 2004. A Geologic Time Scale 2004. Cambridge, UK. NEw York: Cambridge University Press.

Kent, D. V., Gradstein, F.M., 1985. A Cretaceous and Jurassic geochronology. GSA Bulletin 96, 1419–1427.

Laj, C., Channell, J.E.T., 2007. Geomagnetic Excursions, in: Treatise on Geophysics. Elsevier, pp. 373–416.

Lowrie, W., Kent, D. V., 2004. Geomagnetic polarity timescales and reversal frequency regimes, in: Geophysical Monograph Series. pp. 117–129.

Opdyke, M., Channell, J.E., 1996. Magnetic stratigraphy. Academic Press.

Tauxe, L., 2010. Essentials of Rock and Paleomagnetism. University of California Press.

Zijderveld, J.D.A., 1967. Ac Demagnetization of Rocks: Analysis of Results, in: Collinson, D.W., Creer, K.M., Runcorn, S.K. (Eds.), Methods in Palaeomagnetism. Elsevier, Amsterdam, New York, pp. 254–286.

Capítulo 4 . new magnetostratigraphic and numerical age of the fuente nueva-3 site (guadix -baza basin, spain)

Quaternary International 389 (2015) 224–234

Contents lists available at ScienceDirect

Quaternary International

journal homepage: www.elsevier.com/locate/quaint

New magnetostratigraphic and numerical age of the Fuente Nueva-3 site (Guadix-Baza basin, Spain)

C. Álvarez [a, *], J.M. Parés [a], D. Granger [b], M. Duval [a], R. Sala [c], I. Toro [d]

[a] Geochronology Program, CENIEH, Paseo Sierra de Atapuerca 3, 09002 Burgos, Spain
[b] Department of Earth Atmospheric and Planetary Sciences, Purdue University, West Lafayette, IN 47907, USA
[c] IPHES (Institut Català de Paleoecologia Humana i Evolució Social), Área de Prehistòria, Universitat Rovira i Virgili, Plaça Imperial Tarraco 1, 43005 Tarragona, Spain
[d] Museo Arqueológico y Etnológico de Granada, Carrera. Del Darro 41-43, 18010 Granada, Spain

ARTICLE INFO

Article history:
Available online 10 June 2015

Keywords:
Guadix-Baza basin
Magnetostratigraphy
Cosmogenic nuclides
Electron spin resonance
Pliocene–Pleistocene
Olduvai

ABSTRACT

Sediments of the Plio-Pleistocene Guadix – Baza basin have provided a wealth of information on the first hominin populations in Western Europe. To better constrain the age of the Fuente Nueva-3 archaeological site within the basin, and to complement previous magnetostratigraphic studies, two vertical boreholes were taken that provide a continuous record of the lower part of the sequence. Results indicate that the sequence is dominated by negative inclinations, but some additional intervals with positive inclination are also identified in the lower part of the sequence. A new cosmogenic nuclide burial age of 1.50 ± 0.31 Ma helps constrain the magnetostratigraphic record. The abundance of normal polarity directions at the bottom of a borehole may indicate proximity to the Olduvai Subchron; however, further analyses are required to confirm this hypothesis.

1. Introduction

The Guadix-Baza basin, located in the Betic Mountain Range (southern Spain) contains a record of the southernmost and one of the largest Neogene-Quaternary paleolakes in Europe. The lake sediments are rich in organic material and often fossiliferous, and are continuous across the Miocene, Pliocene and Pleistocene epochs (e.g. García Aguilar and Palmqvist, 2011). They have therefore been the target of numerous geologic, paleontological, and archaeological studies. Sites such as Orce, Huéscar, Barranco León, and Fuente Nueva have yielded important information for understanding the Plio-Pleistocene, including faunal events such as the so-called "Villafranchian turnover" and climate events such as the Early-Middle Pleistocene Revolution that marks the transition to longer-period glacial–interglacial cycles (Agustí et al., 2001, 2010; Head et al., 2010). In addition, the basin holds promise to become a European reference for an unprecedented "out-of-Africa lacustrine basin" including both evidence of human occupation and a faunal record for the Pleistocene.

Fuente Nueva-3 (FN-3), in the NE Guadix-Baza basin, is currently considered as one of the oldest sites of hominin occupation in Western Europe (e.g. Martínez-Navarro et al., 1997; Oms et al., 2000b; Toro et al., 2011; Duval et al., 2012a). A previous magnetostratigraphic study at FN-3 revealed a 20 m thick composite stratigraphic section of entirely reversed magnetic polarity that was correlated to the Matuyama Chron, very likely between the Olduvai and Jaramillo Chrons, based on biochronological evidence (Oms et al., 2000b, 2010b). However, the scarcity of the outcrops available in that area and the lack of stratigraphic continuity hampered sampling and precluded a detailed study of a continuous sequence. To address this issue, two boreholes were drilled in the vicinity of FN-3 in July 2011; the paleomagnetic results are presented here. One of the pending questions addressed by this work is whether short polarity chrons, in particular the Jaramillo, are missing due to the limited availability of suitable lithologies for paleomagnetism and due to weathering at the surface. In this paper, we document a new chronostratigraphic study at FN-3 that combines new data derived from the magnetostratigraphy and from cosmogenic nuclide burial dating. These data, combined with the available electron spin resonance (ESR) age results (Duval et al., 2012b), complement the existing geochronologic framework of the site.

* Corresponding author.
E-mail address: claudia.alvarez@cenieh.es (C. Álvarez).

http://dx.doi.org/10.1016/j.quaint.2015.04.044
1040-6182/

2. Geological context

The Guadix-Baza basin (Fig. 1) developed during the Neogene due to tectonic interactions between the Iberian block and the African plate. During the upper Miocene, it was part of the Betic corridor that connected the Mediterranean Sea to the Atlantic Ocean (Sanz de Galdeano, 1990; Sanz de Galdeano and Vera, 1992; Vera, 2000; Pla, 2009 and references therein). Later, in the latest Tortonian-early Messinian, the seaway progressively reduced and eventually closed, isolating the basin from the Mediterranean. Continental sedimentation continued in the lake basin, leaving a continuous record with a thickness of >500 m (and probably up to 2400 m) ranging in age from the Tortonian to the Pleistocene (Soria et al., 1999; Viseras Alarcón et al., 2003; Garcia Aguilar et al., 2010a,b; Hüsing et al., 2010;). During the Plio-Pleistocene, the basin was divided into two main sub-basins hosting distinct environments. The western sector (Guadix sub-basin) was dominated by a fluvial drainage flowing towards the eastern sector (Baza sub-basin), which was mainly occupied by a large and permanent lake (e.g. Viseras and Fernandez, 1992; Garcia Aguilar and Palmqvist, 2011). This duality yielded the identification of two almost coeval lithostratigraphic units for the Plio-Pleistocene deposits of the Guadix-Baza basin (García Aguilar and Martín, 2000; Pla, 2010; Pla et al., 2011): (1) the Guadix Formation, in the western part, which includes sandstones and conglomerates of fluvial and fan-delta origin; and (2) the Baza Formation, mostly exposed in the eastern part and made up of fine-grained lacustrine sediments.

The Baza Formation, the target of this study, hosts a rich mammal fauna near the Plio-Pleistocene transition. A number of Neogene Mammal (MN) zones have been distinguished, including MN 14 to MN 17 for the Pliocene, and the biozones Mm Q1 to MmQ4 defined by Agustí et al. (1987) for the Pleistocene (Agustí and Martínez Suárez, 1984; Agustí, 1985; Agustí et al., 1987; Oms et al., 2000a; Agustí et al., 2001; Oms et al., 2010a; Duval et al., 2011). A number of magnetostratigraphic studies have been carried out to precisely constrain MN boundaries and to furnish some important time lines for lacustrine sedimentation (Peña, 1985; Oms et al., 1994; Garcés et al., 1996, 1997; Oms et al., 1996; Parés and Dinarés-Turell, 1997; Agustí et al., 1999; Oms et al., 2000a; Gibert et al., 2006, 2007; Scott et al., 2007; Oms et al., 2010b, 2011). Overall, these studies place the sequences around the upper Pliocene and Lower Pleistocene, including archaeo-paleontological sites at Venta Micena, Barranco León, Fuente Nueva, Cúllar de Baza and Huescar.

2.1. Fuente Nueva-3 section

The town of Fuente Nueva is located ~7 km east of Orce, in the northeastern part of the Guadix-Baza basin. In the Orce-Fuente Nueva-Venta Micena area, the Baza Fm. has been classically divided in three different members (Vera et al., 1984): (1) an upper member of silty limestone (lacustrine and palustrine environment), which rests on (2) a middle red detrital member (alluvial), and (3) a lower limestone member at the base (shallow lacustrine and palustrine). This formation is especially known for the numerous paleontological and archaeological sites that have been discovered over the last decades (e.g. Toro et al., 2000; Agustí et al., 2010). The most famous are undoubtedly Fuente Nueva-3 and Barranco León, currently considered among the oldest evidence of hominin presence in Western Europe (Martínez-Navarro et al., 1997; Oms et al., 2000b) and the paleontological site of Venta Micena (Arribas and Palmqvist, 1998).

In the area of Fuente Nueva, three paleontological sites have been identified, labeled as “Fuente Nueva-1”, “Fuente Nueva-2” and

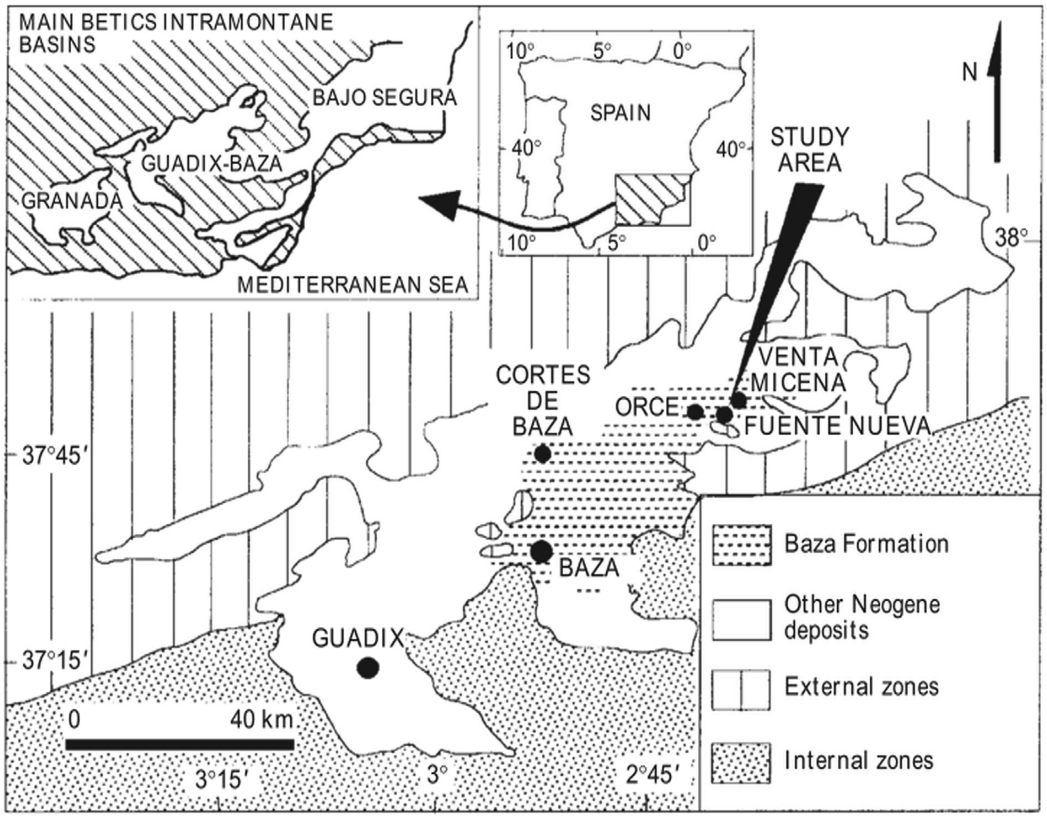

Fig. 1. Geographic location of the Guadix basin – Baza, South Spain (Modified from Martínez-Navarro et al., 1997).

"Fuente Nueva-3" respectively (Fig. 2); this paper will focus on FN-3, the only one with evidence of hominin presence (Martínez-Navarro et al., 1997). The stratigraphic section at Fuente Nueva 3 belongs to the Upper Member of the Baza Fm.; it includes a stratigraphic thickness of up to 25 m of rather uniform lithology deposited in a deep lake system, although superficial debris obscures much of the section (Garcia Aguilar, 2010a,b). The archaeological levels are found in limestones, marls and siltstones of palustrine/lacustrine origin and represent the upper part of the Baza Fm. (Anadón et al., 2003; Duval, 2008; Garcia Aguilar, 2010a,b). Details of the archaeology can be found in Toro et al. (2011).

The chronology of the deposits was originally established by a combination of magnetostratigraphy, biostratigraphy and numerical dating. The rich large mammal assemblage at FN-3 has been attributed to the Late Villafranchian biochron (Rook and Martínez-Navarro, 2010), similarly to other Early Pleistocene European sites such as Dmanisi (Georgia), Venta Micena, Barranco León, Pirro Nord (Italy) and Sima del Elefante TE-9 (Spain). The rodent assemblage at FN-3 shows an association of the species *Mimomys savini* (small) and *Allophaiomys* aff. *lavocati* that places FN-3 into the same biozone with Barranco León in the biozonation of the Guadix-Baza sedimentary record (Agusti et al., 2007). This biozone is younger than the *A. ruffoi* biozone, which includes Venta Micena, but older than the *Iberomys huescarensis–M. savini* biozone with Huéscar-1 site (Agustí et al., 2007, 2010). Previous magnetostratigraphic studies (Oms et al., 1996, 2000a, 2003, 2010a; Garcés et al., 1997; Gibert et al., 2006; Scott et al., 2007) revealed that the upper Member of the Baza Fm. is entirely of reverse polarity, which together with the fossil content correlates the FN-3 section to the Matuyama Chron (2.58–0.78 Ma) in the Lower Pleistocene. More recently, Duval et al. (2012a) published a combined U-series/Electron Spin Resonance (US-ESR) study of fossil teeth, which yielded a chronology of 1.19 ± 0.21 Ma (1σ uncertainty) for the upper archaeological level of Fuente Nueva-3, in excellent agreement with the magneto-biostratigraphic framework. In addition, faunal and paleomagnetic evidence indicate that FN-3 and Barranco León (layer D, ex BL-5) are coeval (Oms et al., 2000b). A recent ESR dating study based on optically bleached quartz grains provided a weighted mean ESR age of 1.43 ± 0.38 Ma for the layer D that encompasses the archaeological layer at Barranco León (Toro Moyano et al., 2013). This age is in apparent good agreement with the one at FN-3, but the large uncertainty precludes a meaningful comparison.

3. Material and methods

3.1. Paleomagnetism

Two vertical boreholes were drilled next to the archaeological site of FN -3 in July 2011; with a TP50 – D boring rig, that uses a hydraulic system. Core sections were obtained and sealed in the field (named Borehole #1 and Borehole #2 respectively). Boreholes were drilled through the sedimentary infill until the basement rock of Jurassic limestone was reached. Core recovery showed a Rock Quality Designation (RQD index) between 75% and 90% for both boreholes, indicating a good recovery rate. At the time of extraction, cores were immediately oriented up and down before be stored in their boxes. All paleomagnetic analyses were carried out at the Paleomagnetism Laboratory of the CENIEH (Burgos, Spain). Natural Remanent Magnetization and its decay during demagnetization were measured on a 755-4K Superconducting Rock Magnetometer (SRM, 2G Enterprises) with a magnetic moment noise less than 1×10^{-12} Am^2 housed in a low-magnetic environment. The SRM has a 3-axis degausser system built in for Alternating Field demagnetization (up to 170 mT). The thermal demagnetization apparatus included a TD-48SC oven (ASC Scientific). Specimens were stored in a μ-metal shielded cylinder during analysis.

After visual inspection of the Zijderveld diagrams (Zijderveld, 1967), characteristic remanent magnetization (ChRM) directions were computed using various programs (paldir- University of Utrecht; pmag- Tauxe; 1998; VDP5 -Ramón and Pueyo; 2011) and inclination-only was used to establish the local magnetic polarity.

Both cores were first stratigraphically correlated to the main sequence initially published by Oms et al., 2000 (Fig. 3). This correlation has been established by the depth of the cores, as well by visual inspection in the field, since boreholes were about 5 meters away from the clomun published by Oms et al. (2003). Core fragments were sub-sampled in the laboratory by slicing several ~10 cc cubes along the sedimentary record. A total of 112 specimens were prepared and measured for paleomagnetism. Both thermal (TH) and alternating field (AF) demagnetization were tested on a pilot set of samples. After inspection of the demagnetization plots, preference was given to the latter, as, it results in a better characterization of the primary component. This could be explained by the low intensity and susceptibility of the samples. Hence, AF demagnetization allows a slower removal of the secondary component yet without compromising the definition of the

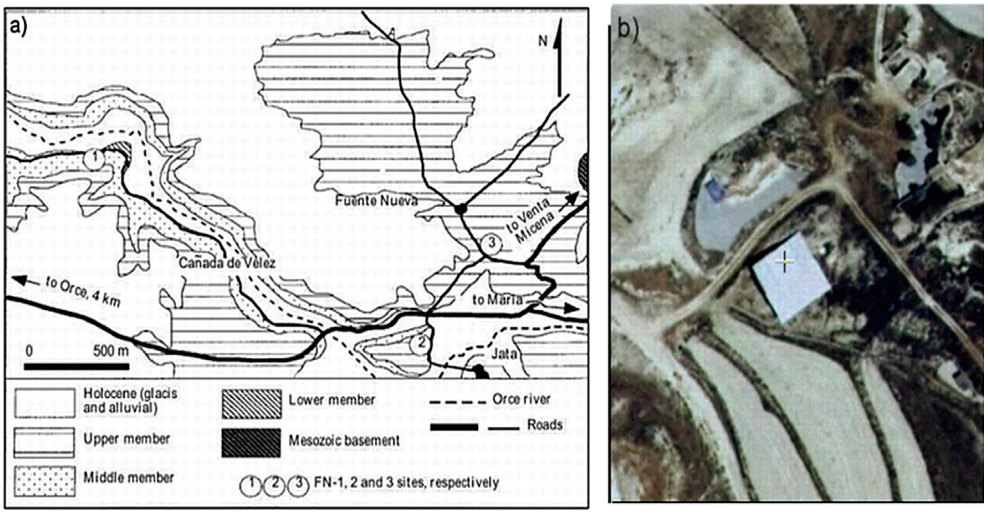

Fig. 2. a) Schematic geological map of the area of Fuente Nueva (Martínez Navarro et al., 1997); b) aerial photo of the location of the Fuente Nueva 3 site (taken from SigPac visor).

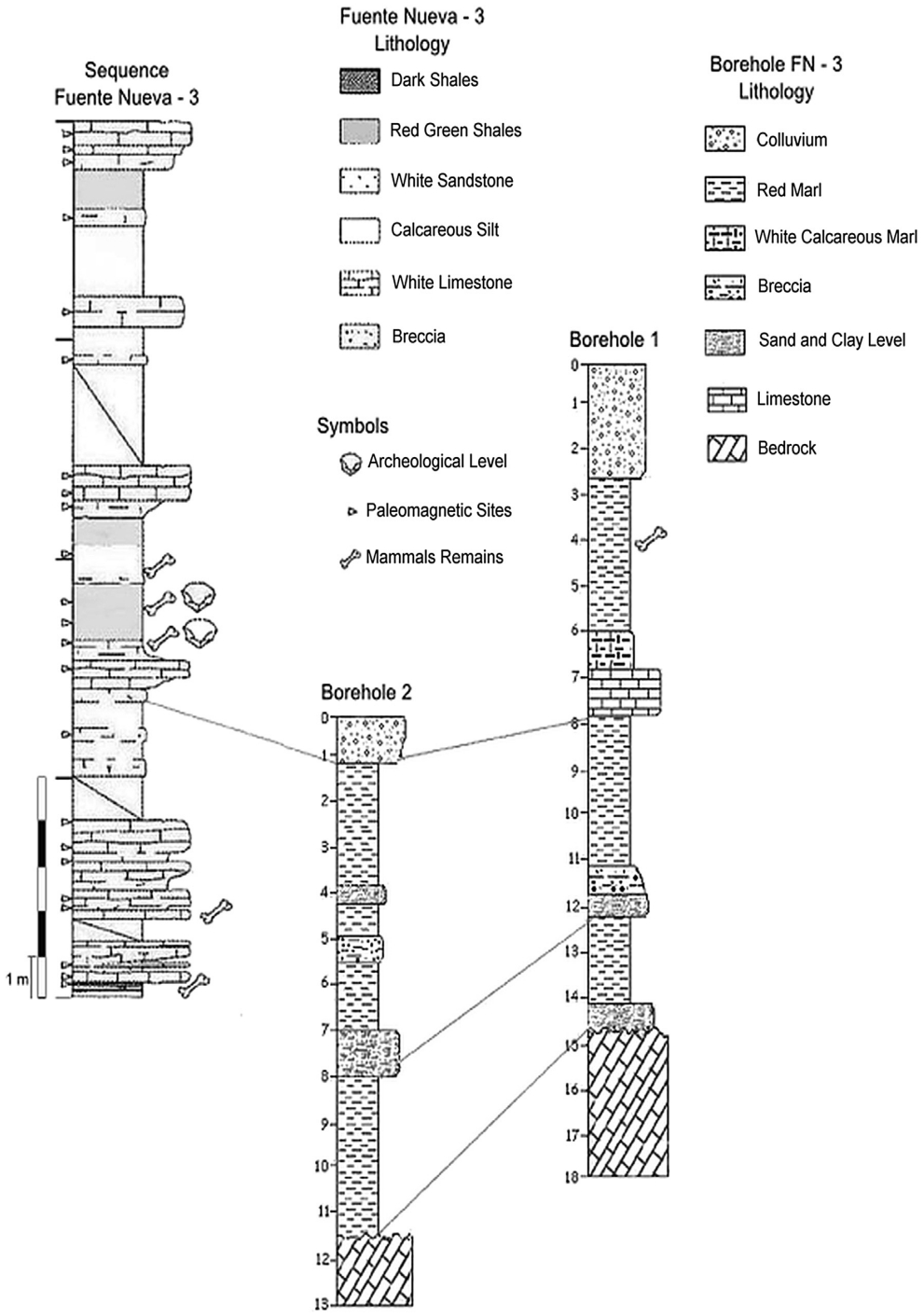

Fig. 3. Correlation between the two boreholes to the stratigraphic column of Fuente Nueva 3, modified Oms et al., 2003.

primary, higher coercivity component. In addition, most samples exhibit an erratic behavior (spurious magnetization) above 460 °C. Such behavior may indicate the presence of iron sulfides (as pyrrhotite or greigite) typical of lacustrine marsh sediments as well as the breakdown of phyllosiclicates at high temperature.

3.1.1. Borehole #1

Located on top of the archaeological site, this core is 18 m long and up to 9 cm in diameter. We obtained a total of 64 cubic samples, of which 32 were thermally demagnetized. Thermal demagnetization was performed at 40 °C intervals up to 460 °C, at which point the intensity was too low or the samples displayed erratic behavior. The remaining samples were demagnetized with the AF method with a peak field of 100 mT or until the magnetization was too low or erratic.

3.1.2. Borehole #2

The second core is 13 m long and was taken 7 m south of the Borehole #1. A total of 48 cubic samples were taken, of which 32 were thermally demagnetized. Thermal demagnetization was done

Table 1
Cosmogenic nuclide data obtained for sample FN081.

Sample name	^{10}Be (10^6 at/g)	^{26}Al (10^6 at/g)	^{26}Al/^{10}Be	Burial age (Ma)
FN081	0.303 ± 0.011	0.967 ± 0.158	3.19 ± 0.53	1.50 ± 0.31

at 60 °C and increased at 30 °C interval up to a maximum temperature of 420 °C. The remaining 16 samples were AF demagnetized with a peak field of 100 mT. The cohesiveness and continuity of some core sections allowed "u-channel"-type sampling. Two segments of 2 × 2 cm in cross section and 21 and 19 cm long respectively, were collected at depths of 8.18 m and 8.50 m. They were taken by cutting the core section lengthwise using a nylon string and ceramic knives. Such u-channels were measured at 2-cm intervals and AF demagnetized up to 100 mT with the SRM 2G magnetometer. Hysteresis loops of selected samples from both boreholes were conducted using a 3900 Magnetometer VSM MicroMag.

3.2. Dating sediment burial dating using ^{26}Al and ^{10}Be cosmogenic nuclides

We used ^{26}Al and ^{10}Be cosmogenic nuclides present in quartz to date sediment burial. Burial dating is based on radioactive decay of these two nuclides, which are produced by secondary cosmic rays near the ground surface. Several factors, including depth of burial, sediment deposition rate and other changes in production rate affect the nuclide concentration and hence the estimate of burial age (Granger and Muzikar, 2001; Granger, 2006). Accurate burial dating requires that several assumptions be met. First, it is important that sediment be deposited only once in the past several million years. If the sediment has been recycled from another deposit then the inferred burial age will be too old (e.g., Hu et al., 2011). Second, it is important that the sediment be buried deeply and quickly enough that postburial production of ^{26}Al and ^{10}Be can be ignored. If the sediment is not buried deeply enough, then the inferred burial age will be too young. In favorable circumstances these assumptions can be tested by constructing an isochron from multiple samples collected at the same burial depth (see Granger and Schaller, 2014) or by analyzing samples of known or zero burial age. Here, we analyze only a single sample and assume that it has no prior burial history. In this case, we calculate a simple burial age and consider it to be a minimum age for the deposit.

We collected 2 L of sediment at the lower archaeological level at Fuente Nueva-3 for burial dating ("unit 2" of Oms et al., 2011). The sampled stratigraphic layer has 10 m of visible sediment on top. Sample preparation and chemical analysis were carried out at the PRIME (Purdue Rare Isotope Measurement) Laboratory, Purdue University. Clean quartz was dissolved in HF/HNO_3 and spiked with ^{9}Be in a carrier solution prepared from beryl. Stable aluminum concentrations were measured on an aliquot of the sample solution by ICP-OES. AMS standards were prepared by Nishiizumi (Nishiizumi, 2004; Nishiizumi et al., 2007). Ages were calculated following Granger and Muzikar (2001), assuming steady erosion prior to burial, and that samples are buried sufficiently deeply that production by muons is negligible. We use a ^{10}Be mean life of 2.005 Ma, and a ^{26}Al mean life of 1.02 Ma. Production rates at the surface prior to burial are taken as 61.8 and 9.1 at/g/yr for ^{26}Al and ^{10}Be, for a latitude of 37.7 N and an altitude of 987 m asl, following Stone (2000) corrected for the ^{10}Be half-life. The calculated ages should be considered as minimum ages, as erosion rate and hence postburial production are unconstrained in detail. Data are shown in Table 1.

However, at the sime time, the calculated cosmogenic burial age could represent a maximum age estimate because we cannot exclude the existence of a prior burial history or exposure cycles in this sedimentary context; particularly given the evidence for sedimentary cyclicity present in the lacustrine sediments of the basin (García Aguilar, 2010). In light of these uncertainties, the age provided by the cosmogenic analysis is taken with caution. At best, it represents a first attempt at using this methodology at this particular site, and further analyses are needed to test the reliability of the burial age presented here.

4. Results

Our palaeomagnetic results show low NRM intensities: 3.6 × 10^{-6} A/m to 7.6 × 10^{-6} A/m for Borehole #1, and

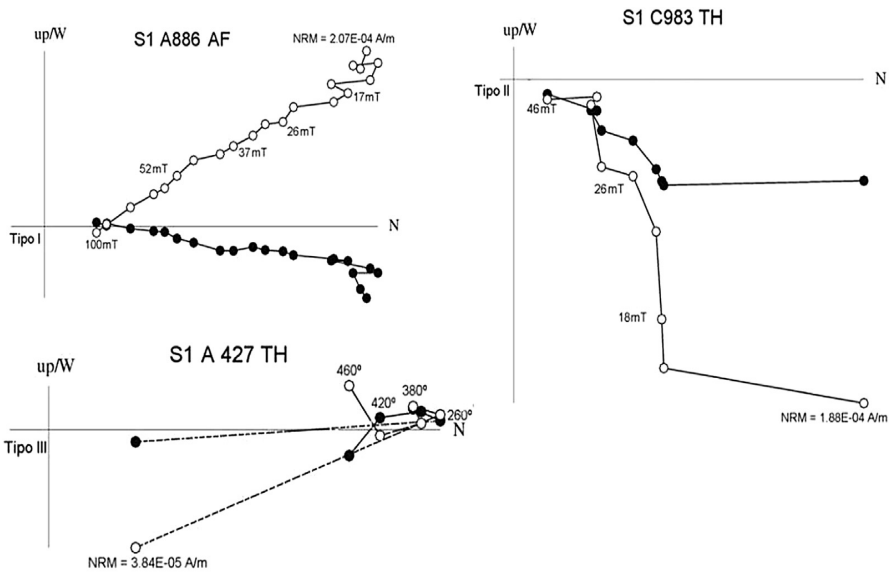

Fig. 4. Orthogonal demagnetization diagrams which represent the three classes defined in the manuscript, corresponding to Borehole #1 (black circles represent declination and white circles represent inclination).

3.97×10^{-6} A/m to 3.21×10^{-6} A/m for Borehole #2; which, along with the noisy results from hysteresis loops possibly indicate the presence of iron sulfides over ferromagnetic materials. Samples were grouped into 3 classes according to their behavior during demagnetization. Class I samples (7.1%) display linear demagnetization trends towards the origin on the Zijderveld diagrams, and the corresponding ChRM direction can unambiguously be computed. A soft component is usually observed but removed at very low AF fields. Class II samples (38.4%) are a little bit noisier but the ChRM directions are also clearly defined. Class III (54.5%) denotes samples having somewhat more noisy demagnetization trends (Figs. 4 and 5). We use those samples for which the primary component could be interpreted, including both Class I and Class II. The Class III samples have been excluded for the interpretation. The samples used to construct the inclination diagram for both boreholes are shown in Fig. 6.

The goal of our study is to complement the magnetostratigraphy done by Oms et al. (2000b; 2003) at FN-3, by obtaining fresher samples from intervals previously not sampled given the outcrop availability in the area. In particular, the two boreholes provide, for the first time, a continuous record of the lower part of the sedimentary sequence. As these boreholes were not oriented, inclination-only data was used to establish the magnetic polarity and our results need to be evaluated in light of the existing paleomagnetic data. We produced a new composite magnetostratigraphy based on the combination of the existing data by Oms

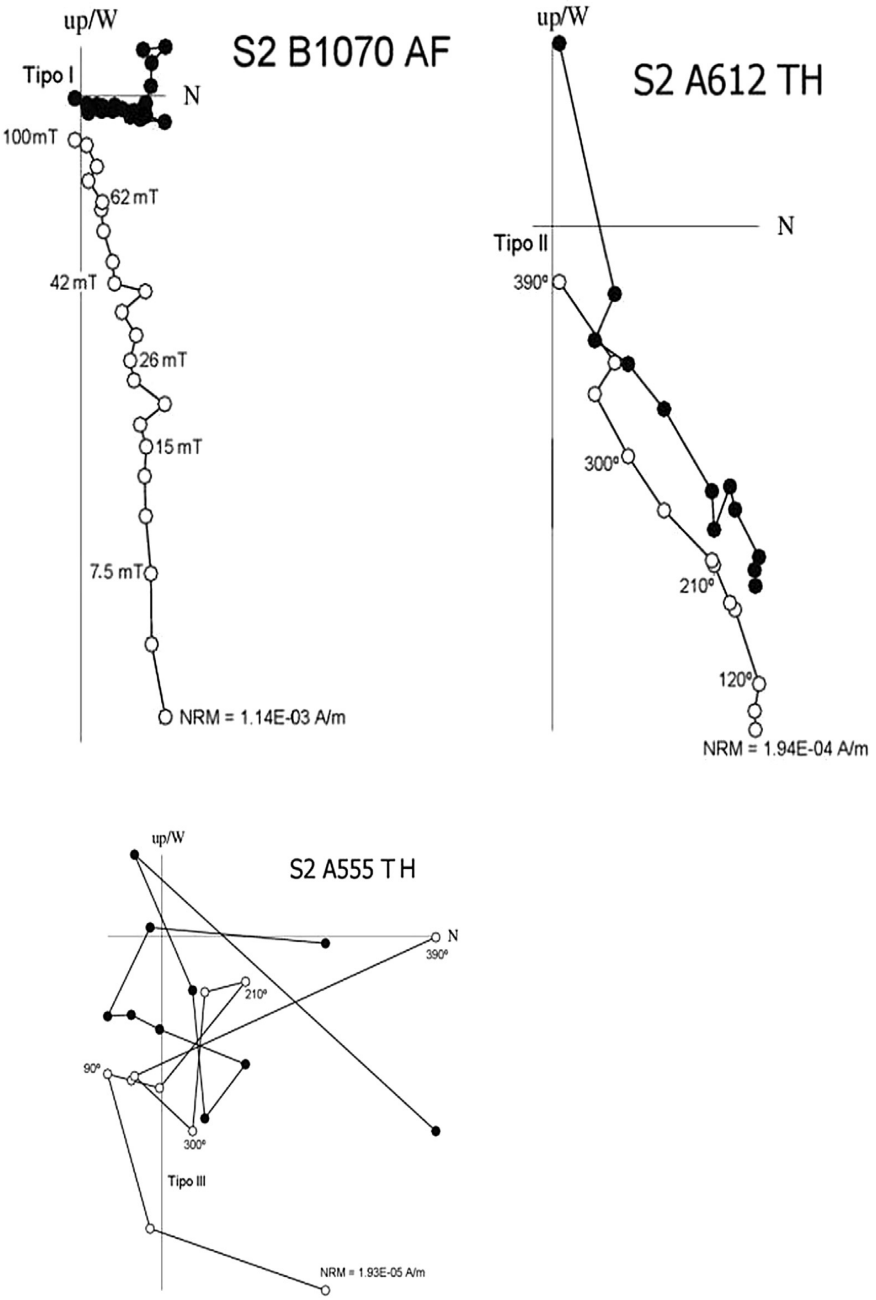

Fig. 5. Orthogonal demagnetization diagrams which represent the three classes defined in the manuscript, corresponding to Borehole #2 (black circles represent declination and white circles represent inclination).

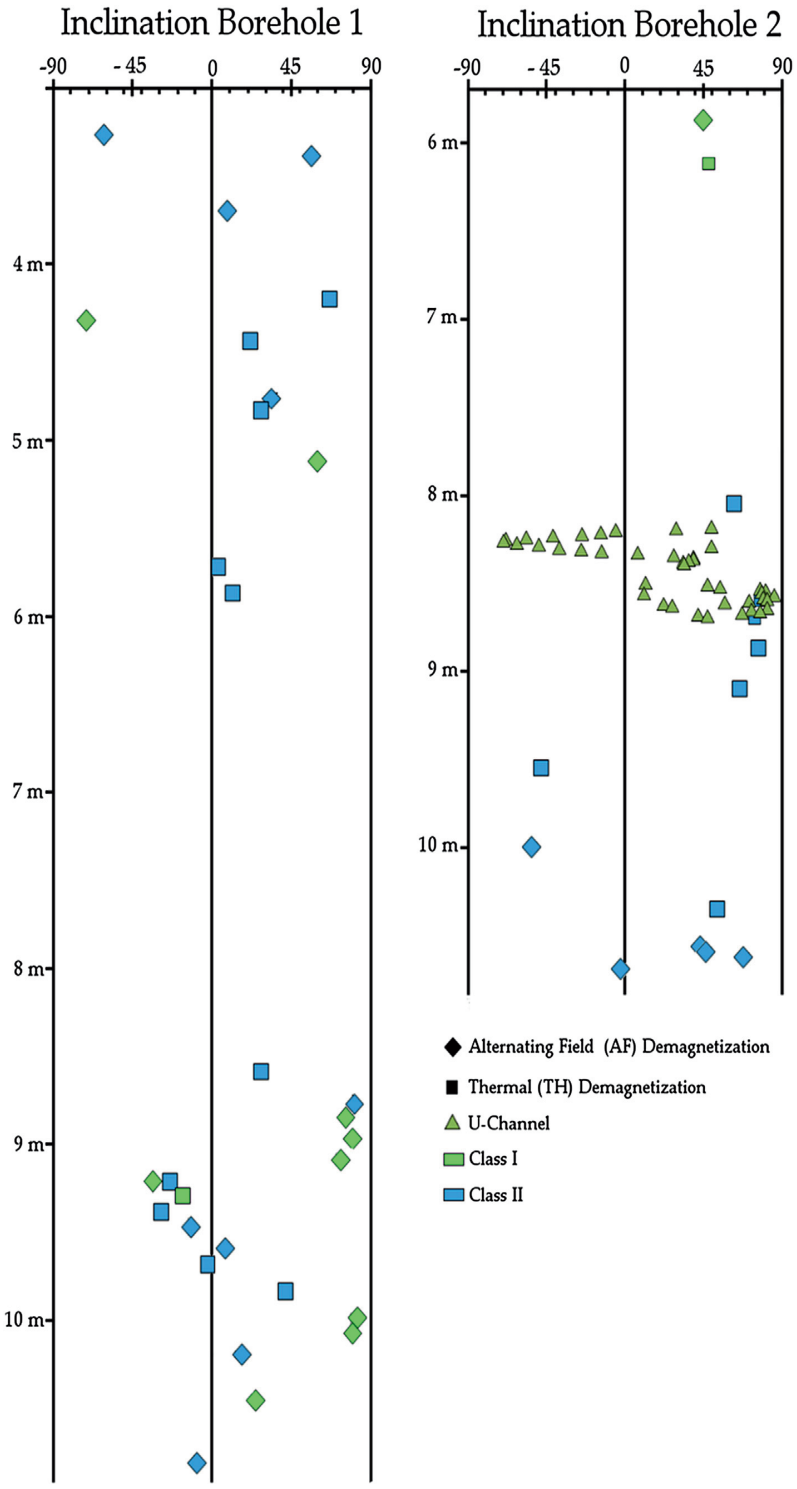

Fig. 6. Inclination only data; from Characteristic Remanent Magnetism (ChRM) direction for both boreholes.

and our own results from the two boreholes. Inclination values range from −70 to 85, and therefore we arbitrarily chose a window between ±25° and ±90° to construct the combined magneto-stratigraphic column (Fig. 7) (see also Merrill et al., 1998).

Three intervals with positive inclination (depths of ~3.5 m, 5 m, and 10 m; Fig. 7) have been identified along the borehole 1, two of them being close to the stratigraphic position of the archaeological levels. However, because some of the data are obtained from the analysis of a single sample only, they should be interpreted with caution. In addition, such positive polarities have not been previously identified by Oms et al. (2000b; 2003). For these reasons these data are represented in gray (Fig. 7). The values from borehole 2 show intervals that are clearly positive (represented in black at depths of ~6 m, 8.5–9.0 m and >10 m; Fig. 7). These intervals are stratigraphically below the sequence studied by Oms, so from layers that have not previously been sampled. Even though our data

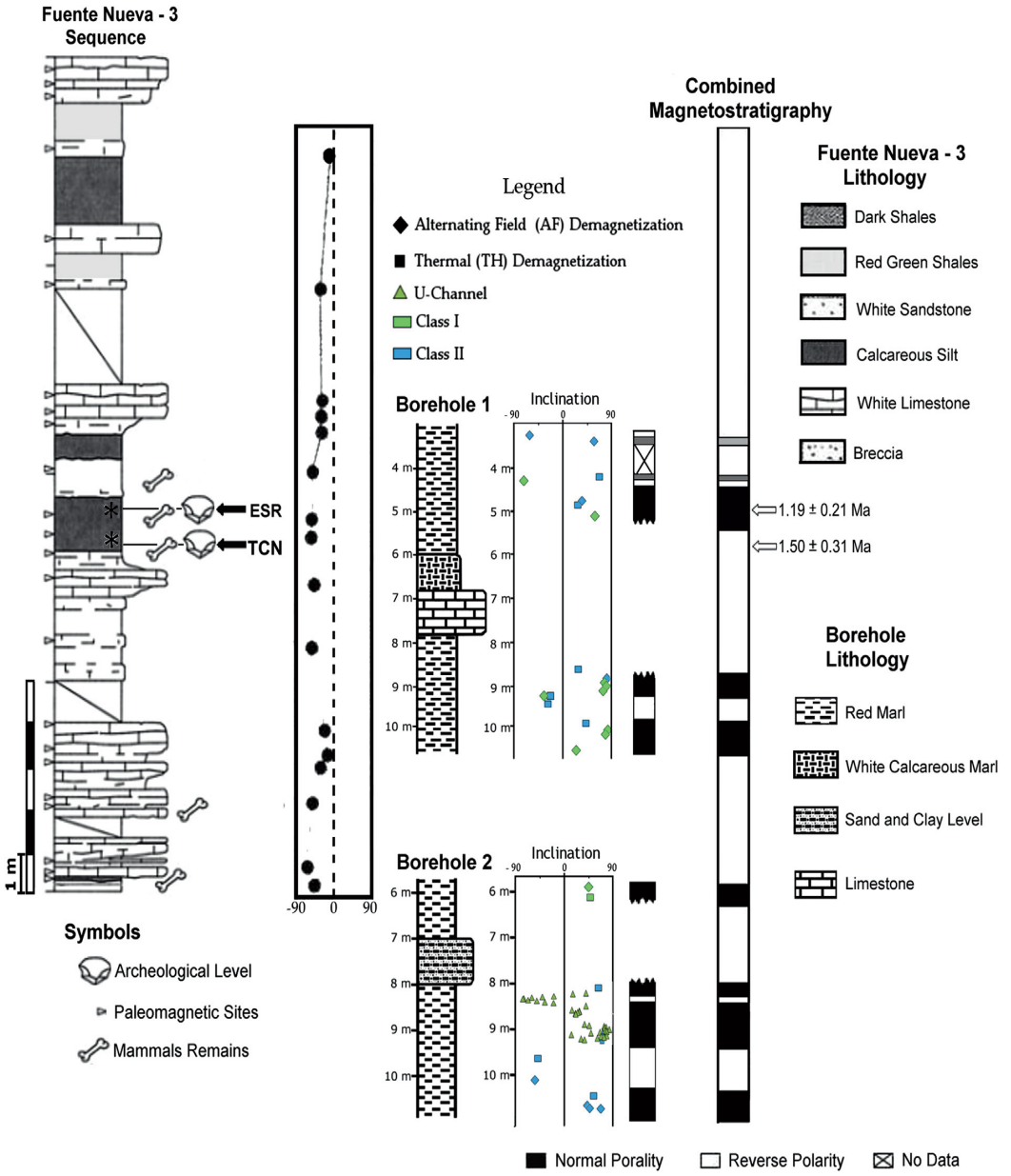

Fig. 7. Comparison of the polarity obtained by Oms et al. (2003) to that obtained in this study. The sequence described by Oms et al. (2003) is indicated on the left; we only show the interval of the each borehole that have provided paleomagnetic results although maintained in the corresponding position with respect to the vertical column stratigraphic from Fuente Nueva 3 (see Fig. 3). The gray bar in the combined magnetostratigraphy denotes a single sample.

are based on inclination only, the stability of AF demagnetization directions, the absence of weathering in the sampled lithologies, and the presence of several consecutive specimens with constant inclination, give us confidence that the ChRM directions are primary and not a recent overprint or artifact. Unfortunately, given the lithology of the deposits, u-channel sampling has been only possible on a small portion of the borehole 2. With the available data we cannot tell whether these three intervals represent a single normal polarity chron; further sampling is warranted.

Additional chronometric dating helps to anchor the local magnetostratigraphy to the Geomagnetic Polarity Time Scale (GPTS). Previous combined U-series/electron spin resonance (US-ESR) dating of one tooth from the upper archaeological level of FN-3 yielded an age of 1.19 ± 0.21 Ma (Duval et al., 2012b). Our cosmogenic nuclide burial dating with ^{26}Al and ^{10}Be in quartz grains gives a minimum age of 1.50 ± 0.31 Ma (1σ uncertainty). Being aware that this age corresponds to a single sample of 2 L (with a 2σ relative uncertainty range of 40%) and the intrinsic limitations discussed above (see Material and Methods, 3.2 section), we need to be cautious with the burial age. The age provided by the cosmogenic nuclides is consistent at 1σ with the US-ESR age and overall in agreement with the paleomagnetic data. The locality of Barranco León, about 3 km W from Fuente Nueva and considered as biochronologically coeval (e.g. Agusti et al., 2007) has recently been studied for ESR dating of optically quartz grains and produced a weighted mean ESR age of 1.43 ± 0.38 Ma for the layer BL-D (Toro-Moyano et al., 2013). This age is in agreement with the new chronology obtained at FN-3. Nevertheless, the

limited precision of these ages does not allow us to establish a meaningful correlation between both sites. Additional samples for cosmogenic nuclide analysis could help improve the precision of the burial age as well as confirm that the samples had no prior burial history.

Taken together, the numerical ages and the new magnetostratigraphy seem to support a Matuyama age for the sediments, and most likely within its upper part and below the Jaramillo subchron. However, we are aware of the margin of error of the ages (both from ESR and cosmogenic nuclides). The paleomagnetic data obtained in this study, reveal that the long reverse chron reported by Oms et al. (2003) is punctuated, in its lower part, by very short intervals with positive inclination. Should these intervals correspond to short periods of normal polarity, they ought to be Olduvai or younger. Additional magnetostratigraphic data (Scott et al., 2007) indicate that the Olduvai Subchron might have been recorded along the stratigraphic section of "Mojona Mine", about 2.5 km west of Fuente Nueva. Oms et al. (2011) suggests that the normal polarity chron at Mojona Mine has to be older, presumably Gauss, based on the integration of all available stratigraphy and biostratigraphy. A number of very short polarity intervals have been identified between Olduvai and Jaramillo Subchrons, including (from old to young) Gilsa (~1.6 Ma), Gardar (~1.5 Ma), Bjorn (~1.3 Ma), Cobb Mountain (~1.2 Ma) and Punaruu (~1.1 Ma) (Singer et al., 1999; Channell et al., 2002); therefore it is likely that we recovered some of those short polarity intervals. These short normal polarity events have been barely identified in the Guadix-Baza basin (e.g. Gilbert et al., 2007; Pla-Pueyo et al., 2011). A more precise correlation of the newly obtained magnetostratigraphy to the Geomagnetic Polarity Time Scale (GPTS) is not possible with the current data set, given the intrinsic uncertainty of the positive inclinations, as well as the uncertainty on numerical ages. Nonetheless, we can use the sediment accumulation rate (SAR) to develop hypotheses to explain these positive magnetization directions at the bottom of the FN-3 section. Based on the normal polarity interval at the "Mojona Mine", Scott et al. (2007) infer a SAR of 9 cm/ky. In their recent study on the geology and chronology of the upper member of the Baza Fm., Oms et al. (2011) re-analyzed the normal magnetozone at Mojona Mine and suggested it could in fact correspond to Gauss, implying a SAR of about 4 cm/ky. The top of the Mojona Mine normal chron is about 44 m below the stratigraphic layers dated in this study. We use the re-evaluated interpretation of La Mojona section in Fig. 8, to try to infer the hypothetical location of Olduvai Subchron at FN-3. A rough estimation of the chronology of the site may be obtained by considering a weighted mean age derived from US-ESR and burial ages in combination with the SAR.

The SAR of 4 cm/ky implied that the top of the observed normal magnetization directions at Fuente Nueva would have an age of around 1.5 Ma, i.e. not far from the age of the top of Olduvai (1.77 Ma). Nevertheless, considering the uncertainties related to (1) age dating, (2) accumulation rate and (3) thickness of the composite section, some (if not all) of the positive inclinations that are observed at the bottom of the section could alternatively correspond to short polarity intervals such as Gardar or Gilsa. Further investigation will be necessary to elucidate the precise origin of the normal polarity intervals found along the section of Fuente Nueva.

5. Conclusion

The current magnetostratigraphic record at FN-3 is consistent with a period of dominantly reverse polarity, punctuated at the bottom by short polarity intervals, such as the time interval between 1.77 and 1.07 Ma, as supported by both the US-ESR ages and cosmogenic nuclide burial dating. Overall, the combined magnetostratigraphic constraint and both ESR and burial ages suggest that the stratigraphic unit containing the archaeopaleontological site of Fuente Nueva 3 has a pre-Jaramillo age, in agreement with the recent ages obtained at the nearby site of Barranco León (Oms et al., 2000b; Toro-Moyano et al., 2013). Some authors (as Muttoni et al., 2013) suggest that a more accurate age for the sites from Orce (specifically Barranco León) is below 0.78 Ma (Brunhes – Matuyama limit) but above the Jaramillo subchron. The paleomagnetic data obtained in this study show short intervals of normal polarity (directions with positive inclination at the bottom of the composite section) which have not been found in other sites of the basin. With that in mind, we are aware that establishing a pre Jaramillo age with these data is risky, especially given the limitations of the cosmogenic nuclides results. However, despite the criticisms by Muttoni et al. (2013), the age provided by Duval (2008) and Duval et al. (2011, 2012a, 2012b) are consistent with the biostratigraphic data, not only with the microfauna analysis (Agustí et al., 2010) but also with the large mammals (Martínez Navarro et al., 2010) which collectively indicate an age of Fuente Nueva of Early Pleistocene, below the age of Jaramillo subchron. This inference, along with the sedimentation rate inferred by Scott et al. (2007), allow us to develop the hypothesis that the sequence of Fuente Nueva-3 studied in this paper could have an age between the Olduvai and Jaramillo subchrons. Future work should include

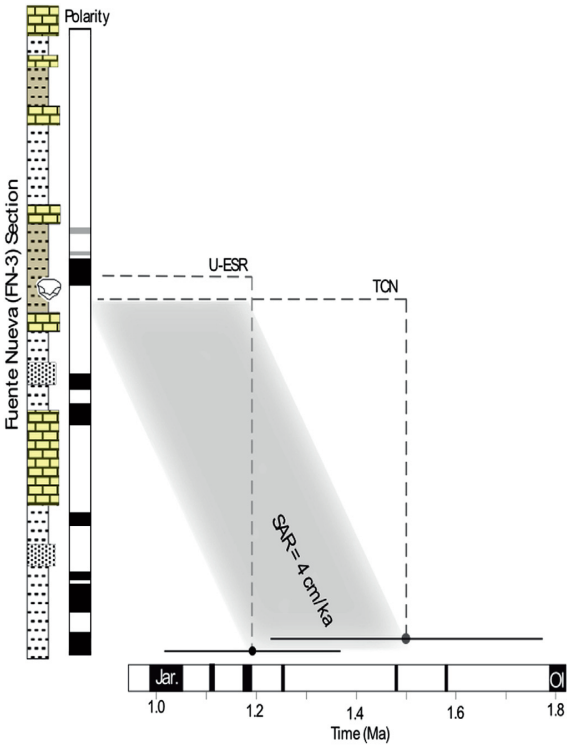

Fig. 8. Combined magnetostratigraphy and suggested correlation of the composite section obtained at FN-3 with the Geomagnetic Polarity Time Scale (GPTS) (Numerical ages by Singer et al. 1999). Short normal chrons between Olduvai and Jaramillo are from right to left: Gilsa, Gardar, Bjorn, Cobb Mountain and Punaruu. A weighted mean age has been computed by combining US-ESR and TCN burial ages. A sediment accumulation rate (SAR) of 4 cm/ka (Oms et al., 2011) has been used to infer the approximated chronology of the positive intervals identified at the bottom of the sequence. The horizontal bar shows the 1σ uncertainties on the numerical. ages for FN-3.

additional sampling for paleomagnetism, as well as for ESR and cosmogenic nuclide burial dating, to better constrain the chronology of FN-3 and confirm our hypothesis.

Acknowledgements

The following research projects contributed to this study: B090678SV18BC (Dirección General de Bienes Culturales, Junta Andalucía): (PI R. Sala); CGL2010-16821 (MINECO): (PI J.M. Parés). MD is currently the recipient of an International Outgoing Fellowship from the People Programme (Marie Curie Actions) of the European Union's Seventh Framework Programme (FP7/2007-2013) under REA grant agreement PIOF-GA-2013-626474. The authors also would like to thank the editor and the reviewers, the time spent in this paper and we appreciate the comments.

References

Agustí, J., 1985. Bioestratigrafía de los depósitos Plio-Pleistocenos de la depresión Guadix–Baza. Paleontología i Evolució 18, 13–18.
Agustí, J., Martin Suarez, E., 1984. El Plioceno continental de la depresión Guadix–Baza (Prov. Granada) y su fauna de micromamíferos. Nota preliminar. Acta Geológica Hispánica 19, 277–281.
Agustí, J., Moyà-Solà, S., Pons-Moya, J., 1987. La sucesión de Mamiferos en el Pleistoceno inferior de Europa: Proposición de una nueva escala bioestratigráfica. Paleontología y Evoluciò, Memoria Especia 1, 287–295.
Agustí, J., Oms, O., Parés, J.M., 1999. Calibration of the Early-Middle Pleistocene transition in the continental beds of the Guadix–Baza basin (SE Spain). Quaternary Science Reviews 18, 1409–1417.
Agustí, J., Cabrera, L., Garcés, M., Krijgsman, W., Oms, O., Parés, J.M., 2001. A calibrated mammal scale for the Neogene of Western Europe. State of the art. Earth Science 52, 247–260.
Agusti, J., Oms, O., Pares, J.M., 2007. Biostratigraphy, paleomagnetism and geology of the Orce ravine (Southern Spain). Comment on the paper by Gibert et al., 2006. Quaternary Science Reviews 26, 568–572.
Agustí, J., Blain, H.-A., Furió, M., Marfá, R. d, Santos-Cubedo, A., 2010. The early Pleistocene small vertebrate succession from the Orce region (Guadix–Baza basin, SE Spain) and its bearing on the first human occupation of Europe. Quaternary International 223, 162–169.
Anadón, P., Julià, R., Oms, O., 2003. Estratigrafía y estudio sedimentológico preliminar de diversos afloramientos en Barranco León y Fuente Nueva (Orce, Granada). Memoria científica campañas 1999-2002. In: Toro, I., Agustí, J., Martínez-Navarro, B. (Eds.), El Pleistoceno Inferior de Barranco León y Fuente Nueva 3, Orce (Granda), Arqueología Monografías. Consejería de Cultura, Junta de Andalucía, Sevilla, pp. 47–72.
Arribas, A., Palmqvist, P., 1998. Taphonomy and Palaeoecology of an assemblage of large mammals: hyaenid activity in the Lower Pleistocene site at Venta Micena (Orce, Guadix–Baza basin, Granada, Spain). Geobios 31, 3–47.
Channell, J., Mazaud, A., Sullivan, P., 2002. Geomagnetic excursions and paleointensities in the Matuyama Chron at Ocean drilling program sites 983 and 984 (Iceland Basin). Journal of Geophysical Research: Solid Earth 107, 1–14.
Duval, M., 2008. Evaluation du potentiel de la méthode de datation par Résonance de Spin Electronique (ESR) appliquée aux gisements du Pléistocène inférieur: étude des gisements d'Orce (bassin de Guadix–Baza, Espagne) et contribution à la connaissance des premiers peuple. Thèse pour obtenir le grade de docteur du Muséum national d'Histoire naturelle, Paris, 1–522. (inédit).
Duval, M., Falguères, C., Bahain, J.-J., GrÃün, R., Shao, Q., Aubert, M., Hellstrom, J., Dolo, J.M., Agustí, J., Martínez-Navarro, B., Plamqvist, P., Toro-Moyano, I., 2011. The challenge of dating early pleistocene fossil teeth by the combined uranium series-electron spin resonance method: the Venta Micena palaeontological site (Orce, Spain). Journal of Quaternary Science 26, 603–615.
Duval, M., Falguères, C., Bahain, J.-J., 2012a. Age of the oldest hominin settlements in Spain: contribution of the combined U-series/ESR dating method applied to fossil teeth. Quaternary Geochronology 10, 412–417.
Duval, M., Falguères, C., Bahain, J.J., Grün, R., Shao, Q., Aubert, M., Dolo, J.M., Agustí, J., Martínez-Navarro, B., Palmqvist, P., Toro-Moyano, I., 2012b. On the limits of using combined U-series/ESR method to date fossil teeth from two Early Pleistocene archaeological sites of the Orce area (Guadix–Baza basin, Spain). Quaternary Research 77, 482–491.
Garcés, M., Agustí, J., Parés, J.M., 1996. Magnetocronología del Plioceno superior continental de la cuenca de Guadix–Baza. Geogaceta 20, 1033–1036.
Garcés, M., Agustí, J., Parés, J.M., 1997. Late Pliocene continental magnetochronology in the Guadix–Baza basin. Earth and Planetary Science Letters 146, 677–687.
García Aguilar, J.M., 2010a. Estratigrafía y sedimentología del yacimiento paleontológico Fuente Nueva 3 (Orce, España). In: Toro, I., Martínez-Navarro, B., Agustí, J. (Eds.), Ocupaciones humanas en el pleistoceno inferior y medio de la cuenca de Guadix–Baza, Arqueología Monografías. Consejería de Cultura, Junta de Andalucía, Sevilla, pp. 39–55.
García Aguilar, J.M., 2010b. Ciclicidad sedimentaria de materiales lacustres de la cuenca Guadix–Baza (Granada). In: Toro, I., Martínez-Navarro, B., Agustí, J. (Eds.), Ocupaciones humanas en el pleistoceno inferior y medio de la cuenca de Guadix–Baza, Arqueología Monografías. Consejería de Cultura, Junta de Andalucía, Sevilla, pp. 25–37.
García Aguilar, J.M., Martín, J.M., 2000. Late Neogene to recent continental history and evolution of the Guadix–Baza basin (SE Spain). Revista de la Sociedad Geológica de España 12, 65–78.
García-Aguilar, J.M., Palmqvist, P., 2011. A model of lacustrine sedimentation for the Early Pleistocene deposits of Guadix–Baza basin (southeast Spain). Quaternary International 243, 3–15.
Gibert Beotas, L., Scott, G.R., Ferràndez-Cañadell, C., 2006. Evaluation of the Olduvai subchron in the Orce ravine (SE Spain). Implications for Plio-Pleistocene mammal biostratigraphy and the age of Orce archeological sites. Quaternary Science Reviews 25, 507–525.
Gibert Beotas, L., Scott, G.R., Martin, R., Gibert i Clols, J., 2007. The Early to Middle Pleistocene boundary in the Baza Basin (Spain). Quaternary Science Reviews 26, 2067–2089.
Granger, D.E., 2006. A review of burial dating methods using ^{26}Al and ^{10}Be. In: Alonso-Zarza, A.M., Tanner, L.H. (Eds.), In situ-produced Cosmogenic Nuclides and Quantification of Geological Processes, Geological Society of America Special Papers, vol. 415, pp. 1–16.
Granger, D.E., Muzikar, P., 2001. Dating sediment burial with cosmogenic nuclides: theory, techniques, and limitations. Earth and Planetary Science Letters 188, 269–281.
Granger, D.E., Schaller, M., 2014. Cosmogenic Nuclides and Erosion at the Watershed Scale. Elements 10, 369–373.
Head, J.W., Marchant, D.R., Dickson, J.L., Kress, A.M., Baker, D.M., 2010. Northern mid-latitude glaciation in the Late Amazonian period of Mars: Criteria for the recognition of debris-covered glacier and valley glacier landsystem deposits. Earth Planetary Science Letters 294, 306–320.
Hu, X., Kirby, E., Pan, B., Granger, D.E., Su, H., 2011. Cosmogenic burial ages reveal sediment reservoir dynamics along the Yellow River, China. Geology 39, 839–842.
Hüsing, S., Oms, O., Agustí, J., Garcés, M., Kouwenhoven, T., Krijgsman, W., Zachariasse, W.-J., 2010. On the late Miocene closure of the Mediterranean-Atlantic gateway through the Guadix basin (southern Spain). Palaeogeography, Palaeoclimatology, Palaeoecology 291, 167–179.
Martínez-Navarro, B., Turq, A., Ballester, J.A., Oms, O., 1997. Fuente Nueva-3 (Orce, Granada, Spain) and the first human occupation of Europe. Journal of Human Evolution 33, 611–620.
Martínez-Navarro, B., Palmqvist, P., Madurell-Malapeina, J., Ros-Montoya, S., Espigares, M.P., Torregrosa, V., Pérez-Claros, J.A., 2010. Lafauna de grandes mamíferos de Fuente Nueva 3 y Barranco León 5. Estado de la cuestión. In: Toro, I., Martínez-Navarro, B., Agustí, J. (Eds.), Ocupaciones humanas en el pleistoceno inferior y medio de la cuenca de Guadix–Baza, Arqueología Monografías. Consejería de Cultura, Junta de Andalucía, Sevilla, pp. 197–236.
Merrill, R.T., McElhinny, M.W., McFadden, P.L., 1998. The magnetic field of the Earth paleomagnetism, the core, and the deep Mantle. International Geophysics 63, 531.
Muttoni, G., Scardia, G., Kent, D.V, 2013. A critique of evidence for human occupation of Europe older than the Jaramillo subchron (~1 Ma): comment on "The oldest human fossil in Europe from Orce (Spain)" by Toro-Moyano et al. (2013). J. Hum. Evol. 65, 746–749.
Nishiizumi, K., 2004. Preparation of ^{26}Al AMS standards. Nuclear Instruments and Methods in Physics Research Section B: Beam Interactions with Materials and Atoms 223, 388–392.
Nishiizumi, K., et al., 2007. Absolute calibration of 10Be AMS standards. Nuclear Instruments and Methods in Physics Research Section B: Beam Interactions with Materials and Atoms 258, 403–413.
Oms, O., Garcés, M., Parés, J.M., Agustí, J., Anadón, P., Julià, R., 1994. Magnetostratigraphic characterization of a thicker Lower Pleistocene lacustrine sequence from the Baza Basin (Betic Chain, Southern Spain). Physics of the Earth and Planetary Interiors 85, 173–180.
Oms, O., Dinarès-Turell, J., Parés, J.M., 1996. Resultados paleomagnéticos iniciales de la sección Plio-Pleistocena de Fuente Nueva (Cuenca de Guadix–Baza, Cordilleras Béticas). Revista de la Sociedad Geológica de España 9, 89–95.
Oms, O., Agustí, J., Gabàs, M., Anadón, P., 2000a. Lithostratigraphical correlation of micromammal sites and biostratigraphy of the Upper Pliocene to Lower Pleistocene in the Northeast Guadix–Baza basin. Journal of Quaternary 15, 43–50.
Oms, O., Parés, J.M., Martínez-Navarro, B., Agustí, J., Toro, I., Martínez-Fernández, G., Turq, A., 2000b. Early human occupation of Western Europe: paleomagnetic dates for two paleolithic sites in Spain. Proceedings of the National Academy of Sciences of the United States of America 97, 10666–10670.
Oms, O., Parés, J.M., Agustí, J., 2003. Datación Magnetoestratigráfica de los yacimientos de Fuente Nueva 3 y Barranco León 5 (Orce, Granada). Memoria científica campañas 1999-2002. In: Toro, I., Agustí, J., Martínez-Navarro, B. (Eds.), El Pleistoceno Inferior de Barranco León y Fuente Nueva 3, Orce (Granda), Arqueología Monografías. Consejería de Cultura, Junta de Andalucía, Sevilla, pp. 105–114.
Oms, O., Agustí, J., Anadón, P., 2010a. El plioceno superior – pleistoceno inferior en el sector Galera-Orce-Fuente Nueva de le cuenca Guadix–Baza. In: Toro, I., Martínez-Navarro, B., Agustí, J. (Eds.), Ocupaciones humanas en el pleistoceno inferior y medio de la cuenca de Guadix–Baza, Arqueología Monografías. Consejería de Cultura, Junta de Andalucía, Sevilla, pp. 97–105.

Oms, O., Agustí, J., Parés, J.M., 2010b. Litoestratigrafía, magnetoestratigrafía y bioestratigrafía de los yacimientos de Barranco León 5 y Fuente Nueva 3. In: Toro, I., Martínez-Navarro, B., Agustí, J. (Eds.), Ocupaciones humanas en el pleistoceno inferior y medio de la cuenca de Guadix–Baza, Arqueología Monografías. Consejería de Cultura, Junta de Andalucía, Sevilla, pp. 107–119.

Oms, O., Anadón, P., Agustí, J., Julià, R., 2011. Geology and chronology of the continental Pleistocene archeological and paleontological sites of the Orce area (Baza basin, Spain). Quaternary International 243, 33–43.

Parés, J.M., Dinarès-Turell, J., 1997. Estado actual de las investigaciones paleomagnéticas en la cuenca de Guadíx-Baza (Cordilleras Béticas). Geogaceta 22, 137–T39.

Peña, J.A., 1985. La depresión de Guadix–Baza. Estudios Geológicos 41, 33–46.

Pla, S., 2009. Contexto estratigráfico y sedimentario de los yacimientos de grandes mamíferos del sector central de la cuenca de Guadix (Cordillera Bética). Tesis Doctoral. Universidad de Granada, 1–273. http://digibug.ugr.es/handle/10481/2373.

Pla, S., 2010. Encuadre estratigráfico de los más significativos yacimientos de macromamíferos continentales localizados en el marco del Proyecto Fonelas (límite Plioceno-Pleistoceno, Cuenca de Guadix, Granada. Boletín Geológico y Minero 117, 483–489.

Pla, S., Viseras, C., Soria, J.M., Tent-Manclús, J.E., Arribas, A., 2011. A stratigraphic framework for the Pliocene-Pleistocene continental sediments of the Guadix basin (Betic Cordillera, S. Spain). Quaternary International 243, 16–32.

Rook, L., Martínez-Navarro, B., 2010. Villafranchian: the long story of a Plio-Pleistocene European large mammal biochronologic unit. Quaternary International 219, 134–144.

Sanz de Galdeano, C., 1990. Geologic evolution of the Betic Cordilleras in the Western Mediterranean, Miocene to the present. Tectonophysics 172, 107–119.

Sanz de Galdeano, C., Vera, J.A., 1992. Stratigraphic record and palaeogeographical context of the Neogene basins in the Betic Cordillera, Spain. Basin Research 4, 23–36.

Scott, G.R., Gibert Beotas, L., Gibert i Clols, J., 2007. Magnetostratigraphy of the Orce region (Baza Basin), SE Spain: new chronologies for Early Pleistocene faunas and hominin occupation sites. Quaternary Science Reviews 26, 415–435.

Singer, B., Hoffman, K., Chauvin, A., 1999. Dating transitionally magnetized lavas of the late Matuyama Chron: toward a new $^{40}Ar/^{39}Ar$ timescale of reversals and events. Journal of Geophysical Research: Solid Earth 104, 679–693.

Stone, J.O., 2000. Air pressure and cosmogenic isotope production. Journal of Geophysical Research 105, 23753–23759.

Toro, I., Turq, A., Agustí, J., Martínez-Navarro, B., Oms, O., 2000. Los yacimientos del pleistoceno inferior de Barranco León y Fuente Nueva 3 de Orce (Granada). Contribución al conocimiento del primero poblamiento humano de Europa. Revista de prehistoria y arqueología de la Universidad de Sevilla 9, 179–188.

Toro, I., Barsky, D., Cauche, D., Celiberti, V., Grégoire, S., Lebegue, F., Moncel, M.H., De Lumley, H., 2011. The archaic stone tool industry from Barranco León and Fuente Nueva 3, (Orce, Spain): evidence of the earliest hominin presence in southern Europe. Quaternary International 243, 80–91.

Toro-Moyano, I., Martínez-Navarro, B., Agustí, J., Souday, C., Bermúdez de Castro, J.M., Martinón-Torres, M., Fajardo, B., Duval, M., Falguères, C., Oms, O., Parés, J.M., Anadón, P., Julià, R., García-Aguilar, J.M., Moigne, A.-M., Espigares, M.P., Ros-Montoya, S., Palmqvist, P., 2013. The oldest human fossil in Europe, from Orce (Spain). Journal of Human Evolution 65, 1–9.

Vera, J.A., 2000. El Terciario de la Cordillera Bética: estado actual de conocimientos. Boletín de la Sociedad Geológica de España 13, 345–373.

Vera, J.A., Fernández, J., López-Garrido, A.C., Rodríguez-Fernández, J., 1984. Geología y estratigrafía de los materiales plioceno- pleistoceno del sector Orce- Venta Micena (Prov. Granada). Paleontología i Evolució 18, 3–12.

Viseras, C., Fernandez, J., 1992. Sedimentary basin destruction inferred from the evolution of drainage systems in the Betic Cordillera, southern Spain. Journal of the Geological Society 149, 1021–1029.

Viseras Alarcón, C., Soria Mingorance, J.M., Durán Valsero, J.J., Arribas Herrera, A., 2003. Contexto geológico y sedimentario del yacimiento de grandes mamíferos Fonelas P-1 (Cuenca de Guadix, Cordillera Bética). Geo Temas 5, 247–250.

Zijderveld, J.D.A., 1967. A.C. demagnetization of rocks: analysis of results. In: Collinson, D.W., Creer, K.M., Runcorn, S.K. (Eds.), Methods of Paleomagnetism. Elsevier Science, New York, pp. 254–268.

Capítulo 5 . new magnetostratigraphic evidence for the age of acheulean tools at the archaeo-palaeontological site "solana del zamborino" (guadix-baza basin, s spain)

www.nature.com/scientificreports

SCIENTIFIC REPORTS

OPEN

New magnetostratigraphic evidence for the age of Acheulean tools at the archaeo-palaeontological site "Solana del Zamborino" (Guadix – Baza Basin, S Spain)

Received: 2 May 2017
Accepted: 2 October 2017
Published online: 18 October 2017

C. Álvarez-Posada[1], J. M. Parés[1], R. Sala[2], C. Viseras[3] & S. Pla-Pueyo[4]

The sedimentary record in the Guadix-Baza Basin (southern Spain) has proved to be a great source of information for the Miocene through the Pleistocene periods, due to the abundant faunal remains preserved, in some cases associated with lithic tools. The Solana del Zamborino (SZ) section has been the subject of controversy ever since a magnetostratigraphic analysis resulted in an age of 750–770 Kyr for Acheulean tools, a chronology significantly older than the ~600 Kyr established chronology for the first Acheulean record in Europe. Although recent findings at the "Barranc de la Boella" site (north-east of the Iberian Peninsula) seem to indicate that an earlier introduction of such technique in Europe around 0.96–0.781 Ma is possible, the precise age of the classical site at SZ is still controversial. The aim of this paper is to constrain the chronology of the site by developing a longer magnetostratigraphic record. For this purpose, we carried out an exhaustive sampling in a new succession at SZ. Our results provide a ~65 m magnetostratigraphic record in which 4 magnetozones of normal polarity are found. Our new magnetostratigraphic data suggest an age range between 300–480 Kyr for the lithic tools, closer to the age of traditional Acheulean sites in Europe.

The Guadix-Baza basin, located in the Betic Mountain Range (southern Spain) contains the most complete sedimentary record in Spain throughout the Miocene to Pleistocene epochs[1–5], including well known palaeontological sites such as Orce, Huéscar, Venta Micena, Fonelas, Barranco León and the three sites of Fuente Nueva locality, which have provided abundant faunal information critical for the Plio-Pleistocene boundary[6–12]. Specifically, sites such as Solana del Zamborino (SZ hereafter) have produced abundant lithic tools that have been claimed to be the oldest Acheulean tools in Europe[13]. The aim of this study is to provide a solid and more complete chronological framework for SZ. Our results are based on new magnetostratigraphy that covers approximately over 65 meters of section, complementing the previous results by Scott and Gibert[13].

Solana del Zamborino is located in the Guadix-Baza Basin (one of the more prominent post-orogenic intramontane depressions of the Betic Range) and developed during the Miocene, with a NE-SW orientation[2,14]. The basin was flooded by sea water during the Tortonian and marine sediments were deposited[15]. Subsequently, the basin was isolated from the sea, due to tectonic tilting related to the activation of a NE-SW fault system, and filled with continental sediments from the late Tortonian to the Upper Pleistocene[16]. During the Villafranchian stage, the basin was divided in two sub-basins separated by a topographic elevation: the Baza sub-basin to the NE and the sub-basin of Guadix to the SW[16]. The Guadix sub-basin holds an abundance of terrigenous sediments, including conglomerates and sands which were deposited by rivers, alluvial fans and lacustrine fan deltas, fed by the surrounding reliefs[17–22].

[1]Geochronology Program, CENIEH, Paseo Sierra de Atapuerca 3, 09002, Burgos, Spain. [2]IPHES (Institut Català de Paleoecologia Humana i Evolució Social). Área de Prehistòria, Universitat Rovira i Virgili, Campus Sescelades-URV, Edifici W3, 43007, Tarragona, Spain. [3]Dpto. Estratigrafía y Paleontología, Facultad de Ciencias, Universidad de Granada, 18071, Granada, Spain. [4]Heriot-Watt University, Edinburgh, EH14 4AS, United Kingdom. Correspondence and requests for materials should be addressed to C.Á.-P. (email: claudiaalvarezposada@gmail.com)

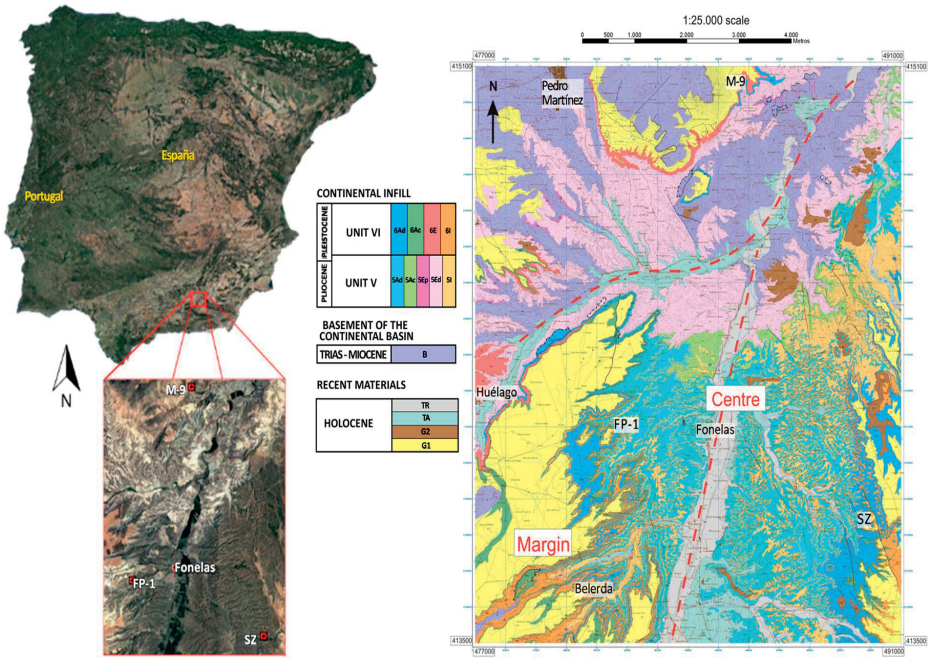

Figure 1. Location of the paleontological sites of Solana del Zamborino (SZ), Mencal (M-9), and Fonelas (FP-1) using Google Earth free program (version 7.1.8.3036. Map data: Google, Digital Globe). The lithostratigraphic map of the Fonelas-Mencal area was created by Pla-Pueyo[20] and digitalised using ArcGis 9.1. (http://www.esri.com/arcgis/about-arcgis). An online version of the map can be found in http://hdl.handle.net/10481/2373. Legend: **TR**, recent terraces; **TA**, ancient terraces; **G2**, glacis 2; **G1**, glacis 1; **5Ad**, luddites, sands and gravels (locally palustrine carbonates), Detrital Axial System; **5Ac**, palustrine-lacustrine limestones (locally tufa), Axial System carbonates; **5Ep**, blocks and gravels, Proximal External Transverse System; **5Ed**, sands, shales and gravels, distal External Transverse System; **5I**, gravel, sand and shale (locally palustrine-calcrete carbonates), External Transverse System; **6Ad**, sands and shales (locally palustrine-lacustrine carbonates), Detrital Axial System; **6Ac**, palustrine-lacustrine carbonates (locally shale), Carbonate Axial System; **6E**, breccia, gravel, sand and shale, External Transverse System, **6I**, gravel, sand and shale, External Transverse System; **B**, basement.

The site targeted for this study is located on the western sector of the Guadix-Baza Basin, where only the Guadix and Gorafe-Huélago formations are exposed (the two lithostratigraphic units that have survived after the different nomenclatures established over time[23–25]). Deposits are horizontal to sub-horizontal and include frequent lateral facies changes; these fluvial deposits are the two most recent units of the continental landfill of the basin, named as units V and VI[20] (Fig. 1). The archaeo-paleontological site of SZ is in the eastern sector of the Guadix sub-basin[21], (Fig. 1), and within the youngest stratigraphic unit (VI, with an age that corresponds to the lower limit of Olduvai subchron, 1.778 My[22]), and south of the highest lacustrine intercalation in Guadix formation as described by Casas *et al.*[24]. Within the site, stratigraphic levels have been traditionally named alphabetically from A to F (from bottom to top) and their detailed description and characteristics are fully included in Casas *et al.*[24].

The excavation consists of an open quarry (Fig. 2), in what is known as "Llano de Zamborino" which began as a palaeontological site excavated in 1972 by members of the Department of Prehistory at the University of Granada, led by Botella[26–28]. The quarry has yielded an abundance of skeletal remains and lithic tools, found in an ensemble of layers composed mainly of silts and grey claystone. The stratigraphic, faunal and lithic studies[24,29,30] have allowed for interpretation of the human occupation of the site, ranging from occasional hunting place to a permanent settlement during periods of hunting and finally to progressive abandonment[26,28,31].

Materials and Methods

During the years 2014 and 2015, two paleomagnetic campaigns were carried out at the site of Solana del Zamborino, in order to obtain as complete magnetostratigraphic record as possible. For this purpose, a stratigraphic column of the section to be sampled was measured. Since the study area is dissected by several badlands, the process consisted of developing two parallel stratigraphic columns. Because beds are flat lying it has been possible to correlate both sections, which overlap 13.5 meters. Therefore, a composite stratigraphic section of about 80 meters was obtained (Fig. 3). This section is predominantly composed of silty-clay sediments, which have determined the process of sampling. The first sampling technique involved retrieving a compact block using a ceramic knife, while for the second consisted of using a cylindrical non-magnetic device sliced longitudinally into two halves and inserted by hammering into the sediment. In both cases, diluted sodium silicate solution was used to preserve the integrity of the sample. All samples were oriented *in situ* with a standard compass and clinometer.

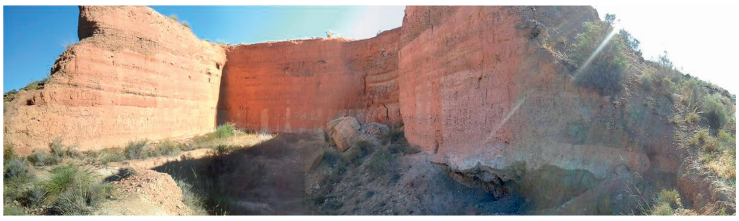

Figure 2. Current state of the paleontological site of Solana del Zamborino. Photograph taken by Claudia Álvarez-Posada. The walls of the quarry are approximately 12 meters in height.

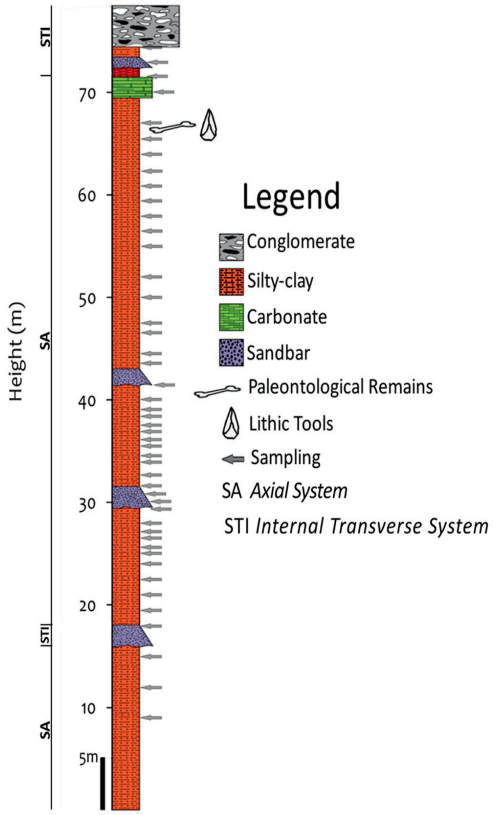

Figure 3. Stratigraphic succession obtained in this study, resulting from combining two parallel sequences measured in SZ in the years 2014 and 2015.

The SZ section is dominated by green-grey fluvial sediments from the fluvial Axial System. Redder sediments corresponding to several progradations of the Internal Transverse System alluvial fans are intercalated among them. From bottom to almost to the top, the sequence predominantly comprises fine-grained sediments (Fig. 3). Towards the middle part of the section, some coarser-grained beds appear. This lithofacies association can be interpreted as a distal fluvial flood plain, subjected to sporadic periods of ponding and into which sandy sediments come from the overbank of fluvial channels[19–21,32]. The top of the site section is marked by palustrine carbonates, a thin layer of clay, and a bed of conglomerates about two meters thick, related to an important progradation of alluvial fan sediments from the Internal Transverse System into the axial valley.

We sampled every meter and a half or less, whenever possible, in a total of 47 sampling sites from which we have obtained 367 individual samples (between 8 cm^3 and 11 cm^3 depending on the process by which the samples were obtained).

The measurement of the natural remanent magnetization (NRM) of the specimens and the progressive demagnetisation was carried out in two different laboratories: a preliminary analysis was carried out in the laboratory of Paleomagnetism and Rock Magnetism at the University of Oxford (England) on a pilot set of specimens. Low field magnetic susceptibility was measured with a Kappabridge model KLY2 with a CS3 oven incorporated.

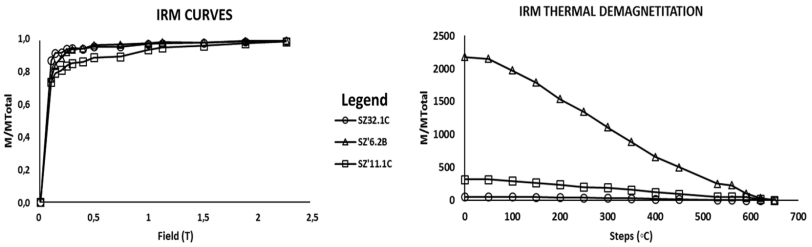

Figure 4. Example of *isothermal remanent magnetization* (IRM) acquisition curves and their respective thermal demagnetisation for some representative specimens. Each symbol corresponds a different sample. Notice a rapid increase in the IRM at fields lower than 1 T (between 300 and 400 mT) and unblocking temperatures just below 600 °C, suggesting magnetite as the main carrier of stable magnetization.

Further analyses were carried out using a cryogenic magnetometer 2 G enterprises DC including an online degausser for alternating field (AF) demagnetization. Subsequently, the remaining specimens were processed at the National Research Center for Human Evolution (CENIEH, Burgos), using an TD-48SC oven (ASC Scientific) for thermal (TH) demagnetization, a cryogenic magnetometer 2 G model 755R-4K with a built in degausser system for AF demagnetization up to 170 mT, and an Impulse Magnetizer, model IM-10–30 (ASC Scientific) for isothermal remanent magnetization (IRM) acquisition curves.

Of the 367 samples obtained, 316 have been analysed, 32 of which have been used to obtain IRM acquisition curves. From the remaining 284 specimens, 175 were analysed by TH demagnetisation with progressive steps of 30°C until 420°C and then increasing the steps to 50 °C up to 670 °C; and the last 109 specimens were analysed using AF to a maximum field of 0.1 T. Finally, after visual inspection of the Zijderveld diagrams, the characteristic remanent magnetization (ChRM) direction, the highest stability component of the NRM, was determined and computed for each specimen using Principal Component Analysis[33], typically anchoring the directions to the origin. We used the Fisherian mean direction[34] of the ChRM to calculate the corresponding virtual geomagnetic pole (VGP) position for each site (using the software packages Pmag-Tauxe, 1988; VDP7 Ramon & Pueyo, 2014). Latitudes of the VGP poles were used to establish the local magnetostratigraphy.

Data Availability. The datasets generated during and/or analysed during the current study are available from the corresponding author upon request. The information about the individual samples analysed, and the statistical result are provided as a supplementary information.

Results

The analysed specimens exhibit a wide range of NRM intensities, which vary from 3.02E-05 A/m to a 6.83E-01 A/m, with an average intensity of 6.63E-02 A/m. The IRM acquisition curves indicate relatively low values of coercivity, reaching saturation rapidly towards field values before 1 T (Fig. 4). Thermal demagnetisation of the IRM suggests Curie temperatures close to 625°– 650°C. Such magnetic behaviour (attributed to a mineralogy rich in iron oxides) has been previously observed and reported[20,21]. Overall, the specimens have a stable behaviour during both, AF and TH, demagnetization, and present normal and reverse polarity directions (Fig. 5). Following the visual observation of the Zijderveld diagrams, we identified the presence of a low temperature component (<270 °C) that moves away from the origin, and can be associated with a recent remagnetization. It is followed by a stable component, directed towards the origin, taken as the primary magnetization.

For the distribution of our samples we proceed by two different methods, a visual inspection at the Zijderveld diagrams about the behaviour of the progressive demagnetisation of each sample, and a statistical distribution of the MAD by calculated mean of all data. In this second method, the value obtained was a mean of 4.7, which we use as reference to classify the data as type I if the MAD value of the individual sample is equal or less at 4.7; and we classified as type II if the MAD is over 4.7. For the samples without possibility to obtain data, the type of such samples has been defined as III. A table with both classifications can be found in the supplementary information (Table 1), and because the difference between them is not so large, we consider maintaining the visual inspection of each Zijderveld diagram of each individual sample. Therefore, samples have been grouped in three different types. Type I (23%) when the ChRM direction is clearly defined with a straight line and pointing towards the origin (Fig. 5a,b); type II (40%) directions are a little bit noisy, but ChRM directions can still be unambiguously defined (Fig. 5c,d); and type III (37%) includes noisy directions that prevent ChRM identification (Fig. 5e,f). We only used those samples in which the primary component could be clearly interpreted, including both type I and type II data, excluding the type III data, to compute mean directions and their corresponding VGP position. Plotting these data against the stratigraphic column produces a local magnetostratigraphy for the Solana del Zamborino site (Fig. 6). There are four magnetozones of normal polarity, labelled N1, N2, N3, and N4 from bottom to top of the sequence, and two reverse magnetozones R1, and R2 in the midsection. Between N1 and N2 levels there is a gap due to the lack of information since it has not been possible to obtain conclusive ChRM directions, therefore we consider such interval as two different magnetozones, but we are aware that a future revision and resampling of that part of the section must be carried out to determine if they are separate magnetozones or not. Nevertheless, to determinate the antipodal nature of the reversal a bootstrap test has been carried out with our data, whose results can be found as the supplementary information (Fig. 1).

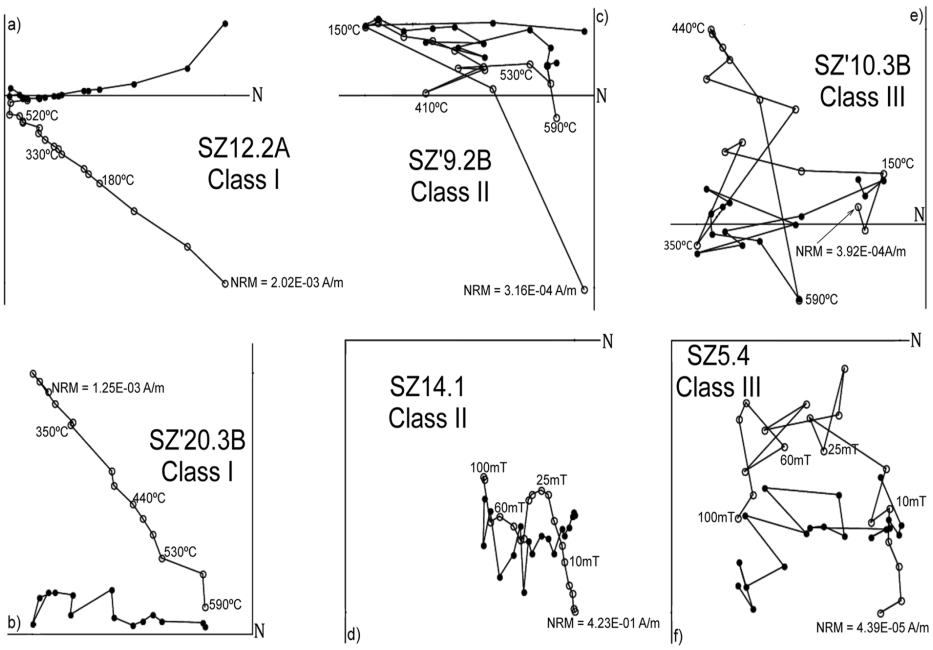

Figure 5. Representative orthogonal demagnetisation diagrams (Zijderveld). Black and white dots represent horizontal and vertical components respectively. Data in geographic coordinates.

Martín Penela (1998) (SZ)	Ruiz-Bustos (1999)
Macaca sylvanus	*Macaca sylvanus*
Mammuthus trogontherii	*Mammuthus trogontherii*
Palaeoloxodon antiquus	*Palaeoloxodon antiquus*
Equus caballus torralbae	*Equus caballus*
Dicerorhinus hemitoechus	*Stephanorhinus hemitoechus*
Cervus elaphus	*Cervus elaphus*
Capreolus	*Capreolus*
Dama sp.	*Dama sp.*
Bos (Bos) primigenius	*Bos primigenius*
Bos (Bison) priscus	*Bison priscus*
Hippopotamus sp.	*Hippopotamus cf. amphibious*
Sus scrofa	*Sus scrofa*
Canis cf. lupus	*Canis lupus*
Panthera (Leo) spelaea	*Panthera leo spelaea*
Lynx cf. Pardina	*Lynx cf. pardina*
Felis sylvestris	*Felis sylvestris*

Table 1. Summary of the published faunal lists of large mammals for Solana del Zamborino (SZ). Modified from Jiménez-Arenas *et al.*[39]. More exhaustive information can be found in the bibliography.

Given the remains of macro vertebrates found at the Solana del Zamborino (Table 1), a chronology of Middle Pleistocene has been traditionally assigned to this site[29,31,35]. Hence, comparing the obtained local magnetostratigraphy to the geomagnetic polarity time scale (GPTS) (Fig. 7), magnetozone N4 found at the top of the section is correlated with the Brunhes Chron (C1n). Therefore, it seems plausible that the next normal magnetozone N3 corresponds to the Jaramillo Subchron, and therefore N2 to the upper limit of Subchron Olduvai. Notice that such correlation (labelled Option I in Fig. 7), implies a rather long Jaramillo Subchron with a concomitant high and variable sedimentation rate. The nearby site of Fonelas (located 5 km away from La Solana, with the Fonelas-Pico 1 (FP-1) section (Fig. 1)) helps in evaluating such correlation. The FP-1 section contains the richest assemblage of vertebrates in the area, which has provided nearly 500 fossil remains that belong to 20 genera of large mammals, as well several remains of small mammals, in which tooth marks by carnivores have been found, without presence of human activity[36,37]. A recent magnetostratigraphy of the section reveals that the Jaramillo Subchron is

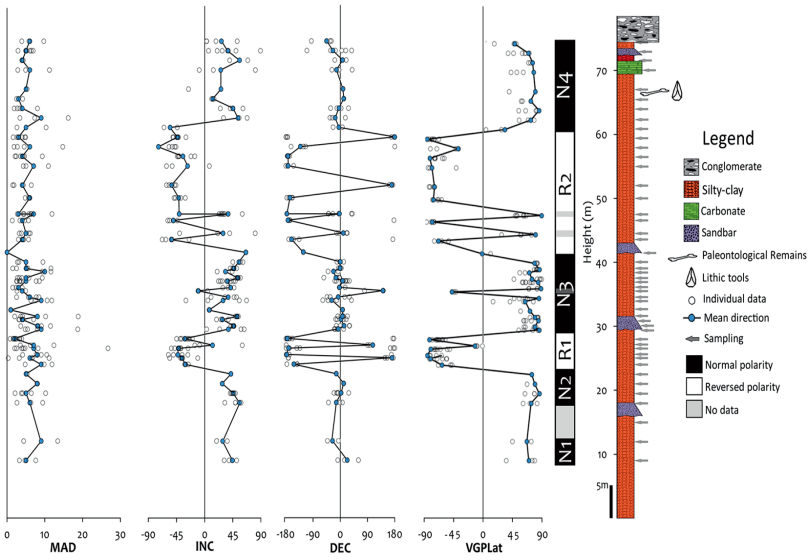

Figure 6. Graphical representation of the virtual geomagnetic pole (VGP) latitude against stratigraphic height, and the resultant local magnetostratigraphy. (MAD: *maximum angular deviation*, Inc/Dec: inclination and declination of each ChRM direction). Four magnetozones with normal polarity, named N1, N2, N3 and N4 and three magnetozones with reversed polarity named R1, R2 have been defined. At least two magnetostratigraphically consecutive sites of the same polarity were required to define a change in polarity, otherwise a grey bar represents a single site.

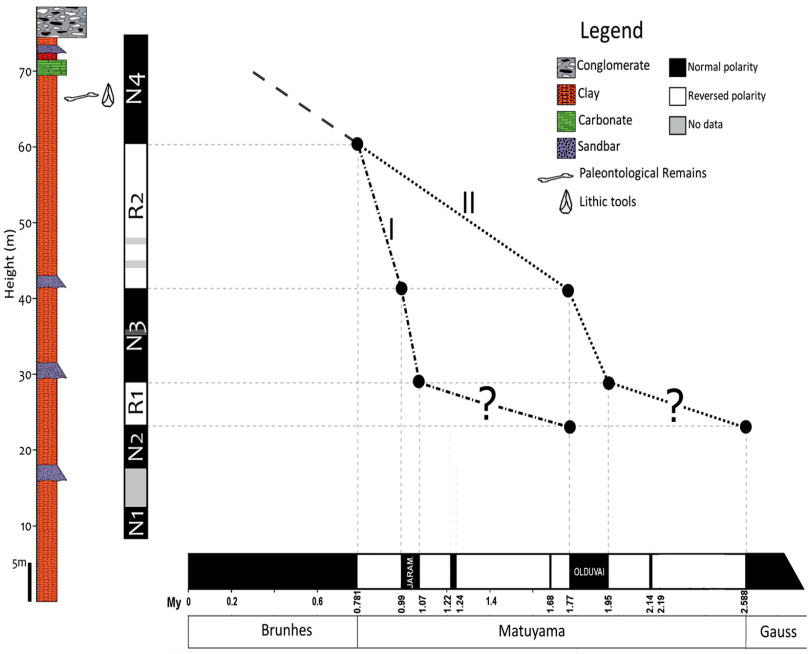

Figure 7. Resultant magnetostratigraphy and suggested correlations to the Global chrono-stratigraphical correlation table for the last 2.7 million years (Cohen and Gibbard[47]). Option II is favoured due to its consistency with the nearby Fonelas magnetostratigraphic section (see text for discussion).

absent[20–22]. In that locality, the stratigraphic record begins at the top of Chron Gauss and finishes in the Brunhes Chron. Therefore, and given the proximity to the SZ section, it seems likely that the Jaramillo could be missing as well in La Solana. Under such assumption, an alternative option (Option II in Fig. 7) includes assigning N3 magnetozone to Olduvai Subchron, and N2 magnetozone to the upper limit of Gauss Chron (C2n).

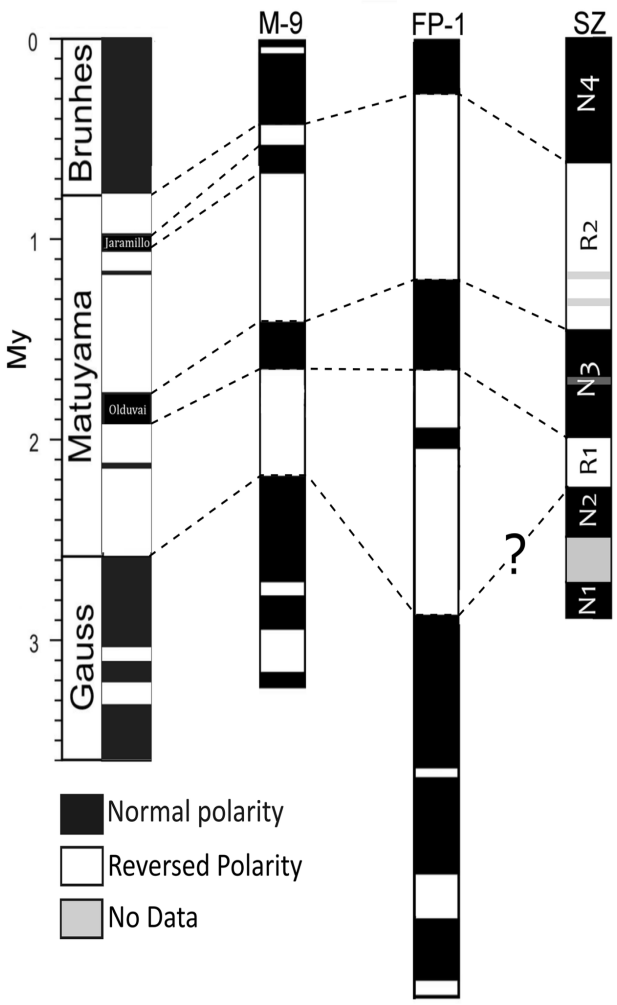

Figure 8. Correlation between Mencal (M9), Fonelas (FP-1) and Solana del Zamborino (SZ) magnetostratigraphies and the Geomagnetic Polarity Time Scale (GPTS 2004[48]) modified from Pla-Pueyo[20].

In support of such interpretation are the bulk sedimentation rates estimated in La Solana, Fonelas and Mencal sites (the last one located at 14 km N form Solana, with the M-9 section[20]), which are of the same order of magnitude (average of 2 cm/kyr[20–22]) (Fig. 8).

Discussion

The ultimate goal of establishing the chronology at SZ resides in the presence of the lithic tools found at a stratigraphic level reported as level B, corresponding to the Guadix Formation (more information can be found in Casas *et al.*[24] and Botella *et al.*[27]). In a previous study[13] the archaeological layer was found above the Brunhes / Matuyama boundary. Based on an inferred accumulation rate, an age of ~760kyr was suggested by these authors. However, because this previous magnetostratigraphy lacks polarity reversals below and above the archaeological layer, an alternative stratigraphic section at the paleontological site of Cúllar-Baza[38] (located more than 50 km away), was used to infer the accumulation rate for La Solana. We would like to emphasize that the section of Cúllar-Baza is not lithologicaly similar to that at La Solana, since the latter is characterised by siliciclastic sediments (silt and clay of fluvial origin), whereas the former sequence is mainly composed of carbonate lacustrine-palustrine sediments[5]. Highly different sediment accumulation rates are expected to be found simply because of the contrasting depositional environment. Jimenez-Arenas *et al.*[39] have also brought up inconsistencies with such an age assignment. According to these authors, there are several errors in the interpretation of the archaeological assemblage for the site, and also discrepancies with the original faunal lists published. In our new study, we have been able to locate three reversals below the archaeological site at La Solana, which allows a firmer interpretation of the local magnetostratigraphy and by inference the approximate chronology of the site. Assuming an average accumulation rate of 2 cm/kyr throughout La Solana section, the stratigraphic position of

the archaeological site would have an estimated age range between 300 Kyr to 480 Kyr, significantly younger than the previously suggested age, and more in line with the conventional chronology proposed for the evolution of Acheulean in Europe[40] and with the faunal record of the SZ site itself[31].

Conclusions

An exhaustive paleomagnetic study of the tool-bearing and paleontological deposits at La Solana del Zamborino, as well as of the older stratigraphic levels, has been carried out:

- A stratigraphic sequence of ~65 meters has been paleomagnetically studied.
- The samples generally present a stable magnetic signal and quality that have allowed us to obtain an interpretable magnetostratigraphy.
- The absence of subchron Jaramillo is consistent with the existing records obtained by Pla-Pueyo[20]and Pla-Pueyo *et al.*[21] in the close palaeontological site of Fonelas P-1.

This new magnetostratigraphic study, based on three polarity reversals, is consistent with existing data from nearby sections (e.g., FP-1 and M-9) and based on the sedimentation rate, the stratigraphic position of the archaeological site at SZ would have an approximate age of ~300–480 Kyr, much younger than the age provided by Scott and Gibbert[1] and, therefore, more similar to the chronology of European Acheulean sites such as L'Arago in France, Boxgrove in England or Atapuerca in Spain[41–46].

References

1. Soria, J., Viseras, C. & Fernández, J. Late Miocene-Pleistocene tectono-sedimentary evolution and subsidence history of the central Betic Cordillera (Spain): a case study in the Guadix intramontane basin. *Geol. Mag.* **135**, 565–574 (1998).
2. Soria, J., Fernández, J. & Viseras, C. Late Miocene stratigraphy and paleogeographic evolution of the Guadix intramontane Basin (Central Betic Cordillera, Spain): implications for Atlantic-Mediterranean connection. *Palaeogeogr. Palaeoclimatol. Palaeoecol.* **151**, 255–266 (1999).
3. Viseras, C., Soria, J. M., Fernández, J. & García García, F. The Neogene-Quaternary basins of the Betic Cordillera: an overview. *Geophys. Res. Abstr.* **7**, 1–5 (2005).
4. Viseras, C., Soria, J., Durán, J. & Arribas, A. Condicionantes geológicos para la génesis de un yacimiento de grandes mamíferos: Fonelas P-1 (límite Plioceno-Pleistoceno, Cuenca de Guadix-Baza, Cordillera Bética). *Boletín Geológico y Min.* **115**, 551–566 (2004).
5. García-Aguilar, J. M. & Palmqvist, P. A model of lacustrine sedimentation for the Early Pleistocene deposits of Guadix-Baza basin (southeast Spain). *Quat. Int.* **243**, 3–15 (2011).
6. Arribas, A. *et al*. A mammalian lost world in Southwest Europe during the Late Pliocene. *PLoS One* **4**, e7127, 1–10 (2009).
7. Gibert, L., Ortí, F. & Rosell, L. Plio-Pleistocene lacustrine evaporites of the Baza Basin (Betic Chain, SE Spain). *Sediment. Geol.* **200**, 89–116 (2007).
8. Lozano-Fernández, I., Blain, H.-A., López-García, J. M. & Agustí, J. Biochronology of the first hominid remains in Europe using the vole Mimomys savini: Fuente Nueva 3 and Barranco León D, Guadix-Baza Basin, south-eastern Spain. *Hist. Biol.* **27**, 1021–1028 (2015).
9. Martínez-Navarro, B. *et al*. The Epivillafranchian and the arrival of pigs intoEurope. *Quat. Int.* **389**, 131–138 (2015).
10. Martínez-Navarro, B., Turq, A., Agustí Ballester, J. & Oms, O. Fuente Nueva 3 (Orce, Granada, Spain) and the first human occupation of Europe. *J. Hum. Evol.* **33**, 611–620 (1997).
11. Oms, O., Anadón, P., Agustí, J. & Julià, R. Geology and chronology of the continental Pleistocene archeological and paleontological sites of the Orce area (Baza basin, Spain). *Quat. Int.* **243**, 33–43 (2011).
12. Agustí, J., Blain, H.-A. A., Furió, M., De Marfá, R. & Santos-Cubedo, A. The early Pleistocene small vertebrate succession from the Orce region (Guadix-Baza Basin, SE Spain) and its bearing on the first human occupation ofEurope. *Quat. Int.* **223–224**, 162–169 (2010).
13. Scott, G. R. & Gibert, L. The oldest hand-axes in Europe. *Nature* **461**, 82–85 (2009).
14. Viseras, C., Soria, J. M. J. M., Fernández, J. & García, F. The neogene-quaternary basins of the betic cordillera: an overview. *Geophys. Res. Abstr.* **7**, 11123–11128 (2005).
15. García-García, F. J.M., S., Viseras, C. & Fernández, J. A model of interplay between climatic oscillations, subsidence and sediment dispersal. *J. Sediment. Res.* **79**, 302–315 (2009).
16. Viseras, C., Soria, J. M. & Fernández, J. in *Geología* de España (ed. Vera, J. A.) 577–581 (IGME, 2004).
17. Viseras, C. & Fernández, J. Sedimentary basin destruction inferred from the evolution of drainage systems in the Betic Cordillera (southern Spain). *J. Geol. Soc. London.* **149**, 1021–1029 (1992).
18. Calvache, M. L. & Viseras, C. Long-term control mechanisms of stream-piracy processes in southeast Spain. *Earth Surf. Process. Landforms* **22**, 93–105 (1997).
19. Viseras, C. *et al*. A large-mammal site in a meandering fluvial context (Fonelas P-1, Late Pliocene, Guadix Basin, Spain). Sedimentological keys for its paleoenvironmental reconstruction. *Palaeogeogr. Palaeoclimatol. Palaeoecol.* **242**, 139–168 (2006).
20. Pla-Pueyo, S. *Contexto estratigráfico y sedimentario de los yacimientos de grandes mamíferos del sector centralal de la Cuenca de Guadix (Cordillera Bética)*. (2009).
21. Pla-Pueyo, S., Viseras, C., Soria, J. M., Tent-Manclús, J. E. & Arribas, A. A stratigraphic framework for the Pliocene-Pleistocene continental sediments of the Guadix Basin (Betic Cordillera, S. Spain). *Quat. Int.* **243**, 16–32 (2011).
22. Pla-Pueyo, S. *et al*. Correlación litológica y magnetoestratigráfica de las secciones continentales del sector occidental de la Cuenca de Guadix (Cordillera Bética, España). *Geo-Temas2* **10**, 171–174 (2008).
23. Vera, J. A. E. E. de la Depresión Guadix-Baza. *Boletín Geológico y Min.* **81**, 429–462 (1970).
24. Casas, J., Ruano, J. A. P. & Torres, J. A. V. Interpretación Geológica Y Estratigráfica Del Yacimiento De La 'Solana Del Zamborino'. *Cuadernos de Prehistoria y Arqueología de la Universidad de Granada* **1**, 5–15 (1976).
25. Viseras, C. Estratigrafía y Sedimentología del relleno aluvial de la Cuenca de Guadix (Cordillera Bética). (PhD dissertation. Universidad de Granada, 1991).
26. Botella, M. C. El cazadero achelense de la Solana de Zamborino (Granada). *Cr{ó}nica del XIII Congreso Arqueol{ó}gico Nacional* 175–184 (1975).
27. Botella, M. C., Merelo, I. M., Ontañón, A., de, B., Rodríguez, A. C. R. & Delgado, M. T. La Excavación Y Sus Resultados Arqueológicos. *Cuadernos de Prehistoria y Arqueología de la Universidad de Granada* **1**, 25–45 (1976).
28. Botella, M. C., Torres, J. A. V. & Porta, J. d.e El Yacimiento Achelense De La 'Solana Del Zamborino'. Fonelas (Granada) (Primera Campaña De Excavaciones). *Cuadernos de Prehistoria y Arqueología de la Universidad de Granada* **1**, 1–4 (1976).
29. de Porta, J. Estudio preliminar sobre la fauna de la 'Solana del Zamborino'. *Cuad. Prehist. la Univ. Granada* **1**, 17–23 (1976).

30. Botella, M. C. Excavaciones arqueológicas en el yacimiento achelense de la 'Solana de Zamborino', Fonelas (Granada). *Noticiario arqueológico hispánico* 25–32 (1976).
31. Martín Penela, A. Los grandes mamíferos del yacimiento Achelense de la Solana del Zamborino, Fonelas (Granada, España). *Antropología y Paleoecología humana* 29–187 (1988).
32. Pla-Pueyo, S. *et al*. Climatic control on palaeohydrology and cyclical sediment distribution in the Plio-Quaternary deposits of the Guadix Basin (Betic Cordillera, Spain). *Quat. Int.* **389**, 56–69 (2015).
33. Kirschvink, J. L. The least-squares line and plane and the analysis of palaeomagnetic data. *Geophys. J. R. Astron. Soc.* **62**, 699–718 (1980).
34. Fisher, R. Dispersion on a Sphere. *Proc. R. Soc. London A Math. Phys. Eng. Sci.* **217**, (1953).
35. Rook, L. & Martínez-Navarro, B. Villafranchian: The long story of a Plio-Pleistocene European large mammal biochronologic unit. *Quat. Int.* **219**, 134–144 (2010).
36. Arribas, A. *et al*. Un nuevo yacimiento de grandes mamíferos villfranquienses en la Cuenca de Guadix-Baza (Granada): Fonelas P-1, primer registro de una fauna próxima al límite Plio-Pleistoceno en la Península Ibérica. *Boletín Geológico y Min.* **112**, 3–34 (2001).
37. Arribas, A. *et al*. Nuevos registros paleontológicos de grandes mamíferos en la Cuenca de Guadix-Baza (Granada): Aportaciones del Proyecto Fonelas al conocimiento sobre las faunas continentales del Plioceno-Pleistoceno europeo. *Bol. Geol. y Min.* **115**, 567–582 (2004).
38. Gibert, L., Scott, G., Martin, R. & Gibert, J. The Early to Middle Pleistocene boundary in the Baza Basin (Spain). *Quat. Sci. Rev.* **26**, 2067–2089 (2007).
39. Jiménez-arenas, J. M., Santonja, M., Botella, M. & Palmqvist, P. The oldest handaxes in Europe: fact or artefact? *J. Archaeol. Sci.* **38**, 3340–3349 (2011).
40. Moncel, M. H. *et al*. Early Evidence of Acheulean Settlement in Northwestern Europe-La Noira site, a 700.00 Year-Old ocupation in the Center of France. *PLoS One* **8**, e75–529 (2013).
41. Roberts, M. B., Stringer, C. B. & Parfitt, S. A. A hominid tibia from Middle Pleistocene sediments at Boxgrove, UK. *Nature* **369**, 311–313 (1994).
42. Falguères, C. *et al*. New U-series dates at the Caune de l'Arago, France. *J. Archaeol. Sci.* **31**, 941–952 (2004).
43. Santonja, M. & Pérez-González, A. Mid-Pleistocene Acheulean industrial complex in the Iberian Peninsula. *Quat. Int.* **223**, 154–161 (2010).
44. Falguères, C. *et al*. Combined ESR/U-series chronology of Acheulian hominid bearing layers at Trinchera Galería site, Atapuerca, Spain. *J. Hum. Evol.* **65**, 168–184 (2013).
45. Ollé, A. *et al*. The Acheulean from Atapuerca: Three steps forward, one step back. *Quat. Int.* **411**, 316–328 (2016).
46. Demuro, M. *et al*. New Luminiscene Ages for the Galeria Complex Archaeological Site: resolving Chronological Uncertainites on the Acheulean Recod of the Sierra de Atapuerca, Northern Spain. *PLoS One* **9**, e110169 (2014).
47. Cohen, K. M. & Gibbard, P. 2011 Global chronostratigraphical correlation table for the last 2.7 million years. Subcommission on Quaternary Stratigraphy (International Commission on Stratigraphy), Cambridge, England.
48. Gibbard, P. & Van Kolfschoten, T. In *A Geological Time Scale 2004* (eds Gradstein, F. M., Ogg, J. G. & Smiths, A. G.) 441–471 (Cambridge University Press, 2004).

Acknowledgements
This work has been possible thanks to the following research grants: B090678SV18BC (General Direction of Cultural Heritage, Junta de Andalucía): PI R. Sala; CGL2010–16821 andCGL2014–62296-EXP (MINECO): PI J.M. Pares, CGL20013–43013R (MINECO-FEDER) and Research Group RNM 369 of the Junta de Andalucía. We also wish to thank the Editorial Board Member handling the manuscript and the reviewer(s) for their time and constructive comments about this work. All of them have helped us to improve this manuscript.

Author Contributions
C.A.-P. and J.M.P. designed the work. C.A.-P. obtained and analysed the data. C.A.-P. and J.M.P. wrote the manuscript with contributions about geological information from C.V. and S.P.-P., and contributions from R.S. about the Acheulean tools ages. R.S. and J.M.P. oversaw and coordinated the research project. All authors discussed and commented on the manuscript.

Additional Information Appendix A
Supplementary information accompanies this paper at https://doi.org/10.1038/s41598-017-14024-5.

Competing Interests: The authors declare that they have no competing interests.

Publisher's note: Springer Nature remains neutral with regard to jurisdictional claims in published maps and institutional affiliations.

Capítulo 6 . a post-jaramillo age for the artefact-bearing layer td4 (gran dolina, atapuerca): new paleomagnetic evidence

Quaternary Geochronology 45 (2018) 1–8

Contents lists available at ScienceDirect

Quaternary Geochronology

journal homepage: www.elsevier.com/locate/quageo

A post-Jaramillo age for the artefact-bearing layer TD4 (Gran Dolina, Atapuerca): New paleomagnetic evidence

Claudia Álvarez-Posada[a,*], Josep María Parés[a], Gloria Cuenca-Bescós[b], Jan Van der Made[c], Jordi Rosell[d], José María Bermúdez de Castro[e], Eudald Carbonell[d,f]

[a] Geochronology Program, CENIEH, Paseo Sierra de Atapuerca 3, 09002 Burgos, Spain
[b] Aragosaurus-IUCA, Departamento de Ciencias de la Tierra, Facultad de Ciencias, Universidad de Zaragoza, c/ Pedro Cerbuna, 12, 50009 Zaragoza, Spain
[c] Departamento de Paleobiología, Museo Nacional de Ciencias Naturales, C.S.I.C., c/ José G. Abascal 2, 28006 Madrid, Spain
[d] Institut Català de Paleoecologia Humana i Evolució Social, IPHES, Campus Sescelades (URV), 43007 Tarragona, Spain
[e] Paleobiology Program, CENIEH, Paseo Sierra de Atapuerca 3, 09002 Burgos, Spain
[f] Universitat Rovira i Virgili, Carrer de l'Escorxador, s/n, 43003 Tarragona, Spain

ARTICLE INFO

Keywords:
Atapuerca
Gran Dolina
Lithic tools
Jaramillo
Early Pleistocene
Biostratigraphy

ABSTRACT

The cave - site of Gran Dolina in Atapuerca preserves one of the most abundant records of Early to Middle Pleistocene sediments known so far. Therefore, establishing the chronology for the stratigraphic levels within the cavity is crucial. Since the early 1990s, subsequent excavations have allowed better access to the older stratigraphic levels TD4, TD5 and TD6 allowing for re-sampling with the aim of providing detailed chronology and testing whether the lithic industries-bearing layer TD4 has a post or pre-Jaramillo age, and hence establishing a better geochronological context for the lithic tools. In this study, we obtained negative magnetic polarity directions for these stratigraphic levels, a result consistent with previous studies that already identified the Matuyama—Brunhes boundary between TD7 and TD8 levels. In addition, several new ESR analysis, recently published, were carried out throughout the sequence, provide an age between 0.77 and 0.85 Ma for the upper limit of TD6 and an age of 0.91 ± 0.25 Ma for the lower limit of TD4. The age provided by ESR for TD6 is consistent with recent luminescence analysis, which provides a mean age of 846 ± 57 ka. The combination of ESR, luminescence, biostratigraphy, with our new paleomagnetic results, supports a post-Jaramillo age for layer TD4 in Gran Dolina.

1. Introduction

The Atapuerca karst system contains one of the largest and most continuous records of Early and Middle Pleistocene age known so far. The cave sediments found in this karst system have been studied since the late 1980s (e.g., Aguirre et al., 1990; Carbonell et al., 1995; Parés and Pérez-González, 1995; Arsuaga et al., 1997; Bermúdez de Castro, 1997) contributing to a much better understanding of human evolution and dispersal outside the African continent.

Within this karstic complex, the Gran Dolina (TD) site has provided abundant archaeological and paleontological remains that document human activity and its relationship to the environment over the last one million years (Carbonell et al., 1995, 2008; Bermúdez-de Castro et al., 2008; Rodríguez et al., 2011; Rodríguez-Gómez et al., 2013). Different stratigraphic layers have been extensively studied and dated using numerous chronological methods such as biostratigraphy, luminescence, electron spin resonance (ESR) and paleomagnetism (Parés and Pérez-González, 1995, 1999; Cuenca-Bescós et al., 1999, 2015; Falguères et al., 1999; García and Arsuaga, 1999; Berger et al., 2008; Parés et al., 2013; Arnold et al., 2015). Successive excavation seasons have expanded access to the sediments that fill the cave of Gran Dolina, making it possible to sample horizons that were not available before. This is particularly significant for magnetic reversal stratigraphy. The aim of this study is to build upon the existing magnetostratigraphy of levels TD6, TD5 and TD-4, which are currently much better and continuous exposed than when the original paleomagnetic study was done at this site, and to provide more information which complement the work reported by Parés et al. (2013).

Specifically, stratigraphic layer TD4 is a key unit, as its upper part contains remains of a lithic industry that confirms human presence in levels well below the Aurora stratum, now TD6-2 (Carbonell et al., 1995), which in turn predates the Matuyama—Brunhes boundary (here after MBB) (Parés and Pérez-González, 1995). The most recent absolute age available for this important layer is due to ESR, which gives an age

* Corresponding author.
E-mail address: cap0035@alu.ubu.es (C. Álvarez-Posada).

https://doi.org/10.1016/j.quageo.2018.01.003
Received 1 November 2017; Received in revised form 10 January 2018; Accepted 19 January 2018
Available online 31 January 2018

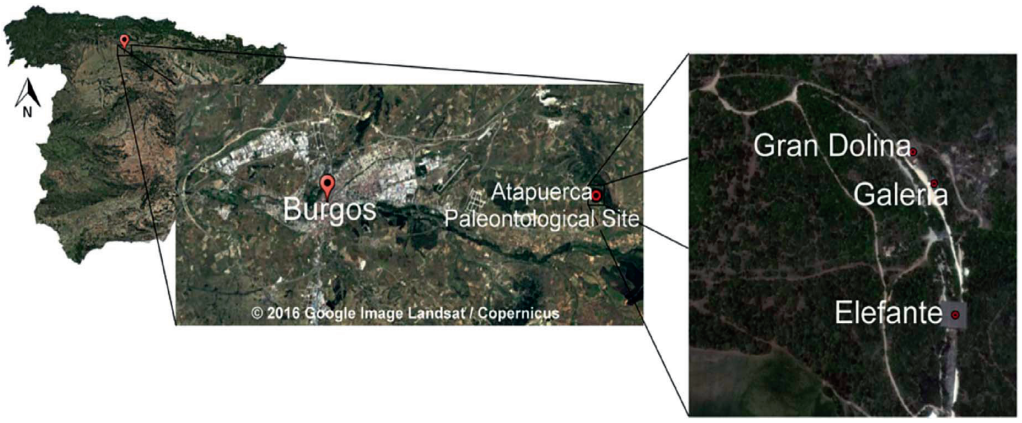

Fig. 1. Location of the Atapuerca karst system site. Images obtained from Google Earth free program (version 7.1.8.3036. Map data © 2016 Google, Digital Globe).

902 ± 149 ka (Moreno et al., 2015) which could be compatible with the presence of the Jaramillo subchron (1001–1.069 ka) within the error margin. Therefore, the main goal of this study is to test whether the Jaramillo subchron is present in the section, thus establishing a better chronological framework for the levels TD4 to TD6 that allow a more accurate temporal range for the lithic industry and fossils found at TD4.

1.1. Geological and stratigraphical context

Sierra de Atapuerca is located about 16 km west of the city of Burgos (Fig. 1) within what is known as the " Bureba Corridor," a passage or connection between two of the largest Cenozoic basins of the Iberian Peninsula, the Duero and Ebro basins (Alonso-Gavilán et al., 2004). The mountain range corresponds to an anticline that structurally is part of the north western most sector of the Iberian chain and has been dissected in the Quaternary by the Arlanzón River (Benito-Calvo, 2004; Benito-Calvo et al., 2008). The mountain range consists mostly of Mesozoic limestones and dolomites, leading to a karst system which includes 4.7 km of explored passages, where numerous archaeological and paleontological remains have been found (Ortega et al., 2013).

1.1.1. Gran Dolina (TD)

This site consists a sedimentary filling, about 20 m thick, divided into 11 individual units labelled TD11 to TD1 from top to bottom (Gil et al., 1987) The stratigraphic nomenclature is still used with some modifications, specifically in the lower part, which includes names such as TDW4b, TD3-TD4 or TD3-4 (Cuenca-Bescós et al., 2001; Pérez-González et al., 2001). A summary of the different nomenclatures can be found in Rodríguez et al. (2011). For the present manuscript, we will use the name of TD4 for this stratigraphic unit present in the lower part.

The sedimentary layers of the TD cavity, now exposed in a continuous vertical outcrop, include both interior facies sediments with little external influence (also known as autochthonous deposits in the literature), and entrance facies sediments, which originate outside the cave or at its entrance and which are deposited by different transport mechanisms mostly forming slope and talus cones. Level TD1 corresponds to a slackwater deposits capped by a speleothem at the base of TD4, and does not contain fossil. Levels TD4 to TD11 overlie the previous units and are formed mainly of pebbles, cobbles and sandy clay, corresponding to talus, slope wash and sliding bed mode deposits, and they contain numerous fossil remains.

A description of the levels addressed in this paper follows below:

- TD4: About 2 m thick dominated by breccia, with a reddish-brown sandy clay matrix and limestone pebbles between 10 and 15 cm.
- TD5: About 2.5 m thick, consisting of a clast-supported breccia with pebbles and cobbles, up to 60 cm of diameter at the bottom, with a mud and sandy matrix and a dark brown clay level at the top.
- TD6: 2–2.5 m thick with abundant clasts ranging from breccia to gravels with a very hard and less abundant clay matrix.

A more comprehensive and detailed description of the sedimentary infill of Gran Dolina can be found in Campaña et al. (2015, 2016).

1.2. Biostratigraphical context of TD4, TD5 and TD6

The mammal assemblages from the TD4, TD5 and TD6 are Biharian in the European biostratigraphy. The preceding Villafranchian Mammal Age is a biochronological unit based on large mammals covering the time interval from the Late Pliocene through most of the Early Pleistocene in Southern Europe. It roughly spans from around 3.5 Ma to about 1.0 Ma (Rook and Martínez-Navarro, 2010) and are found in pre-Jaramillo or Jaramillo layers from several localities in Europe (see Cuenca-Bescós et al., 2015 for a comprehensive review). In Spain, the end of the Villafranchian is characterized by the faunal unit defined in Sima del Elefante as the Atapuerca FU 1 (Cuenca-Bescós and García, 2007). This FU1 records the oldest occurrence of fossil remains of *Homo* in Europe (Carbonell et al., 2008) together with at rodent association dominated by the *Allophaiomys* species *Allophaiomys lavocati* (Laplana and Cuenca-Bescós, 2000), from the Lower Red Units of Sima del Elefante (knows as TELRU levels, López-García et al., 2011), in Atapuerca. This faunal association is unique and is situated in the layers prior to the Jaramillo event in the localities were this event is recorded such as the layer 10 of the site of Vallparadís, EVT 10 (Estació de Vallparadís 10), see Minwer-Barakat et al. (2011) and Duval et al. (2011). The micro fauna from TD4, TD5, TD6 and lower part of TD7, below the MMB and hence Early Pleistocene, is dominated by the *Mimomys savini* which disappears short after the MBB event in Gran Dolina TD8 (level TD8b, Table 1), and from the faunal units FU2 to FU4 (Cuenca-Bescós et al., 2015, 2010).

Relevant large mammal species from TD4 include *Bison voigtstedtensis*, which is assumed to be a descendant of *Bison menneri* (Made et al., 2015), a species of *Eucladoceros* replacing the closely related *Eucladoceros giulii*, *Megaceroides solilhacus*, which is a descendant of *Eucladoceros pliotarandoides* and *Crocuta*, which first appeared in Atapuerca (García and Arsuaga, 2001; Made et al., 2015). The first appearance of *Cervus elaphus* in Europe seems to have been diachronic, appearing before the Jaramillo in Montenegro, within the Jaramillo in Germany, and in TD4 in Spain (Made and Dimitrijevic, 2015). These taxa suggest a post, rather than a pre-Jaramillo age for TD4. A summary of the different stratigraphic ranges of taxa which appears (first or last) in the latest Matuyama until Jaramillo subchron is shown in Fig. 2. Further information about those taxa can be found in the

Table 1
Distribution of the rodents at the Gran Dolina stratigraphic sequence. The upper limit of ATA FU 5 represents the highest appearance of taxa of rodents of "early Pleistocene age" though it appears above the Matuyama–Brunhes boundary, the proposed limit between the Early-Middle Pleistocene.

Paleomagnetic record	Pleistocene subseries	Atapuerca Faunal Units	Gran Dolina	Age	Selected rodent species of the Gran Dolina Sequence, Burgos, Spain																					
					Eliomys quercinus	*Castor fiber*	*Apodemus sylvaticus*	*Allophaiomys chalinei*	*Stenocranius gregaloides*	*Hystrix refossa*	*Terricola arvalidens*	*Microtus seseae*	*Pliomys savini*	*Mimomys savini*	*Iberomys huescarensis*	*Marmota marmota*	*Allocriteus bursae*	*Micromys minutus*	*Microtus ratticepoides*	*Terricola atapuerquensis*	*Iberomys brecciensis*	*Allocricetus correzensis*	*Microtus arvalis*	*Microtus agrestis*	*Pliomys lenki*	*Arvicola sapidus*	*Clethionomys sp.*
Brunhes	Middle	FU6	TD10-11	0.4	x		x									x				x	x	x	x	x	x	x
			TD8b	0.6	x		x													x	x	x				
		FU5	TD8A	<0.6									x	x	x		x		x							
			TD7	0.78			x				x	x	x	x	x	x	x									
Matuyama	Early	FU4	TD6b	0.85		x	x		x	x	x	x	x	x	x	x	x									
		FU3	TD6a			x	x	x	x	x	x	x	x	x	x	x	x	x									
			TD5		x	x	x	x	x		x	x	x	x	x	x	x	x									
		FU2	TD4	~0.9	x	x	x	x	x	x	x	x	x	x	x	x	x									

supplementary data (Appendix A, Tables S1 and S2, and the bibliographical references there contained).

2. Material and methods

Owning to the cohesiveness and hardness of the materials of the studied levels, two different procedures were used to obtain the samples for this study. The top of level TD6 is cohesive and indurated, and an electric radial saw was used in order to obtain hand blocks between 8 and 4 cm, which were processed to obtain individual samples about 8 cm^3 into the laboratory. For levels TD5 and TD4, with more abundant and softer clay matrix a ceramic knife has been used to cut individual samples of sediment in situ. In both cases, samples were oriented in situ with a standard compass and clinometer. Whenever possible, we have tried to obtain consecutive samples in all stratigraphic levels, although given the accessibility to the outcrop (currently a vertical wall) and the abundance of paleontological remains, this has not always been possible. In total, we have sampled 86 sites spread across the three levels studied, obtaining 140 individual specimens of 8 cm^3.

The paleomagnetic analyses were performed at the Paleomagnetism Laboratory of the National Research Center for Human Evolution (CENIEH, Burgos) and consisted in measuring the natural remanent

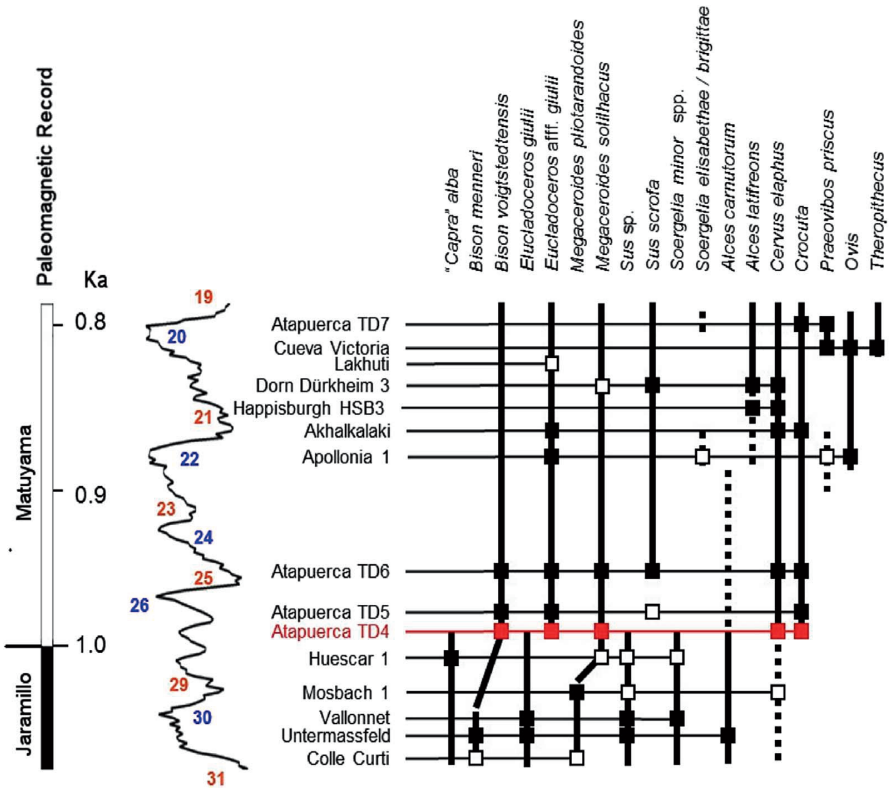

Fig. 2. Stratigraphic ranges of taxa with last appearances in the Jaramillo or first or last appearances in the latest Matuyama and the localities in which they Occur. Modified from Van der Made et al. (2015).

magnetization (NRM) of the samples and their progressive demagnetization. We used a Superconducting Rock Magnetometer model 755-4K (2G Enterprises) with a built in 3-axis degausser system for alternating field demagnetization (AF) up to 170 mT, and an oven model TD-48SC (ASC Scientific) for thermal demagnetization (TH). Also, an Impulse Magnetizer, model IM-10-30 ASC has been used to obtain isothermal remanent magnetization (IRM) acquisition curves.

Of the 140 individual specimens obtained, 118 have been analysed, of which 73 (62%) have been thermally demagnetized, with an initial increase of 50 °C to reach 350 °C, and then reduce the step at 30 °C, reaching 650 °C. 24 specimens (20%) have been demagnetized using AF, reaching up 0.1T. Nine specimens (8%) have been demagnetized first at 130 °C and then with AF until a peak field of 50 mT. Twelve specimens (10%) has been used to obtain the IRM curves, and their progressive thermal demagnetization. The information about the individual samples analysed and the statistical results are provided in the supplementary data (Appendix A Table S3).

After visual inspection of the obtained Zijderveld (1967) diagrams, we have determined, based in the most stable component of the NRM (Natural Remanent Magnetization), the primary component, known as Characteristic Remanent Magnetization (ChRM) direction, which we favour to be the original primary magnetization acquired at the of deposition, for each sample. Afterwards we obtained the fisherian mean of the ChRM directions (appling various programs, such as Pmag, Tauxe, 1988; VPD7, Ramón & Pueyo, 2014), and last, we calculated the Virtual Geomagnetic Pole (VGP) latitude for each site based on the mean ChRM direction.

3. Results

Paleomagnetic results show a moderate NRM intensity, with values ranging between 6.79×10^3 A/m to $3.35x10^{-4}$A/m, well above the noise level of the magnetometer that we used. The IRM acquisition curves present a low coercivity phase, with a saturation below 100 mT, indicating that the main carrier of magnetization is magnetite (Fig. 3).

After visual inspection of the Zijderveld diagrams, samples have been categorized by a statistical distribution of the MAD (maximum angular deviation) by calculated the mean of all data. The value obtained was a numerical mean of 7.05, which we use as a reference to classify the data as: type I (25%) include specimens in which the MAD value is equal or less at 7.05; type II (24%) specimens have a MAD value over 7.05; and type III (52%) for those specimens which show an erratic or noisy behaviour, and there is no possibility to obtain data (Fig. 4). In thermally demagnetized samples having type I and II, we have identified, in almost all of them, the presence of two components: a low temperature, between 20 °C to 350 °C, and high temperature (where ChRM has been determined) which reaches 530 °C. Above this temperature, behaviour typically becomes erratic (Fig. 4). Both observations, mid-unblocking temperature and the saturation curves of the IRM experiments at low fields, confirm magnetite as the major ferromagnetic mineral present in the sediments. This result is coherent with a number of existing paleomagnetic and rock magnetic analysis (Bógalo et al., 2003; Parés et al., 2013).

The orientation of the low temperature component is NW and positive, not distinguishable from the present Earth's magnetic field at the locality, while the high temperature component has a SE and upwards direction. The low stability component (NW positive) has been interpreted as a recent overprinting, and the latter is considered as the primary magnetization (Fig. 5).

The reversal stratigraphy is based on the VGP Latitude position and sites have been classed based on the k precision parameter: class 1 if $k \geq 10$; class 2 if $k < 10$, and class 3 if only one sample was used (Table 2). The VGP Latitude plot values shows a dominance of negative polarities (Fig. 6), ranging from −78 to −33.

The obtained reverse magnetozone encompasses stratigraphic levels TD6, TD5 and TD4, and is interpreted as the Matuyama chron, as a major change in polarity, from reverse to normal observed near the limit between units TD7 and TD8 was assigned to the Matuyama-Brunhes Boundary (Parés and Pérez-González, 1995, 1999) and later corroborated by OSL and ESR dating (e.g., Arnold et al., 2015; Falguères et al., 1999; Moreno et al., 2015). The obtained reverse magnetozone is only interrupted by three non-consecutive sites that show positive magnetization directions which cannot be unambiguously interpreted as geomagnetic short events. These few horizons displaying normal polarity could simply correspond to remagnetized sediments or else due to as an insufficient removal of the present day field overprint and therefore are not included in the discussion and interpretation of the results.

Recent ESR analyses carried out by Moreno et al. (2015) in the lower section of Gran Dolina, and specifically from the mid - lower section of TD4, give an age of 902 ± 149 ka; whereas the upper part of TD6, includes an OSL (Optical Stimulated Luminiscence) chronology by Arnold et al. (2015) which results in a mean age of 846 ± 57 ka for TD6 level, clearly below the – Matuyama-Brunhes limit (Fig. 6). Our new magnetostratigraphic results can then be combined with such absolute ages to interpret the magnetic polarity.

4. Discussion and conclusions

The magnetostratigraphy obtained in this study reveals essentially reverse polarity from TD4 to TD6 levels that agrees with the presence of the MBB at the upper part of level TD7 (Parés and Pérez-González, 1999, 1995). ESR analyses carried out in Aurora stratum (upper part of TD6), just below TD7, show an age between 0.77 and 0.85 Ma for such level (Duval et al., 2012; Falguères et al., 2013, 1999), and is consistent with the average age of 846 ± 57 ka for TD6 provided by luminescence (Arnold et al., 2015). Also, the ESR analyses (Moreno et al., 2015) on quartz grains in the lower section of Gran Dolina, provide an average

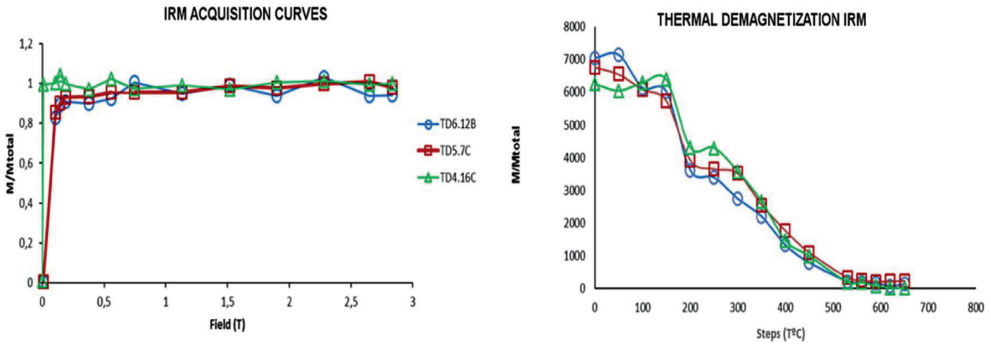

Fig. 3. IRM (isothermal remanent magnetization) diagrams an corresponding thermal demagnetization. The IRM diagrams show a rapid increase of magnetization and a saturation at about 0.1–0.2 mT. Maximum unblocking temperatures are between 550 and 600 °C.

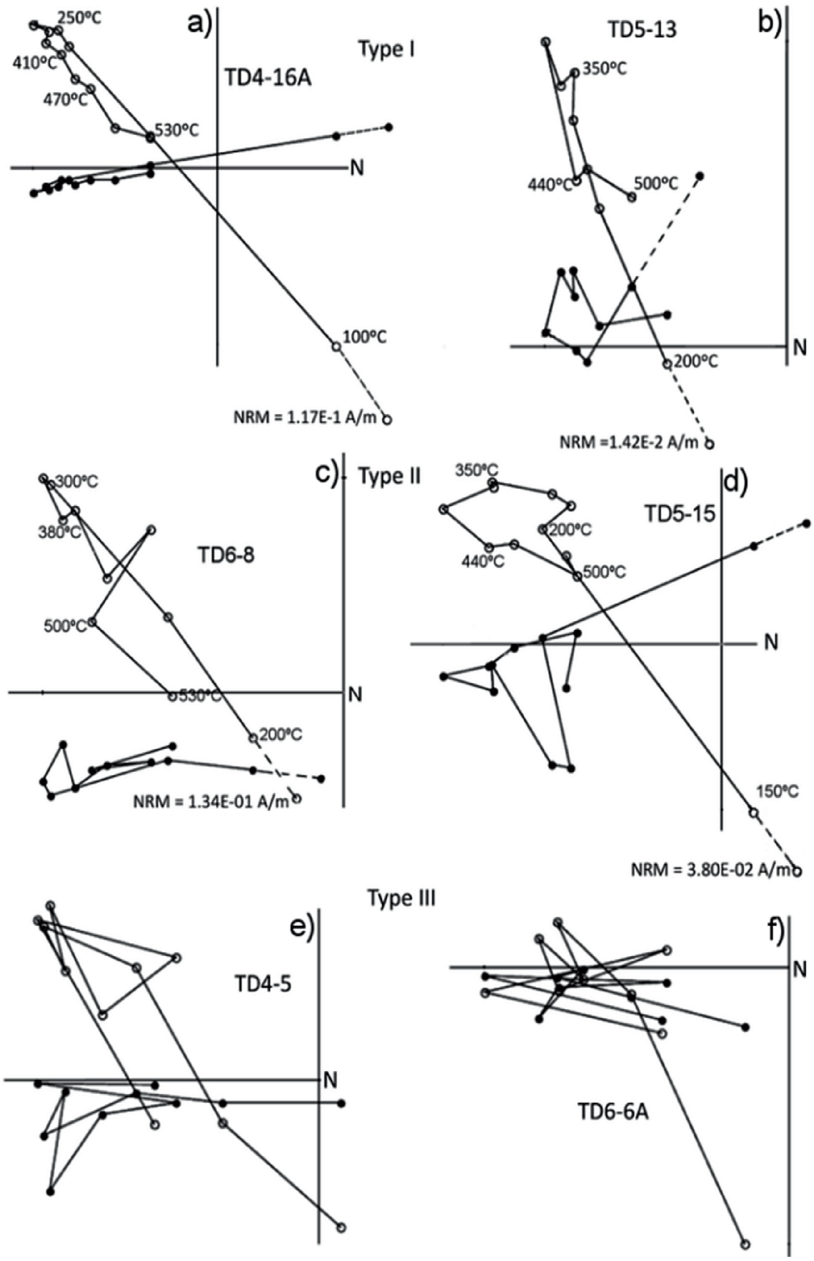

Fig. 4. Orthogonal Zijderveld diagrams representing the three types of behaviour obtained in this study. Open (closed) circles show vertical (horizontal) components of magnetization. Type I, diagrams a) and b); Type II, c) and d); and Type III e) and f).

age for TD4 level of 0.91 ± 0.25 Ma. Hence the window of time comprised in levels TD6 to TD4 levels is constrained between 0.85 and 0.91 Ma. The lower limit of such a window of time, due the uncertainty of the ESR age (~10%), is a priori compatible with the presence of the Jaramillo subchron (1.00–1.07 Ma) in the lower part of the section, a possibility that our new results allow to re-evaluate. The presence of exclusively reverse polarity from TD4 to TD7, together with the ESR age, strongly suggests that such stratigraphic interval was formed after the Jaramillo subchron, so sometime after 1.00 Ma. The Jaramillo subchron has a duration of about 60–70 ka and hence, given that no hiatuses or major erosional surfaces are observed in this part of the stratigraphy (e.g., Campaña et al., 2015), it is unlikely that the Jaramillo Subchron was simply not recorded in the stratigraphic record.

The insectivores (Eulipothyphla) and arvicolines (Rodentia) of levels TD4, TD5, TD6 and lower part of TD7 are characteristic of the end of the Early Pleistocene. These are the late Biharian microfaunas, which are partially correlated with the first two thirds of the Galerian large mammal faunas in the continental European biostratigraphy (Cuenca-Bescós et al., 2010, 2015). These observations are compatible with a post-Jaramillo age for TD4.

Overall, when comparing the magnetostratigraphy obtained in this work with the Quaternary geomagnetic instability time scale (Singer, 2014) (Fig. 7), we can conclude that lithic tool-bearing layer TD4 of Gran Dolina has an early Pleistocene age, and on the basis of all existing data, that the studied section post-dates the Jaramillo Subchron (< 1.0 Ma). Our conclusion is consistent with recent results from Italy (e.g., Muttoni et al., 2010, 2009) in that a significant pulse in human dispersal in southern Europe took place between the Jaramillo subchron and the Brunhes - Matuyama boundary (0.99–0.78 Ma) Whether the lithic tools found in TD4 (Carbonell and Rodríguez, 1994; Carbonell

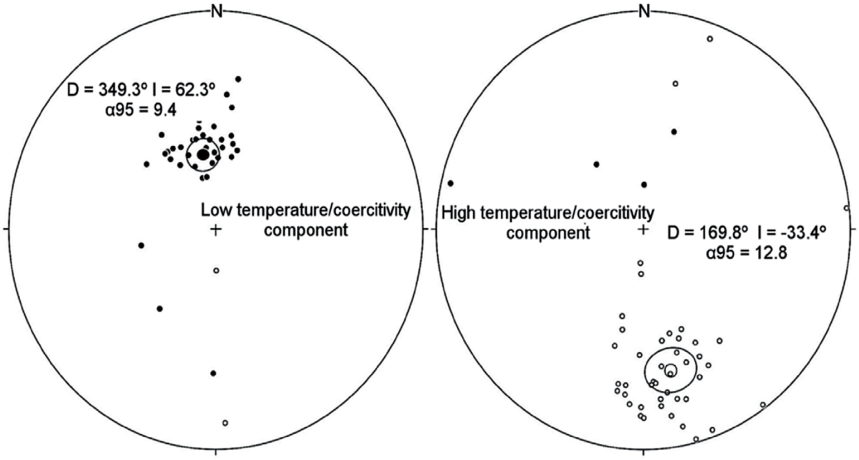

Fig. 5. Equal area, lower hemisphere projection of high and low temperature magnetization components. Each point represents a magnetization component of one individual sample. White and black dots represent vectors onto the upper and lower hemisphere respectively. Alfa-95 circles around the mean directions are also shown. The direction of the low stability components is consistent with the present Earth's field, and is considered to be recent overprint Also the expected GAD inclination is about 61.3°, which is within the error of the mean of the lower temperature component.

Table 2
The samples are grouped in sites and ordered by depth, showing the VGP Latitude calculated for each site. **Depth** = Stratigraphic depth of the sequence beginning from the top of Gran Dolina; **Site** = sampling site; **N** = Number of individual specimens used; **VGPLat°** = latitude of the Virtual Geomagnetic Pole; **Class (K)** = precision parameter; sites are classified according to the value of k: class 1 if k > 10, class 2 if k < 10, and class 3 if one specimen was used.

Depth	Site	N	VGP Lat	Class (K)
7,06	TD6.1	2	−53	1
7,18	TD6.9	1	−58	3
7,2	TD6.10	1	−59	3
7,23	TD6.8	1	−56	3
7,27	TD6.12	1	−65	3
7,4	TD6.15	1	−53	3
7,44	TD6.14	1	−57	3
7,53	TD6.13	1	−65	3
7,55	TD6.7	2	−61	1
7,8	TD6.17	1	−59	3
8	TD6.20	2	−62	1
8,05	TD6.22	1	−69	3
8,09	TD6.23	2	−78	1
8,26	TD6.21	1	−63	3
8,52	TD6.24	1	−61	3
8,95	TD5.2C	1	−33	3
9,1	TD5.15	1	−56	3
9,18	TD5.13	1	−56	6
9,21	TD5.14	1	48	3
9,24	TD5.9	1	−38	3
9,31	TD5.20	1	4	3
9,36	TD5.12	2	−46	1
9,66	TD5.18	1	−61	3
9,68	TD5.17	1	−68	3
10,11	TD4.10	1	−64	3
10,17	TD4.11	2	−71	1
10,21	TD4.1	1	40	3
10,4	TD4.12	1	29	3
10,4	TD4.4	2	−55	1
10,57	TD4-1.1	1	−60	3
11,39	TD4.29	1	40	3
11,66	TD4.31	1	76	3
12,05	TD4.20	2	−35	2
12,12	TD4.18	1	−70	3
12,22	TD4.15	1	−68	3
12,24	TD4.16	2	−37	2
12,26	TD4.17	2	−69	1
12,29	TD4.19	2	−68	1
12,34	TD4.14	1	−63	3
12,41	TD4.13	1	11	3

et al., 2001), which include cores and flakes, were transported in to the cave by natural processes or else they are in situ needs further work. No cut-marks have been observed so far in the large mammal fossils found at the layer, which would suggest transport of the artifacts into the cave, although work in progress will shed more light into this important issue.

Although Gran Dolina TD6 layer holds an unprecedented, well dated record of hominin fossils ca 0.9 Ma, the underlying and hence older stratigraphic layer TD4, which also reveals human presence through lithic tools, confirms that occupation at the site of Gran Dolina was, if not rather continuous, at least highly constant through the Pleistocene.

From a geological point of view, stratigraphic layer TD4 reveals an important change in karst dynamics, as the sediment type, grain size, and texture indicate all together the development of a proximal cave entrance and a significant drop of the water table. Notably, the small mammals recorded in these layers are indicators of dry conditions in comparison with the small mammal assemblages of layers TD5 and TD6. Underlying older levels (TD1) display interior facies (fluvial, slackwater deposits) and proximity to the phreatic level (Parés et al., submt.), with no external connections and hence preventing the accumulation of large fossils or artifacts into the cave. Therefore, a major paleoenvironmental change occurred between the top of TD1 and TD4, which led to the development of a cave entrance in Gran Dolina (TD), allowing the beginning of the accumulation of exterior sediments. As a consequence, the fossiliferous record (external input) of the lower part of Gran Dolina might be biased by the geologic processes associated with such environmental change (transport and accumulation).

Acknowledgments

Access and permission to collect samples in Atapuerca was granted by Junta de Castilla y León. The authors are deeply indebted to the Atapuerca Research Team (EIA) and the Fundación Atapuerca for continuous backup of this research. In particular, to the team of scientists that excavate level TD4 for their cooperation and patience throughout the sampling process. Thank are also debt to the “river team” that wash-sieve the sediments obtained during the excavations. Financial support for this work was obtained from Junta de Castilla y León and from MINECO projects CGL2010-16821 (J.M. Parés) and CGL2015-65387-C3-1-P (J.M. Bermúdez de Castro), and CGL2012-38434-C03-01 (G. Cuenca-Bescós). C. Álvarez-Posada has been the beneficiary of a pre-doctoral MINECO FPI grant BES-2011-048877.

Appendix B Supplementary data

Supplementary data related to this article can be found at http://dx.doi.org/10.1016/j.quageo.2018.01.003.

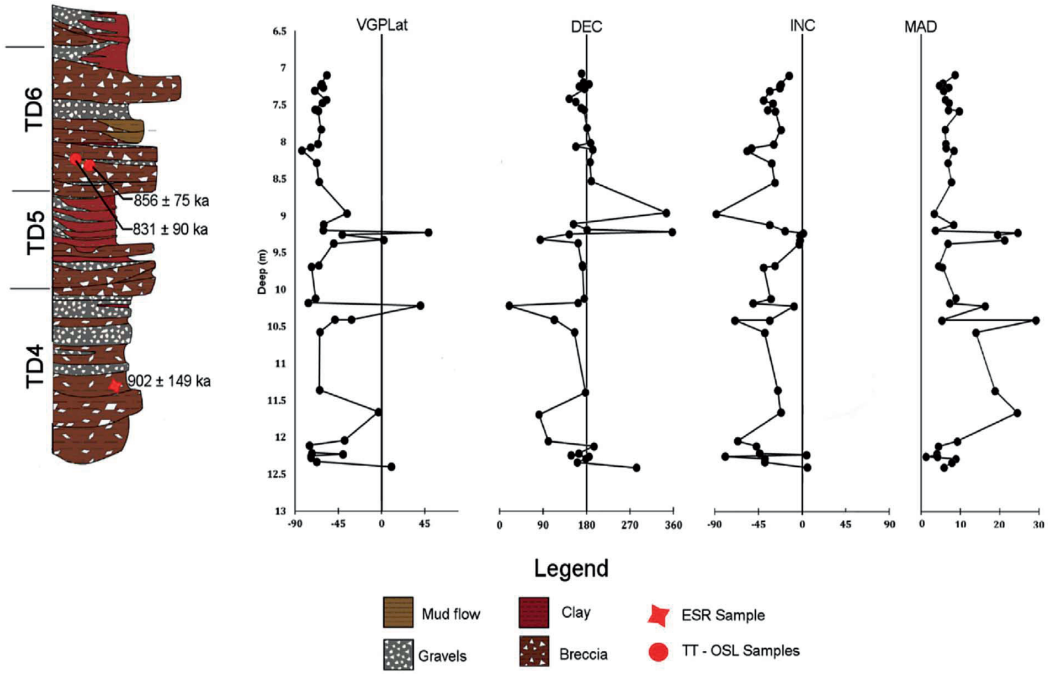

Fig. 6. Resulting magnetostratigraphy expressed as Virtual Geomagnetic Pole latitude (VGPLat°) position. Also, shown is declination (DEC), inclination (INC) and maximum angular deviation (MAD) for each site. The stratigraphic section has been taken and modified from Campaña et al. (2016). The red dots are the two luminescence samples studied by Arnold et al. (2015) by thermally transferred optically stimulated luminescence (TT-OSL) and from which they obtained a mean age of 846 ± 57 ka for unit TD6. The red star is the sample analysed byMoreno et al. (2015) at the TD4 unit. (For interpretation of the references to colour in this figure legend, the reader is referred to the Web version of this article.)

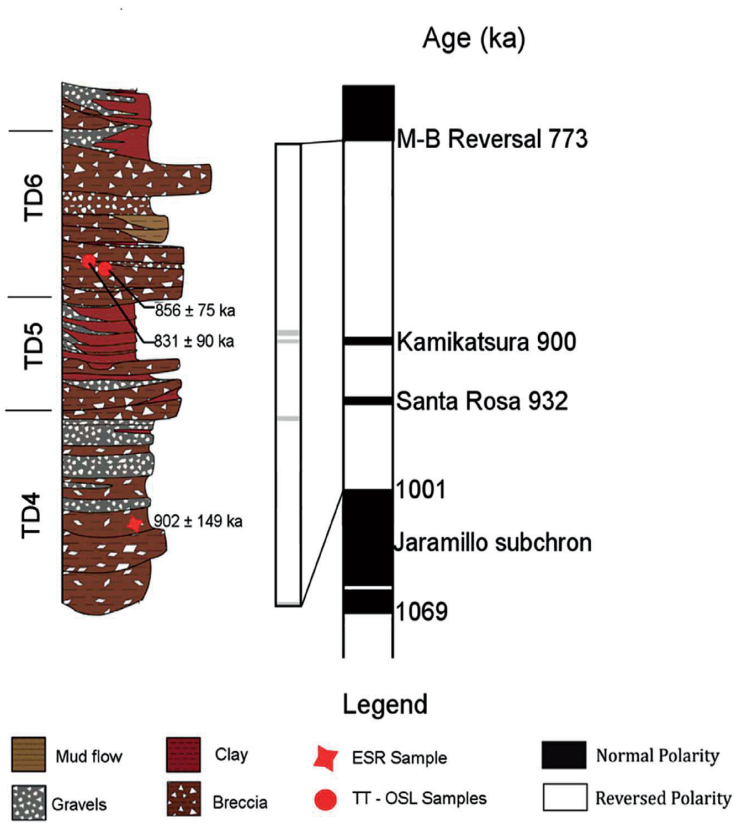

Fig. 7. Comparison of the magnetostratigraphy obtained in this study with the GITS (geomagnetic instability time scale) of Matuyama Reverse Chron (modified from Singer, 2014). The stratigraphic section has been taken and modified from Campaña et al., (2016). Although we find values of normal polarity in depths of 9, 10 and 12.5 m (the grey levels in the magnetostratigraphy) we cannot interpret them in terms of full reversals of the geomagnetic field (see text for discussion).

References

Aguirre, E., Arsuaga, J.L., Bermúdez de Castro, J.M., Carbonell, E., Ceballos, M., Díez, C., Enamorado, J., Fernández-Jalvo, Y., Gil, E., Gracia, A., Martín-Nájera, A., Martínez, I., Morales, J., Ortega, A.I., Rosas, A., Sánchez, A., Sánchez, B., Sesé, C., Soto, E., Torres, T.J., 1990. The Atapuerca sites and the ibeas hominids. Hum. Evol. 5, 55–73. http://dx.doi.org/10.1007/BF02436474.

Alonso-Gavilán, G., Armenteros, I., Carballeira, J., Corrochano, A., Huerta, P., Rodríguez, J., 2004. Cuenca del Duero. In: Vera, J.A. (Ed.), Geología de España. SGE-IGME, Madrid, pp. 531–586.

Arnold, L.J., Demuro, M., Parés, J.M., Pérez-González, A., Arsuaga, J.L., Bermúdez de Castro, J.M., Carbonell, E., 2015. Evaluating the suitability of extended-range luminescence dating techniques over early and Middle Pleistocene timescales: published datasets and case studies from Atapuerca, Spain. Quat. Int. 389, 167–190. http://dx.doi.org/10.1016/j.quaint.2014.08.010.

Arsuaga, J.L., Bermúdez de Castro, J.M., Carbonell, E., 1997. Preface for 'Special Issue: the Sima de los Huesos Hominid Site'. J. Hum. Evol. 33, 105–107.

Benito-Calvo, A., 2004. Análisisgeomorfológico y reconstrucción de paleopaisajes neógenos y cuaternarios en laSierra de Atapuerca y el valle medio del río Arlanzón. Universidad Complutensede Madrid, Servicio de Publicaciones, Madrid doi: ISBN 84-669-2585.

Benito-Calvo, A., Pérez-González, A., Parés, J.M., 2008. Quantitative reconstruction of Late Cenozoic landscapes : a case study in the Sierra de Atapuerca (Burgos, Spain). Earth Surf. Process. Landforms 33, 196–208. http://dx.doi.org/10.1002/esp.

Berger, G.W., Pérez-González, A., Carbonell, E., Arsuaga, J.L., Bermúdez de Castro, J.M., Ku, T.-L.L., 2008. Luminescence chronology of cave sediments at the Atapuerca paleoanthropological site, Spain. J. Hum. Evol. 55, 300–311. http://dx.doi.org/10.1016/j.jhevol.2008.02.012.

Bermúdez-de Castro, J., Perez-Gonzalez, A., Martinon-Torres, M., Gomez-Robles, A., Rosell, J., Prado, L., Sarmiento, S., Carbonell, E., 2008. A new early Pleistocene hominin mandibule from Atapuerca-TD6, Spain. J. Hum. Evol. 55, 729–735.

Bermúdez de Castro, J.M., 1997. A hominid from the lower Pleistocene of Atapuerca, Spain: possible ancestor to neandertals and modern humans. Science 276, 1392–1395. http://dx.doi.org/10.1126/science.276.5317.1392.

Bógalo, M.F., Heller, F., Villaláin, J.J., Calvo, M., Osete, M.L., Pérez-González, A., 2003. Propuesta metodológica para la caracterización de la mineralogía magnética en estudios paleoambientales. Aplicación al yacimiento de Atapuerca. Geogaceta 34, 107–110.

Campaña, I., Benito-Calvo, A., Pérez-González, A., Ortega, A.I., Bermúdez de Castro, J.M., Carbonell, E., 2015. Pleistocene sedimentary facies of the Gran Dolina archaeo-paleoanthropological site (Sierra de Atapuerca, Burgos, Spain). Quat. Int. 1–17. http://dx.doi.org/10.1016/j.quaint.2015.04.023.

Campaña, I., Pérez-González, A., Benito-Calvo, A., Rosell, J., Blasco, R., Bermúdez De Castro, J.M., Carbonell, E., Arsuaga, J.L., 2016. New Interpretation of the Gran Dolina-TD6 Bearing Homo Antecessor Deposits through Sedimentological Analysis. Nature Publishing Group, pp. 1–13. http://dx.doi.org/10.1038/srep34799.

Carbonell, E., Bermúdez de Castro, J.M., Arsuaga, J.L., Díez, C., Rosas, A., Cuenca-Bescós, G., Sala, R., Mosquera, M., Rodríguez, X.P., 1995. Lower Pleistocene hominids and artefacts from Atapuerca - TD6 (Spain). Science 269, 826–829.

Carbonell, E., Bermúdez de Castro, J.M., Parés, J.M., Pérez-González, A., Cuenca-Bescós, G., Ollé, A., Mosquera, M., Huguet, R., Made, J. van der, Rosas, A., Sala, R., Vallverdú, J., García, N., Granger, D.E., Martinón-Torres, M., Rodríguez, X.P., Stock, G.M., Vergès, J.M., Allué, E., Burjachs, F., Cáceres, I., Canals, A., Benito, A., Díez, C., Lozano, M., Mateos, A., Navazo, M., Rodríguez, J., Rosell, J., Arsuaga, J.L., 2008. The first hominin of Europe. Nature 452, 465–469. http://dx.doi.org/10.1038/nature06815.

Carbonell, E., Mosquera, M., Ollé, A., Rodríguez, X.P., Sahnouni, M., Sala, R., Vergès, J.M., Rodriguez, X.P., 2001. Structure morphotechnique de l'industrie lithique du Pléistocène inférieur et moyen d'Atapuerca (Burgos, Espagne). Anthropologie 105, 259–280. http://dx.doi.org/10.1016/S0003-5521(01)80016-9.

Carbonell, E., Rodríguez, X.P., 1994. Early Middle Pleistocene deposits and artefacts in the Gran Dolina site (TD4) of the 'Sierra de Atapuerca' (Burgos, Spain). J. Hum. Evol. 26, 291–311.

Cuenca-Bescós, G., Blain, H.A., Rofes, J., Lozano-Fernández, I., López-García, J.M., Duval, M., Galán, J., Núñez-Lahuerta, C., 2015. Comparing two different Early Pleistocene microfaunal sequences from the caves of Atapuerca, Sima del Elefante and Gran Dolina (Spain): biochronological implications and significance of the Jaramillo subchron. Quat. Int. 389, 148–158. http://dx.doi.org/10.1016/j.quaint.2014.12.059.

Cuenca-Bescós, G., Canudo, J.I., Laplana, C., 2001. La séquence des rongeurs (Mammalia) des sites du Pléistocène inférieur et moyen d' Atapuerca (Burgos, Espagne). Anthropologie 105, 115–130. http://dx.doi.org/10.1016/S0003-5521(01)80009-1.

Cuenca-Bescós, G., García, N., 2007. Biostratigraphic succession of the early and Middle Pleistocene mammals faunas of the Atapuerca caves sites (Burgos, Spain). Courier Forschungsinstitut Senckenberg Weimar 259, 99–101.

Cuenca-Bescós, G., Laplana, C., Canudo, J.I., 1999. Biochronological implications of the arvicolidae (Rodentia, Mammalia) from the lower Pleistocene hominid-bearing level of trinchera Dolina 6 (TD6, Atapuerca, Spain). J. Hum. Evol. 37, 353–373. http://dx.doi.org/10.1006/jhev.1999.0306.

Cuenca-Bescós, G., Rofes, J., López-García, J.M., Blain, H.A., De Marfá, R.J., Galindo-Pellicena, M.A., Bennásar-Serra, M.L., Melero-Rubio, M., Arsuaga, J.L., Bermúdez de Castro, J.M., Carbonell, E., 2010. Biochronology of Spanish Quaternary small vertebrate faunas. Quat. Int. 212, 109–119. http://dx.doi.org/10.1016/j.quaint.2009.06.007.

Duval, M., Falguères, C., Bahain, J.J., Grün, R., Shao, Q., Aubert, M., Dolo, J.M., Agustí, J., Martínez-Navarro, B., Palmqvist, P., Toro-Moyano, I., 2012. On the limits of using combined U-series/ESR method to date fossil teeth from two Early Pleistocene archaeological sites of the Orce area (Guadix-Baza basin, Spain). Quat. Res. 77, 482–491. http://dx.doi.org/10.1016/j.yqres.2012.01.003.

Duval, M., Moreno, D., Shao, Q., Voinchet, P., Falguères, C., Bahain, J.J., Garcia, T., Garcia, J., Martinez, K., 2011. Datacion por ESR del yacimiento arqueologico del Pleistoceno inferior de Vallparadís (Terrassa, Cataluna, Espana). Trab. Prehist. 68, 7–24.

Falguères, C., Bahain, J.-J.J., Yokoyama, Y., Arsuaga, J.L., Bermudez de Castro, J.M., Carbonell, E., Bischoff, J.L., Dolo, J.-M.M., 1999. Earliest humans in Europe: the age of TD6 gran Dolina, Atapuerca, Spain. J. Hum. Evol. 37, 343–352. http://dx.doi.org/10.1006/jhev.1999.0326.

Falguères, C., Bahain, J.J., Bischoff, J., Pérez-González, A., Ortega, A.I., Ollé, A., Quiles, A., Ghaleb, B., Moreno, D., 2013. Combined ESR/U-series chronology of Acheulian hominid bearing layers at Trinchera Galería site, Atapuerca, Spain. J. Hum. Evol. 65, 168–184.

García, N., Arsuaga, J.L., 2001. Les carnivores (Mammalia) des sites dus Pléistocène ancien et moyen d'Atapuerca (Espagne). L'Anthropologie 105, 83–94.

García, N., Arsuaga, J.L., 1999. Carnivores from the Early Pleistocene hominid-bearing Trinchera Dolina 6 (Sierra de Atapuerca, Spain). J. Hum. Evol. 37, 415–430. http://dx.doi.org/10.1006/jhev.1999.0325.

Gil, E., Aguirre, E., Hoyos, M., 1987. Contexto estratigráfico. In: Aguirre, E., Carbonell, E., Bermúdez de Castro, J.M. (Eds.), El Hombre Fósil de Ibeas Y El Pleistoceno de La Sierra de Atapuerca, pp. 47–54 Valladolid.

Laplana, C., Cuenca-Bescós, G., 2000. Una nueva especie de Microtus (Allophaiomys) (Arvicolidae, Rodentia, Mammalia) en el Pleistoceno inferior de la Sierra de Atapuerca (Burgos, España). Rev. Esp. Paleon 15, 77–88.

López-García, J.M., Blain, H.-A., De Marfá, R., García, A., Martinell, J., Bennàsar, M.L., Cuenca-Bescós, G., 2011. Small-mammals from the Middle Pleistocene layers of the Sima del Elefante (Sierra de Atapuerca, Burgos, northwestern Spain). Geol. Acta 9, 29–43.

Made, J van der, Dimitrijevic, V., 2015. Eucladoceros montenegrensis n. sp. and other Cervidae from the lower Pleistocene of trlica (Montenegro). Quat. Int. 2 (389), 90–118.

Made, J van der, Rosell, J., Blasco, R., 2015. Faunas from Atapuerca at the Early-Middle Pleistocene limit: the ungulates from level TD8 in the context of climatic change. Quat. Int. 433, 1–51.

Minwer-Barakat, R., Madurell-Malapeira, J., Alba, D.M., Aurell-Garrido, J., De Esteban-Trivigno, S., Moyà-Solà, S., 2011. Pleistocene rodents from the Torrent de Vallparadís section (Terrassa, northeastern Spain) and biochronological implications. J. Vertebr. Paleontol. 31, 849–865. http://dx.doi.org/10.1080/02724634.2011.576730.

Moreno, D., Falguères, C., Pérez-González, A., Voinchet, P., Ghaleb, B., Despriée, J., Bahain, J.J., Sala, R., Carbonell, E., Bermúdez de Castro, J.M., Arsuaga, J.L., 2015. New radiometric dates on the lowest stratigraphical section (TD1 to TD6) of Gran Dolina site (Atapuerca, Spain). Quat. Int. 30, 535–540. http://dx.doi.org/10.1016/j.quageo.2015.05.007.

Muttoni, G., Scardia, G., Kent, D.V., 2010. Human migration into Europe during the late early Pleistocene climate transition. Palaeogeogr. Palaeoclimatol. Palaeoecol. 296, 79–93. http://dx.doi.org/10.1016/j.palaeo.2010.06.016.

Muttoni, G., Scardia, G., Kent, D.V., Swisher, C.C., Manzi, G., 2009. Pleistocene magnetochronology of early hominin sites at Ceprano and Fontana Ranuccio, Italy. Earth Planet Sci. Lett. 286, 255–268. http://dx.doi.org/10.1016/j.epsl.2009.06.032.

Ortega, A.I., Benito-Calvo, A., Pérez-González, A., Martín-Merino, M.A., Pérez-Martínez, R., Parés, J.M., Aramburu, A., Arsuaga, J., Bermúdez de Castro, J.M., Carbonell, E., 2013. Evolution of multilevel caves in the Sierra de Atapuerca (Burgos, Spain) and its relation to human occupation. Geomorphology 196, 122–137. http://dx.doi.org/10.1016/j.geomorph.2012.05.031.

Parés, J.M., Arnold, L., Duval, M., Demuro, M., Pérez-González, A., Bermúdez de Castro, J.M., Carbonell, E., Arsuaga, J.L., 2013. Reassessing the age of Atapuerca-TD6 (Spain): new paleomagnetic results. J. Archaeol. Sci. 40, 4586–4595. http://dx.doi.org/10.1016/j.jas.2013.06.013.

Parés, J.M., Pérez-González, A., 1995. Paleomagnetic age for hominid fossils at Atapuerca archaeological site, Spain. Science 269, 830–832. http://dx.doi.org/10.1126/science.7638599.

Parés, J.M.M., Pérez-González, A., 1999. Magnetochronology and stratigraphy at gran Dolina section, Atapuerca (Burgos, Spain). J. Hum. Evol. 37, 325–342. http://dx.doi.org/10.1006/jhev.1999.0331.

Pérez-González, A., Parés, J.M., Carbonell, E., Aleixandre, T., Ortega, A.I., Benito, A., Martin Merino, M.Á., 2001. Géologie de la Sierra de Atapuerca et stratigraphie des remplissages karstiques de Galería et Dolina (Burgos, Espagne). L'Anthropologie 105, 27–43. http://dx.doi.org/10.1016/S0003-5521(01)80004-2.

Rodríguez-Gómez, G., Rodríguez, J., Martín-González, J.Á., Goikoetxea, I., Mateos, A., 2013. Modeling trophic resource availability for the first human settlers of Europe: the case of Atapuerca TD6. J. Hum. Evol. 64, 645–657. http://dx.doi.org/10.1016/j.jhevol.2013.02.007.

Rodríguez, J., Burjachs, F., Cuenca-Bescós, G., García, N., Van der Made, J., Pérez González, A., Blain, H.A., Expósito, I., López-García, J.M., García Antón, M., Allué, E., Cáceres, I., Huguet, R., Mosquera, M., Ollé, A., Rosell, J., Parés, J.M., Rodríguez, X.P., Díez, C., Rofes, J., Sala, R., Saladi, P., Vallverdú, J., Bennasar, M.L., Blasco, R., Bermúdez de Castro, J.M., Carbonell, E., 2011. One million years of cultural evolution in a stable environment at Atapuerca (Burgos, Spain). Quat. Sci. Rev. 30, 1396–1412. http://dx.doi.org/10.1016/j.quascirev.2010.02.021.

Rook, L., Martínez-Navarro, B., 2010. Villafranchian: the long story of a Plio-Pleistocene European large mammal biochronologic unit. Quat. Int. 219, 134–144. http://dx.doi.org/10.1016/j.quaint.2010.01.007.

Singer, B.S., 2014. A quaternary geomagnetic instability time scale. Quat. Geochronol. 21, 29–52. http://dx.doi.org/10.1016/j.quageo.2013.10.003.

Zijderveld, J.D.A., 1967. Ac demagnetization of rocks: analysis of results. In: Collinson, D.W., Creer, K.M., Runcorn, S.K. (Eds.), Methods in Palaeomagnetism. Elsevier, Amsterdam, New York, pp. 254–286. http://dx.doi.org/10.1016/j.neuroscience.2010.03.066.

Capítulo 7 . chronology of the cave interior sediments at gran dolina archaeological site, atapuerca (spain)

Quaternary Science Reviews 186 (2018) 1–16

Contents lists available at ScienceDirect

Quaternary Science Reviews

journal homepage: www.elsevier.com/locate/quascirev

Chronology of the cave interior sediments at Gran Dolina archaeological site, Atapuerca (Spain)

J.M. Parés [a, *], C. Álvarez [a], M. Sier [b, c, d], D. Moreno [a], M. Duval [e], J.D. Woodhead [f], A.I. Ortega [a, g], I. Campaña [a], J. Rosell [h, i], J.M. Bermúdez de Castro [a, j], E. Carbonell [h, i]

[a] CENIEH, Paseo Sierra de Atapuerca 3, 09002 Burgos, Spain
[b] Department of Earth Sciences, Oxford University, South Parks Road, OX1 3AN Oxford, United Kingdom
[c] Paleomagnetic Laboratory Fort Hoofddijk, Faculty of Geosciences, Utrecht University, 3584 CD, Utrecht, The Netherlands
[d] Faculty of Archaeology, Leiden University, PO Box 9515, 2300 RA, Leiden, The Netherlands
[e] Australian Research Centre for Human Evolution, Environmental Futures Research Institute, Griffith University, 170 Kessels Road, Nathan, Australia
[f] School of Earth Sciences, University of Melbourne, VIC, 3010, Australia
[g] Fundación Atapuerca, Ctra. de Logroño, 44, 09198 Ibeas de Juarros, Spain
[h] Institut Català de Paleoecologia Humana i Evolució Social, c/ Marcel·lí Domingo s/n, Campus Sescelades, 43007 Tarragona, Spain
[i] Àrea de Prehistoria, Dept. d'Història de l'Art, Univ. Rovira i Virgili, Fac. de Lletres, Av. Catalunya, 35, 43002 Tarragona, Spain
[j] Department of Anthropology, University College London, 14 Taviton Street, London, WC1H 0BW, UK

ARTICLE INFO

Article history:
Received 29 September 2017
Received in revised form
31 January 2018
Accepted 6 February 2018

Keywords:
Karstic cave
Spain
Pleistocene
Interior facies
Paleomagnetism
ESR
U/Pb dating

ABSTRACT

The so-called "Gran Dolina site" (Atapuerca mountain range, N Spain) is a karstic cavity filled by sediments during the Pleistocene, some of which contain a rich ensemble of archaeological and paleontological records. These sediments have contributed significantly to our understanding of early human dispersal in Europe but, in contrast, older, interior facies deposits have received much less of attention. The stratigraphy of Gran Dolina reveals an abrupt sedimentary change of interior to entrance facies from bottom to top, reflecting a significant paleoenvironmental change that promoted the accumulation of sediments transported from the vicinity of the cave by water or "en masse". Since the major magnetic polarity reversal known as the Matuyama-Brunhes boundary (0.78 Ma) was detected within the TD7 unit in the middle of the stratigraphic section, we carried out a new combined paleomagnetic, radiometric (U-Pb), and electron spin resonance (ESR) dating study of the lower part of the sequence in order to constrain the chronology of the interior facies at Gran Dolina. U-Pb analysis of speleothems did not produce age information as the samples proved to be extremely unradiogenic. The magnetic stratigraphy of the cave interior sediments reveals a dominant reverse magnetic polarity, coherent with a Matuyama age, and interrupted by a normal polarity magnetozone interpreted as the Jaramillo Subchron (1.0–1.1 Ma). ESR ages on quartz grains from the upper part of the interior facies sediments are coherent with such an interpretation. We conclude that the fluvial deposits (interior facies) that constitute the cave floor began accumulating before 1.2 Ma. The development of large cave entrances at Gran Dolina occurred shortly after the Jaramillo Subchron but before ca 900 ka ago.

1. Introduction

Research at the Lower Paleolithic cave site of Gran Dolina, Sierra de Atapuerca (northern Spain) (Fig. 1), has led to major advances in our understanding of human evolution and occupation of Eurasia in the Pleistocene. The Gran Dolina site has produced thousands of fossils and artifacts since 1995, when the first hominin remains were reported, and soon became a Pleistocene landmark in studies of early human settlement outside the African continent (Carbonell et al., 1995, 2008). Stratigraphic layer TD6 of Gran Dolina has yielded over 170 human fossil remains, more than 200 lithic artifacts, classified as Mode 1, as well as several thousand small and large vertebrate remains (Bermúdez de Castro et al., 1997; Carbonell et al., 2005; Bermúdez de Castro et al., 2008; Ollé et al., 2013). The initial paleomagnetic dating at Gran Dolina revealed a switch from reverse to normal geomagnetic polarity above TD6 level,

* Corresponding author.
E-mail address: josep.pares@cenieh.es (J.M. Parés).

https://doi.org/10.1016/j.quascirev.2018.02.004
0277-3791/

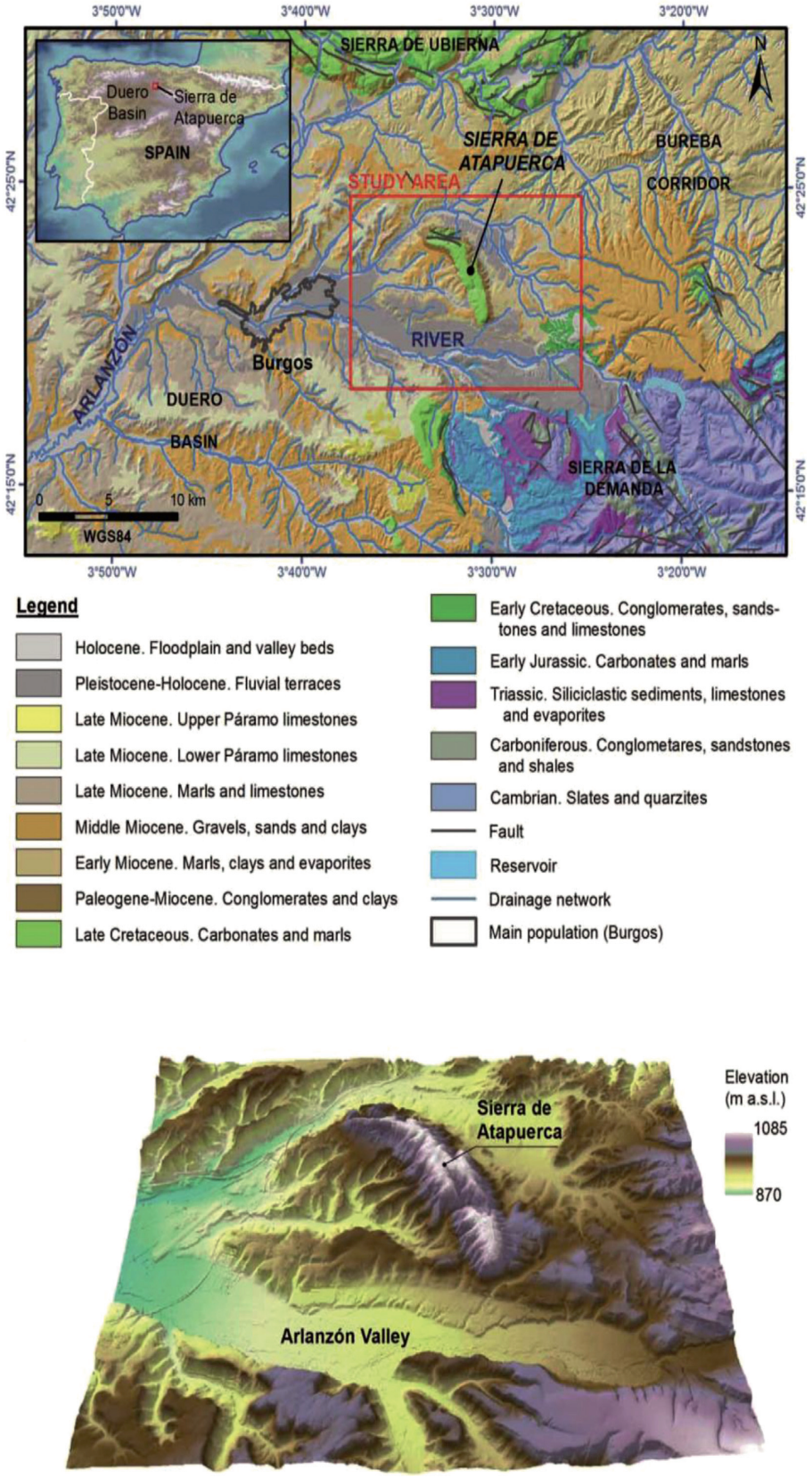

Fig. 1. Regional geological map of the study area showing the main lithological units (above), and a 3D view of the Atapuerca Mountain Range (Benito-Calvo and Pérez-González, 2015).

interpreted as the Matuyama-Brunhes boundary (MBB), providing a minimum age of 0.78 Ma for the archaeo-paleontological layer TD6 (Parés and Pérez-González, 1995). Subsequent chronometric analysis by Electron Spin Resonance (ESR) and luminescence further reinforced the paleomagnetic age (Falguères et al., 1999), and currently an age of around 0.85 Ma is accepted for the TD6 level (Parés et al., 2013; Arnold et al., 2014; Moreno et al., 2015). About four meters below TD6, stratigraphic layer TD4, a breccia of gravel-size clasts in a muddy and sandy matrix, is known to contain archaeological artifacts although no human fossils have been found yet (Carbonell and Rodríguez, 1994) (Fig. 2). The chronology of the ensemble TD4-TD5 levels is constrained by ESR dates on quartz grains and ranges between 0.9 and 1.13 Ma (Moreno et al., 2015). Such an age range overlaps with the Jaramillo Subchron (1.00–1.07 Ma) and therefore paleomagnetism allows testing whether level TD1 has a pre or post-Jaramillo age and in doing so constraining the age of the overlying, lithic-tool bearing layer TD4. Due to the progress of the excavation during the past five years, it has recently been possible to reach the bottom of TD1 stratigraphic layer at Gran Dolina, extending by ten more meters the current stratigraphic profile at the site.

There is very little chronological constraint on the underlying interior cave deposits that make up layer TD1. Interior facies deposits in caves are found in parts that are more remote and far the cave entrance, in total darkness, and typically in the vadose and upper phreatic zone of the cave system. Deposition modes in such areas are determined by the hydrologic conditions and may consist of fluvial gravels, sands and clays, commonly referred as fluvial facies. Even though layer TD1 is sterile, a better age for the sediments would constitute a maximum age for the overlying archaeological layer. Since the MB boundary has been identified in TD7, TD1 is known to be older than 0.78 Ma (Parés et al., 2013). The only direct ages available so far are based on ESR dating of optically bleached quartz grains extracted from the top of TD1. The three samples dated by Moreno et al. (2015) confirm an Early Pleistocene chronology, but the age scatter (from 789 ± 61 to 1249 ± 126 ka) does not provide any further age constraint. In this study we report new paleomagnetic and ESR dating results from cave interior sediments layer TD1, well below the fossiliferous stratigraphic units, and well below the MB boundary recorded in TD7/TD8. Such new chronological constraints will build on the existing chronology in two different ways. First, paleomagnetism can detect the presence of subchrons along the Gran Dolina lower section in TD1 that could help establishing additional time lines in the sedimentary infill. For this purpose we collected numerous paleomagnetic samples through 9 m in layer TD1, including laminated clastic deposits that preceded the opening of large entrances to the cave and the concomitant accumulation of fossils and artifacts. Second, we re-analysed with ESR three quartz samples from the bottom of the sedimentary sequence that were previously dated by Moreno et al. (2015), by measuring the Ti-center and by obtaining new dose rate measurements. Last, we attempted to date two flowstones at the top of TD1 with the U-Pb method.

2. Geological setting

At first glance the Gran Dolina sedimentary deposits reveal a rather common succession in karstic tiered caves that developed in relation to progressive river incision. Passages of phreatic origin form at or just below the water table and are subjected to frequent flooding and associated deposition of slackwater deposits by stream flows. Accumulation of drip-type flowstones such as stalactites and stalagmites will often cap the fine clastic sediments, although these can also form after groundwater draining. In either case, the development of flowstones in caves has been associated with prolonged valley stability (e.g., Frank et al., 2006; Couchoud, 2008; Harmand et al., 2017). As incision lowers the local water table such passages are progressively abandoned and subjected to truncation by valley deepening, collapse, or fissuring that eventually will lead to the formation of a cave entrance. Talus, slope wash, and sliding bed mode deposits will then accumulate at the cave entrance and up to several meters in to the cave. Such processes will produce a variety of gravel accumulation, diamictons, and channel facies, controlled by water availability and particle size (e.g., Bosch and White, 2004). The Gran Dolina stratigraphy has been divided into 12 main units termed TD1 to TD 11 from bottom to top (Campaña et al., 2017). It reflects a broad evolution and includes cave interior deposits at the bottom (including both silts, clays and flowstones) below TD4 unit, and an assemblage of diamictons and gravels often showing channel cut-and-fill structures with abundant sand and silts from TD4 to the top of the sequence (Fig. 2). Cave entrance deposits will not be further considered in this paper and details can be found in Campaña et al. (2017). Below a prominent flowstone at the base of these cave entrance deposits (the basal "stalagmitic crust" of Carbonell and Rodríguez, 1994), the sedimentary record is mostly made up by silts and clays of fluvial origin (Fig. 2). Although a detailed study of such sediments is underway, the source of these cave interior sediments likely includes fluvial deposits and filtrates from soils (terra rossa). Silts and clays are often laminated, a quite common feature in phreatic environments (e.g., Ford and Williams, 2007), although the presence of two flowstones towards the top of the section suggests sporadic proximity to the vadose zone. The lower half of the stratigraphic section is characterized by a conspicuous unit of inclined laminar bedding silts and clays. Laminae are parallel to the depositional surface and therefore the unit corresponds to parallel accretion (Bull, 1981), so deposition of silt and clay laminae that are concordant to the underlying bedrock topography. Locally, such laminated silts and clays form couplets (3–4 cm thick), possibly suggestive of frequent flooding and drawing (Ford and Williams, 2007) by a mechanism linked to climatic events.

Consequently, our sampling was focused on the cave interior deposits TD1-TD2, which basically correspond to a slackwater facies and the capping flowstones, with the ultimate goal of extending the magnetostratigraphy at Gran Dolina to the floor of the cavity. In addition to this 9 m-thick new profile (hereafter called the Vicho section), a shorter one (South Trench) 4 m south and encompassing the layers sampled for ESR was also sampled and paleomagnetically studied and the description can be found somewhere else (Campaña et al., 2017).

3. Sampling and procedures

3.1. Paleomagnetism and rock-magnetism

Owing to the cementation of the cave deposits, two different methods have been used to obtain paleomagnetic samples. In flowstones and cemented siltstones we used a gas-powered drilling machine, equipped with a 1-inch non-magnetic drill bit. Soft, non-cohesive clay and silt deposit samples were obtained by pushing standard 8 cm^3 cubic or cylindrical plastic boxes into a clean, vertical surface. In both cases orientation of the specimens was performed *in situ* using a standard orientation device (compass-inclinometer) to obtain the azimuth and dip of the samples. Paleomagnetic analyses were carried out at the Geochronology facilities at the CENIEH (Burgos, Spain). Measurement of the natural remanent magnetization (NRM) of the samples was performed with a cryogenic magnetometer 2G model 755R–4K, which includes an online AF degausser capable of producing a peak field of 170 mT. Thermal demagnetization of the NRM was carried out with

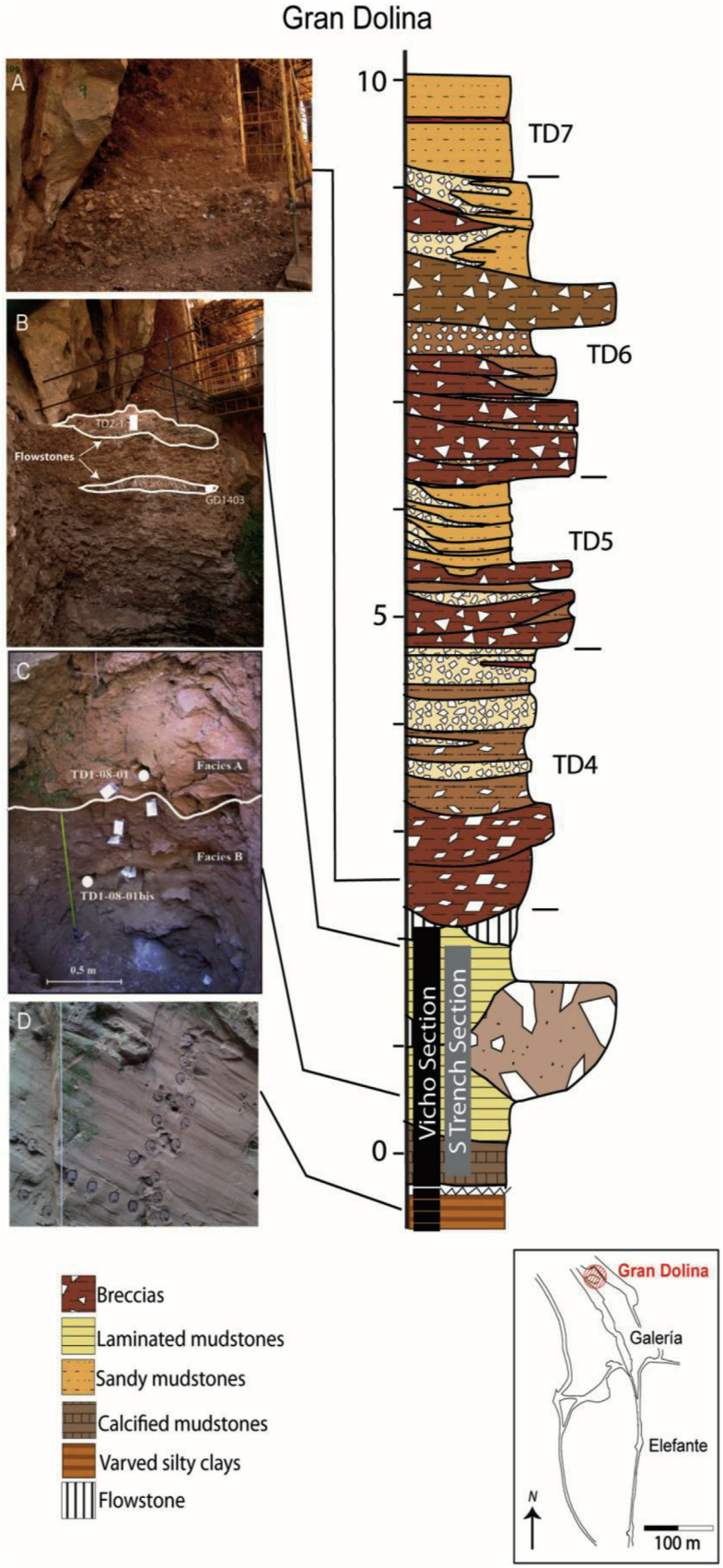

Fig. 2. Gran Dolina sedimentary infill above the interior facies (units TD4 to lower part of TD7). Photographs: A- Breccias of the lower part of unit TD4; B- Speleothems at the top of unit TD1 and location of samples for U-Pb analysis (see text for details); C- Position of the three ESR samples in S Trench section; D- Detail of laminated silty clays in the lower part of the interior facies deposits. Location of the two studied sections is shown at the bottom of the stratigraphic column (Vicho Section and S Trench Section). Facies and stratigraphic section modified from Campaña et al. (2017). Insert shows the general context of the Gran Dolina site on a map view of the excavation area.

an oven (model TD-48, ASC Scientific). Standard orthogonal, Zijderveld-type plots were used to interpret the structure of remanence components to later computing the direction of the Characteristic Remanent Magnetization (ChRM) directions using linear regression, guided by visual inspection of orthogonal demagnetization plots. Rockmagnetic analysis included hysteresis cycles, which were obtained on a 3900 VSM MicroMag (Princeton).

For sedimentary fabric characterization, we have used the anisotropy of magnetic susceptibility (AMS). The low field magnetic susceptibility of a rock (the ratio of magnetization, M, to the applied field H, or K = M/H) is given by the total contribution of its bulk mineralogy, including paramagnetic (e.g., phyllosilicates, iron-bearing feldspars), diamagnetic (e.g., quartz, calcite) and ferromagnetic (*sensu lato*; e.g., magnetite, goethite, hematite) grains. The AMS is defined by an ellipsoid (Nye, 1957) whose semi-axes are the three principal susceptibilities ($K_{max} \geq K_{int} \geq K_{min}$). AMS in siliciclastic rocks depends mostly on the crystallographic preferred orientation of the individual components, mostly phyllosilicates, and compositional layering. Therefore, AMS can be used as a proxy for grain preferred orientation in a variety of rocks (e.g., Tarling and Hrouda, 1993). Some of the advantages of using AMS as opposed to x-ray, or other methods such as neutron diffraction are the speed of the measurement and the integration of thousands of grains as analyses are performed on several cubic centimeters of rock at a time.

AMS was measured on a 1-FA Kappabridge (AGICO Instruments), a fully automated inductive bridge, at a frequency of 976 Hz and with a field of 200 A/m. The measurement takes about 2 min per specimen and is very precise, due to many susceptibility determinations in each plane perpendicular to the axis of specimen rotation. The errors in determination of this tensor are estimated using a method based on multivariate statistics principles Jelinek (1978). There is a plethora of parameters to describe the axial magnitude relationships of the susceptibility ellipsoid (see also Tauxe, 1993; Tarling and Hrouda, 1993). The simplest expressions are the axial ratios L (K_{max}/Kin) (Balsley and Buddington, 1960), F (K_{int}/K_{min}) (Stacey et al., 1960) and P (K_{max}/K_{min}) (Nagata, 1961). Alternatively, other authors use the parameters P' ($P' = \exp 2(a_1^2+a_2^2+a_3^2)]^{1/2}$ (Jelinek, 1981) where $a_1 = \ln(K_{max}/K_b)$, etc. and $K_b=(K_{max} + k_{int} + K_{min})/3$ (Nagata, 1961) to express the fabric intensity as a measure of eccentricity and T ($T = 2(\ln K_{int}-\ln K_{min})/[\ln K_{max}-\ln K_{min}]-1$) (Jelinek, 1981) to define the degree to which the ellipsoid is oblate or prolate, both adopted in this study.

3.2. Electron spin resonance of optically bleached quartz grains

Among the 39 quartz samples previously ESR dated at Gran Dolina by Moreno et al. (2015), three of them (TD1-08-01bis, TD1-08-01 and TD1-08-02) were taken from the upper part of level TD1 layer and are consequently of direct interest for the present study. Full details of the sample preparation, gamma irradiations and laboratory bleaching experiment can be found in Moreno et al. (2015). All the aliquots (i.e., gamma-irradiated, natural and bleached aliquots) of these three quartz samples were re-measured by ESR using the experimental setup at CENIEH (see details in Duval and Guilarte Moreno, 2012) and following the most advanced analytical procedures as in Duval et al. (2017). New *in situ* gamma spectrometry measurements were also carried out at the exact sampling spots with a NaI probe connected to an Inspector1000 multichannel analyzer (Canberra).

In accordance with the Multiple Centre (MC) approach, the ESR signals of both the Al and Ti centres using experimental conditions as in Duval et al. (2017). When possible, the angular dependence of the ESR signal due to sample heterogeneity was taken into account by measuring each aliquot three times after a ~120° rotation in the cavity. However, only one angle of each aliquot was measured for the ESR signal of the Ti centres in samples TD1-08-01 and TD1-08-02 because of the weak ESR intensities that required to significantly increase the number of scans (10–25 scans here) for one given measurement. This resulted in a total measurement time >3 h for a given sample. Beyond this duration the stability of the experimental setup might become an issue and impact the repeatability of the measurements (Duval and Guilarte Moreno, 2012). Furthermore, data reproducibility was checked by running repeated ESR measurements over different days. The ESR intensities of Al and Ti centres were extracted and corrected as in Duval et al. (2017). Following Duval et al. (2015), only option D was evaluated for the Ti centres, as it has been demonstrated to be the most reliable for

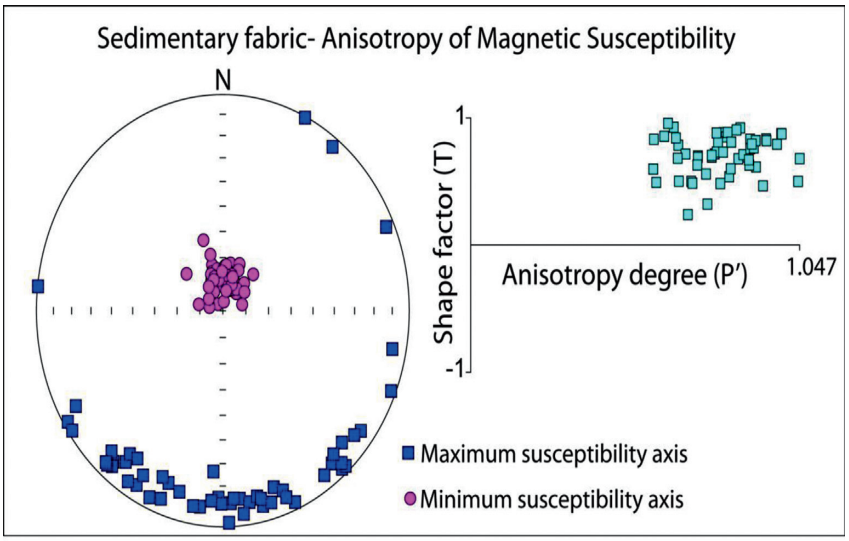

Fig. 3. Sedimentary fabric of the slackwater deposits (interior facies), in the lower part of TD1, as shown by the Anisotropy of Magnetic Susceptibility (AMS). Stereographic projection shows the distribution of the maximum (squares) and minimum (dots) susceptibility axes on to the lower hemisphere. Cartesian diagram on the right shows the shape of the magnetic ellipsoid (T) and the degree of anisotropy (P'). All samples display foliated magnetic anisotropy (T > 0) (see text for discussion), coherent with a depositional fabric on a slightly inclined surface.

Early Pleistocene deposits. Final Dose Response Curves (DRCs) were obtained by pooling all the repeated ESR intensities into a single graph as recommended by Duval (2012).

The equivalent dose (D_E) values were calculated with the Microcal Origin 8.5 software using the Levenberg-Marquardt algorithm by chi-square minimization. For the Al center, a single saturating exponential + linear function (SSE + LIN) was fitted through the experimental points, while the Ti-2 function was employed for the ESR signal of the Ti centers Duval et al. (2017).

New dose rate calculations were carried out using a combination of *in situ* and laboratory measurements. Gamma dose rate values were assessed on site with a NaI probe and evaluated using the Threshold approach as described in Duval and Arnold (2013). External alpha and beta dose rates were derived from U, Th and K concentrations obtained by ICP-MS analysis of ~5 g of powdered dry raw sediment. The dose rate conversion factors are from Guérin et al. (2011). Values were corrected with β and α attenuations for spherical grains (Brennan et al., 1991; Brennan, 2003; Guérin et al., 2012) and water attenuation formulae from Grün (1994). A water content (dry weight) of 15 + 5% was assumed for all samples and an internal dose rate was assumed to be 50 ± 30 μGy/a based on the work from Vandenberghe et al. (2008) and assuming an α-efficiency k-value of 0.15 ± 0.10 (Yokoyama et al., 1985). The cosmic dose rate was calculated from the equations of Prescott and Hutton (1994), with latitude, altitude and depth corrections. ESR age calculation was performed using a non-commercial software based on DRAC (Durcan et al., 2015) which takes into account the uncertainties derived from concentrations, depth, water content, *in situ* gamma dose rate, attenuations and D_E values. The errors associated with total doses, equivalent doses and ESR age results are given at 1σ.

3.3. U-Pb geochronology

Two flowstones were sampled for U-Pb dating, including the top "stalagmitic crust" and a lower flowstone within the upper part of TD1 (Fig. 2). Prior to U-Pb isotope dilution analysis, reconnaissance U-Th-Pb concentration data were obtained by performing laser

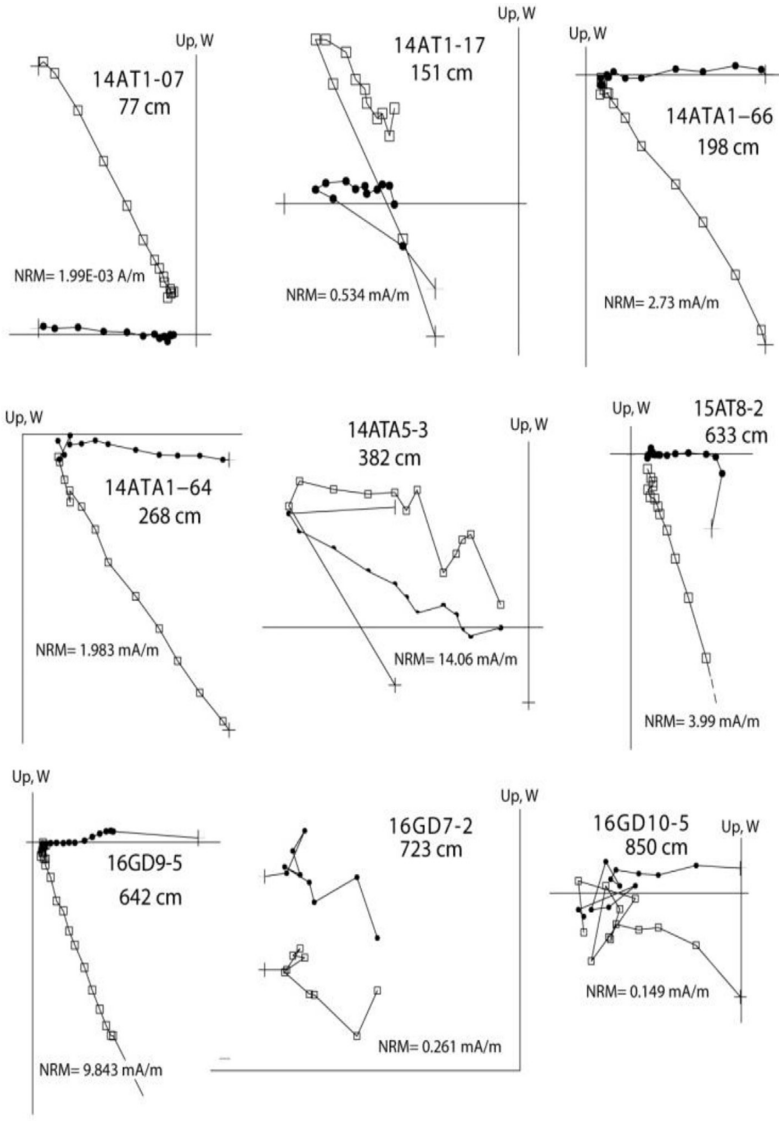

Fig. 4. Examples of progressive alternating field demagnetization displayed by vector end point diagrams (Zijderveld, 1967) of representative samples. Each data point represents the Natural Remanent Magnetization (NRM) end vector for individual demagnetization steps projected onto the horizontal (solid symbols) and vertical (open symbols) plane. Initial value of NRM (A/m) is also shown. Diagrams are shown in geographic coordinates.

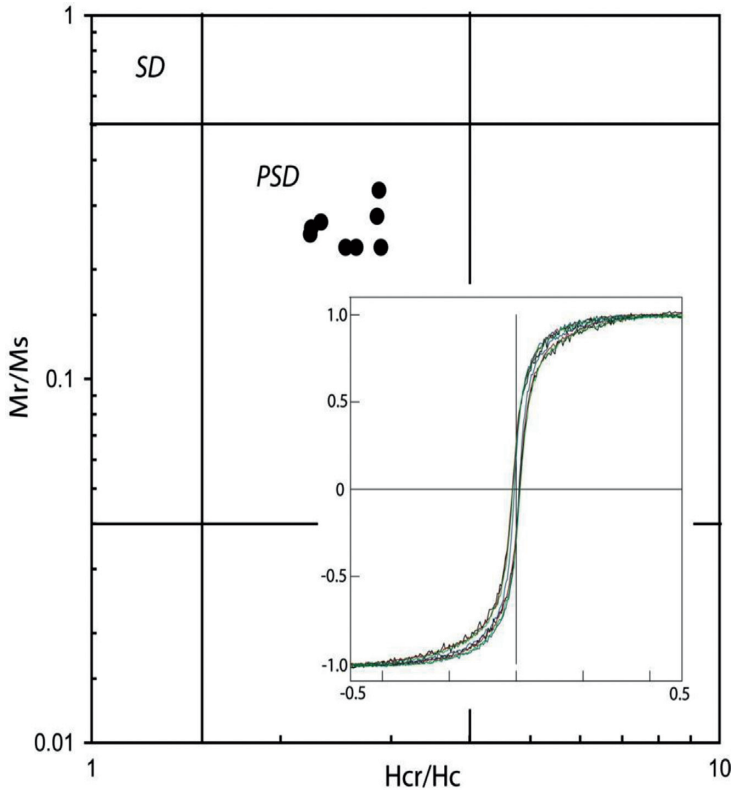

Fig. 5. Examples of representative hysteresis loops (inset) for the clayey siltstones and sandstones of the cave interior facies, and corresponding magnetic grain size on a Day diagram (Day et al., 1977). SD: Single Domain, PSD: Pseudo-single Domain. M_r: Saturation remament magnetization, M_s: Saturation magnetization, H_{cr}: Coercivity of remanence, H_c: Coercivity.

ablation traverses perpendicular to the growth layers of each sample. As noted in Woodhead et al. (2012) this allows location of optimal layers for dating i. e those with high U/Pb ratio.

Analytical methods follow closely those published previously by Woodhead et al. (2006, 2012). Multiple aliquots of solid sample (not powders), typically weighing ~50 mg, are removed from the optimal layers in the speleothem sample identified by the laser ablation analysis, using a dental drill. The pieces of calcite removed in this way are placed into pre-cleaned disposable polyethylene cups and moved to a multiple-HEPA filtered clean room environment. Samples were briefly leached 2 times in very dilute (~0.01 M) three-times teflon distilled HCl, with each cycle lasting around a minute, and then repeatedly washed in ultra-pure water before being dried in a HEPA filtered laminar flow hood. This step is critical to the elimination of Pb contaminants resulting from sample handling which can easily dominate the Pb budget of the entire sample unless removed.

Individual samples were weighed into pre-cleaned teflon beakers and treated with sufficient 6N HCl to ensure complete dissolution. A mixed ^{233}U-^{205}Pb tracer, calibrated against EarthTime (http://www.earth-time.org) reference solutions, was then weighed into the vials and each one sealed and refluxed on the hotplate for several hours to ensure complete sample-spike equilibration. Samples were then dried down and taken up in 0.6N HBr for Pb separation using AG 1X-8 anion exchange resin. The eluate was subsequently processed through the same column now filled with Eichrom TRU ion-specific resin, to separate U.

Isotope ratios were determined on a Nu Plasma MC-ICPMS using a DSN-100 desolvation unit and MicroMist glass nebuliser, operating in the range 50–100 μl/min uptake. Instrumental mass bias effects were monitored and corrected using NIST SRM 981 reference material in the case of Pb, and the sample's internal $^{238}U/^{235}U$ ratio in the case of U. Instrument data files were processed initially using an in-house designed importer, operating within the Iolite environment (Paton et al., 2011), which considers all data and reference material analyses obtained throughout a particular analytical session and permits a variety of corrections for instrumental mass bias and drift. The resulting data, now corrected for instrumental effects, were then processed for isotope-dilution calculations and blank correction using the Schmitz and Schoene (2007) software.

4. Results

4.1. Paleomagnetism

As part of the sedimentary fabric study, the measurement of the AMS was carried out in the inclined laminar bedding silts and clays that appear in the lower part of the stratigraphic section. The distribution of the maximum axes of susceptibility show an overall tilt to the south and parallel to the measured dip of the laminae, whereas the minimum axes of susceptibility are normal to the lamination (Fig. 3). Axis distributions of this type are quite common in sedimentary rocks that have a primary inclination, providing further support for the origin of this cave interior facies. The anisotropy degree of 1.034 is consistent with clay-rich sediments as seen in a number of studies (see Tarling and Hrouda, 1993; Parés et al., 2007, 2010) and so is the shape of the ellipsoid as indicated by the T parameter (Fig. 3). Overall these observations are coherent with parallel accretion concordant to the dip of the underlying bedrock, and with the fluvial origin of this facies.

Demagnetization diagrams (Fig. 4) show generally well

behaved, stable remanent magnetization directions upon stepwise alternating field demagnetization. Many samples have a secondary low-coercivity component, possibly a viscous magnetization as the sediments have not been exhumed or thermally re-activated. Such low stability components are typically removed at fields of 15–20 mT and are apparent in samples where the high coercivity component has a negative inclination (e.g., 14AT.17, 14AT5-3 in Fig. 4). The orientation of this viscous component typically conforms to that of the present day field at the locality and hence has not been further considered in our study. Taken together the demagnetization of the NRM and hysteresis curves (Fig. 5) suggest that PSD magnetite is present in the studied silts and clays, in agreement with our previous studies of sediments from the same cave system (Parés et al., 2016) and with numerous cave deposits elsewhere (e.g., Bosak et al., 2003; Rossi et al., 2016). The magnetostratigraphy of the sampled interval (Fig. 6), expressed as the Virtual Geomagnetic Pole Latitude (VGP Lat) position (Table 1), reveals that, for the most part, the cave interior deposits display reverse polarity. Data from the lowermost cave interior sediments are scarcer, due to the abundance of sandy silts that have produced either inconclusive or non interpretable demagnetization diagrams. A 100 cm-thick interval of normal polarity is observed at a depth between 2 and 3 m, and around a depth of 5.5 and 6.5 two shorter intervals of the same polarity as well (N3, N2, and N1 respectively, Fig. 6).

4.2. ESR dating

The fitting results derived from the Al centre (Fig. 7) show an excellent goodness-of-fit for sample TD1-08-01bis (adjusted $r^2 > 0.99$) resulting in a relative D_E error of 9%. In comparison, TD1-08-01 and TD1-08-02 show instead a regular goodness-of-fit (adj. $r^2 < 0.97$), resulting in somewhat higher relative D_E errors of 22%. In contrast, no reliable ESR data have been obtained from the Ti centres (Option D) in two of the three samples analysed in this work. The low intensity of the signals makes them quite difficult to measure, with noisy spectra resulting in scattered Dose Response Curves (DRC), unsatisfactory goodness-of-fit (adj. $r^2 < 0.85$), and

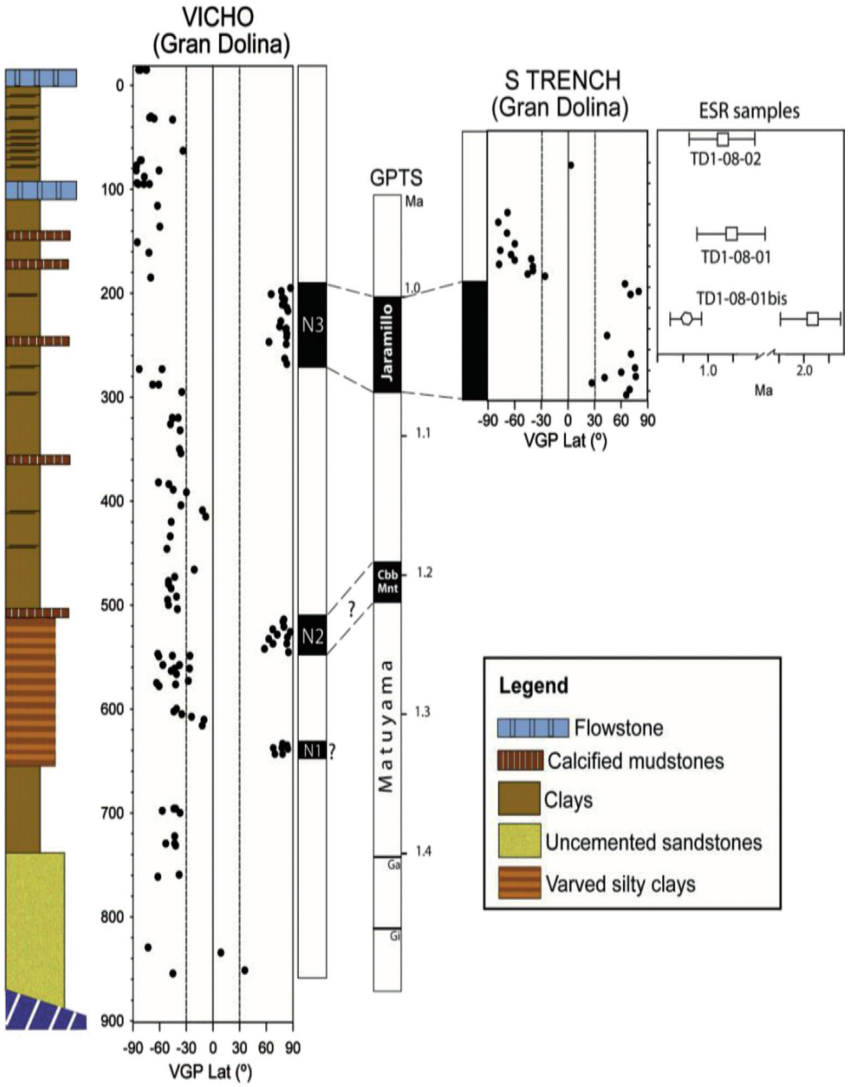

Fig. 6. Virtual Geomagnetic Pole (VGP) latitude positions for both Vicho (left) and South Trench (right) sections. Each dot corresponds to the VGP latitude of a specimen. GPTS (Geomagnetic Polarity Time Scale) shows the Jaramillo Subchron (1.00–1.07 Ma), and three additional, shorter normal polarity intervals within Matuyama: Cobb Mountain (1.19–1.122 Ma), Gardar (Ga, 1.4 Ma) and Gilsa (Gi, 1.5 Ma) (Singer, 2014). Also shown is the location of samples for ESR analysis. Squares (polygon) show Al (Ti) data (see main text for discussion).

Table 1
Paleomagnetic data. Dec & Inc = Declination and Inclination of the Characteristic Remanent Magnetization (ChRM) direction; MAD = Maximum angular deviation; VGP LAT = latitude of the Virtual Geomagnetic Pole Position.

VICHO Section					
Specimen	Depth (cm)	Dec	Inc	MAD	VGP Lat
14AT1.05.B	−15.0	176.4	−55.7	6.1	−83
14AT1.01.A	−15.0	164.2	−53.8	4.5	−75
14AT1.02.A	−15.0	174.7	−54.4	12.3	−82
14AT.03.A	−15.0	189.5	−48.1	7.0	−75
14AT1.05.A	−15.0	185.6	−65.4	18.9	−84
14ATA1-70	30.0	182.7	−39.2	42.6	−70
14ATA1-71	31.0	205.9	−63.2	12.2	−71
14ATA1-72	32.0	192.7	−37.4	32.8	−66
14ATA1-73	33.0	200.6	−3.0	11.3	−45
14AT1.06	63.0	239.4	−30.8	16.8	−34
14AT1.10.A	72.0	192.8	−61.3	2.1	−81
14AT1.10.B	72.0	189.8	−65.0	16.9	−82
14AT1.07	77.0	184.1	−59.0	1.9	−86
14AT1.09.A	82.0	180.9	−64.2	8.9	−86
14AT1.09.B	82.0	206.9	−40.8	38.5	−61
14AT1.12.B	88.0	173.5	−70.3	25.6	−77
14AT1.12.A	94.0	183.9	−58.4	2.1	−86
14AT1.11.A	95.0	185.5	−50.1	9.2	−78
14AT1.11.C	95.0	202.2	−54.7	14.0	−71
14AT1.11.B	95.0	183.4	−56.3	10.5	−84
14AT1.14	116.0	164.4	−79.0	35.6	−62
14AT1.16.A	136.0	206.6	−38.6	31.3	−60
14AT1.17	151.0	184.0	−57.8	8.9	−85
14AT1.18	161.0	185.9	−43.0	33.5	−72
14AT1.20.B	185.0	180.0	−30.0	15.5	−70
14ATA1-65	195.0	3.0	62.1	5.4	88
14ATA1-66	198.0	351.8	50.6	10.1	77
14ATA1-67	201.0	329.2	56.4	14.9	66
14ATA1-68	204.0	9.1	52.7	10.4	78
14ATA1-69	206.0	359.1	52.7	9.2	81
14ATA1-48	208.0	12.0	58.4	8.6	80
14ATA1-49	211.0	353.9	69.6	14.2	78
14ATA1-50	214.0	356.6	66.2	6.7	83
14ATA1-51	217.0	354.5	58.3	7.3	85
14ATA1-53	227.0	341.7	63.3	7.8	77
14ATA1-47	232.0	345.8	52.3	8.2	75
14ATA1-54	234.0	5.9	66.1	7.9	83
14ATA1-55	235.0	350.9	58.5	13.4	82
14ATA1-56	239.0	8.4	59.6	9.7	83
14ATA1-58	247.0	28.7	75.9	12.3	63
14ATA1-59	249.0	357.7	54.6	10.0	83
14ATA1-62	242.0	8.0	58.5	3.6	83
14ATA1-63	263.0	356.9	68.0	7.1	81
14ATA1-64	268.0	1.9	55.3	7.2	83
14AT1.31.A	273.0	190.8	−21.1	24.4	−57
14AT1.32	273.0	171.2	−59.3	21.2	−83
14AT1.33.A	288.0	177.5	−36.5	9.8	−68
14AT1.34.A	288.0	161.3	−33.1	25.0	−61
14AT1.36	295.0	137.8	−4.2	3.1	−35
14AT1.39	320.0	165.4	−0.1	14.2	−46
14AT1.40	320.0	140.0	−11.2	4.8	−39
14AT1.42	326.0	171.3	−1.7	8.4	−48
14AT1.44	332.0	206.9	9.5	6.6	−37
14ATA5-1	350.0	220.6	−8.3	17.0	−38
14ATA5-2	354.0	212.1	6.4	15.7	−36
14ATA5-3	382.0	201.0	−35.6	18.2	−61
14ATA5-4	383.7	209.5	−21.4	12.8	−50
14ATA5-6	389.0	187.1	4.8	19.9	−45
14ATA5-7	391.6	209.8	21.8	11.1	−30
14ATA5-10	404.0	206.0	12.2	19.2	−36
14ATA5-11	409.0	230.7	36.5	20.0	−12
14ATA5-13	415.0	239.7	33.6	16.8	−8
14ATA5-14	420.0	139.0	−31.4	6.0	−47
14ATA5-15	434.0	150.0	−18.7	10.4	−48
14ATA5-17	446.0	142.4	−37.0	20.8	−52
16GD6.13	466.0	211.0	36.0	6.0	−21.0
16GD6.11	473.0	207.0	−3.0	10.0	−43.0
16GD6.10	477.0	178.0	−4.0	4.0	−50.0
16GD6.9	480.0	174.0	−4.0	1.0	−50.0
16GD6.8	484.0	182.0	0.0	6.0	−47.0
16GD6.6	492.0	167.0	10.0	11.0	−41.0

(*continued on next page*)

Table 1 (*continued*)

VICHO Section				
Specimen	Depth (cm)	Dec	Inc	MAD
16GD6.5	495.0	173.0	−7.0	7.0
16GD6.4	500.0	182.0	−5.0	5.0
16GD6.3	504.0	186.0	15.0	3.0
16GD6.2	514.0	1.0	52.0	2.0
16GD6.1	516.0	5.0	52.0	3
15AT8-1	516.0	344.0	59.0	7.0
15AT8-2	520.0	1.0	69.7	7.6
15AT8-3	521.0	13.0	62.4	10.4
15AT8-29	524.0	329.0	66.0	9.0
15AT8-4	526.0	1.9	63.2	9.3
15AT8-5	529.0	22.7	67.0	6.0
15AT8-30	531.0	352.0	63.0	6.0
15AT8-6	533.0	14.5	78.8	21.2
15AT8-7	533.0	6.1	58.5	19.2
15AT8-8	537.0	327.3	74.6	19.4
15AT8-11	537.0	28.9	57.6	15.1
15AT8-14	542.0	336.0	80.8	19.5
15AT8-15	545.0	359.2	65.2	17.9
15AT8-56	547.0	194.0	−32.0	4.4
15AT8-16	549.0	184.5	38.5	8.5
15AT8-36	549.0	165.0	0.1	5.0
15AT8-58	549.0	176.0	−25.0	6.0
15AT8-39	558.0	203.0	11.0	32.0
15AT8-60	558.0	190.8	−19.5	10.0
15AT8-21	561.0	175.0	38.0	23.8
15AT8-61	561.0	215.7	−14.6	8.0
15AT8-41	563.0	200.0	−7.0	22.0
15AT8-42	566.0	191.0	10.0	27.0
15AT8-46	573.0	205.0	29.0	27.0
15AT8-47	575.0	161.0	−38.0	27.0
15AT8-28	577.0	154.2	−0.1	7.7
15AT8-95	578.0	181.0	−25.0	7.0
16GD8-13	600.0	163.0	8.0	13.0
16GD8-12	602.0	159.0	0.0	12.0
16GD8-11	605.0	164.0	21.0	9.0
16GD8-10	608.0	150.0	33.0	15.0
16GD8-9	611.0	147.0	51.0	8.0
16GD8-7	616.0	181.0	55.0	30.0
15AT7-12	632.0	356.0	52.0	4.0
16GD8-2	633.0	3.0	57.0	2.0
16GD8-1	636.0	16.0	59.0	5.0
15AT7-13	636.0	7.0	39.0	6.0
16GD9-3	636.0	12.0	64.0	3.0
16GD7-14	638.0	5.0	62.0	3.0
16GD9-5	642.0	349.0	66.0	2.0
15AT7-16	642.0	23.0	64.0	5.0
16GD7-13	642.0	353.0	40.0	6.0
16GD7-9	696.0	236.0	−44.0	6.0
16GD7-8	696.0	233.0	−45.0	15.0
16GD7-7	698.0	193.0	−22.0	9.0
16GD7-6	700.0	212.0	3.0	13.0
16GD7-2	723.0	218.0	−19.0	6.0
16GD7-1	730.0	203.0	−22.0	10.0
16GD10-25	732.0	222.0	−22.0	7.0
16GD10-20	762.0	202.0	−38.0	10.0
16GD10-19	760.0	219.0	−8.0	6.0
16GD10-10	835.0	325.0	−51.0	6.0
16GD10-9	830.0	166.0	−49.0	8.0
16GD10-8	852.0	300.0	37.0	16.0
16GD10-4	855.0	213.0	−16.0	3.0
S TRENCH Section				
Specimen	Depth (cm)	Dec	Inc	MAD
TD1-13-064	0.0	294.0	−34.0	8.0
TD1-13-056	44.0	177.0	−35.0	10.0
TD1-13-054	53.0	176.0	−49.0	5.5
TD1-13-052	63.0	176.0	−36.0	6.3
TD1-13-050	73.0	221.0	−58.0	7.0
TD1-13-048	79.0	199.0	−66.0	3.2
TD1-13-046	83.0	217.0	−69.0	4.5
TD1-13-044	87.0	248.0	−60.0	6.9
TD1-13-042	88.0	222.0	−61.0	3.2
TD1-13-040	92.0	197.0	−66.0	3.8

Table 1 (*continued*)

S TRENCH Section					
Specimen	Depth (cm)	Dec	Inc	MAD	VGP Lat
TD1-13-038	94.0	235.0	−35.0	4.6	−38.6
TD1-13-036	98.0	230.0	−26.0	8.9	−38.5
TD1-13-034	101.0	222.0	−27.0	6.0	−44.5
TD1-13-032	103.0	238.0	−5.0	7.3	−25.0
TD1-13-030	108.0	7.0	27.0	12.0	61.6
TD1-13-026	118.0	352.0	59.0	5.1	83.6
TD1-13-022	122.0	340.0	50.0	23.8	70.5
TD1-13-018	158.0	305.0	49.0	9.6	44.7
TD1-13-016	175.0	340.0	52.0	2.6	71.6
TD1-13-014	188.0	343.0	57.0	5.2	76.2
TD1-13-013	192.0	331.0	43.0	4.1	60.7
TD1-13-012	196.0	16.0	57.0	3.8	77.0
TD1-13-010	197.0	58.0	48.0	4.2	42.0
TD1-13-008	202.0	334.0	−29.0	9.1	27.7
TD1-13-003	208.0	360.0	39.0	5.1	70.0
TD1-13-005	213.0	26.0	50.0	8.0	66.4

thus meaningless D_E results. However, sample TD1-08-01bis shows a somewhat less scattered DRC, from which D_E has been obtained (Fig. 7). Fitting results with equal weights and data weighted by the inverse of the squared errors provided D_E values of 1387 ± 249 and 1141 ± 181 Gy, respectively. These values differ by about 21%, which is most likely due to the scatter in the experimental data points. Consequently, we consider the mean D_E value 1264 ± 174 Gy as being the best estimate for the burial dose of this sample.

Calculations provide ESR-Al age results of 1.12 ± 0.25, 1.20 ± 0.27 and 2.27 ± 0.22 Ma for samples TD1-08-02, TD1-08-01 and TD1-08-01bis, respectively. Overall, these results are apparently coherent with both the chronostratigraphic framework and previous numerical ages (Moreno et al., 2015) suggesting an Early Pleistocene chronology for TD1. For example, the new age of TD1-08-01 is very similar to that previously obtained by Moreno et al. (2015) (−3%) while it is higher by +41% for sample TD1-08-02. This is mostly because previous age calculations by Moreno et al. (2015) were performed using the same gamma dose rate value as for TD1-08-01. The new *in situ* measurements and the radioelement concentrations obtained by ICP-MS instead reveal that the gamma dose rate at TD1-08-02 site was lower by 35%. Finally, sample TD1-08-01bis yields an age that is more than two times older than those previously obtained by Moreno et al. (2015) (2.3 Ma vs. 0.9 Ma). This difference is mostly due to the D_E values derived from each study (3403 ± 310 vs 1631 ± 332, respectively), although a more limited impact due to a somewhat smaller total dose rate cannot be discounted.

As far as sample TD1-08-01bis, two factors could possibly explain a bias in age. A water content of 15 ± 5% (1σ) was first assumed for the age calculation, in order to cover a wide range of values (5–25%), including the current water content at a 2 sigma confidence level. A slight increase of the water content to 20% instead would result in a moderate age increase to 0.90 ± 0.13 Ma. Moreover, the reliability of the fitting results may be questioned as one may observe that the natural point is actually much lower than any other points in the DRC. This has most likely the effect of decreasing the D_E value and thus the age. To evaluate this impact, we calculated the D_E without taking into account the natural point, obtaining a D_E of 1892 ± 447 (data weighted by the inverse of the squared experimental errors, i.e., $1/s^2$) and 2087 ± 646 (equal weights). Considering the resulting mean D_E value 1990 ± 137 Gy, the resulting ESR-Ti age obtained becomes significantly older (1.33 ± 0.10 Ma), which may be considered as the maximum possible age for the sample. Consequently, it is probable that the true age of TD1-08-01bis is somewhat higher than the 0.84 ± 0.12, although this cannot be exactly quantified.

The new results show an excellent goodness-of-fit ($r^2 > 0.99$), which contrast with the previous data ($r^2 < 0.98$) from Moreno et al. (2015), resulting in a more reliable dose estimate and thus a more accurate age result. However, this ESR-Al age is far older than those obtained for TD1-08-01 and TD1-08-02. This may actually reflect some vertical variations of the sedimentary fluvial environment within the top of TD1 unit. The three ESR samples were indeed collected from two different facies observed within TD1, as defined by Campaña et al. (2017). TD1-08-01bis may be correlated to facies B, comprised of laminated cemented clayey silt, while TD1-08-01 and TD1-08-02 were collected from facies A, a laminated sandy silt with soft nodules. The change from facies B to facies A indicates an increase in the flow energy and the sorting of larger particles (Campaña et al., 2017) (Fig. 2). Therefore, these two sedimentary facies suggest different transport and depositional conditions, and thus bleaching histories for the three samples. The higher energy environment of facies A may indicate a more effective zeroing of the Al-centre for samples TD1-08-01 and TD1-08-02, in comparison with TD1-08-01bis.

In comparison, the Ti-Li signal measured in TD1-08-01bis gives a significantly younger age result of 0.84 ± 0.12 Ma. Based on the principle of the MC approach, such a difference between ESR-Al and ESR-Ti ages for this sample may be interpreted as an incomplete bleaching of the Al signal during transportation, which is consistent with previous observations made on the sedimentary environment. Consequently, we consider the Ti result as the most reliable estimate for the burial age of sample TD1-08-01bis (see Table 2).

4.3. U-Pb Geochronology

The reconnaissance laser ablation data reveal typically low, and relatively constant, uranium concentrations around 50 ppb but with very large variations in Pb concentration from low ppb to high ppm values (Fig. 8). Although areas with the highest U/Pb ratios (identified for analysis using laser ablation techniques) were sampled for the subsequent solution isotope dilution analyses, the U-Pb data reveal no discernible radiogenic ingrowth with increasing U/Pb ratios - at least within analytical uncertainties (see Table 3). As a result no U-Pb age information could be obtained for the two flowstones. At the present time therefore these materials remain undatable with traditional U-Pb isotope dilution methods. Research is however continuing into the development of *in situ* (laser ablation) dating methodologies which might ultimately allow the isolation of more radiogenic horizons suitable for age determination.

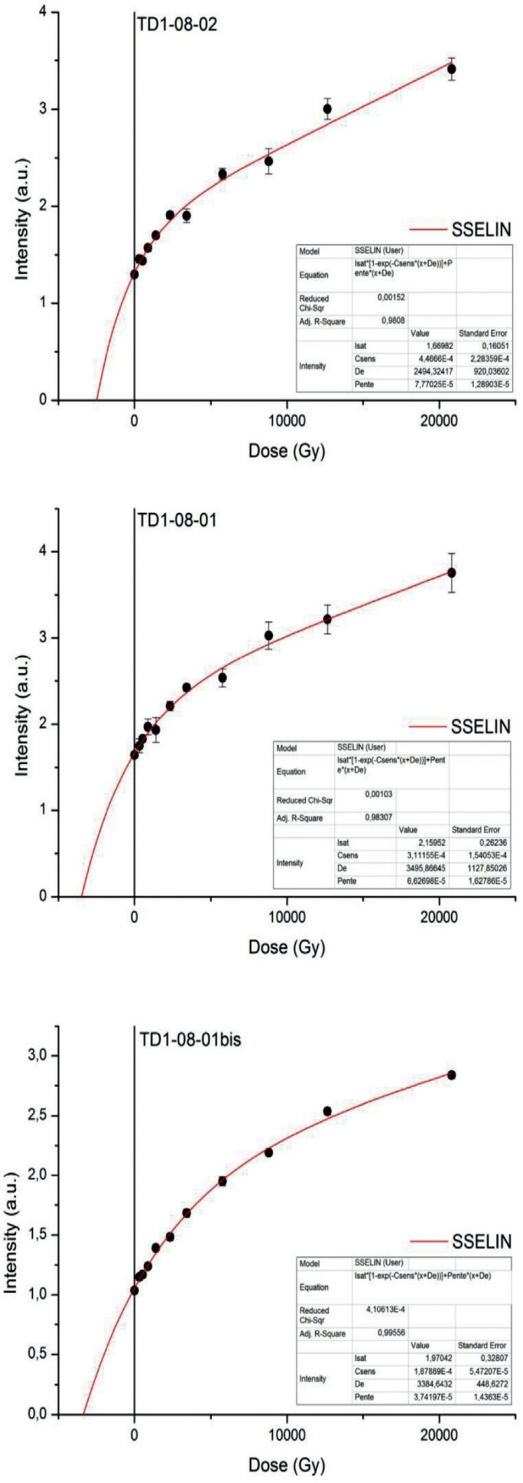

Fig. 7. ESR dose response curves (DRC) of the Al and Ti-Li (option D) signals measured in three quartz samples from the TD1 level in Gran Dolina site. For each sample, final D_E values were derived the pooled ESR intensities, as recommended by Duval (2012).

5. Discussion

The magnetostratigraphic study of the lowermost part of the sequence at Gran Dolina (Vicho section) has led to the unambiguous identification of three normal magnetozones (N3, N2 and N1 from bottom to top) within deposits mostly dominated by a reverse polarity (Fig. 6). In comparison, only one normal and one reverse magnetozone were identified in the shorter Southern trench where ESR samples were collected. A tight litho- and magnetostratigraphic correlation is nevertheless possible for those two sections that are distant by a few meters only, positioning the Southern trench deposits in the top part of the Vicho profile.

The presence of the Matuyama-Brunhes boundary (MBB) near the TD7-TD8 boundary has been reported at about 10 m above the youngest cave interior facies horizon (Parés et al., 2013 for discussion), and recent luminescence dates from TD6 sediments, right below the MBB, produced a weighted mean age of 846 ± 57 ka (Arnold et al., 2014), which can be taken as a *postquem* for the cave interior sediments. On the other hand, our new ESR results reveal ages of 1.12 ± 0.25 (TD1-08-02) and 1.20 ± 0.27 (TD1-08-01) for the reverse magnetozone located at the top of unit TD1 and above magnetozone N3 (Fig. 6). These two ages are derived from the measurement of the Al centre, which means that they should be considered as maximum possible age estimates for the deposits dated. In other words, the true age of those deposits is either similar or younger than the ESR-Al ages obtained. The chronology of the top part of TD1 is thus constrained between the MBB and the weighted mean Al age of 1.16 ± 0.18 Ma derived from the two ESR samples.

Consequently, both the MBB above TD1 and the ESR ages strongly suggest that normal chron N3 of the local magnetostratigraphy corresponds to the Jaramillo Subchron (C1r.1n; 1.00–1.07 Ma). The ESR sample TD1-08-01bis collected within N3 provides an ESR-Al age of 2.27 ± 0.2 Ma and an ESR-Ti age 0.84 ± 12 Ma. While the former should be interpreted as a maximum age, the latter instead may be considered as the best age estimate for the deposits and, as discussed in the previous section, by considering a more realistic water content of 20% the age increases to 0.90 + 0.13 Ma, consistent within error with a Jaramillo chronology.

There are two older short normal polarity intervals in the section, namely N1 and N2, much shorter and hence difficult to interpret. On the GPTS two short-lived normal polarity intervals can be observed below Jaramillo, namely Cobb Mountain (1.19–1.22 Ma) and Bjorn (1.25 Ma) (Singer, 2014), which we can tentatively correlate to polarity intervals N2 and N1 respectively. We are aware that assigning interval N2 to Cobb Mountain implies a reduction of accumulation rate downwards between depths 5 to 2.5 m, but given the nature and accumulation history of cave deposits it is a reasonable hypothesis. The appearance of well laminated, varved sediments at depths 4.8–6.2 m suggests a variable sediment accumulation rate in the section. Hence, because (1) accumulation rates can be rather variable, and (2) there is a number of short-lived, ephemeral normal polarity intervals between 1.7 Ma (top Olduvai) and 1.0 Ma (bottom Jaramillo) (Gradstein et al., 2012), the assignation of intervals N1 and N2 remains at this stage somewhat ambiguous, whereas Jaramillo seems to be rather well documented in the section. In any case the interpretation of N1 does not affect the inference that sedimentation in the cave started within the Matuyama Chron, before Jaramillo, and most likely before the Cobb Mountain normal short interval.

Our new paleomagnetic record of the cave interior sediments (TD1) at the base of the Gran Dolina section adds an important constraint on the overlying stone tool-bearing level TD4. Sedimentary unit TD4 predates both a luminescence age of 850 ka, and the Matuyama-Brunhes boundary (0.78 Ma), and it is younger than the cave interior sediments that recorded the Jaramillo Subchron. These chronological constraints are consistent with the biochronological evidence. Significant microfaunal taxa suggest that level TD4 of Gran Dolina is younger than the lower red units of Sima del Elefante (Cuenca-Bescós et al., 2015), with an estimated burial age of 1.2 Ma±0.16 Ma (Carbonell et al., 2008). They indicate that

Table 2
ESR ages and associated data obtained (Bl = bleaching percentage, expressed as the relative difference between the ESR intensities of the natural and bleached aliquots); D_{cos} = cosmic dose rate; Dint = internal dose rate; Da = total dose rate; DE = equivalent dose).

This study											Moreno et al. (2015)
Sample	Centre	Bl (%)	D_α (μGy/a)	D_β (μGy/a)	D_γ (μGy/a)	D_{cos} (μGy/a)	D_{int} (μGy/a)	D_a (μGy/a)	D_E (Gy)	Age (Ma)	Age (Ma)
TD1-08–02	**Al**	50.6 ± 0.8	44 ± 10	1347 ± 22	639 ± 38	30 ± 3	50 ± 30	2110 ± 54	2374 ± 517	**1.12 ± 0.25**	**0.79 ± 0.06**
TD1-08–01	**Al**	65.7 ± 0.3	65 ± 15	1774 ± 29	1087 ± 63	28 ± 3	50 ± 30	3004 ± 63	3609 ± 798	**1.20 ± 0.27**	**1.25 ± 0.13**
TD1-08–01bis	**Al**	52.4 ± 1.4	31 ± 7	759 ± 13	632 ± 38	27 ± 3	50 ± 30	1499 ± 51	3403 ± 310	**2.27 ± 0.22**	**0.92 ± 0.19**
	Ti-Li (option D)								1264 ± 174 ka	**0.84 ± 0.12**	-

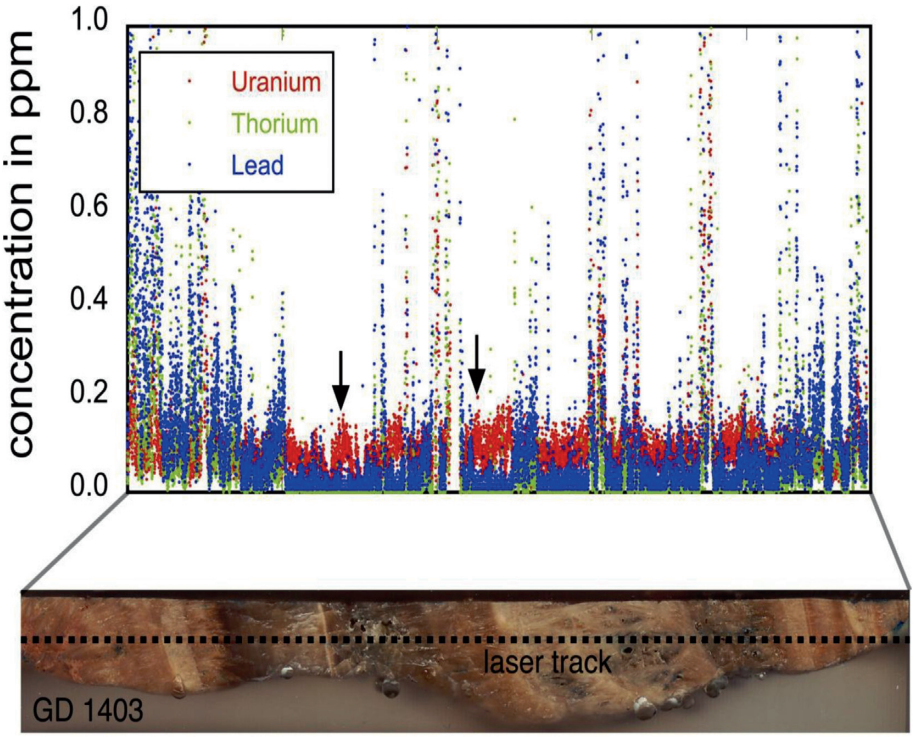

Fig. 8. Laser ablation traverses perpendicular to the growth layers of each sample for reconnaissance of U-Th-Pb concentration data.

Table 3
Uranium and lead isotopic compositions of Gran Dolina TD1 speleothem samples analysed by MC-ICP-MS at the University of Melbourne.

Speleothem	Sample	U (ppm)	Pb (ppm)	$^{238}U/^{206}Pb$	% err	$^{207}Pb/^{206}Pb$	% err	$^{204}Pb/^{206}Pb$	% err	corr. coeff.
TD2-1	1	0.054	0.009	21.142	1.03	0.82879	0.14	0.05279	0.25	−0.76
	2	0.076	0.012	21.094	0.98	0.82855	0.14	0.05262	0.25	−0.75
	3	0.053	0.008	21.865	1.30	0.82760	0.16	0.05242	0.48	−0.82
	4	0.074	0.010	26.893	1.53	0.82797	0.18	0.05287	0.29	−0.85
	5	0.055	0.010	19.766	1.43	0.82849	0.17	0.05262	0.28	−0.80
	6	0.083	0.015	19.550	0.86	0.82921	0.12	0.05387	0.22	−0.77
GD1403	1	0.049	0.008	21.854	1.37	0.81825	0.18	0.05170	0.50	−0.87
	2	0.067	0.009	24.717	53.69	0.84113	12.59	0.04448	0.50	−0.01
	3	0.046	0.012	13.298	0.81	0.82039	0.13	0.05215	0.23	−0.72
	4	0.066	0.004	65.613	3.49	0.82185	0.39	0.05234	0.51	−0.97
	5	0.053	0.010	18.077	1.05	0.82760	0.15	0.05242	0.58	−0.73
	6	0.068	0.005	50.475	1.50	0.82182	0.19	0.05197	0.34	−0.87

TD4 level, which postdates the cave interior sediments, is younger than the Sima Elefante red units (TELRU of Cuenca-Bescós et al., 1999, 2015) fauna.

From a karst evolution point of view, the "stalagmitic crust" at the top of TD1 marks an important step in the Gran Dolina sedimentary infilling history and by inference in the middle tier of the karst. Below such a flowstone sediments are slackwater deposits, whereas on top the sedimentary record shows an abundance of coarse deposits, gravels and sandstones of allochthonous origin for the most part. Such a pronounced change, likely related to an environmental shift that occurred between ca 1.0 and 0.9 Ma (MIS 25?), reflects the development of a cave entrance that allowed the beginning of the allochthonous sediment accumulation in the cavity, and a significant drop of the water table. Although some thin

flowstones are found in younger units (e.g., TD7-TD8), the cavity remains essentially above the phreatic level until it is completely filled up by sediments (unit TD11). The time gap between the development of the basal stalagmitic crust and the first entrance of allochthonous deposits of unit TD4 remains to be determined and will inevitably slightly rejuvenate the age of this geo-unit.

From a broader geological perspective, this geochronological context also helps us to better understanding the development and karst evolution of the Atapuerca system. Gran Dolina is one of several caves in the middle level tier of the karst. The middle karst level tier consists of a sub-horizontal passage located at 1000–1005 m a.s.l. (above sea level) in Cueva Mayor (Ortega et al. 2013, 2014). Along both Galería Baja and Galería del Silo (interior of Cueva Mayor) a unit of sandy clays and silts of unknown total thickness is blanketing the floor of the passages. The visible thickness, in prehistoric silos, is about 150 cm, but the contact with the limestone floor is not exposed. A thin flowstone is capping the clastic sediments in both passages. The magnetostratigraphic sections in these two conduits show similar trends: sediments at the bottom have reverse magnetization directions whereas at the top they have normal polarity. The remains of *Ursus deningeri* in the upper sediments suggests a Middle Pleistocene age (e.g., García

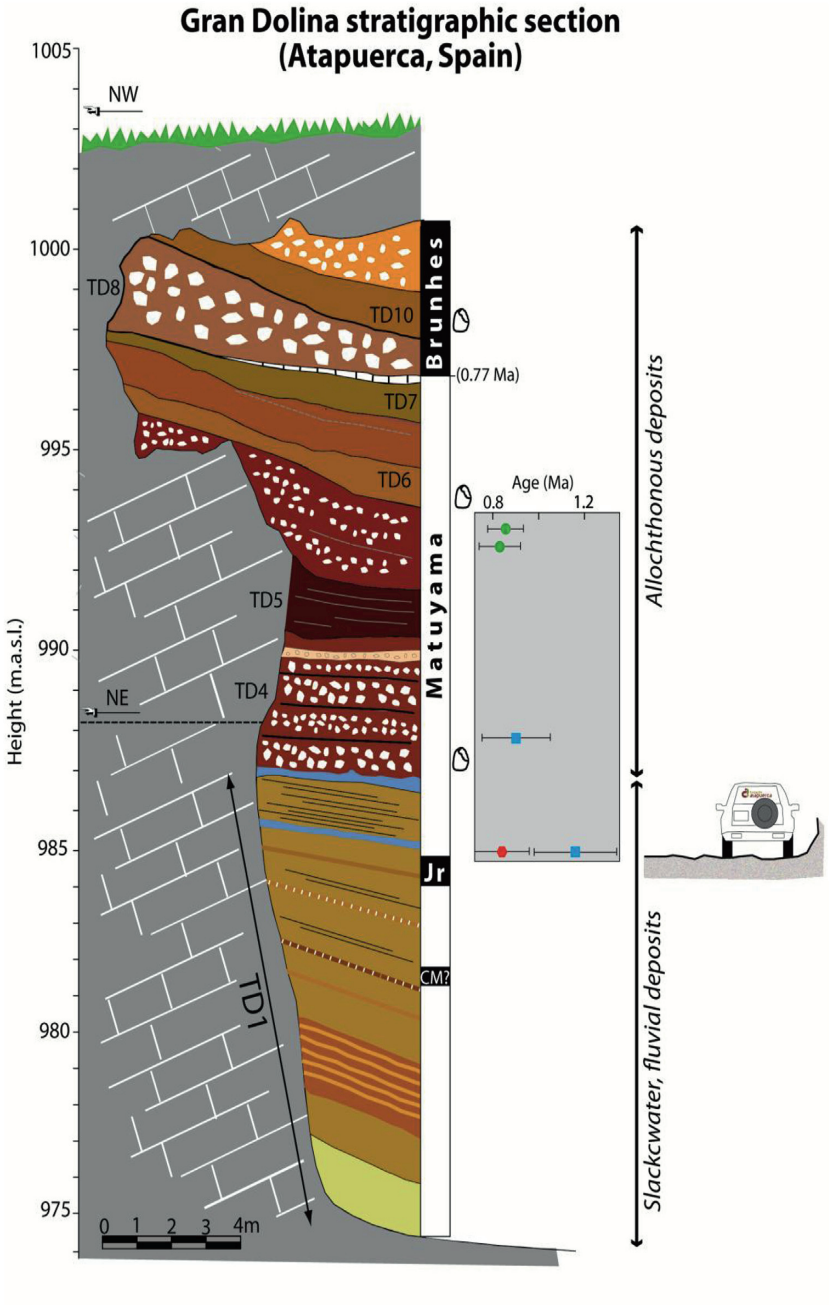

Fig. 9. Sedimentary infill at Gran Dolina site with magnetostratigraphic, OSL, and ESR results. Main lithostratigraphic units adapted from Campaña et al. (2016) and our own field observations. Notice the two main groups of sedimentary facies, including entrance (or allochthonous) facies deposits (TD4 through TD10) at the top, and slackwater, fluvial deposits (TD1) at the bottom, directly overlying the bedrock. In blue are shown the speleothems developed at the bottom unit TD1. Numerical ages include OSL (green) (Arnold et al. (2014), ESR-Al (blue), ESR-Ti (red) (Moreno et al., 2015 and this study). (For interpretation of the references to colour in this figure legend, the reader is referred to the Web version of this article.)

et al., 1997) and accordingly the R→N polarity change has been interpreted as the Matuyama-Brunhes boundary (Parés et al., 2013). The thickness of sediment underneath the sampled section is unknown, and therefore the polarity reversal age is only a minimum age for the cave formation. This is consistent with previous observations in Sima del Elefante (Middle level tier exposed along the railway trench, see Fig. 1), where the lowermost deposits (TE9) have a burial age of 1.22 ± 0.16 Ma (Carbonell et al., 2008). In the upper part of the Elefante section the Matuyama-Brunhes reversal has been described (Parés et al., 2007) and recent luminescence dates confirm such a polarity reversal (Arnold et al., 2014). In summary, current evidence suggests that the middle level tier in the Atapuerca karst system formed well before the Matuyama-Brunhes boundary as suggested by both paleomagnetism and terrestrial cosmogenic burial ages. The cave interior sediments at Gran Dolina targeted in the current study are flooring the middle level tier and have reverse polarity, which is consistent with the previous data, and shows that this level tier formed during in Matuyama times and before the Jaramillo Subchron according to our new data.

6. Conclusions

The archaeological layers at Gran Dolina, including artifact-bearing level TD4, are preceded by about 9 m of sterile, interior fluvial facies cave sediments that were deposited before the appearance of large openings to the cave (Fig. 9). The cave interior sediments are capped by a flowstone and followed by a pile of 15 m of exterior facies sediments (talus, slope, sliding bed deposits), where fossil and artifact-bearing horizons are found. The magnetic stratigraphy of the cave interior sediments reveals a dominant reverse magnetic polarity, coherent with a Matuyama age, and interrupted by a ca. 100 cm normal polarity magnetozone. Re-measured ESR ages on quartz grains in the upper part of TD1 produced an age range between 0.8 and 1.2 Ma, and therefore we interpret the normal magnetozone N3 as the Jaramillo Subchron (1.00–1.07 Ma). The oldest archaeological unit at Gran Dolina and artifact-bearing layer TD4 is overlying the studied layer TD1 and therefore post-dates the Jaramillo Subchron.

The flowstone between units TD1 and TD4 ("stalagmitic crust") indicate the proximity of the cavity to the vadose zone, and its formation shows a major change from interior facies (phreatic-vadose zone) to eventual cave entrances development, an environmental change that allowed the accumulation of slope, talus, and debris cones that contain the fossil and artifact horizons that make the Gran Dolina site so special. Ongoing research on the flowstone that precedes such deposits will help in further constraining the age of such major paleoenvironmental change in the karst evolution and development at Atapuerca.

Acknowledgements

Access and permission to collect samples in Atapuerca was granted by Junta de Castilla y León. The authors are deeply indebted to the Atapuerca Research Team (EIA) and the Fundación Atapuerca for continuous support of this research. We are thankful to Miguel Ángel Martín for preparing field photographs (Fig. 2). Financial support for this work was obtained from Junta de Castilla y León and from MINECO Grants CGL2010-16821 and CGL2015-65387-C3-3-P. M. Duval's research is currently funded by an Australian Research Council Future Fellowship (FT150100215). U-Pb dating at Melbourne was conducted with funding from the Australian Research Council. MJS was funded by the Netherlands Organisation for Scientific Research grants NWO-ALW 823.01.003. We thank the three anonymous reviewers for their helpful constructive comments and suggestions.

References

Arnold, L.J., Demuro, M., Parés, J.M., Pérez-González, A., Arsuaga, J.L., Bermúdez de Castro, J.M., Carbonell, E., 2014. Evaluating the suitability of extended-range luminescence dating techniques over early and Middle Pleistocene time-scales: published datasets and case studies from Atapuerca, Spain. Quat. Int. https://doi.org/10.1016/j.quaint.2014.08.010.

Balsley, J.R., Buddington, A.F., 1960. Magnetic susceptibility anisotropy and fabric of some Adirondack granites and orthogneisses. Am. J. Sci. 258A, 6–20.

Benito-Calvo, A., Pérez-González, A., 2015. Geomorphology of the Sierra de Atapuerca and the Middle Arlanzón Valley (Burgos, Spain). J. Maps 11, 535–544.

Bermúdez de Castro, J.M., Arsuaga, J.L., Carbonell, E., Rosas, A., Martínez, I., Mosquera, M., 1997. A hominid from the lower Pleistocene of Atapuerca, Spain: possible ancestor to Neandertals and modern humans. Science 276, 1392–1395.

Bermúdez de Castro, J.M., Pérez-González, A., Martinón-Torres, M., Gómez-Robles, A., Rosell, J., Prado, L., Sarmiento, S., Carbonell, E., 2008. A new early Pleistocene hominin mandible from Atapuerca-TD6, Spain. J. Hum. Evol. 55, 729–735.

Bosak, P., Pruner, P., Kadlec, J., 2003. Magnetostratigraphy of cave sediments: application and limits. Studia Geophys. Geod. 47, 301–330.

Bosch, R.F., White, W.B., 2004. Lithofacies and transport of clastic sediments in karstic aquifers. In: Sasowsky, I.D., Mylroie, J.E. (Eds.), Studies of Cave Sediments. Kluwer Academic/Plenum Publishers, New York, pp. 1–22.

Brennan, B.J., 2003. Beta doses to spherical grains. Radiat. Meas. 37 (4–5), 299–303.

Brennan, B.J., Lyons, R.G., Philips, S.W., 1991. Attenuation of alpha particle track dose for spherical grains. Int. J. Rad. Appl. Instrum. Part D. Nucl. Tracks Radiat. Meas. 18, 249–253.

Bull, P.A., 1981. Some fine-grained sedimentation phenomena in caves. Earth Surf. Process. Landforms 6, 11–22.

Campaña, I., Pérez-González, A., Benito-Calvo, A., Rosell, J., Blasco, R., Bermúdez De Castro, J.M., Carbonell, E., Arsuaga, J.L., 2016. New interpretation of the Gran Dolina-TD6 bearing Homo antecessor deposits through sedimentological analysis. Sci. Rep. 6, 34799. https://doi.org/10.1038/srep34799.

Campaña, I., Benito-Calvo, A., Pérez-González, A., Ortega, A.I., Bermúdez de Castro, J.M., Carbonell, E., 2017. Pleistocene sedimentary facies of the Gran Dolina archaeo-paleoanthropological site (Sierra de Atapuerca, Burgos, Spain). Quat. Int. 433, 68–84.

Carbonell, E., Rodríguez, X.P., 1994. Early-Middle Pleistocene deposits and artefacts in the Gran Dolina site (TD4) of the Sierra de Atapuerca (Burgos, Spain). J. Hum. Evol. 26, 291–311.

Carbonell, E., Bermúdez de Castro, J.M., Arsuaga, J.L., et al., 1995. Lower Pleistocene hominids and artifacts from Atapuerca-TD6 (Spain). Science 269, 826–829.

Carbonell, E., Bermúdez de Castro, J.M., Arsuaga, J.L., Allué, E., Bastir, M., Benito, A., Cáceres, I., Canals, T., Díez, J.C., Van der Made, J., Mosquera, M., Ollé, A., Pérez-González, A., Rodríguez, J., Rodríguez, X.P., Rosas, A., Rosell, J., Sala, R., Vallverdú, J., Vergés, J.M., 2005. An early Pleistocene hominin mandible from Atapuerca-TD6, Spain. Proc. Natl. Acad. Sci. U.S.A. 102, 5674–5678.

Carbonell, E., Bermúdez de Castro, J.M., Parés, J.M., Pérez-González, A., Cuenca-Bescós, G., Olle, A., Mosquera, M., Huguet, R., van der Made, J., Rosas, A., Sala, R., Vallverdú, J., García, N., Granger, D.E., Martinón-Torres, M., Rodríguez, X.P., Stock, G.M., Vergès, J.M., Allué, E., Burjachs, F., Cáceres, I., Canals, A., Benito, A., Díez, C., Lozano, M., Mateos, A., Navazo, M., Rodríguez, J., Rosell, J., Arsuaga, J.L., 2008. The first hominin of Europe. Nature 452, 465–470.

Couchoud, I., 2008. Les spéléothèmes, archives des variations paléoenvironnementales. Quaternaire 19 (4), 255–274.

Cuenca-Bescós, G., Laplana, C., Canudo, J.I., 1999. Biochronological implications of the Arvicolidae (Rodentia, Mammalia) from the lower Pleistocene hominid-bearing level of Trinchera Dolina 6 (TD6, Atapuerca, Spain). J. Hum. Evol. 37, 353–373.

Cuenca-Bescós, G., Blain, H.A., Rofes, J., Lozano-Fernández, I., López-García, J.M., Duval, M., Galán, J., Núñez-Lahuerta, C., 2015. Comparing two different Early Pleistocene microfaunal sequences from the caves of Atapuerca, Sima del Elefante and Gran Dolina (Spain): biochronological implications and significance of the Jaramillo subchron. Quat. Int. 389, 148–158.

Day, R., Fuller, M.D., Schmidt, V.A., 1977. Hysteresis properties of titanomagnetites: grain size and composition dependence. Phys. Earth Planet. In. 13, 260–266.

Durcan, J.A., King, G.E., Duller, G.A.T., 2015. DRAC: dose rate and age calculator for trapped charge dating. Quat. Geochronol. 28, 54–61.

Duval, M., 2012. Dose response curve of the ESR signal of the Aluminum center in quartz grains extracted from sediment. Ancient TL 30 (2), 1–9.

Duval, M., Guilarte Moreno, V., 2012. Assessing the influence of the cavity temperature on the ESR signal of the Aluminum center in quartz grains extracted from sediment. Ancient TL 30 (2), 11–16.

Duval, M., Arnold, L.J., 2013. Field gamma dose-rate assessment in natural sedimentary contexts using LaBr3(Ce) and NaI(Tl) probes: a comparison between the "threshold" and "windows" techniques. Appl. Radiat. Isot. 74 (0), 36–45.

Duval, M., Sancho, C., Calle, M., Guilarte, V., Peña-Monné, J.L., 2015. On the interest of using the multiple centers approach in ESR dating of optically bleached quartz grains: some examples from the Early Pleistocene terraces of the Alcanadre River (Ebro basin, Spain). Quat. Geochronol. 29, 58–69.

Duval, M., Arnold, L.J., Guilarte, V., Demuro, M., Santonja, M., Pérez-González, A., 2017. Electron spin resonance dating of optically bleached quartz grains from

the Middle Palaeolithic site of Cuesta de la Bajada (Spain) using the multiple centres approach. Quat. Geochronol. 37, 82–96.
Falguères, C., Bahain, J.J., Yokoyama, Y., Arsuaga, J.L., Bermúdez de Castro, J.M., Carbonell, E., Bischoff, J.L., Dolo, J.M., 1999. Earliest humans in Europe: the age of TD6 gran Dolina, Atapuerca, Spain. J. Hum. Evol. 33, 343–352.
Ford, D., Williams, 2007. Karst Hydrogeology and Geomorphology. John Wiley & Sons, Ltd.
Frank, N., Kober, B., Mangini, A., 2006. Carbonate precipitation, U-series dating and U-isotopic variations in a Holocene travertine platform at Bad Langensalza - Thuringia Basin, Germany. Tufs calcaires et travertins quaternaires: morphogenèse, biocénoses, paléoclimats et implantations paléolithiques. 2ème partie. Quaternaire 17 (4), 333–342 (2006).
García, N., Arsuaga, J.L., Torres, T., 1997. The carnivore remains from the Sima de los Huesos Middle Pleistocene site (Sierra de Atapuerca, Spain). J. Hum. Evol. 33, 155–174.
Gradstein, F.M., Ogg, J.G., Schmitz, M.D., Ogg, G.M. (Eds.), 2012. The Geologic Time Scale 2012, vol. 1. Elsevier, p. 144.
Grün, R., 1994. A cautionary note: use of the water content and depth for cosmic ray dose rate in AGE and DATA programs. Ancient TL 12, 50–51.
Guérin, G., Mercier, N., Adamiec, G., 2011. Dose-rate conversión factors: update. Ancient TL 19 (1), 5–8.
Guérin, G., Mercier, N., Nathan, R., Adamiec, G., Lefrais, Y., 2012. On the use of the infinite matrix assumption and associated concepts: a critical review. Radiat. Meas. 47 (9), 778–785.
Harmand, D., Adamson, K., Rixhon, G., Jaillet, S., Losson, B., Devos, A., Hez, G., Calvet, M., Audra, P., 2017. Relationships between fluvial evolution and karstification related to climatic, tectonic and eustatic forcing in temperate regions. Quat. Sci. Rev. https://doi.org/10.1016/j.quascirev.2017.02.016.
Jelinek, V., 1978. Statistical processing of anisotropy of magnetic susceptibility measured on groups of specimens. Studia Geophys. et geol. 22, 50–62.
Jelinek, V., 1981. Characterization of the magnetic fabric of rocks. Tectonophysics 79, 63–67.
Moreno, D., Falguères, C., Pérez, A., Voinchet, P., Ghaleb, B., Despriée, Bahain, J.J., Sala, R., Carbonell, E., Bermúdez de Castro, J.M., Arsuaga, J.L., 2015. New radiometric dates on the lowest stratigraphical section (TD1 to TD6) of Gran Dolina site (Atapuerca, Spain). Quat. Geochronol. 30, 535–540.
Nagata, T., 1961. Rock Magnetism. Maruzen, Tokyo, p. 350.
Nye, J.F., 1957. The Physical Properties of Crystals. Clarendon Press, Oxford, p. 322.
Ollé, A., Mosquera, M., Rodríguez, X.P., de Lombera-Hermida, A., García-Antón, M.D., García-Medrano, P., Peña, L., Menéndez, L., Navazo, M., Terradillos, M., Bargall, o, A., Márquez, B., Sala, R., Carbonell, E., 2013. The Early and Middle Pleistocene technological record from Sierra de Atapuerca (Burgos, Spain). Quat. Int. 295, 138–167.
Ortega, A.I., Benito-Calvo, A., Pérez-González, A., Martín-Merino, M.A., Pérez-Martínez, R., Pares, J.M., Aramburu, A., Arsuaga, J.L., Bermúdez de Castro, J.L., Carbonell, E., 2013. Evolution of multilevel caves in the Sierra de Atapuerca (Burgos, Spain) and its relation to human occupation. Geomorphology 196, 122–137.
Ortega, A.I., Benito-Calvo, A., Pérez-González, A., Arsuaga, J.L., Bermúdez de Castro, J.L., Carbonell, E., 2014. Atapuerca karst and its palaeoanthropological sites. In: Gutiérrez, F., Gutiérrez, M. (Eds.), Landscapes and Landforms of Spain, World Geomorphological Landscapes. Springer Science+Business Media Dordrecht 2014, pp. 101–111.
Parés, J.M., Pérez-González, A., 1995. Paleomagnetic age for hominid fossils at Atapuerca Archaeological site, Spain. Science 269, 830–832.
Parés, J.M., Hassold, N.J.C., Rea, D.K., van der Pluijm, B.A., 2007. Paleocurrent directions from paleomagnetic reorientation of magnetic fabrics in deep-sea sediments at the Antarctic Peninsula Pacific margin (OPD Sites 1095, 1101). Mar. Geol. 242, 261–269.
Parés, J.M., Pérez-González, A., Arsuaga, J.L., Bermúdez de Castro, J.M., Carbonell, E., Ortega, A., 2010. Characterizing sedimentary history of cave deposits, using archaeomagnetism and rockmagnetism, Atapuerca (N Spain). Archaeometry 52 (5), 882–898.
Parés, J.M., Lee, A., Duval, M., Demuro, D., Pérez-González, A., Bermúdez de Castro, J.M., Carbonell, E., Arsuaga, J.L., 2013. Reassessing the age of Atapuerca TD-6 (Spain): new paleomagnetic data. J. Archaeol. Sci. 40, 4586–4595.
Parés, J.M., Ortega, A.I., Benito-Calvo, A., Aranburu, A., Arsuaga, J.L., Bermúdez de Castro, J.M., Carbonell, E., 2016. Paleomagnetic constraints on the Atapuerca karst development (N Spain). In: Feinberg, J., Gao, Y., Alexander Jr., E.C. (Eds.), Caves and Karst across Time: Geological Society of America Special Paper 516, pp. 285–300. https://doi.org/10.1130/2016.2516(22).
Paton, C., Hellstrom, J., Paul, B., Woodhead, J., Hergt, J., 2011. Iolite: freeware for the visualisation and processing of mass spectrometric data. J. Anal. At. Spectrom 26 (12), 2508–2518.
Prescott, J.R., Hutton, J.T., 1994. Cosmic ray contributions to dose rates for luminescence and ESR dating: large depths and long-term time variations. Radiat. Meas. 23, 497–500.
Rossi, C., Villalaín, J.J., Lozano, R.P., Hellstrom, J., 2016. Paleo-watertable definition using cave ferromanganese stromatolites and associated cave-wall notches (Sierra de Arnero, Spain). Geomorphology 57–75.
Singer, B.S., 2014. A Quaternary geomagnetic instability time scale. Quat. Geochronol. 21, 29–52.
Schmitz, M.D., Schoene, B., 2007. Derivation of isotope ratios, errors, and error correlations for U-Pb geochronology using 205Pb-235U-(233U)-spiked isotope dilution thermal ionization mass spectrometric data. G-cubed. https://doi.org/10.1029/2006GC001492.
Stacey, F.D., Joplin, G., Lindsay, J., 1960. Magnetic anisotropy and fabric of some foliated rocks from SE Australia. Geophysica Pura Appl. 47, 551–556.
Tarling, D.H., Hrouda, F., 1993. The Magnetic Anisotropy of Rocks. Chapman and Hall, London, p. 217.
Tauxe, L., 1993. Paleomagnetic Principles and Practice. Kluwer Academic Publishers, Dordrecht, p. 297.
Vandenberghe, D., De Corte, F., Buylaert, J.P., Kucera, J., Van den haute, P., 2008. On the internal radioactivity in quartz. Radiat. Meas. 43, 771–775.
Woodhead, J., Hellstrom, J., Pickering, R., Drysdale, R., Paul, B., Bajo, P., 2012. U and Pb variability in older speleothems and strategies for their chronology. Quat. Geochronol. 14, 105–113.
Woodhead, J., Hellstrom, J., Maas, R., Drysdale, R., Zanchetta, G., Devine, P., Taylor, E., 2006. U-Pb geochronology of speleothems by MC-ICPMS. Quat. Geochronol. 1, 208–221.
Yokoyama, Y., Falgueres, C., Quaegebeur, J.P., 1985. ESR dating of quartz from quaternary sediments: first attempt. Nucl. Tracks Radiat. Meas. 10 (4–6), 921–928.
Zijderveld, J.D.A., 1967. AC demagnetization of rocks: analysis of results. In: Collinson, D.W., Runcorn, S.K., Creer, K.M. (Eds.), Methods in Paleomagnetism. Elsevier, New York, pp. 254–286.

Capítulo 8. Resultados Pendientes de Publicación

Capítulo 8. Resultados pendientes de publicación

Durante el desarrollo de esta tesis se han llevado a cabo una serie de análisis en dos cuencas con evidencia humana, con la intención de establecer un mejor marco cronológico tanto de la evolución de las mismas como de los yacimientos en ellas situados. Una corresponde a la cuenca de Aïn Bni Mathar en Marruecos, y la otra es la cuenca del Duero, en la Península Ibérica. Los resultados obtenidos están todavía en proceso de análisis a la espera de su publicación, sin embargo, se expone a continuación un resumen de los resultados paleomagnéticos iniciales.

8.1 Resultados preliminares de la aplicación del paleomagnetismo en la cuenca de Aïn Bni Mathar (Marruecos)

Se han estudiado cuatro localizaciones cerca de la región de Aïn Bni Mathar, que da nombre a la cuenca (Figura 8.1), analizándose secuencias estratigráficas con una litología similar en todas ellas, en la que predominan niveles inferiores de arenas y arcillas rojas, presencia de niveles conglomerados y travertinos en algunos casos y niveles superiores de calizas, encontrándose costra calcárea en superficie en alguna de las localizaciones. Las secuencias se han nombrado en función de la localidad más próxima: Guefait, con dos columnas estudiadas, numeradas 2 y 4, Garat Soultana y Aïn Tebouda. El

proceso de estudio ha sido el mismo en las cuatro localizaciones: realización de la columna estratigráfica y muestreo *in situ*.

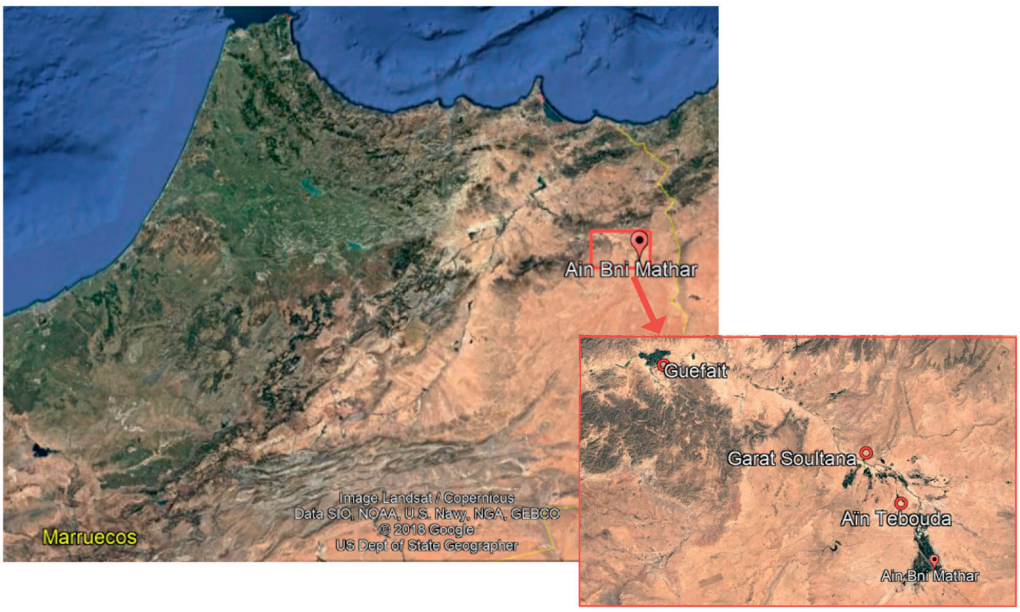

Figura 8.1 Situación de las cuatro localizaciones muestreadas en el noreste de Marruecos, cerca de la ciudad de Aïn Bni Mathar que da nombre a la cuenca. Imagen tomada de Google Earth.

- Guefait 2: Secuencia de 150 m en la que se han obtenido un total de 360 ejemplares, de los cuales se han procesado 259.

- Guefait 4: Con una secuencia de unos 60m, se han obtenido un total de 45 ejemplares de los cuales se han procesado 44.

- Garat Soultana: Secuencia de aproximadamente 17 metros, las muestras obtenidas han sido un total de 70 ejemplares de los que se han analizado 47.

- Aïn Tebouda: Con 15 metros de altura, es la secuencia más corta de las cuatro localizaciones. Se han obtenido un total de 33 ejemplares de los que se han procesado 29.

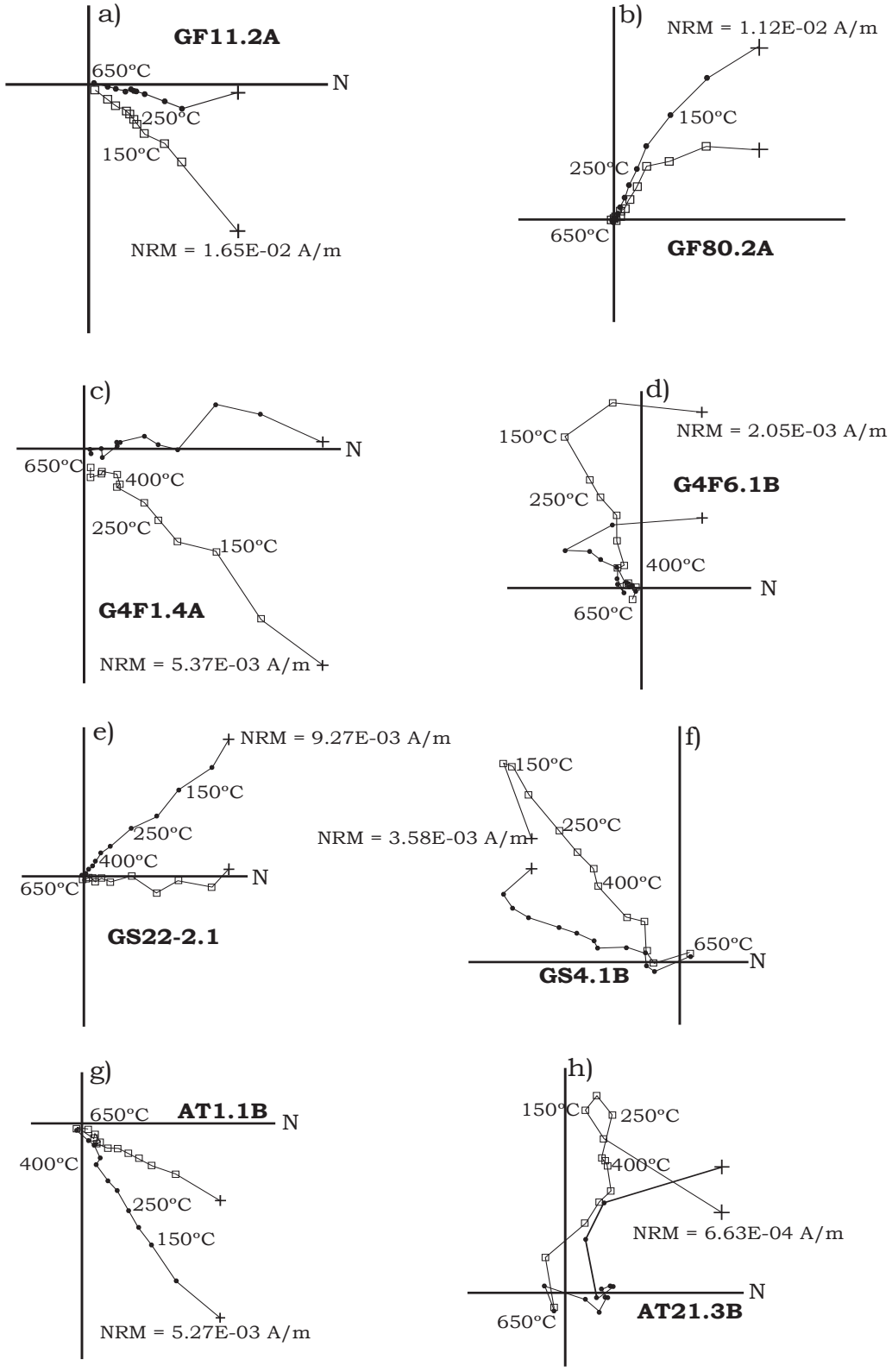

Figura 8.2 Algunos de los diagramas de Zijderveld obtenidos, a) y b) pertenecen a la secuencia de Guefait 2, c) y d) a la de Guefait 4, e) y f) a Garat Soultana y g) y h) a Aïn Tebouda.

Las muestras analizadas presentan valores de NRM que oscilan entre 8.94E-05 A/m y 6.88E-02 A/m, se trata de muestras magnéticamente fuertes, y en general presentan una mejor desmagnetización mediante lavado térmico, llegando a alcanzar temperaturas de 650°C (Figura 8.2). En conjunto se han analizado más de 300 ejemplares que han dado como resultado la obtención de cuatro secuencias magnetoestratigráficas en las que mayoritariamente se observan polaridades inversas con magnetozonas normales.

Actualmente los resultados finales están en proceso de redacción pues forman parte de un trabajo conjunto con otros investigadores y otras técnicas cronológicas, a la espera de ser publicados próximamente.

8.2 Resultados preliminares de los análisis paleomagnéticos en el estudio de la evolución de la Cuenca del Duero

La zona de estudio de la evolución de la cuenca del Duero se ha localizado en los sectores central y oriental de la cuenca y las terrazas pertenecientes a la subcuenca de Almazán. Se ha muestreado en un total de ocho localidades distintas, entre terrazas y secuencias estratigráficas; distribuyéndose de la siguiente manera (Figura 8.3)

a) Terrazas fluviales:

-Río Arlanza: terrazas de Tordomar y Santa Inés. Materiales correspondientes a arcillas, limos y areniscas.

-Río Arlanzón: terrazas de Zalduendo y Villacienzo. Sedimentología correspondiente a conglomerados, areniscas y arcillas.

-Río Duero (Subcuenca de Almazán): terraza de Alconaba. Materiales arenosos.

Figura 8.3. Esquema de la Cuenca del Duero y localización de las zonas muestreadas. 1 -> terrazas de Tordomar, 2 -> terrazas de Santa Inés, 3 -> terraza de Zalduendo, 4 -> terraza de Villacienzo, 5 -> terrazas de Alconaba, 6 -> secuencia de Peñafiel, 7 -> secuencia de Adrada de Haza y 8 -> secuenca de Vallejera. Imagen modificada de Google Earth.

Las muestras analizadas presentan una susceptibilidad magnética muy baja, y valores de MRN que oscilan entre 2.65E-05 A/m y 1.01E-03 A/m, se trata de muestras magnéticamente débiles. Analizando los diagramas de Zijderveld obtenidos (Figura 8.4, a, b y c) se aprecia que en general presentan un solo componente y de baja temperatura, lo que puede indicar que el mineral ferromagnético mayoritario en las muestras sea de alta coercitividad (hematites).

b) Secuencias estratigráficas: sedimentos lacustres carbonatados, con niveles de limos y arcillas arenosas. Se han nombrado en función de las localidades donde se han muestreado.

-Peñafiel; secuencia de 85,5 m en la que se han obtenido 88 muestras individuales.

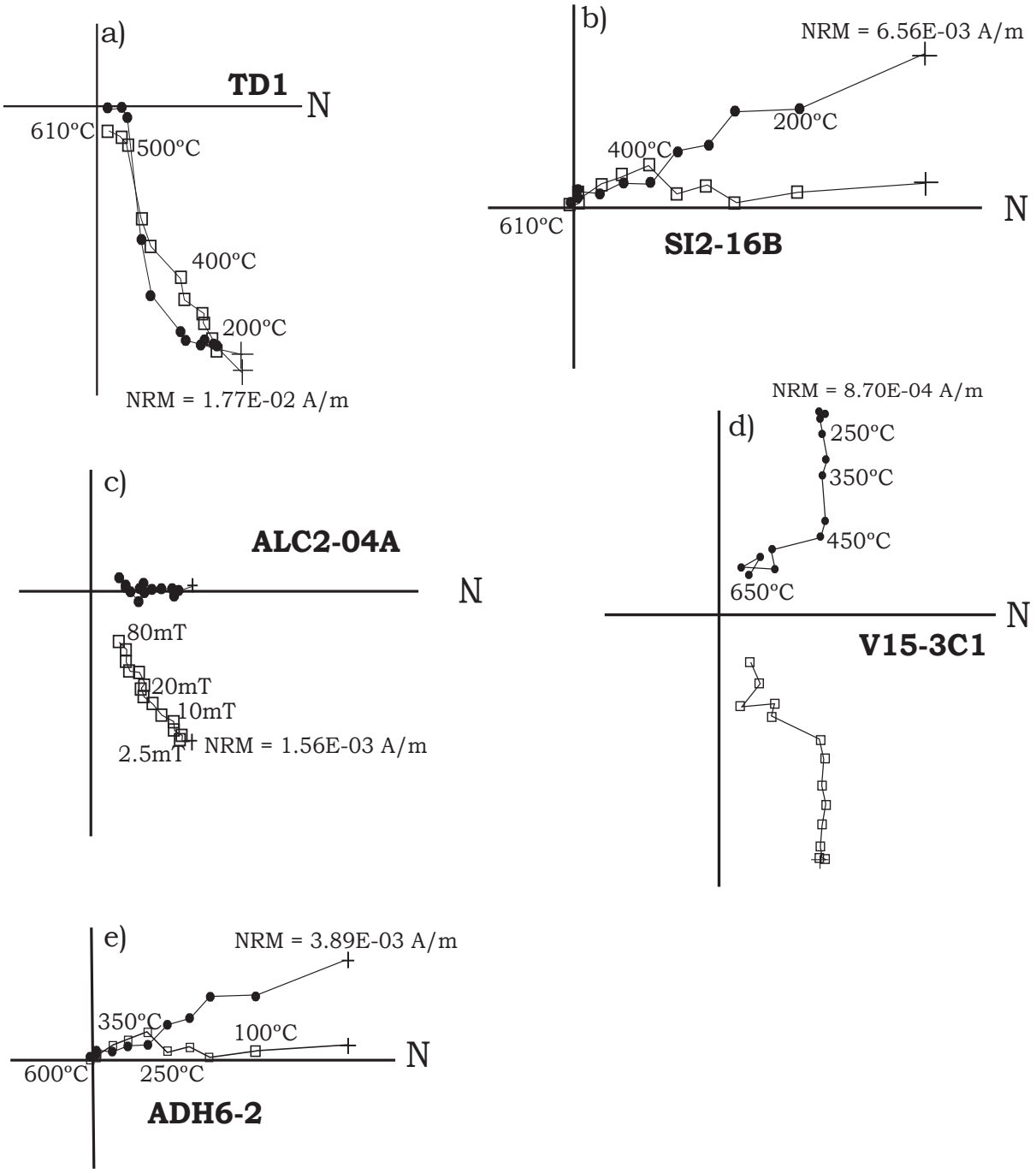

Figura 8.4. Ejemplo de algunos de los diagramas de Zijderveld analizados. TD -> Tordomar, SI2 -> Santa Ines, ALC -> Alconaba, V -> Vallejera, ADH -> Adrada de Haza

-Adrada de Haza: secuencia de 43,5 m, con un total de 68 muestras individuales.

-Vallejera: secuencia de 73,5 m y un total de 185 muestras individuales obtenidas.

Las muestras presentan baja susceptibilidad y valores de NRM altos, oscilan entre 9.18E-05 A/m y 8.57E-03 A/m para Vallejera; 8.49E-05 A/m y 2.92E-04 A/m para Peñafiel, y 8.49E-06 A/m y 1.30E-03 A/m para Adrada de Haza; son en general muestras magnéticamente muy débiles (Figura 8.4, d y e). En el caso de los resultados correspondientes a la Cuenca del Duero, se plantea la posibilidad de remuestrear de nuevo las localizaciones, dada la baja intensidad que muestran los ejemplares analizados. Por tanto, es un proyecto a considerar en el futuro.

Capítulo 9. Discusión

Capítulo 9. Discusión

Los yacimientos analizados a lo largo del desarrollo de esta tesis, y que han dado lugar a artículos publicados, son tres de los yacimientos más importantes en la Península Ibérica en cuanto a presencia humana en el Paleolítico inferior se refiere. Tener, por tanto, un marco temporal lo más delimitado posible es un elemento fundamental. Para ello se ha tratado de establecer con la mayor precisión posible la presencia o ausencia del subcron Jaramillo (0,99 – 1,07 Ma) o al menos situarlo en contexto para determinar con claridad la presencia humana en dichas regiones.

9.1 Yacimientos de Fuente Nueva 3 y Solana del Zamborino (Orce, Granada)

El sector de la Cuenca de Guadix-Baza, en Granada, es una de las zonas del oeste europeo más importantes en cuanto a información dentro del periodo Neógeno – Cuaternario. Posee uno de los registros más abundantes sobre la fauna de esa época; con yacimientos que abarcan desde el Plioceno superior, como el de Huélago; abundante información del Pleistoceno inferior con enclaves como Venta Micena (VM), Barranco León (BL), Fuente Nueva-3 (FN-3) y Huéscar; y en lo referente al Pleistoceno medio, localidades como Solana del Zamborino (SZ) y Cúllar-Baza (Arribas et al., 2004; Toro et al., 2000).

Pero no solo presentan información faunística; contienen también evidencia

de presencia humana, la cual ha recaído mayormente en la abundante presencia de industria lítica hallada en los yacimientos de FN-3, BL y SZ (Botella et al., 1976; Toro et al., 2000), pues desde el polémico resto hallado en VM en 1982 nombrado VM-0 (Gibert et al., 1983), los hallazgos posteriores en BL (Gibert et al., 1999) y otros más encontrados en VM (Gibert et al., 2002) han generado amplia controversia. De hecho, en lo que respecta a VM-0 se ha demostrado que pertenece a una especie de rumiante (Martínez-Navarro, 2002).

Ante esta situación es, como se indicaba anteriormente, la industria lítica encontrada en BL y FN-3 la que evidencia la presencia humana en el suroeste de Europa antes del millón de años, pues los artefactos encontrados en ambos yacimientos, considerados contemporáneos, se han atribuido al Modo 1 u Olduvayense del este de África y datado entre 1,5 y 2 Ma (Martínez-Navarro et al., 1997). Así mismo, las dataciones combinadas de ESR y series de uranio realizadas en FN-3 avalan esa cronología (> 1 Ma) al aportar una edad de ~1,2 Ma para el nivel arqueológico superior del yacimiento (Duval et al., 2012a). Pese a todo, no es hasta 2013 que se acepta de manera concluyente la presencia humana en la Cuenca de Guadix-Baza, con la aparición de un molar de leche de un individuo de unos 10 años de edad en Barranco León, y datado en aproximadamente 1,4 Ma (Toro-Moyano et al., 2013), que junto con la abundante industria lítica asociada, parece indicar que la colonización del oeste de Europa ocurrió menos de 0,5 Ma después de la primera expansión del genéro *Homo*, la cuál tuvo lugar alrededor de hace 1,8 Ma como aporta la datación de Dmanisi (García et al., 2010).

Sin embargo, algunos autores, como Muttoni et al., (2018) sostienen que establecer la ocupación humana en Europa antes de 1 Ma es altamente improbable. Consideran la presencia o ausencia del subcron Jaramillo como referente para establecer la cronología de aquellos yacimientos con posible

evidencia humana anterior a 1 Ma, y ponen en duda la eficacia y exactitud de las técnicas aplicadas en aquellas localizaciones en las que se ha establecido una cronología pre Jaramillo, entre ellos los yacimientos de Barranco León y Fuente Nueva-3. En lo que corresponde al diente hallado en BL sugieren inexactitudes de las dataciones de ESR propuestas por Toro-Moyano et al., (2013) debido a una distancia de transporte insuficiente de los granos de cuarzo para que se reiniciara la señal de ESR de los mismos, por lo que las fechas aportadas podrían no ser efectivas para diferenciar claramente entre momentos pre y post Jaramillo, lo que daría lugar a una sobreestimación de la edad de deposición de la sección y no corresponder al periodo de polaridad inversa del cron Matuyama situado entre los subcrones de Jaramillo y Olduvai. Además, señalan que si, como parece indicar la ESR, la sección supera los 0,7 Ma de duración, no se explica porqué siguen sin encontrarse dichos subcrones. Es esta ausencia también el motivo por el que dudan de la cronología pre Jaramillo atribuida al nivel de industria lítica de FN-3, y no excluyen la posibilidad de que este subcron se sitúe en los niveles inferiores de la secuencia, lo que daría lugar a una cronología más joven (< 1Ma) al yacimiento, pero anterior al límite Brunhes-Matuyama (0,78 Ma). No obstante, estos autores no han tenido en cuenta los datos obtenidos del análisis magnetoestratigráfico y de nucleidos cosmogénicos, realizados sobre los dos sondeos llevados a cabo en FN-3, y que son parte de esta tesis (Álvarez et al., 2015). Los resultados expuestos en este artículo avalan el predominio de polaridad inversa para FN-3, con un intervalo de tiempo comprendido entre 1,77 y 1,07 Ma, propio de una edad previa a Jaramillo, cronología que respaldan los datos de ESR realizados por Duval et al., (2012b). Aunque bien es cierto que no se ha demostrado la presencia del subcron Jaramillo, si se han hallado en la parte inferior de la secuencia una serie de intervalos de polaridad normal que no se han encontrado en otras zonas de la cuenca. Tomando en conjunto todos los datos cronológicos referentes a FN-3, tanto de ESR (Duval et al., 2012a, 2012b, 2011), microfauna (Agustí et al.,

2010) y macrofauna (Martínez-Navarro et al., 2010), nos permiten plantear la hipótesis de que la secuencia de FN-3 estudiada tiene una edad comprendida entre Jaramillo y Olduvai y que los intervalos de polaridad normal registrados correspondan alguno de los intervalos cortos que se han definido entre esos dos subcrones, tales como Gilsa (~1,6 Ma), Gardar (~1,5 Ma), Bjorn (~1,3 Ma) o Cobb Mountain (~1,2 Ma) (Channell, 2002; Laj and Channell, 2007; Singer et al., 1999). Por tanto, sería posible esa cronología superior al millón de años para el yacimiento de Fuente Nueva-3 y extrapolable a Barranco León.

En el caso del yacimiento de Solana del Zamborino, esta localidad ha aportado más de 1000 piezas líticas (Botella, 1975; Botella et al., 1976) que se han clasificado como industria perteneciente al Modo 2 o Achelense y, por tanto, situaría la presencia humana en ese yacimiento hace unos 0,4 – 0,34 Ma. El primer análisis paleomagnético del yacimiento fue llevado a cabo por Scott y Gibert (2009) aportando una edad de 0,77 – 0,75 Ma, inmediatamente por encima del límite Brunhes-Matuyama, convirtiendose así, en la industria lítica Achelense más antigua de Europa. Sin embargo dicho trabajo presenta una serie de incongruencias tal como indican Jiménez-Arenas et al. (2011) y que generan dudas con respecto a las fechas obtenidas. Por ejemplo, la discrepancia en la tasa de sedimentación aportada. La usada por Scott y Gibert corresponde a la del yacimiento de Cúllar – Baza, a 50 km de Solana del Zamborino y que tiene origenes deposicionales distintos, dado que Cúllar – Baza presenta una composición siliciclástica de origen fluvial, mientras que Solana del Zamborino aunque también presenta relleno siliciclástico, es mayormente relleno carbonático de origen palustre - lacustre. Así mismo presentan incongruencias entre la fauna presentada en el artículo y las listas originales publicadas. Por tanto, se hacía imprescindible realizar un nuevo análisis magnetoestratigráfico para determinar con certeza la edad de la industria lítica encontrada en SZ. El trabajo realizado (Álvarez-Posada et al.,

2017), consistió en un muestreo de ~65 m incluyendo el propio yacimiento y niveles inferiores. Los resultados obtenidos presentan una magnetoestratigrafía interpretable sobre el propio entorno del yacimiento, sin necesidad de recurrir a la proporcionada por Cúllar-Baza, y con una tasa de sedimentación propia (Pla-Pueyo, 2009; Pla-Pueyo et al., 2011). Al igual que el trabajo de Scott y Gibert, el yacimiento se encuentra situado en un nivel de polaridad claramente normal, asociado al cron Brunhes, por encima del límite Brunhes-Matuyama. Sin embargo, se han localizado otros tres niveles de polaridad normal por debajo del yacimiento, el más inmediato al límite Brunhes-Matuyama se ha asociado al subcron Olduvai, dada la tasa de sedimentación y la correlación con el yacimiento próximo de Fonelas (FP-1) (Pla-Pueyo, 2006; Pla-Pueyo et al., 2011) en el que Jaramillo también está ausente (ver Figura 8, capítulo V de esta tésis.) En consecuencia, la posición estratigráfica del yacimiento de Solana del Zamborino estaría situada en una cronología más próxima a los 0,30 – 0,48 Ma, más en la línea de la cronología propuesta para la industria lítica Achelense en Europa.

9.2 Yacimiento de Gran Dolina

El yacimiento de Gran Dolina (TD), en Atapuerca, ha aportado amplia información para enteder la dispersión humana por Europa, con el descubrimiento de *Homo antecessor*, y la presencia de abundante industria lítica, tanto del Modo 1 como del Modo 2. Por estos motivos tener una cronología lo más acotada posible, tanto del proceso de relleno de la cavidad como de la presencia humana de la misma, se hace imprescindible. Mientras que la presencia del límite Brunhes – Matuyama (MBB) se ha establecido claramente en la parte superior del nivel TD7 (Parés y Pérez González, 1995, 1999; Parés et al., 2013; Pérez González et al., 2001), no está tan clara la presencia del subcron Jaramillo, que aportaría un mejor marco cronológico

no solo de los restos de *Homo antecesssor* y de la industria lítica presente en los depósitos interiores de la sima (como el propio nivel TD6 o TD4), si no que permitiría contextualizar mejor la cronología de los restos de *Homo sp.* hallados en Trinchera Elefante (Carbonell et al., 2008), y establecer de manera inequívoca la presencia humana en la Sierra de Atapuerca antes del millón de años. En este sentido, la magnetoestratigrafía obtenida para los niveles inferiores de Dolina, TD6 a TD4 (Álvarez-Posada et al., 2018) indican una polaridad claramente inversa, propia del cron Matuyama y acorde con la presencia del límite MMB entre los niveles TD7 y TD8, y posterior al subcron Jaramillo de acuerdo con los datos aportados por la ESR (Moreno et al., 2015) y la luminiscencia (Arnold et al., 2015) que indican unas edades para TD6 de 0,91±0,25 Ma y 0,85±0,57 Ma respectivamente, por lo que es justificable pensar que Jaramillo debería encontrarse en los siguientes niveles de TD, en algún punto entre TD3 y TD1. Las sucesivas campañas de excavación en los últimos años han permitido acceder recientemente al nivel inferior de TD1 y realizar un completo análisis cronológico de los niveles inferiores (Parés et al., 2018), aplicando tanto métodos paleomagnéticos como de ESR. En conjunto, presentan una polaridad mayormente inversa pero interrumpida por una magnetozona de polaridad normal a unos 5 metros de TD4, en la parte superior de TD1 (ver figura 9, capítulo 7), en la que los análisis de ESR indican una edad entre 0,8 y 1,2 Ma que puede intepretarse como Jaramillo.

9.3 Referencias

Agustí, J., Blain, H.-A.A., Furió, M., De Marfá, R., Santos-Cubedo, A., 2010. The early Pleistocene small vertebrate succession from the Orce region (Guadix-Baza Basin, SE Spain) and its bearing on the first human occupation of Europe. Quaternary International 223–224, 162–169.

Álvarez-Posada, C., Parés, J.M., Cuenca-Bescós, G., Van der Made, J., Rosell, J., Bermúdez de Castro, J.M., Carbonell, E., 2018. A post-Jaramillo age for the artefact-bearing layer TD4 (Gran Dolina, Atapuerca): New paleomagnetic evidence. Quaternary Geochronology 45, 1–8.

Álvarez-Posada, C., Parés, J.M., Sala, R., Viseras, C., Pla-Pueyo, S., 2017. New magnetostratigraphic evidence for the age of Acheulean tools at the archaeo-palaeontological site “Solana del Zamborino” (Guadix – Baza Basin, S Spain). Scientific Reports 7, 13495.

Álvarez, C., Parés, J.M., Granger, D., Duval, M., Sala, R., Toro, I., 2015. New magnetostratigraphic and numerical age of the Fuente Nueva-3 site (Guadix-Baza basin, Spain). Quaternary International 389, 224–234.

Arnold, L.J., Demuro, M., Parés, J.M., Pérez-González, A., Arsuaga, J.L., Bermúdez de Castro, J.M., Carbonell, E., 2015. Evaluating the suitability of extended-range luminescence dating techniques over early and Middle Pleistocene timescales: Published datasets and case studies from Atapuerca, Spain. Quaternary International 389, 167–190.

Arribas, A., Baeza, E., Bermúdez, D., Blanco, S., Durán, J.J., Garrido, G., Gumiel, J.C., Hernández, R., Soria, J.M., Viseras, C., 2004. Nuevos registros paleontológicos de grandes mamíferos en la Cuenca de Guadix-Baza (Granada): Aportaciones del Proyecto Fonelas al conocimiento sobre las faunas con-

tinentales del Plioceno-Pleistoceno europeo. Boletin Geologico y Minero 115, 567–582.

Botella, M.C., 1975. El cazadero achelense de la Solana de Zamborino (Granada). Crónica del XIII Congreso Arqueológico nacional 175–184.

Botella, M.C., Torres, J.A. V., Porta, J. de, 1976. El Yacimiento Achelense De La 'Solana Del Zamborino'. Fonelas (Granada) (Primera Campaña De Excavaciones). Cuadernos de Prehistoria y Arqueología de la Universidad de Granada 1.

Carbonell, E., Bermúdez De Castro, J.M., Parés, J.M., Pérez-González, A., Cuenca-Bescós, G., Ollé, A., Mosquera, M., Huguet, R., Van Der Made, J., Rosas, A., Sala, R., Vallverdú, J., García, N., Granger, D.E., Martinón-Torres, M., Rodríguez, X.P., Stock, G.M., Vergès, J.M., Allué, E., Burjachs, F., Cáceres, I., Canals, A., Benito, A., Díez, C., Lozano, M., Mateos, A., Navazo, M., Rodríguez, J., Rosell, J., Arsuaga, J.L., 2008. The first hominin of Europe. Nature 452, 465–469.

Channell, J.E.T., 2002. Geomagnetic excursions and paleointensities in the Matuyama Chron at Ocean Drilling Program Sites 983 and 984 (Iceland Basin). Journal of Geophysical Research 107, 2114.

Duval, M., Falguères, C., Bahain, J.-J., Grün, R., Shao, Q., Aubert, M., Hellstrom, J., Dolo, J.-M., Agusti, J., Martínez-Navarro, B., Palmqvist, P., Toro-Moyano, I., 2011. The challenge of dating early pleistocene fossil teeth by the combined uranium series-electron spin resonance method: the Venta Micena palaeontological site (Orce, Spain). Journal of Quaternary Science 26, 603–615.

Duval, M., Falguères, C., Bahain, J.-J.J., 2012a. Age of the oldest hominin settlements in Spain: Contribution of the combined U-series/ESR dating method applied to fossil teeth. Quaternary Geochronology 10, 412–417.

Duval, M., Falguères, C., Bahain, J.-J.J., Grün, R., Shao, Q., Aubert, M., Dolo, J.-M.M., Agustí, J., Martínez-Navarro, B., Palmqvist, P., Toro-Moyano, I., 2012b. On the limits of using combined U-series/ESR method to date fossil teeth from two Early Pleistocene archaeological sites of the Orce area (Guadix-Baza basin, Spain). Quaternary Research 77, 482–491.

García, T., Féraud, G., Falguères, C., de Lumley, H., Perrenoud, C., Lordkipanidze, D., 2010. Earliest human remains in Eurasia: New40Ar/39Ar dating of the Dmanisi hominid-bearing levels, Georgia. Quaternary Geochronology 5, 443–451.

Gibert, J., Agustí, J., Moyà-Solà, S., 1983. Presencia de Homo sp. en el yacimiento del Pleistoceno inferior de Venta Micena (Orce, Granada). Paleontologia i Evolucio 1–9.

Gibert, J., Gibert, L., Albadalejo, S., Ribot, F., Sánchez, F., Gibert, P., 1999. Molar tooth fragment BL5-0: the oldest human remain found in the Plio-Pleistocene of Orce (Granada province, Spain). Human Evolution 14, 3–19.

Gibert, J., Sanchez, F., Ribot, F., Gibert, L., Ferrandez, C., Iglesias, A., Gibert, P., González, F., 2002. Restes humains dans les sédiments du Pléistocène inférieur de la région d'Orce et de Cueva Victoria (sud-est de l'Espagne). L'Anthropologie 106, 669–683.

Jiménez-Arenas, J.M., Santonja, M., Botella, M., Palmqvist, P., 2011. The oldest handaxes in Europe: Fact or artefact? Journal of Archaeological Science 38, 3340–3349.

Laj, C., Channell, J.E.T., 2007. Geomagnetic Excursions, in: Treatise on Geophysics. Elsevier, pp. 373–416.

Martínez-Navarro, B., Turq, A., Agustí Ballester, J., Oms, O., 1997. Current events. Fuente Nueva-3 (Orce, Granada, Spain) and the first human occupation of Europe. Journal of Human Evolution 33, 611–620.

Martínez-Navarro, B., 2002. The skull of Orce: parietal bones or frontal bones? Journal of Human Evolution 43, 265–270.

Martínez-Navarro, B., Palmqvist Barrena, P., Madurell-Malapeira, J., Ros-Montoya, S., Espigares Ortiz, M.P., Torregrosa, V., Pérez Claros, J.A., 2010. La fauna de grandes mamíferos de Fuente Nueva-3 y Barranco León-5 estado de la cuestión, in: Martínez-Navarro, B., Agustí i Ballester, J., Toro, I. (Eds.), Ocupaciones Humanas En El Pleistoceno Inferior y Medio de La Cuenca de Guadix-Baza. Junta de Andalucía, Consejería de Cultura, Dirección General de Bienes Culturales., Sevilla, pp. 197–236.

Moreno, D., Falguères, C., Pérez-González, A., Voinchet, P., Ghaleb, B., Despriée, J., Bahain, J.J., Sala, R., Carbonell, E., Bermúdez de Castro, J.M., Arsuaga, J.L., 2015. New radiometric dates on the lowest stratigraphical section (TD1 to TD6) of Gran Dolina site (Atapuerca, Spain). Quaternary International 30, 535–540.

Muttoni, G., Scardia, G., Kent, D. V., 2018. Early hominins in Europe: The Galerian migration hypothesis. Quaternary Science Reviews 180, 1–29.

Parés, J.M., Pérez-González, A., 1995. Paleomagnetic age for hominid fossils at Atapuerca archaeological site, Spain. Science 269, 830–832.

Parés, J.M., Pérez-González, A., 1999. Magnetochronology and stratigraphy at Gran Dolina section, Atapuerca (Burgos, Spain). Journal of Human Evolution 37, 325–342.

Parés, J.M., Álvarez, C., Sier, M., Moreno, D., Duval, M., Woodhead, J., Ortega, A., Campaña, I., Rosell, J., Bermúdez de Castro, J., Carbonell, E., 2018. Chronology of the cave interior sediments at Gran Dolina archaeological site, Atapuerca (Spain). Quaternary Science Reviews 186, 1–16.

Parés, J.M., Arnold, L., Duval, M., Demuro, M., Pérez-González, A., Bermúdez de Castro, J.M., Carbonell, E., Arsuaga, J.L., 2013. Reassessing the age of Atapuerca-TD6 (Spain): New paleomagnetic results. Journal of Archaeological Science 40, 4586–4595.

Pérez González, A., Parés, J.M., Carbonell, E., Aleixandre, T., Ortega, A.I., Benito, A., Martin Merino, M.Á., 2001. Géologie de la Sierra de Atapuerca et stratigraphie des remplissages karstiques de Galería et Dolina (Burgos, Espagne). L'Anthropologie 105, 27–43.

Pla-Pueyo, S., 2009. Contexto estratigráfico y sedimentario de los yacimientos de grandes mamíferos del sector centralal de la Cuenca de Guadix (Cordillera Bética). Tesis Doctoral. Universidad de Granada.

Pla-Pueyo, S., 2006. Encuadre estratigráfico de los más significativos yacimientos de macromamíferos continentales localizados en el marco del Proyecto Fonelas (límite Plioceno-Pleistoceno, Cuenca de Guadix, Granada, España). Boletin Geologico y Minero 117, 483–489.

Pla-Pueyo, S., Viseras, C., Soria, J.M., Tent-Manclús, J.E., Arribas, A., 2011. A stratigraphic framework for the Pliocene-Pleistocene continental sediments of the Guadix Basin (Betic Cordillera, S. Spain). Quaternary International 243, 16-32.

Scott, G.R., Gibert, L., 2009. The oldest hand-axes in Europe. Nature 461, 82–85.

Singer, B.S., Hoffman, K.A., Chauvin, A., Coe, R.S., Pringle, M.S., 1999. Dating transitionally magnetized lavas of the late Matuyama Chron: Toward a new 40 Ar/ 39 Ar timescale of reversals and events. Journal of Geophysical Research: Solid Earth 104, 679–693.

Toro-Moyano, I., Martínez-Navarro, B., Agustí, J., Souday, C., Bermúdez de Castro, J.M., Martinón-Torres, M., Fajardo, B., Duval, M., Falguères, C., Oms, O., Parés, J.M., Anadón, P., Julià, R., García-Aguilar, J.M., Moigne, A.-M., Espigares, M.P., Ros-Montoya, S., Palmqvist, P., 2013. The oldest human fossil in Europe, from Orce (Spain). Journal of Human Evolution 65, 1–9.

Toro, I., Turq, A., Agustí, J., Martínez-Navarro, B., Oms, O., Agustp, J., Martínez-Navarro, B., Oms, O., 2000. Los yacimientos del Pleistoceno inferior de Barranco León y Fuente Nueva 3 de Orce (Granada). Contribución al conocimiento del primer poblamiento humano de Europa. SPAL. Revista de Prehistoria y Arqueología de la Universidad de Sevilla 9, 179–188.

Capítulo 10. Conclusions / Conclusiones

Chapter 10. Conclusions

Paleomagnetism used as a chronological dating methodology reveals a powerful tool that can help us to delimit human dispersion into a time frame. In this Thesis, a concrete application of this technique has been made, obtaining magnetostratigraphies in several locations belonging to the Circummediterranean basin. The conclusions are detailed below, grouped according to the sites studied.

10.1 Application of paleomagnetism in the site of Fuente Nueva - 3 (Orce, Granada)

- The magnetostratigraphy obtained is consistent with a period of reverse dominant polarity, between 1.77 and 1.07 Ma, with the presence of brief intervals of normal polarity in the lower part, which have not been found in nearby sites.

- The age provided by the ESR dates for the deposit is consistent with the biostratigraphic data and indicate a chronology of lower Pleistocene, prior to the Jaramillo subchron.

- Therefore, it can be interpreted that the analyzed FN-3 locality analyzed has an age between the Olduvai and Jaramillo subchrons, older than a million years.

10.2 New magnetostratigraphic analyses at the Solana del Zamborino site (Orce, Granada)

- As the sequence has been expanded, three new levels of normal polarity were obtained below the paleontological site, which were not observed in previous studies (Scott and Gibert, 2009).

- The obtained sedimentation rate of the sequence, is similar to that of the nearest deposits of Fonelas and Mencal, and is consistent with the absence of Jaramillo. sedimentation rate and biostratigraphic data indicate that the stratigraphic position of the archaeological layer presents a much younger chronology than that proposed by Scott and Gibert (2009) and more similar to that established for the Acheulean in Europe.

10.3 New paleomagnetic evidence and chronology for the Gran Dolina site (Atapuerca, Burgos)

- The presence of the Brunhes - Matuyama boundary is clearly defined between TD7 and TD8 levels.

- The paleomagnetic data obtained from levels TD6 to TD4 clearly indicate a reverse polarity, which together with the ESR and luminescence analyzes establish an age clearly post Jaramillo for these levels.

- The new outcrop of to the lower strata, reaching the base of TD1, has allowed a more exhaustive analyses of this unit, and although overall the sequence below the MBB limit presents an eminently reverse polarity, a magnetozone with normal polarity has been located in the upper level of TD1 which has been attributed to Jaramillo.

- Therefore, the chronology corresponding to the levels of lithic industry and *Homo antecessor* would be 0.9 - 0.78 Ma, interval between the MBB limit

and the Jaramillo subchron, indicating a human presence in Gran Dolina close to one million years. Results supported by a recent study conducted by Duval et al. (2018) dating a *antecessor* tooth from TD6 which provides and estimated age form 624 to 949 ka.

Definitely, in view of the results of the works presented in this thesis, it can be concluded that, paleomagnetism, specifically the obtained magnetostratigraphies in combination with others chronological methods (ESR, cosmogenic nuclides) can provided a strong evidence to identify human presence prior to the Jaramillo subchron, close enough to a million years, despite the abundance of hominid remains after said subchron.

10. 4 Preliminar Results

As far as our studies in progress we expected that the papers that are still in process of being published will develope further research that will allow us to know a better chronological framework of human dispersion outsie of Africa.

10.5 References

Duval, M., Grün, R., Parés, J.M., Martín-Francés, L., Campaña, I., Rosell, J., Shao, Q., Arsuaga, J.L., Carbonell, E., Bermúdez de Castro, J.M., 2018. The first direct ESR dating of a hominin tooth from Atapuerca Gran Dolina TD-6 (Spain) supports the antiquity of Homo antecessor. Quaternary Geochronology 47, 120–137.

Scott, G.R., Gibert, L., 2009. The oldest hand-axes in Europe. Nature 461, 82–85.

Capítulo 10. Conclusiones

La aplicación del paleomagnetismo como método cronológico se ha revelado como una herramienta potente que puede ayudar a acotar un marco temporal para la dispersión humana. En la presente tesis se ha realizado una aplicación específica de esta técnica: la obtención de magnetoestratigrafías en emplazamientos concretos pertenecientes a la cuenca Circummediterranea. Las conclusiones obtenidas, se detallan a continuación, agrupadas en función de los yacimientos estudiados.

10.1 Aplicación del paleomagnetismo en el yacimiento de Fuente Nueva - 3 (Orce, Granada)

- La magnetoestratigrafía obtenida es consistente con un periodo de polaridad dominante inversa, comprendida entre 1,77 y 1,07 Ma, con presencia de breves intervalos de polaridad normal en los niveles inferiores que no se han hallado en yacimientos próximos.

- La edad aportada por las dataciones de ESR para el yacimiento es consistente con los datos bioestratigráficos que indican una cronología propia del Pleistoceno inferior, anterior al cron Jaramillo.

- Se puede interpretar, por tanto, que la secuencia de FN-3 analizada tiene una edad comprendida entre los subcrones Olduvai y Jaramillo, anterior al

millón de años.

10.2 Nuevo análisis magnetoestratigráfico en el yacimiento de Solana del Zamborino (Orce, Granada)

- Al ampliarse la secuencia se han obtenido tres nuevos niveles de polaridad normal por debajo del yacimiento, que no estaban reconocidos en el trabajo publicado por Scott y Gibert en 2009.

- La tasa de sedimentación obtenida, propia de la secuencia, es similar a la de los yacimientos más próximos de Fonelas y Mencal, y es consecuente con la ausencia de Jaramillo, ya que dicha tasa de sedimentación y los datos bioestratigráficos indican que la posición estratigráfica del yacimiento presenta una cronología mucho más joven que la propuesta por Scott y Gibert y más similar a la establecida para el Achelense en Europa.

10.3 Nueva evidencia paleomagnetica y cronológica para el yacimiento de Gran Dolina (Atapuerca, Burgos)

- La presencia del límite Brunhes - Matuyama está claramente definida entre los niveles TD7 y TD8.

- Los datos paleomagneticos obtenidos de los niveles TD6 a TD4 indican una polaridad inversa, que junto con los análisis de ESR y luminiscencia establecen una edad claramente post Jaramillo para dichos niveles.

- El mejor acceso a los estratos inferiores, llegando a la base de TD1, ha permitido realizar un análisis más exhaustivo de los mismos, y aunque en conjunto el yacimiento por debajo del límite MBB presenta una polaridad eminentemente inversa, se ha localizado una magnetozona de polaridad normal en el nivel superior de TD1 atribuible a Jaramillo.

- Por tanto, la cronología correspondiente a los niveles de industria lítica y de *Homo antecessor* estaría comprendida entre 0,9 - 0.78 Ma, intervalo entre el límite MBB y el subcron Jaramillo, indicando una presencia humana en Gran Dolina cercana al millón de años. Resultados que avala un reciente estudio realizado por Duval et al. (2018) sobre un diente de *antecessor* procedente de TD6 y con una fecha estimada entre 624 a 949 ka.

En definitiva, ante el resultado de los trabajos expuestos en la presente tesis, se puede concluir que el paleomagnetismo, concretamente las magnetoestratigrafías, en combinación con otros métodos de datación (ESR, nucleidos cosmogénicos) puede aportar pruebas lo suficientemente sólidas como para inidicar evidencia de presencia humana previa al subcron Jaramillo, próxima por tanto al millón de años, a pesar de la abundancia de restos de homínidos posteriores a dicho subcron.

10. 4 Resultados pendientes de publicación

En lo que se refiere a los trabajos todavía en proceso de publicación, se espera seguir desarrollando la investigación en los mismos y poder ampliar los resultados que permitan un mejor marco cronológico de la dispersión humana fuera de África.

10.5 Referencias

Duval, M., Grün, R., Parés, J.M., Martín-Francés, L., Campaña, I., Rosell, J., Shao, Q., Arsuaga, J.L., Carbonell, E., Bermúdez de Castro, J.M., 2018. The first direct ESR dating of a hominin tooth from Atapuerca Gran Dolina TD-6 (Spain) supports the antiquity of Homo antecessor. Quaternary Geochronology 47, 120–137.

Scott, G.R., Gibert, L., 2009. The oldest hand-axes in Europe.Nature 461, 82–85.

Appendix / Apéndices

Appendix A - new magnetostratigraphic evidence for the age of acheulean tools at the archaeo-palaeontological site "solana del zamborino" (guadix-baza basin, s spain)

Supplementary Information.

New magnetostratigraphic evidence for the age of Acheulean tools at the archaeo-palaeontological site "Solana del Zamborino" (Guadix – Baza Basin, S Spain)

C. Álvarez-Posada[1*]; J.M. Parés[1]; R. Sala[2]; C. Viseras[3]; S. Pla-Pueyo[4]

[1]Geochronology Program, CENIEH, Paseo Sierra de Atapuerca 3, 09002-Burgos, Spain
[2]IPHES (Institut Català de Paleoecologia Humana i Evolució Social). Área de Prehistòria, Universitat Rovira i Virgili, Campus Sescelades-URV, Edifici W3. 43007 Tarragona
[3]Dpto. Estratigrafía y Paleontología, Facultad de Ciencias, Universidad de Granada. 18071, Granada, Spain.
[4]Heriot-Watt University, Edinburgh. EH14 4AS United Kingdom
* Corresponding author. E-mail address: claudiaalvarezposada@gmail.com

This supplementary information contains one table and one figure.

Table 1

Summary of the paleomagnetic data.

Height (m): Stratigraphic height of the sequence beginning from the bottom,. SZ sites are those from the sequence carried out in 2014, and SZ' are those sampling at the sequence carried out in 2015. **Analysis:** paleomagnetic demagnetization and analysis carried out for each sample (**TH** thermal demagnetization; **AF**, demagnetization by alternating fields; and **IRM** the isothermal remanent magnetization curves). **ChRM Directions:** Characteristic Remanent Magnetization direction of each sample; **Dec/Inc are** the declination/Inclination of each individual sample; and **MAD** is the maximum angular deviation. **Type: visual**, is the visual inspection of the Zijderveld diagrams of each sample and their behaviour during the demagnetization, grouped the samples in three different types, type I (23%), type II (40%) and type III (35%); **MAD**, in this distribution we have calculated first the mean of the MAD of all the individual samples, obtained a value of 4.7 which we use as reference to classify the data as type I if the MAD value of the individual sample is ≤4.7; and we classified as type II if the MAD is > 4.7. For the samples without possibility to obtain data the type has been defined as III. **N:** number of data points. **Dec:** mean declination of the sampling site. **Inc:** mean inclination of the sampling site. ***K*:** the precision parameter. **Class:** statistical classification of the data by using the precision parameter, *k*, in which $k \geq 10$ = class I, $k < 10$ = class II, and when just a one sample has been used to calculate the mean data, *k* = class 3. **Watson's_f:** is the Watson's test for randomness, where **F stats** is the Watson's F statistics of the directional data of each sampling site, and the next column named as **Beat**, is the number to beat for the F stats; if the first columns has a value greater than the required number to beat, the data failed to pass the test and are randomly distributed.

Field Data			Analysis			ChRM directions			Sample Type		Site Mean Distribution				Watsons_f	
Height (m)	Sampling Site	Individual Sample	Dec / Inc	TH	AF	IRM	Dec	Inc	MAD	Visual	MAD	N	Dec	Inc	k	Class	F stats	Beat
9	SZ'1	SZ'1.1A	020/70	X			352	39	4,7	I	II							
		SZ'1.1B	020/70	x			-	-	-	III	III							
		SZ'1.2A	023/74	x			-	-	-	III	III							
		SZ'1.2B	023/74	X			14	51	3,3	I	I	3	23,5	44,5	8,1	2	0	4,46
		SZ'1.2C	023/74		X		60	31	7,6	II	II							
		SZ'1.3	088/63	x			-	-	-	III	III							
		SZ'1.4	045/66			x												
10,5	SZ'2	SZ'2.1A	103/61	X			-	-	-	III	III							
		SZ'2.1B	103/61		X		-	-	-	III	III							
		SZ'2.1C	103/61	x			-	-	-	III	III							
		SZ'2.2A	131/52			x												
		SZ'2.3A	106/55	x			-	-	-	III	III							
		SZ'2.3B	106/55	X			-	-	-	III	III							
12	SZ'3	SZ'3.1A	092/22	x			-	-	-	III	III							
		SZ'3.1B	092/22			x												
		SZ'3.1C	092/22		X		354	36	4,4	I	I	2	334.6	28.7	10.3	1	0	4,46
		SZ'3.2A	125/32		X		-	-	-	II	II							
		SZ'3.2B	125/32	x			-	-	-	III	III							
		SZ'3.3A	123/55	X			318	19	13,4	I	II							
13,5	SZ'4	SZ'4.1A	0/0	X			-	-	-	III	III							
		SZ'4.1B	0/0	x			-	-	-	III	III							
		SZ'4.1C	0/0			x												
		SZ'4.1D	0/0		X		-	-	-	III	III							
		SZ'4.2A	0/0	x			-	-	-	III	III							
		SZ'4.2B	0/0	X			-	-	-	III	III							
		SZ'4.2C	0/0		X		-	-	-	III	III							
15	SZ'5	SZ'5.1A	358/70	x			-	-	-	III	III							
		SZ'5.1B	358/70			x												
		SZ'5.1C	358/70	X			-	-	-	III	III							
		SZ'5.2A	332/70	X			-	-	-	III	III							
		SZ'5.2B	332/70	x			-	-	-	III	III							
		SZ'5.2C	332/70		X		-	-	-	III	III							
		SZ'5.3A	286/38	x			-	-	-	III	III							
		SZ'5.3B	286/38	X			-	-	-	III	III							
		SZ'5.3C	286/38		X		-	-	-	III	III							
		SZ'5bisA	0/0	x			-	-	-	III	III							
18	SZ'6	SZ'6.1A	244/53	x			-	-	-	III	III							
		SZ'6.1B	244/53			x												
		SZ'6.2A	0/0	X			7	49	6,3	II	II	3	352	47,9	#####	1	0	4,5
		SZ'6.2B	0/0		X		321	58	9,4	II	II							
		SZ'6.2C	0/0		x		359	32	9	II	II							

Field Data			Analysis			ChRM directions			Sample Type		Site Mean Distribution				Watsons_f	
Height (m)	Sampling Site	Individual Sample	TH	AF	IRM	Dec	Inc	MAD	Visual	MAD	N	Dec	Inc	k	Class	F stats	Beat
19,5	SZ'7	SZ'7.1A	x			-	-	-	III	III							
		SZ'7.1B		X		352	44	3,8	II	I							
		SZ'7.2A	x			-	-	-	III	III							
		SZ'7.2B	X			348	47	6,4	II	II	3	3,1	45,5	25,4	1	0	4,46
		SZ'7.2C			x												
		SZ'7.3A	x			-	-	-	III	III							
		SZ'7.3B	X			28	41	10,2	II	II							
22,5	SZ'8	SZ'8.1A	x			-	-	-	III	III							
		SZ'8.1B	X			-	-	-	III	III							
		SZ'8.1C		X		11	28	7,9	II	II	1	11	28	-	3	-	-
		SZ'8.2A	x			-	-	-	III	III							
		SZ'8.2B	X			-	-	-	III	III							
24	SZ'9	SZ'9.2A	x			-	-	-	III	II							
		SZ'9.2B	X			218	-26	4,8	II	II							
		SZ'9.2C		X		-	-	-	III	III							
		SZ'9.3A	x			-	-	-	III	III	3	207	-30,6	22,4	1	0	4,46
		SZ'9.4A	x			-	-	-	III	III							
		SZ'9.4B	X			184	-32	9,8	II	II							
		SZ'9.4C		X		218	-31	11,9	II	II							
25	SZ9	SZ9.1A	x			189	-56	11,1	II	II							
		SZ9.1B		X		155	-38,5	3,2	II	I							
		SZ9.2A	X			189	-11	0,3	II	I	5	170,8	-36,5	13,4	1	0	3,63
		SZ9.2B		X		147	-36	6,6	I	II							
		SZ9.2C		X		175	-35	6,6	II	II							
		SZ9.3	X			-	-	-	III	III							
25,5	SZ'10	SZ'10.1A	x			-	-	-	III	III							
		SZ'10.1B	X			183	-50	10,5	II	II							
		SZ'10.1C		X		169	-58	4,1	II	I							
		SZ'10.1D			x												
		SZ'10.2A	x			-	-	-	III	III							
		SZ'10.2B	X			182	-36	9	II	II	4	182,9	-43	27,9	1	0	3,89
		SZ'10.2C		X		-	-	-	III	III							
		SZ'10.3A	x			-	-	-	III	III							
		SZ'10.3B	X			-	-	-	III	III							
		SZ'10.3C		X		192	-27	7,7	II	II							

Field Data				Analysis			ChRM directions			Sample Type		Site Mean Distribution					Watsons_f	
Height (m)	Sampling Site	Individual Sample	Dec / Inc	TH	AF	IRM	Dec	Inc	MAD	Visual	MAD	N	Dec	Inc	k	Class	F stats	Beat
		SZ10.1A	0 / 0	x			226,9	-53,2	26,7	II	II							
		SZ10.1B	0 / 0		X		180	-38	3,9	II	I							
		SZ10.1C	0 / 0			x												
		SZ10.2A	0 / 0	X			182	-38	4,7	I	II							
		SZ10.2B	0 / 0		X		176	-26,8	2,5	II	I							
26,5	SZ10	SZ10.2C	0 / 0		x		180	-30	5	I	II	8	187,9	-41	21,6	1	0	3,34
		SZ10.3A	0 / 0	x			-	-	-	III	III							
		SZ10.3B	0 / 0		x		165	-41	8,2	I	II							
		SZ10.3C	0 / 0		X		192,4	-47,8	2	II	I							
		SZ10.3D	0 / 0	x			216,5	-41,3	4,3	II	I							
		SZ'11.1A	0/0	x			-	-	-	III	III							
		SZ'11.1B	0/0	X			97	-16	12,4	II	II							
		SZ'11.1C	0/0		X		82	-20	8,8	II	II							
		SZ'11.2A	0/0	x			-	-	-	III	III							
27	SZ'11	SZ'11.2B	0/0	X			90	-8	3,5	I	I	5	95,5	-1,5	3,5	2	0	3,63
		SZ'11.2C	0/0		X		83	-12	4,2	II	I							
		SZ'11.3A	0/0	x			-	-	-	III	III							
		SZ'11.3B	0/0	X			182	60	6,2	II	II							
		SZ'11.3C	0/0			x												
		SZ11.1A	0 / 0	x			190	-24	1,6	I	I							
		SZ11.1B	0 / 0		X		181	-32	3,9	I	I							
		SZ11.1C	0 / 0			x												
		SZ11.2A	0 / 0	X			192	-39	2,5	I	I							
		SZ11.2B	0 / 0		X		183,7	-37,1	0,8	I	I					1	0	3,29
28	SZ11	SZ11.2C	0 / 0	X			185	-45	1,7	II	I	9	184,3	-32,8	49,3			
		SZ11.3	0 / 0		X		202	-26	3,4	II	I							
		SZ11.4A	0 / 0	x			177	-20	2,3	II	I							
		SZ11.4B	0 / 0		X		174	-29	3,3	II	I							
		SZ11.4C	0 / 0		x		173	-40	2,8	I	I							
		SZ12.1	0 / 0	x			-	-	-	III	III							
		SZ12.2A	0 / 0		X		350	58	4,8	I	II							
29,5	SZ12	SZ12.2B	0 / 0	X			341	63	5,4	I	II	4	12,5	46,6	27,4	1	0	3,89
		SZ12.3A	0 / 0	x			343	24	8	II	II							
		SZ12.3B	0 / 0		x		11	3	18,7	II	II							
		SZ'12.1A	0/0	x			-	-	-	III	III							
		SZ'12.1B	0/0	X			360	45	3,6	II	I							
		SZ'12.1C	0/0		X		30	46	9,1	II	II							
		SZ'12.2A	0/0	x			-	-	-	III	III							
30	SZ'12	SZ'12.2B	0/0	X			-	-	-	III	III	4	9	53,9	19,6	1	0	3,89
		SZ'12.2C	0/0			x												
		SZ'12.3A	0/0	x			-	-	-	III	III							
		SZ'12.3B	0/0	X			347	47	11,5	II	II							
		SZ'12.3C	0/0		X		31	42	8,2	II	II							

Field Data				Analysis			ChRM directions			Sample Type		Site Mean Distribution					Watsons_f	
Height (m)	Sampling Site	Individual Sample	Dec / Inc	TH	AF	IRM	Dec	Inc	MAD	Visual	MAD	N	Dec	Inc	k	Class	F stats	Beat
31	SZ13	SZ13.1A	0 / 0	x			20	26	4,2	I	I	5	5,9	30,1	24,1	1	0	3,63
		SZ13.1B	0 / 0		X		345	28	7	I	II							
		SZ13.1C	0 / 0		x		22	35	5	I	II							
		SZ13.2A	0 / 0	X			350	38	3,1	I	I							
		SZ13.2B	0 / 0		X		11	19	3,2	I	I							
31,5	SZ'13	SZ'13.1A	0/0	x			-	-	-	III	III	5	7,4	52,1	116,3	1	0	3,63
		SZ'13.1B	0/0	X			10	54	3,6	II	I							
		SZ'13.1C	0/0		X		352	51	2	II	I							
		SZ'13.2A	0/0	x			-	-	-	III	III							
		SZ'13.2B	0/0	X			2	49	4,1	II	I							
		SZ'13.2C	0/0		X		24	52	10,2	II	II							
		SZ'13.3A	0/0	x			-	-	-	III	III							
		SZ'13.3B	0/0	X			10	52	18,8	II	II							
		SZ'13.3C	0/0			x												
32,5	SZ14	SZ14.1	0 / 0	x			-	-	-	III	III	1	8	8	-	3		
		SZ14.2	0 / 0		x		10	12	2	II	I							
34	SZ15	SZ15.1A	0 / 0	x			348	67	6,3	II	II	4	331,7	29,5	2,3	2	0	3,89
		SZ15.1B	0 / 0		X		302	-30	7,5	II	II							
		SZ15.2A	0 / 0	X			-	-	-	III	III							
		SZ15.2B	0 / 0		X		320	5	10,6	II	II							
		SZ15.2C	0 / 0			x					I							
		SZ15.3A	0 / 0	X			-	-	-	III	III							
		SZ15.3B	0 / 0		X		37	55,3	11,8	II	II							
34,5	SZ'14	SZ'14.1A	0/0	x			-	-	-	III	III	5	353,1	37,6	7,9	2	0	3,63
		SZ'14.1B	0/0	X			15	32	5,6	II	II							
		SZ'14.1C	0/0		X		316	51	2,5	II	I							
		SZ'14.2A	0/0	x			-	-	-	III	III							
		SZ'14.2B	0/0	X			30	47	7,7	II	II							
		SZ'14.2C	0/0		X		327	10	8,4	II	II							
		SZ'14.3A	0/0	x			-	-	-	III	III							
		SZ'14.3B	0/0	X			359	32	2,6	II	II							
		SZ'14.3C	0/0			x												
35,5	SZ16	SZ16.1A	0 / 0	x			158	4,9	5	II	II	3	154,4	-0,3	32,1	1	0	4,46
		SZ16.1B	0 / 0		X		142	-11	3	II	I							
		SZ16.1C	0 / 0		X		-	-	-	III	III							
		SZ16.2	0 / 0		x		163	6	4,7	II	I							

Field Data				Analysis			ChRM directions			Sample Type		Site Mean Distribution					Watsons_f	
Height (m)	Sampling Site	Individual Sample	Dec / Inc	TH	AF	IRM	Dec	Inc	MAD	Visual	MAD	N	Dec	Inc	k	Class	F stats	Beat
		SZ'15.1A	0/0	x			-	-	-	III	III							
		SZ'15.1B	0/0		X		357	47	1,5	I	I							
		SZ'15.1C	0/0			x												
		SZ'15.2A	0/0	x			-	-	-	III	III							
36	SZ'15	SZ'15.2B	0/0	X			16	37	2,4	I	I	5	357,1	41,6	39,6	1	0	3,63
		SZ'15.2C	0/0	x			358	29	4	I	I							
		SZ'15.3A	0/0	x			-	-	-	III	III							
		SZ'15.3B	0/0	X			353	49	4,1	II	I							
		SZ'15.3C	0/0		X		339	43	2,1	II	I							
		SZ17.1A	0 / 0	x			30	35	3,7	II	I							
		SZ17.1B	0 / 0		X		347	25	3,4	II	I							
		SZ17.1C	0 / 0		X		342	22	8,5	I	II							
37	SZ17	SZ17.1D	0 / 0	X			16	28	2,6	II	I	7	8,2	36,5	19,3	1	0	3,4
		SZ17.3A	0 / 0	X			23	49	3,3	II	I							
		SZ17.3B	0 / 0		X		18	46	2,5	II	I							
		SZ17.4	0 / 0		X		10	42	7,7	II	II							
		SZ'16.1A	0/0	x			-	-	-	III	III							
		SZ'16.1B	0/0	X			357	53	3,9	I	I							
		SZ'16.1C	0/0		X		358	52	3,2	I	I							
		SZ'16.2A	0/0	x			-	-	-	III	III							
37,5	SZ'16	SZ'16.2B	0/0	X			349	54	5,8	I	II	6	345,6	52,8	37,3	1	0	3,49
		SZ'16.2C	0/0		X		357	57	2,7	I	I							
		SZ'16.3A	0/0	x			-	-	-	III	III							
		SZ'16.3B	0/0	X			306	50	9,3	I	I							
		SZ'16.3C	0/0		X		347	42	5,3	II	I							
		SZ'16.3D	0/0			x												
		SZ18.1A	0 / 0	x			-	-	-	III	III							
38,5	SZ18	SZ18.1B	0 / 0		X		320	44	11,6	II	II	2	338.8	33,1	10	1	0	6,94
		SZ18.2	0 / 0		x		353	20	9,3	II	II							
		SZ'17.1A	0/0	x			-	-	-	III	III							
		SZ'17.1B	0/0	X			4	47	11,6	I	II							
		SZ'17.1C	0/0			x												
		SZ'17.2A	0/0	X			0	47	1,5	I	I							
39	SZ'17	SZ'17.2B	0/0		X		360	45	5,5	I	II	5	359,5	46,2	346,2	1	0	3,63
		SZ'17.2C	0/0	x			-	-	-	III	III							
		SZ'17.3A	0/0	x			-	-	-	III	III							
		SZ'17.3B	0/0	X			354	51	2,5	I	I							
		SZ'17.3C	0/0		X		359	41	5,2	I	II							
		SZ19.1A	0 / 0	x			359	45	9,5	II	II							
40	SZ19	SZ19.1B	0 / 0		X		349	61	3,1	II	I	3	360	54,6	62,2	1	0	4,46
		SZ19.2	0 / 0		X		11	57	2,7	II	I							

Field Data			Analysis			ChRM directions			Sample Type		Site Mean Distribution				Watsons_f	
Height (m)	Sampling Site	Individual Sample	Dec / Inc	TH	AF	IRM	Dec	Inc	MAD	Visual	MAD	N	Dec	Inc	k	Class	F stats	Beat
41,5	SZ20	SZ20.1	0 / 0	x			238	66	3.2	II	I	2	239,8	68	720,5	1	0	6,94
		SZ20.2	0 / 0		x		242	70	3.8	II	I							
43,5	SZ'18	SZ18'.1A	0/0	x			-	-	-	III	III	4	199,4	-53,2	13,1	1	0	3,89
		SZ18'.1B	0/0	x			-	-	-	III	III							
		SZ18'.1C	0/0		x		224	-52	4,4	II	I							
		SZ18'.2A	0/0	x			-	-	-	III	III							
		SZ18'.2B	0/0	x			206	-62	3	II	I							
		SZ18'.2C	0/0		x		190	-25	5,7	II	II							
		SZ18'.3A	0/0	x			-	-	-	III	III							
		SZ18'.3B	0/0	x			174	-68	4,2	II	I							
		SZ18'.3C	0/0		x		-	-	-	III	III							
44,5	SZ'19	SZ18'.1D	0/1			x						4	10,7	28,1	2,6	2	0	3,89
		SZ22.1A	0 / 0	x			355,2	80,6	3,8	II	I							
		SZ22.1B	0 / 0		x		21	-40	6,1	II	II							
		SZ22.2A	0 / 0	x			348	40	5,8	II	II							
		SZ22.2B	0 / 0		x		-	-	-	III	III							
		SZ22.2C	0 / 0	x			-	-	-	III	III							
		SZ22.2D	0 / 0		x		23	21	3,2	II	I							
45	SZ'19	SZ'19.1A	306/52	x			-	-	-	III	III							
		SZ'19.1B	306/52	x			-	-	-	III	III							
		SZ'19.2A	004/65		x													
		SZ'19.2B	004/65	x			-	-	-	III	III							
		SZ'19.3A	323/77	x			-	-	-	III	III							
		SZ'19.3B	323/77	x			-	-	-	III	III							
46,5	SZ'20	SZ'20.1A	348/28	x			-	-	-	III	III	5	187,4	-50,2	84,8	1	0	3,63
		SZ'20.1B	348/28	x			192	-59	4,6	I	I							
		SZ'20.1C	348/28			x												
		SZ'20.2A	0/0	x			-	-	-	III	III							
		SZ'20.2B	0/0	x			195	-50	5,7	I	II							
		SZ'20.2C	0/0		x		177	-56	1,4	I	I							
		SZ'20.3A	0/0	x			-	-	-	III	III							
		SZ'20.3B	0/0	x			189	-44	3,4	I	I							
		SZ'20.3C	0/0		x		184	-41	2,7	I	I							
47,5	SZ24	SZ24.1A	0 / 0	x			321	60	4,3	II	I	6	57,6	37,6	6,6	2	0	3,49
		SZ24.1B	0 / 0		x		355	23	11,9	I	II							
		SZ24.1C	0 / 0			x												
		SZ24.2	0 / 0	x			-	-	-	III	III							
		SZ24.3A	0 / 0	x			40	26	6,4	II	II							
		SZ24.3B	0 / 0		x		37	28	4,5	II	I							
		SZ24.4A	0 / 0	x			321	30	5,8	II	II							
		SZ24.4B	0 / 0		x		336	32	6,3	I	II							

Field Data				Analysis			ChRM directions			Sample Type		Site Mean Distribution					Watsons_f	
Height (m)	Sampling Site	Individual Sample	Dec / Inc	TH	AF	IRM	Dec	Inc	MAD	Visual	MAD	N	Dec	Inc	k	Class	F stats	Beat
		SZ26.1A	0 / 0	x			191	-49	6	II	II							
		SZ26.1B	0 / 0		X		184	-31	5,7	II	II							
		SZ26.1D	0 / 0			x												
50	SZ26	SZ26.2A	0 / 0	X			200	-47	4,8	II	II	4	194,2	-41,5	57,4	1	0	3,89
		SZ26.2B	0 / 0		X		-	-	-	III	III							
		SZ26.3A	0 / 0	X			203	-38	5,9	I	II							
		SZ26.3B	0 / 0		X		-	-	-	III	III							
		SZ27.1A	0/0	x			-	-	-	III	III							
		SZ27.1B	0/0	X			170	-46	4,3	II	I							
		SZ27.1C	0/0		X		165	-48	1,5	II	I							
52	SZ'27	SZ27.2A	0/0	x			-	-	-	III	III	4	169,4	-53	117,2	1	0	3,89
		SZ27.3A	0/0	x			-	-	-	III	III							
		SZ27.3B	0/0	X			170	-57	6,4	II	II							
		SZ27.3C	0/0		X		174	-61	1,8	II	I							
		SZ29.1A	150 / 4	x			206	7,4	10,9	II	II							
		SZ29.1A	0/0	x			-	-	-	III	III							
		SZ29.1B	150 / 4		X		187	-52	4	II	I							
		SZ29.1C	0/0		X		-	-	-	III	III							
55	SZ29	SZ29.2A	0 / 10	X			336	-42	12,8	II	II	5	232,7	-56	2,5	2	0	3,63
		SZ29.2B	0 / 10		X		293	-46	5,9	II	II							
		SZ29.2C	0/10	X			187	-52	4,3	II	I							
		SZ29.2D	0 / 10			x												
		SZ30.1A	0 / 0	x			193	-44	3,5	I	I							
		SZ30.1B	0 / 0		X		188	-42	9,3	II	II							
		SZ30.1C	0 / 0			x												
56,5	SZ30	SZ30.2A	0 / 0	X			187	-22	2,4	I	I	6	187,7	-34,6	42,9	1	0	3,49
		SZ30.2B	0 / 0		X		185	-16	4,3	II	I							
		SZ30.3A	0 / 0	X			189	-42	2,1	I	I							
		SZ30.3B	0 / 0		X		186	-41	4,6	II	I							
		SZ31.1A	40 / 8	x			198	-46	4,5	II	I							
		SZ31.1B	40 / 8		X		246	-57	14,7	II	II							
		SZ31.1C	40 / 8			x												
58	SZ31	SZ31.2A	40 / 8	X			238	-52	1,8	II	I	4	213,2	-53,7	16,4	1	0	3,89
		SZ31.2B	40 / 8		X		180	-48	2,7	II	II							
		SZ31.3A	90 / 20	X			-	-	-	III	III							
		SZ31.3B	90 / 20		X		-	-	-	III	III							

Field Data			Analysis			ChRM directions			Sample Type		Site Mean Distribution				Watsons_f	
Height (m)	Sampling Site	Individual Sample	Dec / Inc	TH	AF	IRM	Dec	Inc	MAD	Visual	MAD	N	Dec	Inc	k	Class	F stats	Beat
59,5	SZ32	SZ32.1A	250 / 10	x			178	-30	4,9	II	II							
		SZ32.1B	250 / 10		X		186	-43	4	II	I							
		SZ32.1C	250 / 10			x												
		SZ32.2A	0 / 10	X			169	-51	1,6	II	I	6	175,7	-44,2	43,7	1	0	3,49
		SZ32.2B	0 / 10		X		181	-50	2,6	II	I							
		SZ32.3A	0 / 10	X			181	-45	4,7	II	II							
		SZ32.3B	0 / 10		X		187	-42	3,1	II	I							
61	SZ33	SZ33.1	90 / 10	x			7	-44	10,3	II	II	2	356	-55,4	18,4	1	0	6,94
		SZ33.2A	90 / 10		X		336,7	-65	2,6	II	I							
62,5	SZ0	SZ0.1	0 / 0	x			334	68	3,4	I	I	3	343,3	53,3	10,1	1	0	4,46
		SZ0.2	0 / 0		X		326	30	16,2	II	II							
		SZ0.3	0 / 0	X			17	55	7,3	II	II							
64	SZ1	SZ1.1A	0 / 0	x			349	61	8	I	II	4	355,8	45,3	11,6	1	0	3,89
		SZ1.1B	0 / 0		X		328	25	2,7	I	I							
		SZ1.2A	0 / 0	X			27	41	3,4	I	I							
		SZ1.2B	0 / 0		X		3	45	1,9	I	I							
		SZ1.3A	0 / 0			x												
65,5	SZ2	SZ2.1	0 / 0	x			12	15	2,5	I	I	2	11,5	13	774,8	1	0	6,94
		SZ2.2	0 / 0		X		11	11	4,1	I	I							
67	SZ3	SZ3.1	0 / 0	x			9	-26	5,3	I	II	1	9	-26	-	3		
		SZ3.2	0 / 0			x												
70	SZ5	SZ5.1	0 / 0	x			356	14	11,2	II	II	3	347,6	28,1	2,8	2	0	4,46
		SZ5.1bis	0 / 0		x		39	81	2,8	I	I							
		SZ5.2	0 / 0		X		332	-8,6	4,9	I	II							
		SZ5.4	0 / 0	x			-	-	-	III	III							
71,5	SZ6	SZ6.1	323 / 35	x			20	40	4,3	I	I	2	8,1	55,8	10,6	1	0	6,94
		SZ6.2	313 / 38		X		342	69	3,9	I	I							
		SZ6.4	329 / 32			x												
73	SZ7	SZ7.1A	0 / 0	x			18	28	6,9	I	II	6	366,6	36,8	3,1	2	0	3,49
		SZ7.1B	0 / 0		X		-	-	-	III	III							
		SZ7.2A	0 / 0	X			250	89	4,9	II	II							
		SZ7.2B	0 / 0		X		5	20	5,2	I	II							
		SZ7.3A	0 / 0	x			-	-	-	III	III							
		SZ7.3B	0 / 0		X		328	6	6,4	I	II							
		SZ7.4A	0 / 0	X			344	38	2,9	I	I							
		SZ7.4B	0 / 0		X		261	5	11,7	I	II							
		SZ7.4C	0 / 0			x												
74,5	SZ8	SZ8.1A	0 / 0	x			331	3	9,7	I	II	3	315	26,7	4,5	2	0	4,46
		SZ8.1B	0 / 0		X		265	52	3,9	I	I							
		SZ8.1C	0 / 0			x												
		SZ8.2A	0 / 0	X			-	-	-	III	III							
		SZ8.2B	0 / 0		X		327	18	5,8	I	II							

Figure 2

Reversal Test.

We have used a bootstrap test for a common mean to perform a reversal test (Tauxe, 1998), which is based on comparing the Cartesian coordinates of the bootstrapped means. This figure shows histograms of Cartesian coordinates of means of para-data sets drawn from the ChRM directions from Table I. The reversed polarity directions have been flipped to the antipode to test for a common mean of the two modes, normal and reversed. Because the confidence bounds from the two data sets overlap in all three components, the means of the reversed and normal modes cannot be distinguished at the 95% level of confidence. We therefore can conclude that the data set passes the bootstrap reversal test.

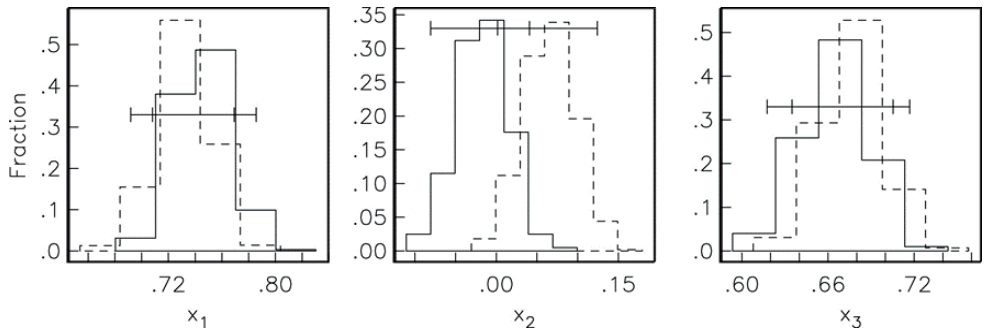

Appendix B - a post-jaramillo age for the artefact-bearing layer td4 (gran dolina, atapuerca): new paleomagnetic evidence

Supplementary data.

This supplementary information contains three tables.

Table S1
References to the ages and faunas of the localities in Figure 2.

Locality	Age	Reference to age	Reference to fauna
Atapuerca TD7	latest Matuyama	Parés et al., 2013	Van der Made et al., 2015
Cueva Victoria	latest Matuyama	Ferràndez-Cañadell et al., 2014	Gibert, Ferràndez-Cañadell, 2014 Van der Made et al., 2015-online
Lakhuti	latest Matuyama		Vangengeim et al., 1988
Dorn Dürkheim 3	latest Matuyama	Franzen et al., 2000	Franzen et al., 2000
Happisburg HSB3	latest Matuyama MIS 21 / 25	Parfitt et al., 2010	Parfitt et al., 2010
Akhalkalaki			Vekua, 1986
Apollonia 1	Biochronology: 0.6-0.9 Ma	Koufos, Kostpoulos, 1997, fig. 2	Koufos, Kostpoulos, 1997; Kostopoulos, 1997
Atapuerca TD6	below Monte Rosa/Kamikatsura	Parés et al., 2013	Van der Made, 1999; García , Arsuaga, 1999
Atapuerca TD5	below Monte Rosa/Kamikatsura	Parés et al., 2013	García , Arsuaga, 2001; Van der Made et al., 2015-online
Atapuerca TD4 (TD3)	below Monte Rosa/Kamikatsura	Parés et al., 2013	Soto, 1987; García , Arsuaga, 2001; Van der Made et al., 2015-online
Huescar 1	Brunhes/Jaramillo OSL: ~420-570 ka	Gibert , Scott, 2009; Demuro et al., in press	Alberdi , Bonadonna, 1989
Mosbach 1	Jaramillo	Von Koenigswald , Tobien, 1987	Von Koenigswald , Tobien, 1987; Von Koenigswald , Heinrich, 1999
Vallonnet	Jaramillo	De Lumley et al., 1988	Moullé et al., 2006
Untermassfeld	Jaramillo	Wiegank, 1997	R.D. Kahlke, 1997, 2001a, 2001b, 2006; H.D: Kahlke, 1997; Sher, 1997; Guérin , Faure, 1997

Collecurti	earliest Jaramillo	Coltorti et al., 1998	Coltorti et al., 1998

Table S2
Reference to the taxonomy of the taxa in Figure 2.

Taxon	**Reference**
Theropithecus	Gibert et al., 1995; Ferràndez Cañadel, et al., 2014
Crocuta	García , Arsuaga, 2001
Sus	Van der Made et al., 2015-online
Alces	Van der Made et al., 2015
Eucladoceros	Van der Made , Dimitrijevic, 2015; Van der Made, 2015
Megaceroides	Van der Made, 2015
Cervus	Van der Made et al., 2014
Bison	Van der Made et al., 2015-online
Soergelia	Van der Made et al., 2015-online
Praeovibos	Van der Made et al., 2015-online
Ovis	Crégut-Bonnoure, 2007
"Capra" alba	Van der Made et al., 2008

Table S3

Summary of the paleomagnetic data.

Level: stratigraphical levels of the Gran Dolina (TD) site analysed. **Deep (m)**: Stratigraphic deep of the sequence beginning from the top of the TD. **Individual sample**: each individual sample obtained in each level. **Dec:** declination of each individual sample, oriented in situ. **Inc:** inclination of each individual sample, oriented in situ. **Analysis:** paleomagnetic demagnetization and analysis carried out for each sample (**TH** thermal demagnetization; **AF**, demagnetization by alternating fields; **130º+AF;** samples demagnetized first at 130^{o}C and then with alternatin field; and **IRM**, the isothermal remanent magnetization curves). **ChRM Directions:** Characteristic Remanent Magnetization direction of each sample; **Dec/Inc are** the declination/Inclination of each individual sample; and **MAD** is the maximum angular deviation. **Sample Type:** distribution of each sample in three different types, using the MAD; we have calculated first the mean of the MAD of all the individual samples, obtained a value of 7.05 which we use as reference to classify the data as type I if the MAD value of the individual sample is ≤7.05; and we classified as type II if the MAD is > 7.05. For the samples without possibility to obtain data the type has been defined as III. **N:** number of data points. **Dec:** mean declination of the sampling site. **Inc:** mean inclination of the sampling site. ***K*:** the precision parameter. **Class:** statistical classification of the data by using the precision parameter, *k*, in which *k*≥10 = class I, *k<10* = class II, and when just a one sample has been used to calculate the mean data, *k* = class 3.

Field Data					Analysis				ChRM directions			Sample Type	PCA SUMMARIZE (Fisher Vector Distribution)						
Level	Deep (m)	Individual Sample	Dec	Inc	TH	AF	130° + AF	IRM	Dec	Inc	Mad		N	Dec	Inc	α95	α99	kappa	Class
TD6	6,82	TD6.5	0	0	x				-	-	-	III							
		TD6.6A	0	0	x				-	-	-	III							
		TD6.6B	0	0				x											
	7,02	TD6.4	0	0	x				-	-	-	III							
	7,06	TD6.1A	0	0	x				168	-10	11,2	II	2	169,5	-13	14,6	33,7	294,9	1
		TD6.1B	0	0			x		171	-16	7,2	II							
	7,1	TD6.2A	0	0	x				-	-	-	III							
		TD6.2B	0	0				x											
	7,14	TD6.3A	0	0	x				-	-	-	III							
		TD6.3B	0	0															
		TD6.3C	0	0		x			-	-	-	III							
	7,18	TD6.9	0	0	x				174	-21	6,2	I	1	174	-21	-	-	-	3
	7,2	TD6.10	0	0	x				185	-22	5,6	I	1	185	-22	-	-	-	3
	7,23	TD6.8	0	0	x				168	-22	7,5	II	1	165	-22	-	-	-	3
		TD6.11	0	0	x				-	-	-	III							
	7,27	TD6.12A	0	0	x				176	-32	6,4	I	1	176	-32	-	-		3
		TD6.12B	0	0				x										-	
	7,4	TD6.15	0	0	x				144	-38	7	I	1	144	-38	-	-	-	3
	7,43	TD6.16	0	0	x				-	-	-	III							
	7,44	TD6.14	0	0	x				158	-29	7,9	II	1	158	-29	-	-	-	3
	7,53	TD6.13A	0	0	x				169	-34	7,6	II	1	169	-34	-	-	-	3
		TD6.13B	0	0															
	7,55	TD6.7A	0	0	x				174	-24	7,05	I	2	175	-26,5	11,6	26,7	465,7	1
		TD6.7B	0	0			x		176	-29	5,4	II							
	7,8	TD6.17	0	0	x				181	-21	6,7	I	1	181	-21	-	-	-	3
		TD6.18	0	0	x				-	-	-	III							
	8	TD6.20A	0	0			x		190	-30	8,2	II	2	188,5	-28	10,5	24	570,7	1
		TD6.20B	0	0	x				187	-26	6,4	I							
	8,04	TD6.19	0	0	x				-	-	-	III							
	8,05	TD6.22	0	0	x				158	-50	7,1	II	1	158	-50	-	-	-	3
	8,09	TD6.23B	0	0	x				193	-52	7,8	II	2	193	-54,5	11,2	25,8	498,6	1
		TD6.23A	0	0			x		195	-57	9,8	II							
	8,26	TD6.21	0	0	x				187	-30	7,5	II	1	187	-30	-	-	-	3
	8,52	TD6.24	0	0	x				190	-27	8,4	II	1	190	-27	-	-	-	3
	8,58	TD6.25A	0	0	x				-	-	-	III							
		TD6.25B	0	0															

	Field Data				Analysis				ChRM directions			Sample	PCA SUMMARIZE (Fisher Vector Distribution)						
Level	Deep (m)	Individual Sample	Dec	Inc	TH	AF	130º + AF	IRM	Dec	Inc	Mad	Type	N	Dec	Inc	α95	α99	kappa	Class
TD5	8,91	TD5.1	0	0	x				-	-	-	III							
	8,95	TD5.2C	0	0		x			345	-85	4	I							
		TD5.2B	0	0	x				-	-	-	III	1	345	-85	-	-	-	3
		TD5.2A	0	0		x													
	9	TD5.3B	0	0		x			-	-	-	III							
		TD5.3A	0	0	x				-	-	-	III							
		TD5.3C	0	0															
	9,05	TD5.4A	0	0	x				-	-	-	III							
		TD5.4C	0	0		x			-	-	-	III							
		TD5.4B	0	0				x											
	9,08	TD5.5C	0	0		x			-	-	-	III							
		TD5.5A	0	0	x				-	-	-	III							
		TD5.5B	0	0															
	9,1	TD5.15	0	0	x				153	-32	8,9	II	1	153	-32	-	-	-	3
	9,13	TD5.6C	0	0		x			-	-	-	III							
		TD5.6A	0	0	x				-	-	-	III							
		TD5.6B	0	0		x													
	9,16	TD5.7A	0	0	x				-	-	-	III							
		TD5.7B	0	0		x													
		TD5.7C	0	0				x											
	9,18	TD5.13	0	0	x				181	-17	4,3	I	1	181	-17	-	-	-	3
	9,2	TD5.8A	0	0	x				-	-	-	III							
		TD5.8B	0	0															
	9,21	TD5.14B	0	0		x			357	1	25	II	1	357	1	-	-	-	3
		TD5.14A	0	0	x				-	-	-	III							
		TD5.14C	0	0		x													
	9,24	TD5.9A	0	0	x				144	-2	20	II	1	144	-2	-	-	-	3
		TD5.9C	0	0		x			-	-	-	III							
		TD5.9B	0	0		x													
	9,27	TD5.10A	0	0	x				-	-	-	III							
		TD5.10C	0	0		x													
		TD5.10B	0	0				x											
	9,31	TD5.20	0	0	x				84	-2	21,7	II	1	84	-2	-	-	-	3
	9,32	TD5.11	0	0	x				-	-	-	III							
	9,36	TD5.12A	0	0	x				165	-2	6,3	I	2	162,5	-3	11,7	27	454	1
		TD5.12B	0	0			X		160	-4	8,5	II							
	9,41	TD5.16	0	0	x				-	-	-	III							
	9,62	TD5.19	0	0	x				-	-	-	III							
	9,66	TD5.18	0	0	x				171	-27	5,2	I	1	171	-27	-	-	-	3
	9,68	TD5.17	0	0	x				172	-38	6,2	I	1	172	-38	-	-	-	3

Field Data					Analysis				ChRM directions			Sample Type	PCA SUMMARIZE (Fisher Vector Distribution)						
Level	Deep (m)	Individual Sample	Dec	Inc	TH	AF	130º + AF	IRM	Dec	Inc	Mad		N	Dec	Inc	α95	α99	kappa	Class
TD4	10,11	TD4.10	0	0	x				175	-31	9,3	II	1	175	-31	-	-	-	3
	10,17	TD4.11A	0	0	x				161	-47	6	I	2	162,9	-48,5	8,7	20	820	1
		TD4.11B	0	0			x		165	-50	10,2	II							
	10,21	TD4.1	0	0	x				20	-8	16,7	II	1	20	-8	-	-	-	3
	10,38	TD4.9	0	0	x				-	-	-	III							
	10,39	TD4.7	0	0	x				-	-	-	III							
	10,4	TD4.12	0	0	x				113	-32	5,9	I	1	13	-32	-	-	-	3
		TD4.4A	0	0	x				173	-14	16,1	II	2	176,5	-15	15,4	35,7	264,2	1
		TD4.4B	0	0			x		180	-16	13,4	II							
	10,4	TD4.5	0	0	x				-	-	-	III							
	10,42	TD4.8	0	0	x				-	-	-	III							
		TD4.6A	0	0	x				-	-	-	III							
		TD4.6B	0	0				x											
	10,49	TD4-1.2C	304	46	x				-	-	-	III							
		TD4-1.2B	304	46		x			-	-	-	III							
		TD4-1.2A	304	46				x											
	10,57	TD4-1.1B	0	0	x				155	-37	14,5	II	1	155	-37	-	-	-	3
		TD4-1.1A	0	0															
	10,74	TD4.21	0	0															
	10,96	TD4.22B	0	0		x			-	-	-	III							
		TD4.22A	0	0	x				-	-	-	III							
	11,03	TD4.23	0	0				x											
	11,09	TD4.24A	0	0		x			-	-	-	III							
		TD4.24B	0	0	x				-	-	-	III							
	11,12	TD4.33	0	0				x											
	11,16	TD4.25A	0	0		x			-	-	-	III							
		TD4.25B	0	0	x				-	-	-	III							
	11,24	TD4.26A	0	0		x			-	-	-	III							
		TD4.26B	0	0	x				-	-	-	III							
	11,26	TD4.27	0	0				x											
	11,36	TD4.28																	
	11,39	TD4.29B	0	0		x			277	76	2,3	I	1	277	77	-	-	-	3
		TD4.29A	0	0	x				-	-	-	III							
	11,51	TD4.30	0	0															
	11,66	TD4.31	0	0	x				348	52	4,9	I	1	348	52	-	-	-	3
	11,99	TD4.32	0	0															
	12,03	TD4.2	0	0	x				-	-	-	III							

Field Data					Analysis			ChRM directions			Sample	PCA SUMMARIZE (Fisher Vector Distribution)					
Level	Deep (m)	Individual	Dec	Inc	TH	AF	130º +	IRM	Dec	Inc	Mad	Type	N	Dec	Inc	α95	α99	kappa	Class
TD4	12,05	TD4.20B	0	0		x			36	-50	4,8	I							
		TD4.20A	0	0	x				154	-43	9,7	II	2	101,1	-63,8	100	100	2,6	2
		TD4.20C	0	0		x			-	-	-	III							
		TD4.3	0	0	x				-	-	-	III							
	12,12	TD4.18	0	0	x				195	-45,3	5	I	1	195	-45,3	-	-	-	3
	12,22	TD4.15	0	0	x				164	-42	4,7	I	1	164	-42	-	-	-	3
	12,24	TD4.16B	0	0		X			121	56	9	II							
		TD4.16A	0	0	x				170	-48	4,4	I	2	147,8	4,4	-	-	1,1	2
		TD4.16C	0	0				x											
	12,26	TD4.17A	0	0	x				184	-74	2	I							
		TD4.17B	0	0			x		186	-78	0,9	I	2	184,9	-76	8,8	20,2	809,2	1
	12,29	TD4.19A	0	0	x				175	-31	4,3	I							
		TD4.19C	0	0			x		182	-43	5,1	I	2	178,2	-37,1	29,2	70,3	75,1	1
		TD4.19B	0	0		x			-	-	-	III							
	12,34	TD4.14	0	0	x				161	-37	8,4	II	1	161	-37	-	-	-	3
	12,41	TD4.13	0	0	x				283	5	6,5	I	1	283	5	-	-	-	3